Integrated Model-Based Impact Assessment of Climate Change and Land Use Change on the Occoquan Watershed

Ayden A. Baran

Dissertation submitted to the faculty of the Virginia Polytechnic Institute and State University in partial fulfillment of the requirements for the degree of

Doctor of Philosophy

In

Civil Engineering

Adil N. Godrej Committee Chair

Glenn E. Moglen Co-Chair

John C. Little

Mark A. Widdowson

Justin A. Bartlett

December 13, 2018

Manassas, VA

Keywords: climate change, land use change, integrated environmental modeling, water quantity, water quality, impact assessment, water resources management

Integrated Model-Based Impact Assessment of Climate Change and Land Use Change on the Occoquan Watershed

Ayden A. Baran

ABSTRACT

Forecasted changes to climate and land use were used to model variations in the streamflow characteristics of Occoquan watershed and water quality in the Occoquan reservoir. The combination of these two driving forces has created four themes and an integrated complexly-linked watershed-reservoir model was used to run the simulations. Two emission scenarios from the fourth assessment report of the Intergovernmental Panel on Climate Change (IPCC), along with four General Circulation Models (GCMs) by using two statistical downscaling methods, were applied to drive the Hydrological Simulation Program—Fortran (HSPF) and CE-QUAL-W2 (W2) in two future time periods (2046-2065 and 2081-2100). Incorporation of these factors yielded 68 simulation models which were compared with historical streamflow and water quality data from the late 20th century. Climate change is projected to increase surface air temperature and precipitation depth in the study area in the future. Using climate change only, an increase in high and median flows and decrease in low flows are projected. Changes in flow characteristics are more pronounced when only future land use changes are considered, with increases in high, median and low flows. Under the joint examination of the driving forces, an amplifying effect on the high flows and median flows observed. In contrast, climate change is projected to dampen the extreme increases in the low flows created by the land use change. Surface water temperatures are projected to increase as a result of climate change in the Occoquan reservoir, while these changes are not very noticeable under the effect of land use change only. It is expected that higher water temperatures will promote decreased oxygen solubility and greater heterotrophy. Moreover, longer anoxic conditions are projected at the bottom of the reservoir. Results indicate that higher water temperature will increase the denitrifying capacity of the reservoir, especially during summer months, further reducing the nitrate concentration in the reservoir.

Integrated Model-Based Impact Assessment of Climate Change and Land Use Change on the Occoquan Watershed

Ayden A. Baran

GENERAL AUDIENCE ABSTRACT

Water resources managers are facing a new set of challenges of developing strategies to address the regional impacts of climate change and land use change, especially in metropolitan areas. Simulating climate change and land use change scenarios can shed light on mitigation and adaption approaches for water resources management as well as future designs (for example, infrastructure, agriculture, irrigation, etc. among other sectors).

The focus of this study is the Occoquan watershed with an area of 1530 km^2 (590 square miles) which includes the 1700-acre Occoquan reservoir that yields about 40% of the drinking water supply of near 2.0 million residents in northern Virginia. The Occoquan watershed located approximately 40 km to the southwest of Washington, D.C. and is situated in the Mid-Atlantic region of the United Sates with four distinct seasons and is part of a bigger watershed known as the Potomac River Watershed.

The primary aim of this research is to provide an improved, quantitative understanding of the potential impacts of climate change and land use change on the Occoquan watershed. The findings of this research can benefit future water supply reliability and mitigation strategies in the study area considering this watershed's essential role as a water supplier in northern Virginia.

Dedication

To my advisors

and

Tom

Acknowledgements

The author wishes to express his thanks and appreciation to Dr. Adil N. Godrej and Dr. Glenn E. Moglen, for giving him an opportunity to work on this interesting topic and for their continuous guidance and patience.

Sincere gratitude is bestowed upon Dr. John C. Little, Dr. Mark A. Widdowson, and Dr. Justin A. Bartlett for serving in author's graduate committee and their support through the course of this research work. The author also would like to extend his appreciation to the late Dr. Thomas J. Grizzard for his unwavering commitment in the establishment and operation of the Occoquan program and the Occoquan Watershed Monitoring Laboratory (OWML) for over 40 years.

Thanks to all of the field, laboratory, and administrative staff as well as students at the OWML for their contributions towards author's research and making the lab a friendly place to work.

An additional note of thanks is owed to OWML and Australian Water Quality Centre (SA Water) for their financial assistance during this study.

Last, but not least, the author wishes to thank his parents, family and friends for their interest and support while he was completing this degree.

Table of Contents

Table of Contents ..... **vi**
List of Tables ..... **x**
List of Figures ..... **xii**
Abbreviations and Acronyms ..... **xix**
Chapter 1 Research Objectives **1**
1.1 Introduction 1
1.2 Study Motivations 1
1.2.1 Climate Change 1
1.2.2 Land Use Change 2
1.3 Study Objectives 2
1.3.1 Climate Change and Projections Variability 2
1.3.2 Impacts of Climate Change and Land Use Change on Water Quantity 3
1.3.3 Impacts of Climate Change and Land Use Change on Water Quality 3
1.4 Document Organization 4
1.5 References 4
Chapter 2 Occoquan Watershed and Occoquan Reservoir Background Information: Site Characteristics and Current Conditions **5**
2.1 Study Area 5
2.2 Sampling Stations 9
2.3 Occoquan Model 10
2.4 Projection Model Factors and Variables 12
2.5 References 13
Chapter 3 Quantifying the Hydrological Impact of Climate Change on a Watershed in Northern Virginia **14**
3.1 Abstract 14
3.2 Introduction 15
3.3 Study Area and Data 18
3.4 Models and Methods 19
3.4.1 Modeling Climate Change Impact 19
3.4.2 Emission Scenarios 19

3.4.3 GCMs 20
3.4.4 Statistical Downscaling of Precipitation and Surface Air Temperature Time Series 20
3.4.5 Delta Change Method 20
3.4.6 Quantile Mapping Method 21
3.4.7 Simulation Time Period 22
3.4.8 Hydrological Simulation Model 22
3.4.9 Flow Regime Indicators 23
3.5 Results and Discussion 23
3.5.1 Surface Air Temperature 23
3.5.2 Precipitation 24
3.5.3 Surface Air Temperature and Precipitation Interaction 25
3.5.4 Streamflow Alterations 25
3.6 Summary and Conclusions 28
3.7 Acknowledgments 29
3.8 References 29
Chapter 4 An Integrated System Modeling for Studying the Individual and Combined Impacts of Climate and Land Use Changes on Occupation Watershed Streamflows in Northern Virginia 47
4.1 Abstract 47
4.2 Introduction 48
4.3 Study Area and Observed Data 50
4.4 Models and Methods 52
4.4.1 Watershed Model 52
4.4.2 Modeling Climate Change Impact 53
4.4.3 Emission Scenarios 53
4.4.4 GCMs 54
4.4.5 Statistical Downscaling 54
4.4.6 Modeling Land Use Change Impact 56
4.4.7 Simulation Periods 56
4.4.8 Simulation Scenarios 57

4.5 Results and Discussion 58
4.5.1 Climate Change 58
4.5.2 Land Use Change 59
4.5.3 Streamflow Alterations 60
4.5.4 Flow Duration Curve 62
4.6 Summary and Conclusions 62
4.7 Acknowledgments 63
4.8 References 64
Chapter 5 Climate Change and Land Use Change Impacts on Water Quality in the Occoquan Reservoir, Virginia, USA 99
5.1 Abstract 99
5.2 Introduction 100
5.3 Study Area and Observed Data 102
5.4 Models and Methods 104
5.4.1 Occoquan Watershed Model 104
5.4.2 Modeling Climate Change Impact 106
5.4.3 Emission Scenarios 106
5.4.4 GCMs 106
5.4.5 Statistical Downscaling 106
5.4.6 Modeling Land Use Changes Impact 108
5.4.7 Simulation Periods 109
5.4.8 Simulated Scenarios 109
5.5 Results and Discussion 110
5.5.1 Climate Change 110
5.5.2 Land Use Change 111
5.5.3 Impacts of Climate Change and Land Use Change on Occupation Reservoir Water Temperature 112
5.5.4 Dissolved Oxygen 113
5.5.5 Nutrients 114
5.6 Summary and Conclusions 115
5.7 Acknowledgment 116

5.8 References 116
Chapter 6 Summary, Conclusions, and Recommendations for Further Study .. 151
6.1 Summary 151
6.2 Conclusions 153
6.3 Recommended Future Research 156
6.4 References 157
Appendix 158
A.1 Model Implementation 158
A.2 Data Management Plan 158
A.2.1 Global Circulation Models Data 158
A.2.2 Land Use Data 159
A.2.3 Local Data and Data Infilling 160
A.2.4 An example of model selection procedure for infilling the historical precipitation data. A case study: Upper Broad Run subbasin 163
A.2.5 Data Management System 175
A.3 References 176

List of Tables

Table 2-1. Summary of Occoquan reservoir and Lake Manassas physical characteristics. 8
Table 2-2. Occoquan watershed monitoring stations. 9
Table 2-3. Occoquan reservoir monitoring stations. 10
Table 2-4. Projection scenarios and model factors used in this study. 12
Table 2-5. Climate variables used in this study. 12
Table 3-1. Baseline meteorological data for the study area from 1981 to 2000. 33
Table 3-2. GCMs used in this study. 34
Table 3-3. The time horizon for historical and GCM data. 35
Table 3-4. Hydrologic streamflow alteration indices. 36
Table 3-5. α values and % change in magnitude of difference between mean annual flows of the projected models and historical values. 37
Table 3-6. Water quantity characteristics for mid and late 21st century. 38
Table 4-1. Baseline meteorological data for the study area from 1981 to 2000. 68
Table 4-2. Performance criteria for calibration and validation of the Occoquan Model. 69
Table 4-3. GCM used in this study. 70
Table 4-4. Climate variables used in this study. 71
Table 4-5. Time horizons for observed and GCM data. 72
Table 4-6. Developed themes for assessing the impacts of climate change and land use change. 73
Table 4-7. Streamflow characteristics caused by climate change and land use change in mid and later 21st century. 74
Table 5-1. Baseline meteorological data for the study area from 1981 to 2000. 120
Table 5-2. Summary of Occoquan reservoir physical characteristics (Xu et al. 2007). 121
Table 5-3. Performance criteria for calibration and validation. 122
Table 5-4. Calibration performance criteria for calibration of the Occoquan reservoir. 123
Table 5-5. GCM used in this study. 124
Table 5-6. Climate variables used in this study. 125
Table 5-7. Time horizons for observed and GCM data. 126

Table 5-8. Developed themes for assessing the impacts of climate change and land use change. 127
Table 5-9. Projected monthly differences between surface and bottom (surface-bottom) layers for water temperature. 128
Table 5-10. Projected monthly differences between surface and bottom (surface-bottom) layers for DO concentrations. 129

List of Figures

Figure 2-1. Occoquan watershed within the Potomac River Watershed. 5
Figure 2-2. Occoquan watershed location and subbasins. 6
Figure 2-3. Occoquan reservoir and stream gages for two major drainage tributaries (Bull Run and Occoquan Creek) to the Occoquan reservoir..... 7
Figure 2-4. Schematic of Occoquan linked watershed-reservoir model. 11
Figure 3-1. Location of the Broad Run watershed within the Occoquan watershed with major streams and streamflow stations. 39
Figure 3-2. Monthly variation of projected surface air temperature for the mid 21st century..... 40
Figure 3-3. Monthly variation of projected surface air temperature for the late 21st century..... 41
Figure 3-4. Monthly variation of projected precipitation for the mid 21st century. 42
Figure 3-5. Monthly variation of projected precipitation for the late 21st century. 43
Figure 3-6. Increase in the median of annual surface air temperature against percent change in the median of annual precipitation for mid 21st century..... 44
Figure 3-7. Increase in the median of annual surface air temperature against percent change in the median of annual precipitation for late 21st century. 45
Figure 3-8. Interactions of model groups for four-way ANOVA design with consideration of four different impacting factors (i.e., a choice of emission scenario (two levels), a choice of GCM (four levels), a choice of downscaling method (two levels) and a choice of simulation period (two levels)). 46
Figure 4-1. Occoquan watershed with major streams and subbasins. 75
Figure 4-2. Designed study framework for quantifying streamflow alteration due to the climate change and land use change in the study area..... 76
Figure 4-3. Schematic of Occoquan linked watershed-reservoir model. 77
Figure 4-4. Overview of ICLUS modeling process (Bierwagen and Morefield 2014). ... 78
Figure 4-5. Future climate change (green) and land use change (orange) horizons for two future time periods (2046-2065 (F1) and 2081-2100 (F2)). 79

Figure 4-6. Monthly variations of projected Climate Change (CC) surface air temperatures for the mid 21st century (F1). The solid blue line represents the historical values and the light green shaded area envelopes the possible maximums and minimums of the projections while the dashed lines are depicting the medians of climate change projected surface air temperatures categorized based on A2 and B1 emission scenarios. 80
Figure 4-7. Monthly variations of projected Climate Change (CC) surface air temperatures for the late 21st century (F2). The solid blue line represents the historical values and the light green shaded area envelopes the possible maximums and minimums of the projections while the dashed lines are depicting the medians of climate change projected surface air temperatures categorized based on A2 and B1 emission scenarios. 81
Figure 4-8. Monthly variations of projected Climate Change (CC) precipitations for the mid 21st century (F1). The solid blue line represents the historical values and the light green shaded area envelopes the possible maximums and minimums of the projections while the dashed lines are depicting the medians of climate change projected precipitations categorized based on A2 and B1 emission scenarios. 82
Figure 4-9. Monthly variations of projected Climate Change (CC) precipitations for the late 21st century (F2). The solid blue line represents the historical values and the light green shaded area envelopes the possible maximums and minimums of the projections while the dashed lines are depicting the medians of climate change projected precipitations categorized based on A2 and B1 emission scenarios. 83
Figure 4-10. Estimate percent impervious surface areas for Occoquan watershed in the historical period. Further delineation (gray lines) was carried out based on 1) rainfall or important meteorological data; 2) soil type; 3) land use conditions; 4) reach characteristics; 5) any other important physical characteristic (infiltration, overland slope, etc.) (Xu et al. 2007). 84
Figure 4-11. Estimate percent impervious surface for Occoquan watershed for future projections in Bull Run and Occoquan Creek using A2 and B1 emission scenarios. 85

Figure 4-12. Estimate percent impervious surface areas in Occoquan watershed for middle of mid 21st period (2055) using A2 emission scenario. 86
Figure 4-13. Estimate percent impervious surface areas in Occoquan watershed for middle of later 21st period (2090) using A2 emission scenario. 87
Figure 4-14. Estimate percent impervious surface areas in Occoquan watershed for middle of mid 21st period (2055) using B1 emission scenario. 88
Figure 4-15. Estimate percent impervious surface areas in Occoquan watershed for middle of late 21st period (2090) using B1 emission scenario. 89
Figure 4-16. Median of monthly variations of flows using Climate Change (CC), Land Use Change (LUC) and combined (CC+LUC) effects for Bull Run in mid 21st century (2046-2065). The solid blue line represents the historical values and the light green shaded area envelopes the possible maximums and minimums of the projections while the dashed lines are depicting the medians of models grouped based on climate change and land use change projections and A2 and B1 emission scenarios. 90
Figure 4-17. Median of monthly variations of flows using Climate Change (CC), Land Use Change (LUC) and combined (CC+LUC) effects for Bull Run in late 21st century (2081-2100). The solid blue line represents the historical values and the light green shaded area envelopes the possible maximums and minimums of the projections while the dashed lines are depicting the medians of models grouped based on climate change and land use change projections and A2 and B1 emission scenarios. 91
Figure 4-18. Median of monthly variations of flows using Climate Change (CC), Land Use Change (LUC) and combined (CC+LUC) effects for Occoquan Creek in mid 21st century (2046-2065). The solid blue line represents the historical values and the light green shaded area envelopes the possible maximums and minimums of the projections while the dashed lines are depicting the medians of models grouped based on climate change and land use change projections and A2 and B1 emission scenarios. 92
Figure 4-19. Median of monthly variations of flows using Climate Change (CC), Land Use Change (LUC) and combined (CC+LUC) effects for Occoquan Creek in late

21st century (2081-2100). The solid blue line represents the historical values and the light green shaded area envelopes the possible maximums and minimums of the projections while the dashed lines are depicting the medians of models grouped based on climate change and land use change projections and A2 and B1 emission scenarios. 93
Figure 4-20. Median of monthly variations of flows for Bull Run and Occoquan Creek grouped based on Climate Change (CC), Land Use Change (LUC) and combined effects (CC+LUC) and A2 and B1 emission scenarios in mid and late 21st century (2046-2065 (F1) and 2081-2100 (F2)). 94
Figure 4-21. Flow duration curves for Bull Run using Climate Change (CC), Land Use Change (LUC) and combined (CC+LUC) effects in mid 21st century (2046-2065). The solid blue line represents the historical values and the light green shaded area envelopes the possible maximums and minimums of the projections while the dashed lines are depicting the medians of models grouped based on climate change and land use change projections and A2 and B1 emission scenarios. 95
Figure 4-22. Flow duration curves for Bull Run using Climate Change (CC), Land Use Change (LUC) and combined (CC+LUC) effects in mid late century (2081-2100). The solid blue line represents the historical values and the light green shaded area envelopes the possible maximums and minimums of the projections while the dashed lines are depicting the medians of models grouped based on climate change and land use change projections and A2 and B1 emission scenarios. 96
Figure 4-23. Flow duration curves for Occoquan Creek using Climate Change (CC), Land Use Change (LUC) and combined (CC+LUC) effects in mid 21st century (2046-2065). The solid blue line represents the historical values and the light green shaded area envelopes the possible maximums and minimums of the projections while the dashed lines are depicting the medians of models grouped based on climate change and land use change projections and A2 and B1 emission scenarios. 97
Figure 4-24. Flow duration curves for Occoquan Creek using Climate Change (CC), Land Use Change (LUC) and combined (CC+LUC) effects in late 21st century (2081-

2100). The solid blue line represents the historical values and the light green shaded area envelopes the possible maximums and minimums of the projections while the dashed lines are depicting the medians of models grouped based on climate change and land use change projections and A2 and B1 emission scenarios. 98
Figure 5-1. Occoquan reservoir within the Occoquan watershed with major streams and subbasins. 130
Figure 5-2. Designed study framework for quantifying water quality alteration due to the climate change and land use change in the study area. 131
Figure 5-3. Schematic of Occoquan linked watershed-reservoir model. 132
Figure 5-4. Occoquan reservoir segmentations and monitoring station locations. 133
Figure 5-5. Overview of ICLUS modeling process (Bierwagen and Morefield 2014). 134
Figure 5-6. Future climate change (green) and land use change (orange) horizons for two future time periods (2046-2065 (F1) and 2081-2100 (F2)). 135
Figure 5-7. Monthly variations of projected Climate Change (CC) surface air temperatures for the mid 21st century (F1). The solid blue line represents the historical values and the light green shaded area envelopes the possible maximums and minimums of the projections while the dashed lines are depicting the medians of climate change projected surface air temperatures categorized based on A2 and B1 emission scenarios. 136
Figure 5-8. Monthly variations of projected Climate Change (CC) surface air temperatures for the late 21st century (F2). The solid blue line represents the historical values and the light green shaded area envelopes the possible maximums and minimums of the projections while the dashed lines are depicting the medians of climate change projected surface air temperatures categorized based on A2 and B1 emission scenarios. 137
Figure 5-9. Monthly variations of projected Climate Change (CC) precipitations for the mid 21st century (F1). The solid blue line represents the historical values and the light green shaded area envelopes the possible maximums and minimums of the projections while the dashed lines are depicting the medians of climate change projected precipitations categorized based on A2 and B1 emission scenarios. 138

Figure 5-10. Monthly variations of projected Climate Change (CC) precipitations for the late 21st century (F2). The blue solid line represents the historical values and the light green shaded area envelopes the possible maximums and minimums of the projections while the dashed lines are depicting the medians of climate change projected precipitations categorized based on A2 and B1 emission scenarios… 139
Figure 5-11. Estimate percent impervious surface areas for Occoquan watershed in the historical period. Further delineation (gray lines) was carried out based on 1) rainfall or important meteorological data; 2) soil type; 3) land use conditions; 4) reach characteristics; 5) any other important physical characteristic (infiltration, overland slope, etc.) (Xu et al. 2007)..... 140
Figure 5-12. Estimate percent impervious surface for Occoquan watershed for future projections in Bull Run and Occoquan Creek using A2 and B1 emission scenarios..... 141
Figure 5-13. Estimate percent impervious surface areas in Occoquan watershed for middle of mid 21st period (2055) using A2 emission scenario. 142
Figure 5-14. Estimate percent impervious surface areas in Occoquan watershed for middle of later 21st period (2090) using A2 emission scenario. 143
Figure 5-15. Estimate percent impervious surface areas in Occoquan watershed for middle of mid 21st period (2055) using B1 emission scenario. 144
Figure 5-16. Estimate percent impervious surface areas in Occoquan watershed for middle of late 21st period (2090) using B1 emission scenario..... 145
Figure 5-17. Projected monthly variations of surface and bottom water temperatures for the Occoquan reservoir at RE02 using Climate Change (CC), Land Use Change (LUC) and combined (CC+LUC) effects in mid and late 21st century (F1 and F2). The solid blue line represents the historical values and the light green shaded area envelopes the possible maximums and minimums of the projections while the dashed lines are depicting the medians of models grouped based on climate change and land use change projections and A2 and B1 emission scenarios..... 146
Figure 5-18. Projected monthly variations of surface and bottom dissolved oxygen concentration levels for the Occoquan reservoir at RE02 using Climate Change (CC), Land Use Change (LUC) and combined (CC+LUC) effects in mid and late

21st century (F1 and F2). The solid blue line represents the historical values and the light green shaded area envelopes the possible maximums and minimums of the projections while the dashed lines are depicting the medians of models grouped based on climate change and land use change projections and A2 and B1 emission scenarios. 147
Figure 5-19. Projected monthly variations of surface and bottom ammonia concentration levels for the Occoquan reservoir at RE02 using Climate Change (CC), Land Use Change (LUC) and combined (CC+LUC) effects in mid and late 21st century (F1 and F2). The solid blue line represents the historical values and the light green shaded area envelopes the possible maximums and minimums of the projections while the dashed lines are depicting the medians of models grouped based on climate change and land use change projections and A2 and B1 emission scenarios..... 148
Figure 5-20. Projected monthly variations of surface and bottom nitrate-nitrite nitrogen concentration levels for the Occoquan reservoir at RE02 using Climate Change (CC), Land Use Change (LUC) and combined (CC+LUC) effects in mid and late 21st century (F1 and F2). The solid blue line represents the historical values and the light green shaded area envelopes the possible maximums and minimums of the projections while the dashed lines are depicting the medians of models grouped based on climate change and land use change projections and A2 and B1 emission scenarios. 149
Figure 5-21. Projected monthly variations of surface and bottom orthophosphate phosphorus concentration levels for the Occoquan reservoir at RE02 using Climate Change (CC), Land Use Change (LUC) and combined (CC+LUC) effects in mid and late 21st century (F1 and F2). The solid blue line represents the historical values and the light green shaded area envelopes the possible maximums and minimums of the projections while the dashed lines are depicting the medians of models grouped based on climate change and land use change projections and A2 and B1 emission scenarios..... 150

Abbreviations and Acronyms

°C	degree Celsius
%	percent
γ	parameter learning rate
μ	mean
σ	standard deviation
ac	acre
AEA	alternate electron acceptor
AHS	adaptive harmony search
at	surface air temperature
BMP	best management practice
bw	bandwidth
cm	centimeter
CSTR	continuously-stirred tank reactor
CV	coefficient of variation
d	day
DO	dissolved oxygen
EH	redox potential
ft	foot
gal	gallon
GCM	global circulation model
Gg	gigagram
GHS	global-best harmony search
GHz	gigahertz
GOF	goodness-of-fit
ha	hectare
HMCR	harmony memory considering rate
HMS	harmony memory size
HS	harmony search
HSPF	Hydrologic Simulation Program – Fortran
hr	hour
kg	kilogram
km	kilometer
L	liter
lb	pound
m	meter
Max	Maximum
MCL	maximum contaminant level
mg	milligram
mi	mile
Min	Minimum
N	nitrogen
NSE	Nash-Sutcliffe Efficiency
Obs	observed data
OP	orthophosphate

ORP	oxidation-reduction potential
OWML	Occoquan Watershed Monitoring Laboratory
OWMP	Occoquan Watershed Monitoring Program
Ox-N	oxidized nitrogen
P	phosphorus
p	probability
PAR	pitch adjusting rate
PBIAS	percent bias
pr, prec	precipitation
prec	precipitation
RAM	random access memory
redox	oxidation-reduction
RMSE	root mean square error
RSR	RMSE–observed standard deviation ratio
SAHS	self-adaptive harmony search
SD	standard deviation
Sim	simulated data
SOD	sediment oxygen demand
TKN	total Kjeldhal nitrogen
TN	total nitrogen
UOSA	Upper Occoquan Service Authority
VSWCB	Virginia State Water Control Board
W2	CE-QUAL-W2
WQO	water quality objective
WRF	water reclamation facility
yr	year

Chapter 1 Research Objectives

1.1 Introduction

This document presents an integrated water quantity and quality modeling research to assess the impacts of climate change and land use change on the Occoquan watershed in northern Virginia, USA. To simulate the hydrology and water quality, the Occoquan Model, a complexly-linked network of seven watershed models and two reservoir models was used.

Hydrological simulations were performed using Hydrological Simulation Program - FORTRAN (HSPF) and the reservoir models were developed and executed using the water quality modeling software CE-QUAL-W2 (W2). The following sections of this chapter provide the motivations for and summaries of the research presented in the subsequent chapters of this document.

1.2 Study Motivations

1.2.1 Climate Change

Among various driving forces affecting a watershed, climate change considered as one of the primary components that can have long term impact on the hydrology of a watershed. The possible alterations can effect various hydrological processes such as precipitations, snow and land ice, evapotranspiration, soil moisture, and runoff and river discharge (Bates 2009).

Climate change is linked to human-induced activities and associated with alterations in the gaseous composition of the atmosphere, specifically increased levels of the Carbon Dioxide (CO_2) concentrations in the atmosphere (Doorghen-Gorden et al. 2018). The impact of climate change is projected to continue and may even accelerate in the future while these projections can be different between climatic regions (Chithra et al. 2018).

The Occoquan reservoir, in the study area, is one of the major resources of drinking water in northern Virginia. Climate change can lead to uncertainties in the future water supply in the study area. As a response to these risks, creative strategies and integrated solutions should be developed. This study can provide a better understanding of the effects of future climate change on the water quantity and quality in the study area, equipping decision-makers with information that can be used to address the potential impact of climate change leading to climate resiliency in the Occoquan watershed.

1.2.2 Land Use Change

In the past, unmanaged environmental resource utilization, in particular, water demand from demographic growth and urbanization has resulted in a series of environmental crises (Corson 1990). The study area has experienced rapid population growth and increases in potable water demand during the last few decades. Urbanization is an ongoing theme in the study area that can greatly influence a watershed's response to precipitation (Leopold 1968). These increases in population and urbanization are projected to continue and were simulated using two Special Report on Emissions Scenarios (SRES) storylines for two future time periods (2046-2065 and 2081-2100).

The findings of can shed light on the necessity to evaluate the state of watersheds for future planning and development with a close consideration of the impact of land use change and urbanization.

1.3 Study Objectives

The primary objective of this study is to develop a framework to quantify the impacts of climate change and land use change on water quantity and quality in the Occoquan watershed and explore the uncertainties in the simulated model results.

1.3.1 Climate Change and Projections Variability

In the first part of this research, the individual effect of climate change has been investigated and projection variabilities have been explored. Two emission scenarios from the fourth assessment report of the Intergovernmental Panel on Climate Change (IPCC), along with four General Circulation Models (GCMs) using two statistical downscaling methods, were applied to drive the HSPF models in two future time periods (2046-2065 and 2081-2100). Incorporation of these factors yielded 32 runoff simulation models which were compared with historical streamflow data from the late 20th century. Changes in streamflow were compared using median flows, low flows, and high flows. In addition, statistical tests were conducted to identify the main factors that affected variations in future climate projections.

The objectives of this study were to (a) simulate future streamflow conditions in the study area for the mid and late 21st century, (b) analyze climate change impact on the watershed

quantifying flow regime alterations, and (c) explore the primary sources of uncertainty that arise from differing emission scenarios, GCMs, downscaling methods, and projection periods.

1.3.2 Impacts of Climate Change and Land Use Change on Water Quantity

In the second study described in this document, the individual and combined impacts of climate change and land use change on water quantity in the Occoquan watershed were studied. The combination of these two driving forces have created four themes, and an integrated complexly-linked watershed-reservoir model was used to run the simulations. Ensembles of climate change projections were created using two emission scenarios, four GCMs, and two downscaling methods for two future time periods (2046-2065 and 2081-2100). Increases in population and urbanization are simulated using two SRES storylines for the two future time periods (2046-2065 and 2081-2100). The alteration in streamflow responses to the climate change and land use change were evaluated at two streamflow gages draining to the Occoquan reservoir.

The objective of this research effort was to address the following question: a) How will the streamflow characteristics change if the climate change and land use change are imposed separately or jointly? b) Which of the driving forces has a stronger effect? c) Do these driving forces exacerbate or offset their individual effects on the streamflow characteristics?

1.3.3 Impacts of Climate Change and Land Use Change on Water Quality

The third research study focused on water quality alterations in the Occoquan reservoir caused by climate change and land use change. For this purpose, combinations of climate change and land use change scenarios using the four themes describes earlier in the section 1.3.2 yielded to 68 scenarios that compared with historical values of the late 20th century.

This study aimed to address the following questions: a) How will the water quality characteristics change if climate change and land use change are imposed separately or jointly? b) Which of these driving forces has a stronger effect? c) Do these driving forces exacerbate or offset their individual effects on the water quality characteristics?

1.4 Document Organization

The remainder of this document is organized as follows:

Chapter 2 presents background information regarding the Occoquan watershed and reservoir, Occoquan policy and Occoquan Model.

Chapter 3 is a research paper on the hydrological impact of climate change in the study area and special focus on the possible sources of uncertainties in the projections. This research paper has been submitted to the ASCE Journal of Hydrologic Engineering.

Chapter 4 is a research paper regarding the incorporation of both climate change and land use change scenarios to assess the individual and combined impacts of these driving forces on water quantity.

Similarly, **Chapter 5** contains a research paper exploring the individual and combined impacts of climate change and land use change on water quality in the Occoquan reservoir.

Chapter 6 contains a summary of the research efforts detailed in this document, an outline of the research's key findings, as well as recommendations for further study.

1.5 References

Bates, B. (2009). *Climate Change and Water: IPCC technical paper VI*, World Health Organization.

Chithra, N., Thampi, S. G., Shahul, D., Muralidhar, S., Unnikrishnan, U., and Rajendran, K. A. (2018). "Change Point Analysis of Air Temperature in India." *Climate Change Impacts*, Springer, 147-155.

Corson, W. H. (1990). *The Global Ecology Handbook: What You Can Do about the Environmental Crisis*, ERIC.

Doorghen-Gorden, J., Nowbuth, M. D., and Proag, V. (2018). "Assessing the Implementation of Eco-Driving in Mauritius—A Climate Change Mitigation Measure." *The Nexus: Energy, Environment and Climate Change*, Springer, 367-381.

Leopold, L. B. (1968). "Hydrology for urban land planning: A guidebook on the hydrologic effects of urban land use."

Chapter 2 Occoquan Watershed and Occoquan Reservoir Background Information: Site Characteristics and Current Conditions

2.1 Study Area

The Occoquan watershed with approximate area of 1500 km^2 is located in the Mid-Atlantic region of the United States, approximately 40 km to the southwest of Washington, D.C., with coordinates between [38.50 - 38.95] N, [77.25 - 77.85] W. The watershed is part of the Chesapeake Bay Watershed encompasses portions of four northern Virginia counties (Fairfax, Fauquier, Loudoun, and Prince William), and contains two independent cities (Manassas and Manassas Park) (Figure 2-1).

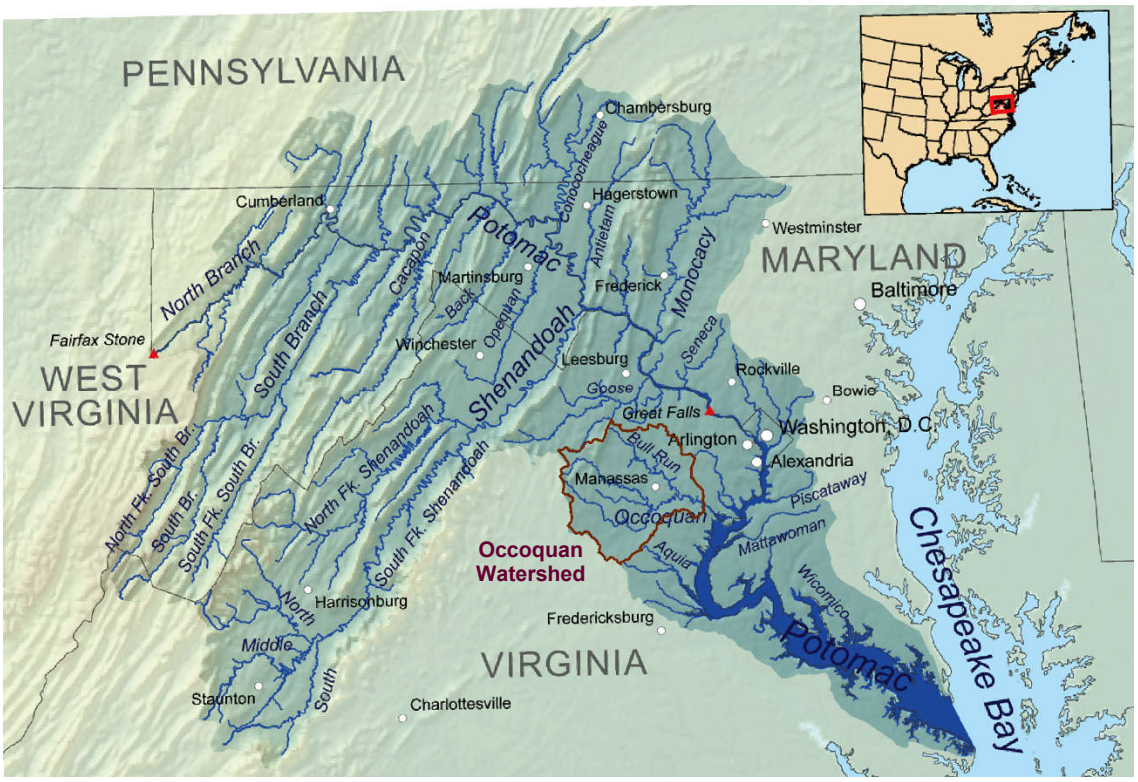

Figure 2-1. Occoquan watershed within the Potomac River Watershed.

The Occoquan watershed has four distinct seasons (refers to the temperature and precipitation differences on a seasonal and annual basis) and is classified in Cfa (humid subtropical climate) zone in Köppen climate classification.

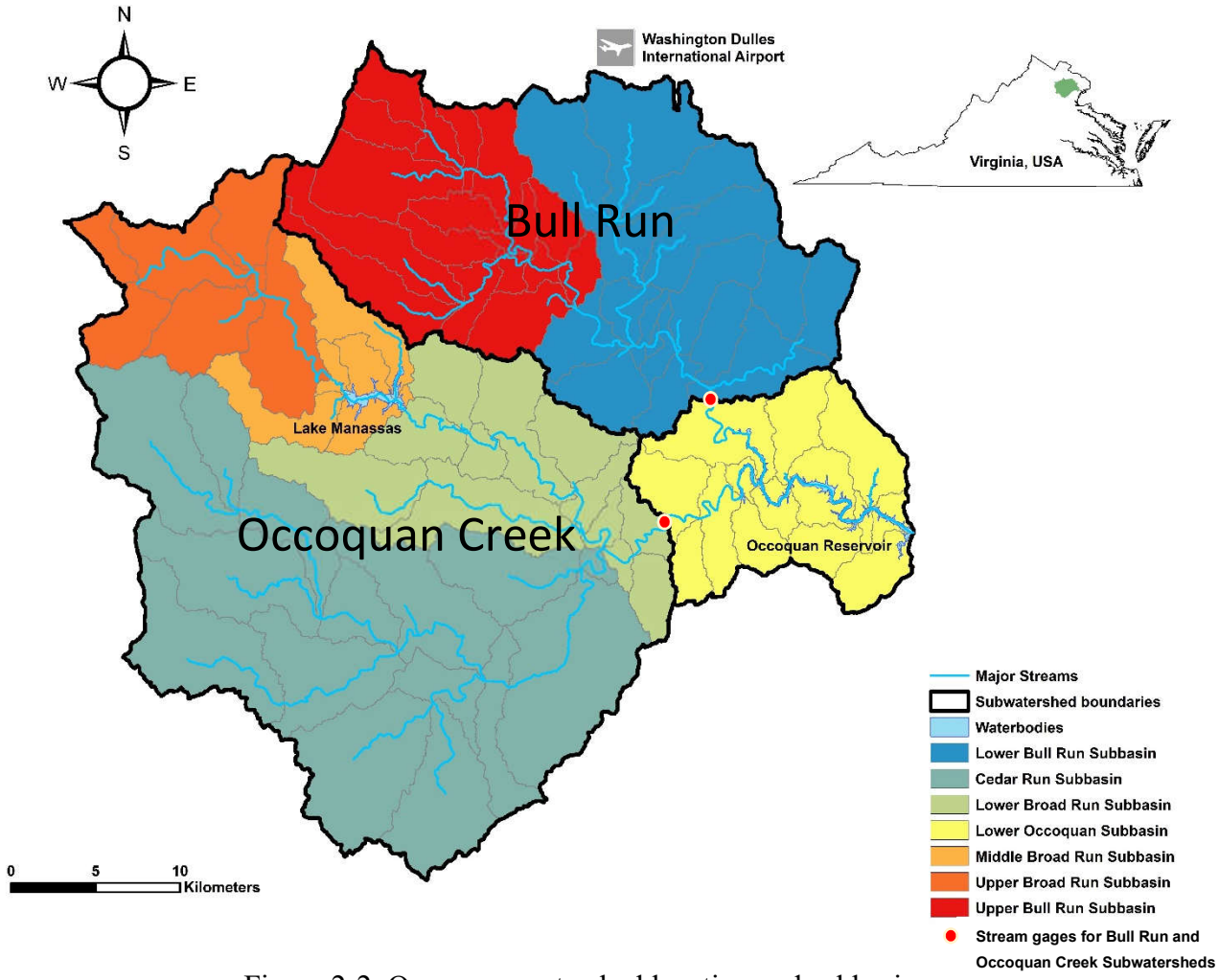

Figure 2-2. Occoquan watershed location and subbasins.

The Occoquan watershed drains to the Occoquan reservoir (Figure 2-2). The major drainage tributaries to the Occoquan reservoir can be divided into two primary sub watersheds, namely Bull Run and Occoquan Creek. Bull Run is in the northern part of the watershed, constitutes of Upper Bull Run and Lower Bull Run subbasins with an aggregate drainage area of 471 km^2.

The confluence of Broad Run and Cedar Run form Occoquan Creek. Broad Run, itself, constitutes of Upper Broad Run, Middle Broad Run and Lower Broad Run subbasins. Upper Broad Run and Middle Broad Run drain to Lake Manassas. Lake Manassas is a primary drinking water source for the City of Manassas, City of Manassas Park, and the surrounding areas (Liu 2011). Occoquan Creek flows directly into the headwaters of the Occoquan reservoir with an of 888 km^2.

The Occoquan reservoir is one of the source primary sources of drinking water for near two million residents in northern Virginia. The reservoir is constructed impoundment with a relatively long and narrow shape. The volume and area of full pool of the Occoquan reservoir are 3.1×10^7 m³ (8.3 billion gal) and 620 ha (1,500 ac), respectively. The average reservoir depth is about 5.1 m with a maximum depth of 19 m at the Occoquan dam. The mean hydraulic residence time is less than 20 days. Table 2-1 summarizes the physical characteristics of the Occoquan reservoir and Lake Manassas (Xu et al. 2007).

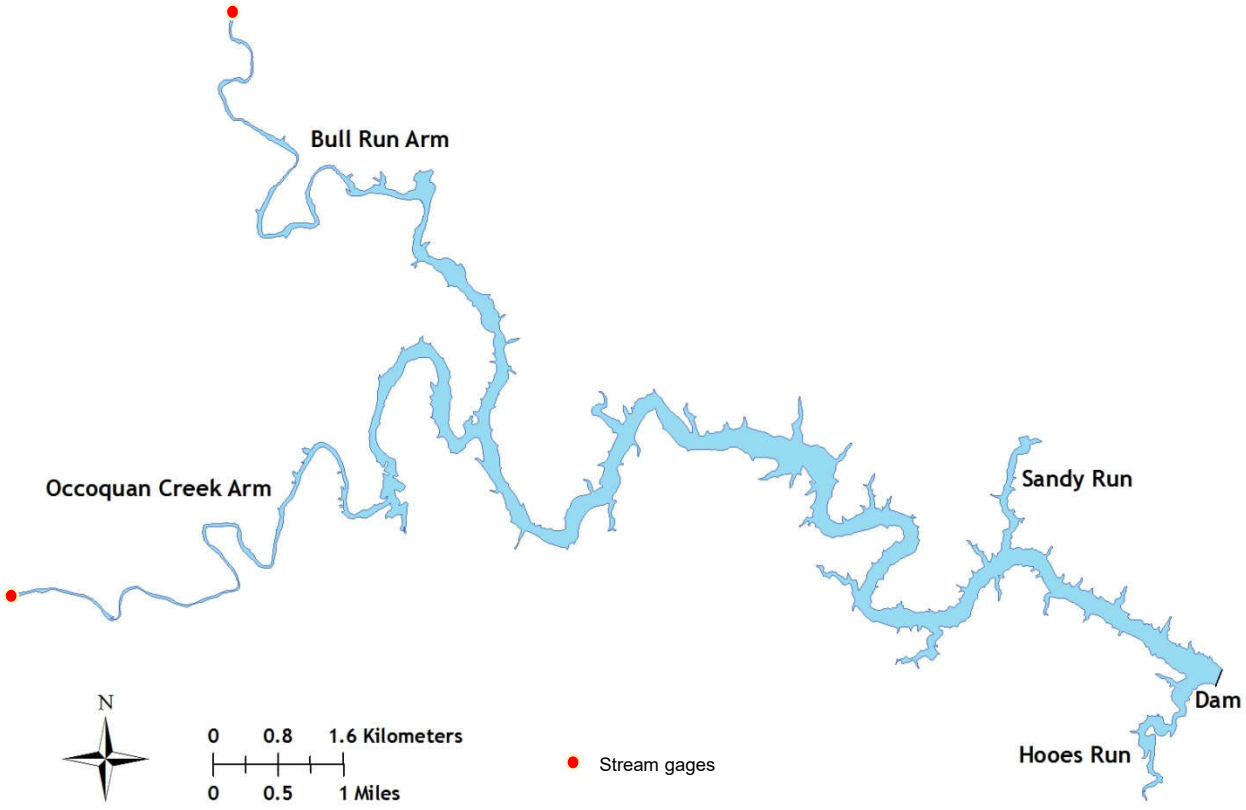

Figure 2-3. Occoquan reservoir and stream gages for two major drainage tributaries (Bull Run and Occoquan Creek) to the Occoquan reservoir.

Table 2-1. Summary of Occoquan reservoir and Lake Manassas physical characteristics.

Physical characteristics	Occoquan reservoir	Lake Manassas
Watershed drainage area (km^2)	1480	189
Volume (m^3)	31.4×10^6	15.4×10^6
Surface Area (ha)	616	282
Length (m)	2.25×10^4	5.97×10^3
Mean Depth (m)	5.1	5.5
Maximum Depth (m)	19	15
Mean Width (m)	150	353
Maximum Width (m)	275	724
Safe Yield (m^3/day)	2.5×10^5	6.4×10^4
Average Inflow (m^3/day)	1.6×10^6	1.3×10^5
Dam Crest Height above Mean Sea Level (m)	37.2	86.7
Hydraulic Residence Time (day)	19.6	118.5

After rapid population growth and land use change within the watershed in the 1960s, water quality degraded dramatically in the Occoquan reservoir and led to a highly eutrophic environment and several algal blooms. At the time, eleven small publicly owned municipal wastewater treatment plants (also referred to as Publicly Owned Treatment Works - POTW) were discharging their treated water into the watershed. The Virginia State Water Control Board (VSWCB) commissioned a study by Metcalf & Eddy Inc., where in these eleven POTWs were identified as the primary cause of the eutrophication. As a response, in 1972, the VSWCB adopted a policy known as the "Occoquan Policy" to manage the wastewater treatment facilities and water quality standards within the Occoquan watershed ("A Policy for Waste Treatment and Water Quality Management in the Occoquan Watershed" (VSWCB, 1971))(Den Bos and Cara 2003).

The policy mandated the replacement of the poor-performing POTWs with state of the art (at the time) wastewater treatment utility known as the Upper Occoquan Service Authority (UOSA), which began its operation in 1978. The UOSA an advanced water reclamation facility (WRF) discharges treated waste loads into Bull Run, upstream of the reservoir. The Fairfax County Water Authority (Fairfax Water) withdraws water at the Occoquan dam as a drinking water supply, resulting in as indirect potable water reuse of reclaimed wastewater. The Occoquan Policy also called for the creation of an independent entity to monitor and screen the Occoquan reservoir's water quality and evaluate the basin's water quality management strategies. As a

result, the Occoquan Watershed Monitoring Laboratory (OWML) was established by Virginia Tech's Department of Civil and Environmental Engineering and began its operations in 1972.

Throughout years, OWML has developed an extensive database using hydrologic and water quality data acquisition and analysis system to monitor the water quantity and quality of the Occoquan watershed. In the recent years, with the human induced climate change and land use change, new questions have arisen that these driving forces may have far reaching consequences for society, economy, and freshwater ecosystem in the area. Therefore, given the history of the Occoquan watershed and using the reclaimed water to supplement potable water supply, there was a need to study the impacts of climate change and land use change on catchment scale water resources. Accordingly, decision making bodies, including governments, will be able to incorporate climate change and land use change related risks into their decision making.

2.2 Sampling Stations

OWML operates a system of automated stream and rainfall stations that provide spatial coverage of Occoquan watershed along with the Occoquan reservoir. Data recorded over time by monitoring stations shown in Table 2-2 and Table 2-3 were used to build and calibrate the Occoquan Model.

Table 2-2. Occoquan watershed monitoring stations.

Station	STORET NO.	Distance Above Dam		Drainage Area		Date Active
		km	mi	km^2	mi^2	
Occoquan Reservoir Outlet	ST01	0	0	1484	573	01/01/1982
Occoquan River near Manassas	ST10	25.8	16	888	343	NA
Cedar Run near Aden	ST25	46.1	28.8	401	155	10/01/1972
Broad Run near Bristow	ST30	46.6	29.1	232.1	89.6	10/01/1974
Bull Run at 28 near Yorkshire	ST45	29.9	18.6	385.9	149	11/16/1984
Cub Run near Bull Run	ST50	34.9	21.8	129.2	49.9	10/01/1972
Bull Run near Catharpin	ST60	49.9	31.2	66.8	25.8	05/01/1969
Broad Run near Buckland	ST70	59.7	37.3	130.8	50.5	10/01/1950

An additional dataset was used in this study from other meteorological stations in the vicinity of the watershed area. The three long-established meteorological stations in this region are Washington Dulles International Airport, Reagan National Airport, and the Plains. Altogether these observed historical data were used in developing climate change and land use change models.

Table 2-3. Occoquan reservoir monitoring stations.

Station	STORET No.	Distance Above Occoquan Dam	
		km	mi
Occoquan Reservoir at Occoquan Dam	RE01	0	0
Occoquan Reservoir at 2nd power line	RE02	0.5	0.3
Occoquan Reservoir below Sandy Run	RE05	2.9	1.8
Occoquan Reservoir at Jacob's Rock	RE10	6.4	4.0
Occoquan Reservoir at Ryan's Dam	RE15	9.8	6.1
Occoquan Reservoir below confluence	RE20	12.6	7.9
Occoquan Creek above con. Bull Run	RE25	15.8	9.9
Occoquan Reservoir (Bull Run)	RE30	16.8	10.5
Occoquan Creek at Ravenwood Bridge	RE35	18.0	11.2

2.3 Occoquan Model

A set of a set of complexly linked computer models, also collectively known as the Occoquan Model were created and maintained by OWML (Xu 2005; Xu et al. 2007). The Occoquan Model consists of seven watershed models, corresponding to Occoquan watershed subbasins, and two reservoir models. One of the reservoir models represents Occoquan reservoir hydrodynamics and water quality, while the other model simulates the Lake Manassas. Figure 2-4 depicts the schematic representation of the Occoquan Model.

The simulation of subbasin models was performed using the Hydrologic Simulation Program – Fortran (HSPF) (Bicknell et al. 2001). HSPF is jointly supported by the United States Environmental Protection Agency and the U.S. Geological Survey. HSPF is a comprehensive process-based watershed model that has the ability to integrate watershed hydrology and water quality simulations. The extended period structure of HSPF allows users to simulate pervious and impervious land surfaces as well as in-stream hydraulic and sediment-chemical interactions (US-EPA 2015). HSPF has been widely used as an analytical tool for planning, designing, and operating water resources systems throughout North America and numerous countries around the globe with different climatic regimes (US-EPA 2015).

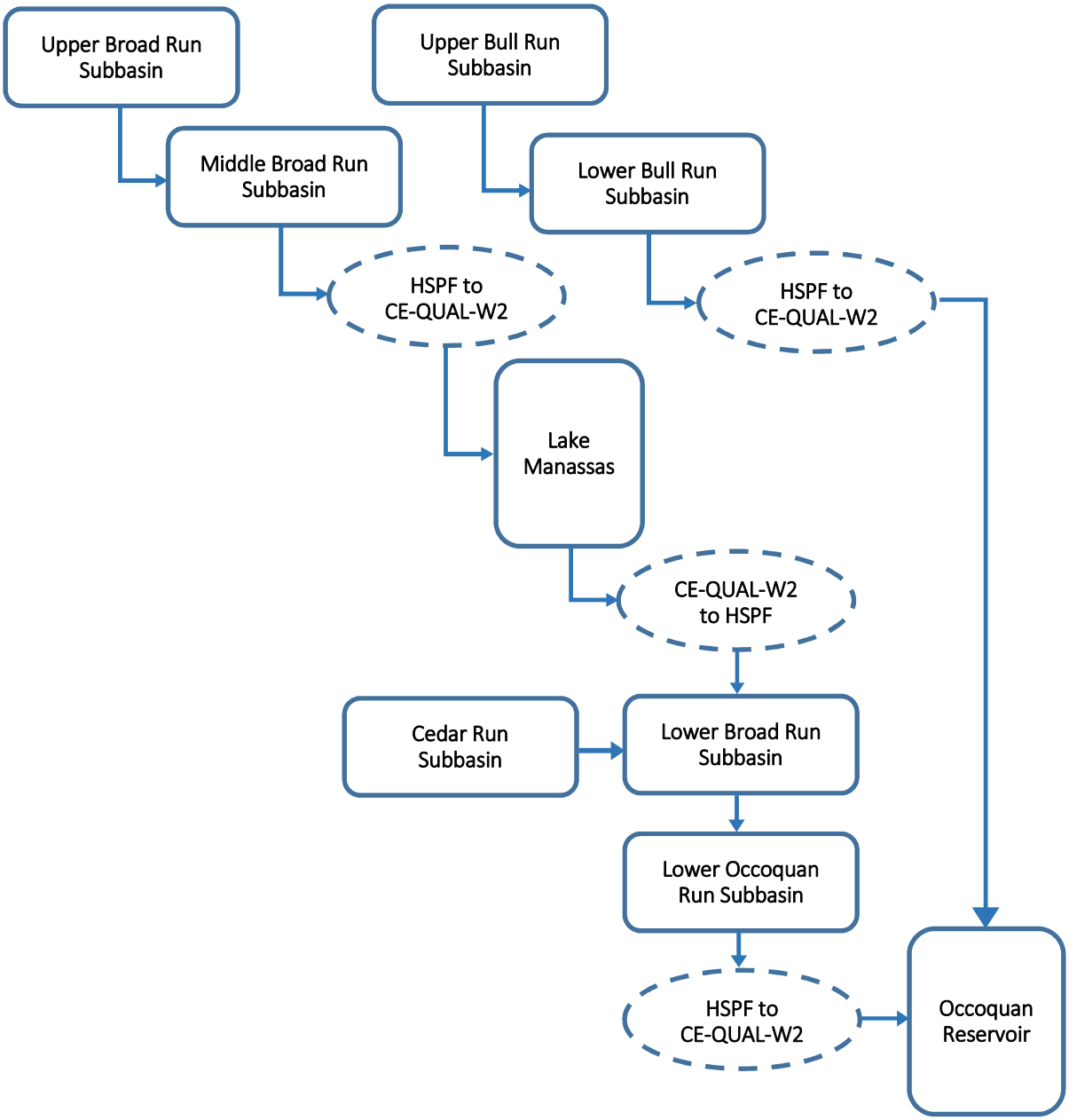

Figure 2-4. Schematic of Occoquan linked watershed-reservoir model.

Watershed models' outputs serve as upstream boundary conditions for the Occoquan reservoir and Lake Manassas models which are simulated using CE-QUAL-W2. CE-QUAL-W2 is a two dimensional hydrodynamic and water quality model that can provide a detailed description of hydrodynamics and water quality processes in receiving waterbodies, such as rivers, lakes, reservoirs, and estuaries (Cole and Wells 2006). In CE-QUAL-W2, waterbodies are defined by a series of laterally averaged, 2-dimensional systems (Xu et al. 2007). CE-QUAL-W2 has been

applied extensively to simulate waterbodies worldwide, and the example applications can be found in Cole and Wells (2006).

Finally, the scope of this study was to examine the impact of climate change and land use change (non-point impact) on the Occoquan watershed and possible impact of UOSA facility (point impact) was not considered in this modeling effort. As such, the inflows and nutrient concentration levels were set as the historical values.

2.4 Projection Model Factors and Variables

As will be explained in more details in the following chapters, for analyzing the impact of climate change and land use change, 68 model projections were compared to the historical values in the Occoquan watershed (total of 69 models). Development of these model projections carried out by combination of different climate and land use factors that included two emission scenarios, two downscaling methods, four GCMs, and two downscaling methods for two future time periods (2046-2065 and 2081-2100) as shown in Table 2-4.

Table 2-4. Projection scenarios and model factors used in this study.

Scenario	Factors	Possible Choices		Number of Choices
Climate	Emission Scenarios	A2	B1	2
	GCM Models	CSIRO MK3	GFDL CM2.0	4
		MPIM:ECHAM5	MRI-CGCM2.3.2	
	Downscaling Method	Delta Change (DC)	Quantile Mapping (QM)	2
	Future Time Periods	2046-2065 (F1)	2081-2100 (F2)	2
Land Use	Emission Scenarios	A2	B1	2
	Future Time Periods	2046-2065 (F1)	2081-2100 (F2)	2

The climate variables that are used in this study are shown in Table 2-5.

Table 2-5. Climate variables used in this study.

Predictor Variables	Precipitation
	Surface Air Temperature
	Maximum Surface Air Temperature
	Minimum Surface Air Temperature
	Wind

2.5 References

Bicknell, B. R., Imhoff, J. C., Kittle Jr, J. L., Jobes, T. H., Donigian Jr, A. S., and Johanson, R. (2001). "Hydrological simulation program-Fortran: HSPF version 12 user's manual." *AQUA TERRA Consultants, Mountain View, California*.

Cole, T. M., and Wells, S. A. (2006). "CE-QUAL-W2: A two-dimensional, laterally averaged, hydrodynamic and water quality model, version 3.5."

Den Bos, V., and Cara, A. (2003). "A water quality assessment of the Occoquan Reservoir and its tributary watershed: 1973-2002." Virginia Tech.

Liu, Y. (2011). "Effective Modeling of Nutrient Losses and Nutrient Management Practices in an Agricultural and Urbanizing Watershed." Virginia Tech.

US-EPA (2015). "BASINS 4.1 (Better Assessment Science Integrating point & Non-point Sources) Modeling Framework." <https://www.epa.gov/ceam/better-assessment-science-integrating-point-and-non-point-sources-basins>. (23/09/2018).

Xu, Z. (2005). "A complex, linked watershed-reservoir hydrology and water quality model application for the Occoquan watershed, Virginia." Virginia Tech.

Xu, Z., Godrej, A. N., and Grizzard, T. J. (2007). "The hydrological calibration and validation of a complexly-linked watershed–reservoir model for the Occoquan watershed, Virginia." *Journal of Hydrology*, 345(3-4), 167-183.

Chapter 3 Quantifying the Hydrological Impact of Climate Change on a Watershed in Northern Virginia

Ayden A. Baran[1]; Glenn E. Moglen[2]; Adil N. Godrej[3]
Occoquan Watershed Monitoring Laboratory, 9408 Prince William Street, Manassas, VA 20110, U.S.A.

[1] Ph.D. Candidate, Occoquan Watershed Monitoring Laboratory, Virginia Tech, Manassas, VA, USA, (corresponding author). Email: abaran@vt.edu,

[2] Supervisory Research Hydrologist, USDA-ARS Hydrology and Remote Sensing Laboratory, Beltsville, MD, USA,

[3] Research Associate Professor, Occoquan Watershed Monitoring Laboratory, Virginia Tech, Manassas, VA, USA.

Submitted to the ASCE Journal of Hydrologic Engineering

3.1 Abstract

Forecasted changes to climate were used to model variations in the streamflow characteristics of a northern Virginia catchment. We applied two emission scenarios from the fourth assessment report of the Intergovernmental Panel on Climate Change (IPCC) along with four General Circulation Models (GCMs) by using two statistical downscaling methods to drive the Hydrological Simulation Program—Fortran (HSPF) in two future time periods (2046-2065 and 2081-2100). Incorporation of these factors yielded 32 runoff simulation models which were compared with historical streamflow data from the late 20th century. Changes in streamflow were compared using median flows, low flows, and high flows. Results showed a general increase in median flows in both the mid and late 21st century. Low flows were projected to decrease whereas high flows were projected to increase, creating a larger range between low flows and high flows. In addition, we conducted statistical tests to identify the main factors that affected variations in future climate projections. The choice of the downscaling method emerged as the main source of uncertainty.

Results support the importance of comprehensive climatic change research and the need to develop an ensemble of projections for regional water resources climate change impact studies. These findings can benefit future water supply reliability and mitigation strategies in the study area considering this catchment's essential role as a water supplier in northern Virginia.

Keywords: Climate change; hydrological impact; scenario development; water supply; water resources management

3.2 Introduction

The effects of anthropogenic climate change on the water cycle has been a focus of many studies in recent years (Haddeland et al. 2014; Ichoku and Adegoke 2016; Stocker and Raible 2005). Commonly, recorded time series of observed data and historical events are used to analyze, design, plan, and manage water resource systems for future events. Many of these procedures assume a stationary state for observed data that carry over to future estimates. These assumptions thus do not reflect possible additional needs caused by future climate change and may not be suitable for future plans and designs (Moglen and Rios Vidal 2014). General Circulation Models (GCMs) are often implemented to predict the effects of climate change. GCMs are mathematical representations of climatic variables that incorporate carbon dioxide as one of the major anthropogenic contributors to the greenhouse effect. GCMs use internally coherent physical and, in some cases, chemical characteristics of climate to simulate and quantify the climatic responses to future human-induced activities (Bernstein et al. 2008).

Climate change impact assessments often require a higher resolution than otherwise provided by GCMs. Different downscaling methods have been developed to translate temporal and spatial climate information from coarse resolution GCM outputs to local and regional scales. Regionalization of the GCMs or downscaling methods can be categorized as either statistical or dynamical procedures (Bernstein et al. 2008). Statistical downscaling methods are based on the premise that the regional climate is conditioned by, first, the large-scale climatic state and, second, the local physiographic features (Wilby et al. 2004). In this context, quantitative relationships can be established between the large-scale climate variables (predictors) and regional variables (predictands) (Abatzoglou and Brown 2012). Primary types of statistical downscaling methods include (1) weather classification schemes, (2) transfer functions, and (3) weather generators. In contrast, dynamical downscaling methods are based on Regional Climate Models (RCMs) nested within the domain of the GCMs, resulting in higher resolution than the original GCM output. The quality of RCMs is not only dependent upon initial conditions (e.g., soil moisture, soil temperature) but is also dictated by the validity of boundary conditions defined in the GCMs (Wilby et al. 2004).

Xu et al. (2005) arrayed a general scheme for assessing the effects of climate change on hydrological regimes based on (1) employment of GCMs representing future climate scenarios as a consequence of increasing greenhouse gases, (2) application of downscaling techniques to downscale GCMs to compatible scales for hydrological modeling, and (3) implementation of hydrological models to simulate the response of hydrological regimes due to climate change. There are several sources of uncertainties in each section of this framework. As an example, for Greenhouse Gas (GHG) emission scenarios in the future, the rate of conversion of a specific GHG emission into atmospheric concentrations, the range of responses of various climate models to a given radiative force, and the method of constructing high resolution information from global climate model outputs, all contribute as sources of uncertainty (Mearns et al. 2001). The possible consecutive uncertainties in this framework are known as a "cascade of uncertainties" (Mearns et al. 2001). It is a general practice to consider this cascade of uncertainties when developing climate related scenarios for climate change impact, adaptation, and mitigation assessment studies (Smithson 2002). To incorporate the aforementioned physical uncertainties in the climate system models of this study, combinations of different Greenhouse Gas (GHG) emission scenarios, GCMs and downscaling methods, and time periods have been considered.

Kay et al. (2009) investigated the uncertainty of the climate change impact on flood frequency in England. They considered six different sources of uncertainty: (1) future greenhouse gas emissions, (2) General Circulation Models (GCMs), (3) downscaling from GCMs (along with an RCM), (4) hydrological models, (5) hydrological model parameters, and (6) internal variability of the climate system. They concluded that the uncertainty arising from future climate models is larger than the corresponding emission scenarios and hydrological modeling which made GCMs the primary source of uncertainty. Veijalainen et al. (2010) used 20 different GCMs to assess climate change on flooding in Finland. They suggested that GCMs are a greater source of uncertainty compared to emission scenarios and recommended that outputs of several GCMs be used in climate change impact studies on flooding. Camici et al. (2013) explored the impacts of climate change on flood frequency in central Italy using two GCMs, one emission scenario, and two statistical downscaling methods for the late 21st century. They concluded that the choice of GCMs and downscaling methods play a substantial role in determining the effects of future climate change on flood frequency. Sunyer et al. (2012) used four different regional climate

models and five various statistical downscaling methods to estimate rainfall extremes under climate change in Denmark from the period of 2071 to 2100 using an A1B emission scenario. They observed significant uncertainties in the mean, standard variation, skewness, the probability of dry days, and extreme events by using different downscaled projections. They also concluded that a considerable source of uncertainty comes from the choice of climate models. Dobler et al. (2012) quantified various sources of uncertainty in an Alpine watershed using three GCMs, three RCMs, and three bias correction techniques for downscaling. In their study, uncertainty from bias correction was found to have the highest impact on extreme river flow projections. They also mentioned that one of the techniques (Quantile-Quantile mapping) showed more reliable results compared to the other two methods (delta change and local scaling). In this context, LaFond et al. (2014) downscaled an ensemble of nine GCMs using two different downscaling methods for a watershed in Kentucky and concluded that the delta change downscaling method was suitable for estimating extreme events in flood impact assessments. Vetter et al. (2017) evaluated the sources of uncertainty of projected climate models for 12 river basins around the globe by applying nine hydrological models, four greenhouse gas concentration trajectories, and five GCMs. They used ANOVA to determine the sources of uncertainties and concluded that the choice of GCMs had the largest share of uncertainty compared to the other factors.

Our study area is located in the mid-Atlantic region of the United States, where recent observations and previous studies have indicated a change in precipitation trends and an increase in air temperature (Bernstein et al. 2008; Moglen and Rios Vidal 2014). Maldonado and Moglen (2012) studied the effects of climate change and land use change on the Occoquan reservoir with a focus on low flow variations. They concluded that land use/demand change has a more substantial impact than climate change on the water supply system, particularly in the mid 21st century of the study area. Moglen and Rios Vidal (2014) investigated the effects of climate change on stormwater infrastructure in the mid-Atlantic region of the United States. They indicated that detention ponds, and likely other stormwater infrastructure systems, would not function as previously envisioned due to the changes in future precipitation intensity and volume. Observed trends of climate change in the study area as well as this watershed's important role in providing water supply in northern Virginia necessitates a more comprehensive climate change impact study.

To account for different sources of uncertainties, this work employs future precipitation and surface air temperature time series from four GCMs using two GHG emission scenarios. For regional use, these time series are subsequently downscaled to the watershed by applying two statistical downscaling methods for the projection periods of 2046-2065 and 2081-2100. The objectives of this study are to (a) simulate future streamflow conditions in the study area for the mid and late 21st century, (b) analyze climate change impact on the watershed quantifying flow regime alterations, and (c) explore the main sources of uncertainty that arise from differing emission scenarios, GCMs, downscaling methods, and projection periods.

3.3 Study Area and Data

The study area is a part of the Mid-Atlantic region of the United States and has four distinctive seasons. The Broad Run watershed is part of a larger watershed system known as the Occoquan watershed in northern Virginia, which is located immediately west of Washington, DC (Figure 3-1). This watershed is a major contributor to the Lake Manassas water supply. Lake Manassas is a primary drinking water source for the City of Manassas, City of Manassas Park, and the surrounding areas (Liu 2011). Rapid population growth in northern Virginia has increased the demand for water supply, calling for new strategies to meet future needs. According to the United States Census Bureau, the population in one of the major counties within the Occoquan watershed (Prince William County) increased 260% from 1970 to 2010. Urbanization is an ongoing theme in the study area which can greatly influence a watershed's response to precipitation (Leopold 1968). The Broad Run watershed has moderate to high slopes with elevations ranging from 122 m to 305 m. The general structure of soils is loamy with approximately 67% in group B of NRCS (Natural Resources Conservation Service) hydrological soil groups (Liu 2011).

Daily meteorological data are collected at several weather stations within and near the study location. Cloud coverage, dew point temperatures, solar radiation, and wind speeds are obtained from Washington Dulles International Airport. Air temperature and precipitation data are obtained from three stations within the Broad Run watershed. Observed annual precipitation varies from 670 mm to 1360 mm with a yearly average of 960 mm. Observed mean annual surface air temperature is roughly 12.4 °C with a maximum monthly mean surface air temperature of 30.6 °C in July and a minimum monthly mean surface air temperature of -4.5 °C

in January. Table 3-1 depicts the observed meteorological data for the study area. Evapotranspiration was simulated using Hamon's potential evapotranspiration formula which relates potential evapotranspiration to maximum possible incoming radiant energy and saturation vapor pressure (Lu et al. 2005). The potential moisture-holding capacity of the air was calculated at the prevailing air temperature. Radiant energy is computed using daylight hours, sunset hour angle, Julian day of the year, and latitude of the study area.

3.4 Models and Methods

The adopted methodology for analyzing the climate change impact on streamflow is described in the following sections.

3.4.1 Modeling Climate Change Impact

Climate change impact studies often consider an ensemble of models to address the uncertainties arising from each factor of the modeling process (Camici et al. 2013; Dobler et al. 2012; Moglen and Rios Vidal 2014). A similar procedure has been implemented in this study.

3.4.2 Emission Scenarios

GHG emissions are exacerbated by anthropogenic activity. Quantifying the evolution of future trends of GHG emissions is complicated. The driving forces of GHG emission scenarios are highly dynamic, connecting several components such as demographic development, socio-economic progress, agricultural practices, and technological changes (Smithson 2002). Using available data and existing knowledge of GHG patterns, the Intergovernmental Panel on Climate Change (IPCC) has developed different storylines and scenario families to cover the extensive range of possible uncertainties and future changes (Bernstein et al. 2008). Four scenario families have been established as the main driving forces of GHG emissions (Bernstein et al. 2008). To address the uncertainty within GHG emission scenarios in this study, two extremes of the Special Report on Emissions Scenarios (SRES) spectrum have been considered giving rise to the full range of emission possibilities. On the upper side of the range, the A2 scenario focuses on regional and economic growth counting for increasing global population, locally oriented economic growth, and fragmented and slower technological advancement. On the lower side of the range, the B1 scenario assumes greater environmental awareness and global growth

attributed to convergent global population after the mid 21st century, introduction of clean technologies, and environmental sustainability (Bernstein et al. 2008).

3.4.3 GCMs

Each GCM represents the Earth's climate system under different initial and boundary conditions. To address the uncertainty specifically arising from the GCMs, an ensemble of four GCMs have been considered. However, only one realization of each GCM was employed, meaning that the internal variability simulated in each GCM is not reflected (Table 3-2).

3.4.4 Statistical Downscaling of Precipitation and Surface Air Temperature Time Series

Simulated data from GCMs are primarily used to demonstrate the Earth's climate system on a global scale. However, for regional use, these models should be translated to the scale of the watershed being studied. For this reason, the use of an appropriate downscaling method is required. In this study, two statistical downscaling methods, Delta Change (Anandhi et al. 2011; Arnell 1996; Camici et al. 2013; Wilby et al. 2004) and Quantile Mapping (Bennett et al. 2014; Camici et al. 2013; Maurer and Hidalgo 2008; Piani et al. 2010; Thrasher et al. 2012; Wood et al. 2004), were applied to produce the needed regional data sets. The essential advantages of using statistical downscaling are computational efficiency and the ability to develop GCM ensembles from multiple GCMs (Abatzoglou and Brown 2012). Moreover, this method can directly assimilate site-specific observations which can be crucial for many operative and managerial climate change impact studies (Wilby et al. 2004).

3.4.5 Delta Change Method

The Delta Change (DC) method is one of the simplest forms of downscaling transfer functions and change factor methodologies. In this method, different formulations based on temporal scales and mathematical operations (generally additive or multiplicative) are implemented. Many researchers use additive formulations as an estimate of the absolute change in temperature and the relative change for future precipitation time series (Anandhi et al. 2011). In the case of downscaling, surface air temperature data using additive change factors may be preferable because multiplicative change factors may encounter an undefined or unrealistically small or large variable. On the other hand, some meteorological variables, such as precipitation, have a lower limit (i.e., 0) and additive change factors must be checked for negative values. In this

study, an additive change factor (Equations 3-1 and 3-2) was applied to produce future surface air temperatures projections and a multiplicative change factor (Equations 3-3 and 3-4) was applied to create future precipitation time series.

$$\delta_{at} = FC_{at} - HC_{at} \tag{3-1}$$

$$LF_{at} = LH_{at} + \delta_{at} \tag{3-2}$$

where, FC_{at} is the future climate surface air temperature, HC_{at} is the historical climate surface air temperature, δ_{at} is the change factor for surface air temperatures, LH_{at} is the local historical surface air temperatures, and LF_{at} is the local future surface air temperature.

$$\delta_{pr} = FC_{pr} \big/ HC_{pr} \tag{3-3}$$

$$LF_{pr} = LH_{pr} \times \delta_{pr} \tag{3-4}$$

where, FC_{pr} is the future climate precipitation, HC_{pr} is the historical climate precipitation, δ_{pr} is the change factor for precipitation, LH_{pr} is the local historical precipitation, and LF_{pr} is the local future precipitation.

3.4.6 Quantile Mapping Method

In the Quantile Mapping (QM) method, cumulative distribution functions (CDFs) of observed and GCMs time series are generated for the variable(s) of interest (i.e., temperature and precipitation). One CDF is based on the GCMs simulations and the other is based on the aggregated observations. The mapping procedure is a simple nonparametric lookup that matches statistical moments of the observed data to the simulated ones. The QM method can reflect changes in the mean and variance of climate variables matching all statistical moments of GCMs with the corresponding observed variables, whereas the Delta Change method can only consider the mean change of the GCMs variables. Different variations of QM methods have been developed by researchers. In this study, bijective (the predictors are the same parameters as the predictands) and parameter-free (empirical cumulative distribution function) QM were implemented. The Equidistant Cumulative Distribution Function (EDCDF) matching method

was used for downscaling surface air temperatures (Equation 3-5) (Li et al. 2010). EDCDF has limitations for bias correcting precipitation where negative values are not acceptable. As a result, some researchers have tried to fit a theoretical distribution to their data to overcome this shortcoming. Alternatively, in this study, the Equiratio Cumulative Distribution Function (ERCDF) matching method was implemented to downscale precipitation data for prevailing this drawback (Equation 3-6) (Wang and Chen 2014).

$$LF_{at} = FC_{at} + \left(LH_{at}^{-1}(FC_{at})\right) - \left(HC_{at}^{-1}(FC_{at})\right) \tag{3-5}$$

$$LF_{pr} = FC_{pr} \times \left(LH_{pr}^{-1}(FC_{pr})\right) \Big/ \left(HC_{pr}^{-1}(FC_{pr})\right) \tag{3-6}$$

3.4.7 Simulation Time Period

In this study, the impact of future climate change is analyzed over two time periods, the mid 21st century and the late 21st century. The period of the mid 21st century consists of simulations from 2046 to 2065 and the period of the late 21st century entails simulations from 2081 to 2100. Table 3-3 summarized the historical and GCM data examined in this study.

3.4.8 Hydrological Simulation Model

Reliable rainfall-runoff modeling for a watershed is a priority for measuring streamflow alteration in climate change impact studies. In this paper, hydrological simulations were performed using Hydrological Simulation Program - FORTRAN (HSPF). HSPF is jointly supported by the United States Environmental Protection Agency and the U.S. Geological Survey. HSPF is a comprehensive process-based watershed model that has the ability to integrate watershed hydrology and water quality simulations. The extended period structure of HSPF allows users to simulate pervious and impervious land surfaces as well as in-stream hydraulic and sediment-chemical interactions (US-EPA 2015). HSPF has been widely used as an analytical tool for planning, designing, and operating water resources systems throughout North America and numerous countries around the globe with different climatic regimes (US-EPA 2015).

For this watershed, delineation and segmentation have been performed based on local geographic characteristics such as topography, land use, and soil properties (Liu 2011). The HSPF model contains three application modules: PERLND, IMPLND, and RCHRES. These modules can be

used to simulate runoff and water quality constituents in pervious and impervious lands as well as free flow reaches/well-mixed impoundments. Several parameters, including seven principal hydrologic calibration parameters, were used to calibrate the hydrological model using observed data from stream station ST70 (Figure 3-1) (Liu 2011). The model was validated by maximizing the Nash-Sutcliffe efficiency (NSE) (Nash and Sutcliffe 1970), and by minimizing the percent bias (PBIAS) (Moriasi et al. 2007).

3.4.9 Flow Regime Indicators

Despite the development of several streamflow alteration indicators in hydrological analyses in previous studies, in many cases the impact of future climate change on runoff have been expressed solely by using percent change of the magnitude of runoff with respect to natural conditions in the baseline period. Olden and Poff (2003) reviewed 171 different hydrological indices for characterizing streamflow regimes. The main classifications of indices in their study were: magnitude, frequency, duration, timing, and rate of change in flow events. These indices are calculated daily, monthly, or annually. Researchers have used and adapted various indices to address the alterations in streamflow due to climate change. Döll and Schmied (2012) studied the impact of climate change on freshwater resources using mean annual runoff (MAR), statistical low and high flows (monthly discharges that exceed the 90th and 10th percentile of flows), and mean seasonal discharge. Laizé et al. (2014) adopted a set of monthly flow regimes indicators (MFRIs) based on Indicators of Hydrologic Alteration (IHA) (Richter et al. 1996) for assessing flow alterations and ecological risks for Pan-European rivers. In this context, Thompson et al. (2014) used MFRIs to assess environmental flows and ecological risks for the Mekong river in Southeast Asia. In our study, a set of indices to quantify streamflow alterations was adopted, as shown in Table 3-4.

3.5 Results and Discussion

3.5.1 Surface Air Temperature

All models predicted an annual increase in average surface air temperature, ranging from 0.9 to 4.8 °C. The smallest change in annual surface air temperature was from the MRI model using emission scenario B1 and the DC downscaling method for the mid 21st century horizon. The highest annual surface air temperature was projected by the GFDL model using emission

scenario A2 and the QM downscaling method in the late 21st century. On average, an increase of 11% and 19% for annual surface air temperature was predicted across all models for the 2046-2065 and 2081-2100 periods, respectively. The annual maximum surface air temperature was also projected to increase by 7% and 13% on average for the first and second time periods. The highest change in annual maximum surface air temperature was 24%, which was projected by the GFDL model using emission scenario A2 and the QM downscaling method for the second time period. The smallest change in annual maximum surface air temperature was 4%, projected by the CSIRO model using emission scenario B1 and the DC downscaling method for the mid 21st century. Annual minimum surface air temperatures showed a 21% and 36% increase for the first and second time periods, respectively, compared to the annual minimum surface air temperatures in the baseline period. All models showed increases in maximum and minimum surface air temperatures with minimum temperatures predicted to rise at slightly higher amounts. This led to a decrease in the annual average of diurnal temperature range, which is the difference between the daily maximum and minimum temperatures. This range decreased more in the second period. Increases in maximum and minimum temperatures could affect future physiological processes of plant ecosystems and biogeochemical cycling modes in significant ways, including phenophase transitions to spring and budburst timing, autumn leaf abscission, and cold hardening (Team 2008).

Figure 3-2 and Figure 3-3 illustrate monthly surface air temperatures for all models in both the mid and late 21st century periods. The highest rise (9%) in average monthly surface air temperature was projected during the summer months (June, July, and August). August had peak monthly average surface air temperatures of 27.3 and 31.6 °C for the mid and late 21st centuries, respectively, using the GFDL model, emission scenario A2 and the QM downscaling method. Maximum monthly surface air temperature, like the average monthly surface air temperatures, increase most during the summer months. However, the monthly average minimum surface air temperature was anticipated to change more in the fall (September, October, and November) with an increase of 1.7 and 2.8 °C for the first and second future periods, respectively.

3.5.2 Precipitation

Mean annual precipitation was projected to increase, ranging from 2% to 17%, with the medians of 9% and 11% increases for the mid and late 21st century, respectively. Among the GCMs,

CSIRO showed the greatest change for the first time period whereas GFDL showed the highest change for the second period. For both periods, MRI projected the least amount of increase in precipitation. Overall, the A2 emission scenario forecasted more precipitation than the B1 scenario. The DC downscaling method produced slightly higher increments of precipitation than the QM method. The median precipitation volumes were higher for all months, except September, with the highest projected precipitation for May in both periods. The seasonal increases in median precipitation ranged from 3% in fall to 13% in spring. Figure 3-4 and Figure 3-5 display the monthly variations of precipitation for the mid and late 21st centuries.

3.5.3 Surface Air Temperature and Precipitation Interaction

Figure 3-6 and Figure 3-7 show contour plots of 16 different climate model projections for each of the mid and late 21st century periods. In these figures, the median of annual precipitation and the median of annual mean surface air temperatures were compared to the historical precipitation and surface air temperatures of the late 20th century. Three level monotonically increasing density grades were applied to show the composition and proportion of summed densities for each period. Increases in the median of annual precipitation and the median of annual mean surface air temperature were projected for both periods. The median of annual mean surface air temperatures were expected to increase 1.6 and 2.3 °C, for mid and late 21st century periods, respectively. Percent changes in the median of annual precipitation were projected to increase by 9% and 11% for the mid and late 21st century periods, respectively. Overall, the ranges of both median annual precipitation and a median annual surface air temperature of projected models were higher for the late 21st century period.

3.5.4 Streamflow Alterations

A statistical test was applied to explore the differences between the projected mean annual flows and the historical data. The null hypothesis was that the mean annual flows in the future would be the same as those experienced in the late 20th century. In more detail, the null hypothesis assumed that the mean annual flows in the projected models came from the same population as the observed data. A nonparametric method, the Wilcoxon signed rank test (Wilcoxon et al. 1963) was implemented. Projection models in which the null hypothesis with 95% confidence interval ($\alpha = 0.05$) was rejected are presented in Table 3-5. Rejecting the null hypotheses for

these cases indicated statistically significant changes in mean annual flows with respect to historical values. The Hodges–Lehmann estimator (Hodges Jr and Lehmann 2004) was subsequently implemented to estimate the magnitude of differences between the projected models and the historical data. As presented in Table 3-5 some of the projections showed up to a 30% change in the magnitude of mean annual flows.

Table 6 shows the details of changes in the characteristics of flow in the study area. In general, model projections showed increasing trends in the mean annual flows. These results are in agreement with previous findings, which signified an increase in mean monthly and yearly flows (Stagge and Moglen 2017). Projections using the DC method showed higher changes in the mid 21st century while the QM method projected greater changes in the late 21st century. Moreover, changes using A2 scenarios were more pronounced than B1 scenarios.

Q_{10} is an indicator of high flows, which is defined as the flow that exceeds 90% of the flows on a monthly basis in the overall period. Percent change in Q_{10} for any given model is calculated as the percent change between the Q_{10} of the projected model and the historical data. The same procedure was performed for Q_{90} and Q_{IQR} , as shown in Table 3-6. Unlike the model group QM-B1, all other model groups showed increases in high flows (Q_{10}) for the future periods. In contrast, low flows showed decreasing trends, suggesting that wider intervals between higher and lower deciles result in higher variabilities in the future flows. In other words, the model projected a higher amount of high flows and a higher amount of low flows in the future. An increase in the amount of high flows will amplify the risk of floods and a decrease in the amount of low flows will intensify the dry spells and cause ecological risks. As presented in Table 3-6, this trend also affected the interquartile range. The A indicates the dispersion of the central 50% of data. On average, this range increased by 13% and 14% for the mid and late 21st century periods, respectively.

Percent change in the number of months above and below the threshold was calculated to note not just the change in magnitude but also change in frequency of the months that have higher or lower flows. To compute percent change in number of months above and below the threshold, the number of months that exceeded the Q_{10} and Q_{90} thresholds in the historical data were first calculated. Then, the number of monthly flows in the projection models that exceeded historical Q_{10} and Q_{90} thresholds were counted. The percent change between these numbers is shown in

the Table 3-6 for each of the different group models during the mid and late 21st centuries. As presented in Table 3-6, generally, the number of months that exceed the Q_{10} and Q_{90} thresholds increase in both periods. As a result, climate change can cause a shift in location, an increase in scale, and also an increase in the frequency of high and low flows in this catchment.

To quantify the relative impact on the different projection models examined, an ANOVA (analysis of variance) model was employed to determine which modeling factor had the largest impact on model outcomes. Two different data transformation methods were used prior to the ANOVA design. TheE first data transformation was applied using a power transformation (Helsel and Hirsch 2002) to provide an approximately normal and constant variance data set. Since water flow regimes are usually positively skewed, the log transformation was applied as the first data transformation method. The rank transformation method (Helsel and Hirsch 2002) was performed as the second data transformation method with the benefit of being an asymptotically distribution-free method. The nonparametric four-way ANOVA with fixed factors was thus designed in consideration of four different impacting factors (i.e., a choice of emission scenario (two levels), a choice of GCM (four levels), a choice of downscaling method (two levels) and a choice of simulation period (two levels)). In this design, there were four main effects and eleven interactions between factors.

In practice, ANOVA methods are intended to help parse experimental data. This case is an example of using ANOVA for simulation data identifying the degree of variability in the models. In principle, ANOVA was used to determine the relative effects of different factors in future climate projections. In this design, Type III sum of squares was used (Langsrud 2003). However, since the design was orthogonal, meaning that there were equal amounts of simulations in every model, the type of sum of squares did not affect the overall results. The null hypothesis for the rank transformation method, as one of the forms of data transformation, looked for heterogeneity of the mean rank as an estimate of the median among all model groups. The null hypothesis was determined as if the median was the same between the model groups for all factor levels.

The results of ANOVA using both data transformation methods presented similar outcomes, both indicating a rejection of the null hypothesis. The rejection of the null hypothesis gives the conclusion that the medians of the mean annual flows differed between model groups. Among the main factors, the downscaling method with α-value denoted that responses for levels DC or

QM were significantly different. Effects of other levels for the remainder of the main factors were not statistically significant, suggesting that only the choice of the downscaling method among other set of choices had a statistically significant effect on changes in the responses (mean annual flows).

Figure 3-8 shows that there were some variations across the interactions of the factors. However, these variations were not statistically significant, indicating no evidence of two-way or more than two-way interactions between factor levels.

3.6 Summary and Conclusions

In this paper, the hydrological impact of climate change on a water supply watershed located in northern Virginia were studied. An ensemble of model groups was developed consisting of two emission scenarios, four GCMs, two downscaling methods, and two periods, resulting in a total of 32 model projections.

All projection models showed increases in mean annual surface air temperatures. The shift in location and dispersal in mean annual surface air temperatures were higher in the late 21st century than the mid 21st century. Also, both the maximum and minimum surface air temperatures were projected to increase in both time periods. Overall, these changes are projected to affect the lower tropospheric temperature profile, as higher amounts of precipitation are anticipated in the study area in both future periods. The precipitation depth was predicted to be slightly higher in the late 21st century by about 2%. The higher temperatures in this period resulted in a 5% increase in evapotranspiration and a 3% reduction in water yield, compared to mid 21st century.

To compute the alteration in streamflow regimes, a nonparametric test was carried out to compare differences in mean annual flows. Some of the model projections estimated up to a 30% positive shift in the median of mean annual flows. On average, an 8% change in the median of mean annual flows was anticipated for both the mid and late 21st century. It is expected that high flows will increase in both the mid and late 21st century, and the decrease of low flows in the late 21st century will be greater than during the mid century. At the same time, the Q_{IQR}, which is understood to represent the dispersion of the scale parameter, was projected to increase in both time horizons. These changes were more prominent using the QM downscaling method. In

essence, these dynamics can result in projected flows with higher intensity runoff, resulting changes in the statistical moments of flood probability distribution function.

An ANOVA test was implemented to identify the major factors affecting in climate change projection models by considering two emission scenarios, four GCMs, two downscaling methods and two periods in the mid and late 21st century. Results indicated that the choice of downscaling method had a statistically significant effect on the mean response, whereas the other main factors and the interactions between factor levels did not. The result of this analysis further affirmed the importance of using an ensemble of climate model projections for climate change impact studies.

3.7 Acknowledgments

The authors gratefully acknowledge the financial support provided by Australian Water Quality Centre (SA Water) and Occoquan Watershed Monitoring Laboratory (OWML) for this study. The views expressed in the paper are those of the authors and not necessarily of the funding bodies.

3.8 References

Abatzoglou, J. T., and Brown, T. J. (2012). "A comparison of statistical downscaling methods suited for wildfire applications." International Journal of Climatology, 32(5), 772-780.

Anandhi, A., Frei, A., Pierson, D. C., Schneiderman, E. M., Zion, M. S., Lounsbury, D., and Matonse, A. H. (2011). "Examination of change factor methodologies for climate change impact assessment." Water Resources Research, 47(3).

Arnell, N. W. (1996). Global warming, river flows and water resources, John Wiley & Sons Ltd.

Bennett, J. C., Grose, M. R., Corney, S. P., White, C. J., Holz, G. K., Katzfey, J. J., Post, D. A., and Bindoff, N. L. (2014). "Performance of an empirical bias-correction of a high-resolution climate dataset." International Journal of Climatology, 34(7), 2189-2204.

Bernstein, L., Bosch, P., Canziani, O., Chen, Z., Christ, R., and Riahi, K. (2008). "IPCC, 2007: climate change 2007: synthesis report." IPCC.

Camici, S., Brocca, L., Melone, F., and Moramarco, T. (2013). "Impact of climate change on flood frequency using different climate models and downscaling approaches." Journal of Hydrologic Engineering, 19(8), 04014002.

Dobler, C., Hagemann, S., Wilby, R., and Stötter, J. (2012). "Quantifying different sources of uncertainty in hydrological projections in an Alpine watershed." Hydrology and Earth System Sciences, 16(11), 4343-4360.

Döll, P., and Schmied, H. M. (2012). "How is the impact of climate change on river flow regimes related to the impact on mean annual runoff? A global-scale analysis." Environmental Research Letters, 7(1), 014037.

Haddeland, I., Heinke, J., Biemans, H., Eisner, S., Flörke, M., Hanasaki, N., Konzmann, M., Ludwig, F., Masaki, Y., and Schewe, J. (2014). "Global water resources affected by human interventions and climate change." Proceedings of the National Academy of Sciences, 111(9), 3251-3256.

Helsel, D., and Hirsch, R. (2002). "Statistical methods in water resources: US Geological Survey Techniques of Water Resources Investigations, book 4, chap." A3.

Hodges Jr, J., and Lehmann, E. L. (2004). "Hodges—Lehmann Estimators." Encyclopedia of statistical sciences, 5.

Ichoku, C., and Adegoke, J. (2016). "Synthesis and review: African environmental processes and water-cycle dynamics." Environmental Research Letters, 11(12), 120206.

Kay, A., Davies, H., Bell, V., and Jones, R. (2009). "Comparison of uncertainty sources for climate change impacts: flood frequency in England." Climatic change, 92(1-2), 41-63.

LaFond, K. M., Griffis, V. W., and Spellman, P. "Forcing Hydrologic Models with GCM Output: Bias Correction vs. the" Delta Change" Method." Proc., World Environmental and Water Resources Congress 2014, 2146-2155.

Laizé, C., Acreman, M., Schneider, C., Dunbar, M., Houghton-Carr, H., Flörke, M., and Hannah, D. (2014). "Projected flow alteration and ecological risk for pan-European rivers." River Research and Applications, 30(3), 299-314.

Langsrud, Ø. (2003). "ANOVA for unbalanced data: Use Type II instead of Type III sums of squares." Statistics and Computing, 13(2), 163-167.

Leopold, L. B. (1968). "Hydrology for urban land planning: A guidebook on the hydrologic effects of urban land use."

Li, H., Sheffield, J., and Wood, E. F. (2010). "Bias correction of monthly precipitation and temperature fields from Intergovernmental Panel on Climate Change AR4 models using equidistant quantile matching." Journal of Geophysical Research: Atmospheres, 115(D10).

Liu, Y. (2011). "Effective Modeling of Nutrient Losses and Nutrient Management Practices in an Agricultural and Urbanizing Watershed." Virginia Tech.

Lu, J., Sun, G., McNulty, S. G., and Amatya, D. M. (2005). "A comparison of six potential evapotranspiration methods for regional use in the southeastern United States." Journal of the American Water Resources Association, 41(3), 621-633.

Maldonado, P. P., and Moglen, G. E. (2012). "Low-flow variations in source water supply for the Occoquan reservoir system based on a 100-year climate forecast." Journal of Hydrologic Engineering, 18(7), 787-796.
Maurer, E. P., and Hidalgo, H. G. (2008). "Utility of daily vs. monthly large-scale climate data: an intercomparison of two statistical downscaling methods."
Mearns, L., Hulme, M., Carter, T., Leemans, R., Lal, M., Whetton, P., Hay, L., Jones, R., Kittel, T., and Smith, J. (2001). "Climate scenario development." Climate change 2001: the science of climate change, Cambridge University Press, 739-768.
Moglen, G. E., and Rios Vidal, G. E. (2014). "Climate change and storm water infrastructure in the mid-Atlantic region: Design mismatch coming?" Journal of Hydrologic Engineering, 19(11), 04014026.
Moriasi, D. N., Arnold, J. G., Van Liew, M. W., Bingner, R. L., Harmel, R. D., and Veith, T. L. (2007). "Model evaluation guidelines for systematic quantification of accuracy in watershed simulations." Transactions of the ASABE, 50(3), 885-900.
Nash, J. E., and Sutcliffe, J. V. (1970). "River flow forecasting through conceptual models part I—A discussion of principles." Journal of hydrology, 10(3), 282-290.
Olden, J. D., and Poff, N. (2003). "Redundancy and the choice of hydrologic indices for characterizing streamflow regimes." River Research and Applications, 19(2), 101-121.
Piani, C., Weedon, G., Best, M., Gomes, S., Viterbo, P., Hagemann, S., and Haerter, J. (2010). "Statistical bias correction of global simulated daily precipitation and temperature for the application of hydrological models." Journal of hydrology, 395(3-4), 199-215.
Richter, B. D., Baumgartner, J. V., Powell, J., and Braun, D. P. (1996). "A method for assessing hydrologic alteration within ecosystems." Conservation biology, 10(4), 1163-1174.
Smithson, P. A. (2002). "IPCC, 2001: climate change 2001: the scientific basis. Contribution of Working Group 1 to the Third Assessment Report of the Intergovernmental Panel on Climate Change, edited by JT Houghton, Y. Ding, DJ Griggs, M. Noguer, PJ van der Linden, X. Dai, K. Maskell and CA Johnson (eds). Cambridge University Press, Cambridge, UK, and New York, USA, 2001. No. of pages: 881. Price£ 34.95, US 49.95,ISBN0-521-01495-6(paperback).£90.00,US 130.00, ISBN 0-521-80767-0 (hardback)." International Journal of Climatology: A Journal of the Royal Meteorological Society, 22(9), 1144-1144.
Stagge, J. H., and Moglen, G. E. (2017). "Water Resources Adaptation to Climate and Demand Change in the Potomac River." Journal of Hydrologic Engineering, 22(11), 04017050.
Stocker, T. F., and Raible, C. C. (2005). "Climate change: water cycle shifts gear." Nature, 434(7035), 830.
Sunyer, M., Madsen, H., and Ang, P. (2012). "A comparison of different regional climate models and statistical downscaling methods for extreme rainfall estimation under climate change." Atmospheric Research, 103, 119-128.
Team, B. A. (2008). Assessment of climate change for the Baltic Sea basin, Springer Science & Business Media.
Thompson, J., Laizé, C., Green, A., Acreman, M., and Kingston, D. (2014). "Climate change uncertainty in environmental flows for the Mekong River." Hydrological Sciences Journal, 59(3-4), 935-954.
Thrasher, B., Maurer, E. P., Duffy, P. B., and McKellar, C. (2012). "Bias correcting climate model simulated daily temperature extremes with quantile mapping."

US-EPA (2015). "BASINS 4.1 (Better Assessment Science Integrating point & Non-point Sources) Modeling Framework." <https://www.epa.gov/ceam/better-assessment-science-integrating-point-and-non-point-sources-basins>. (23/09/2018).
Veijalainen, N., Lotsari, E., Alho, P., Vehviläinen, B., and Käyhkö, J. (2010). "National scale assessment of climate change impacts on flooding in Finland." Journal of Hydrology, 391(3-4), 333-350.
Vetter, T., Reinhardt, J., Flörke, M., van Griensven, A., Hattermann, F., Huang, S., Koch, H., Pechlivanidis, I. G., Plötner, S., and Seidou, O. (2017). "Evaluation of sources of uncertainty in projected hydrological changes under climate change in 12 large-scale river basins." Climatic change, 141(3), 419-433.
Wang, L., and Chen, W. (2014). "Equiratio cumulative distribution function matching as an improvement to the equidistant approach in bias correction of precipitation." Atmospheric Science Letters, 15(1), 1-6.
Wilby, R. L., Charles, S., Zorita, E., Timbal, B., Whetton, P., and Mearns, L. (2004). "Guidelines for use of climate scenarios developed from statistical downscaling methods." Supporting material of the Intergovernmental Panel on Climate Change, available from the DDC of IPCC TGCIA, 27, -.
Wilcoxon, F., Katti, S., and Wilcox, R. A. (1963). Critical values and probability levels for the Wilcoxon rank sum test and the Wilcoxon signed rank test, American Cyanamid Company.
Wood, A. W., Leung, L. R., Sridhar, V., and Lettenmaier, D. (2004). "Hydrologic implications of dynamical and statistical approaches to downscaling climate model outputs." Climatic change, 62(1-3), 189-216.
Xu, C.-y., Widén, E., and Halldin, S. (2005). "Modelling hydrological consequences of climate change—progress and challenges." Advances in Atmospheric Sciences, 22(6), 789-797.

Table 3-1. Baseline meteorological data for the study area from 1981 to 2000.

Month	Surface Air Temperature (tas) (°C)	Maximum Surface Air Temperature (tasmax) (°C)	Minimum Surface Air Temperature (tasmin) (°C)	Precipitation (P) (mm)	Evapotranspiration (ET) (mm)
January	0.3	5.4	-4.5	75	34
February	2.3	7.8	-2.9	66	20
March	6.3	12.4	0.5	87	28
April	11.9	18.4	5.4	78	32
May	17.0	23.4	10.6	96	59
June	21.9	28.1	15.9	80	61
July	24.5	30.6	18.7	79	71
August	23.3	29.4	17.5	92	79
September	19.3	25.5	13.4	87	75
October	12.8	19.6	6.3	68	54
November	7.4	13.4	1.6	88	63
December	2.2	7.3	-2.5	68	34
Average ([a]) or Sum ([s])	12.4[a]	18.4[a]	6.7[a]	964[s]	610[s]

Table 3-2. GCMs used in this study.

Model Name	Agency/Organization	Country	Abbreviation used in this manuscript
CSIRO MK3	Australia's Commonwealth Scientific and Industrial Research Organization	Australia	CSIRO
GFDL CM2.0	Geophysical Fluid Dynamics Laboratory	USA	GFDL
MPIM:ECHAM5	Max Planck Institute for Meteorology	Germany	MPIM
MRI-CGCM2.3.2	Meteorological Research Institute, Japan Meteorological Agency	Japan	MRI

Table 3-3. The time horizon for historical and GCM data.

Model set		Period	Abbreviation used in this paper
Historical		1981-2000	Baseline
GCM	Historical	1981-2000	20c3m
	Future	2046-2065	F1
		2081-2100	F2

Table 3-4. Hydrologic streamflow alteration indices.

Hydrological variable	Indicator	Temporal resolution	Flow type	Regime characteristics	Description
Q_{mean}	% Change	Annually	Mean flow	Magnitude	Percent change in mean annual flows
Q_{10}	Quantile	Monthly	High flow	magnitude	Monthly flow that exceeds ninety percent of months
Q_{IQR}	Quartile	Monthly	Median flow	Magnitude	IQR: difference between 75 and 25 percentiles
Q_{90}	Quantile	Monthly	Low flow	Magnitude	Monthly flow that exceeds ten percent of months
Number of months above threshold in observed data	Quantile	Monthly	High flow	Magnitude, frequency	Threshold: Q_{10}
Number of months below threshold in observed data	Quantile	Monthly	Low flow	Magnitude, frequency	Threshold: Q_{90}

Table 3-5. **α** values and % change in magnitude of difference between mean annual flows of the projected models and historical values.

Model name	Emission scenario	Downscaling method	Period	α-value	% Change in magnitude of difference
CSIRO	A2	DC	2046-2065	0.00	30%
CSIRO	B1	DC	2046-2065	0.00	26%
GFDL	B1	DC	2081-2100	0.00	24%
MPIM	A2	DC	2046-2065	0.04	19%
CSIRO	A2	DC	2081-2100	0.01	15%
MRI	B1	DC	2046-2065	0.02	14%
GDFL	B1	DC	2046-2065	0.01	12%

Table 3-6. Water quantity characteristics for mid and late 21st century.

Hydrological variable	DC-A2		DC-B1		QM-A2		QM-B1	
	2046-2065	2081-2100	2046-2065	2081-2100	2046-2065	2081-2100	2046-2065	2081-2100
% Change in median of mean annual Q	15.3	12.6	15.3	12.2	2.2	6.7	-0.6	2.0
% Change Q_{10}	15.6	13.1	17.7	11.1	11.1	10.8	-1.4	4.7
% Change Q_{IQR}	7.9	6.0	6.7	3.5	24.3	30.8	14.8	16.1
% Change Q_{90}	-3.5	4.6	7.6	-23.8	-40.8	-36.2	-23.8	-35.8
% Change in number of months above threshold in observed data ($Q_{10\text{-}Obs}$)	38.0	31. 5	33.7	25.0	21.7	29.3	4.3	7.6
% Change in number of months below threshold in observed data ($Q_{90\text{-}Obs}$)	15.3	23.6	20.8	18.1	111	132	95.8	124

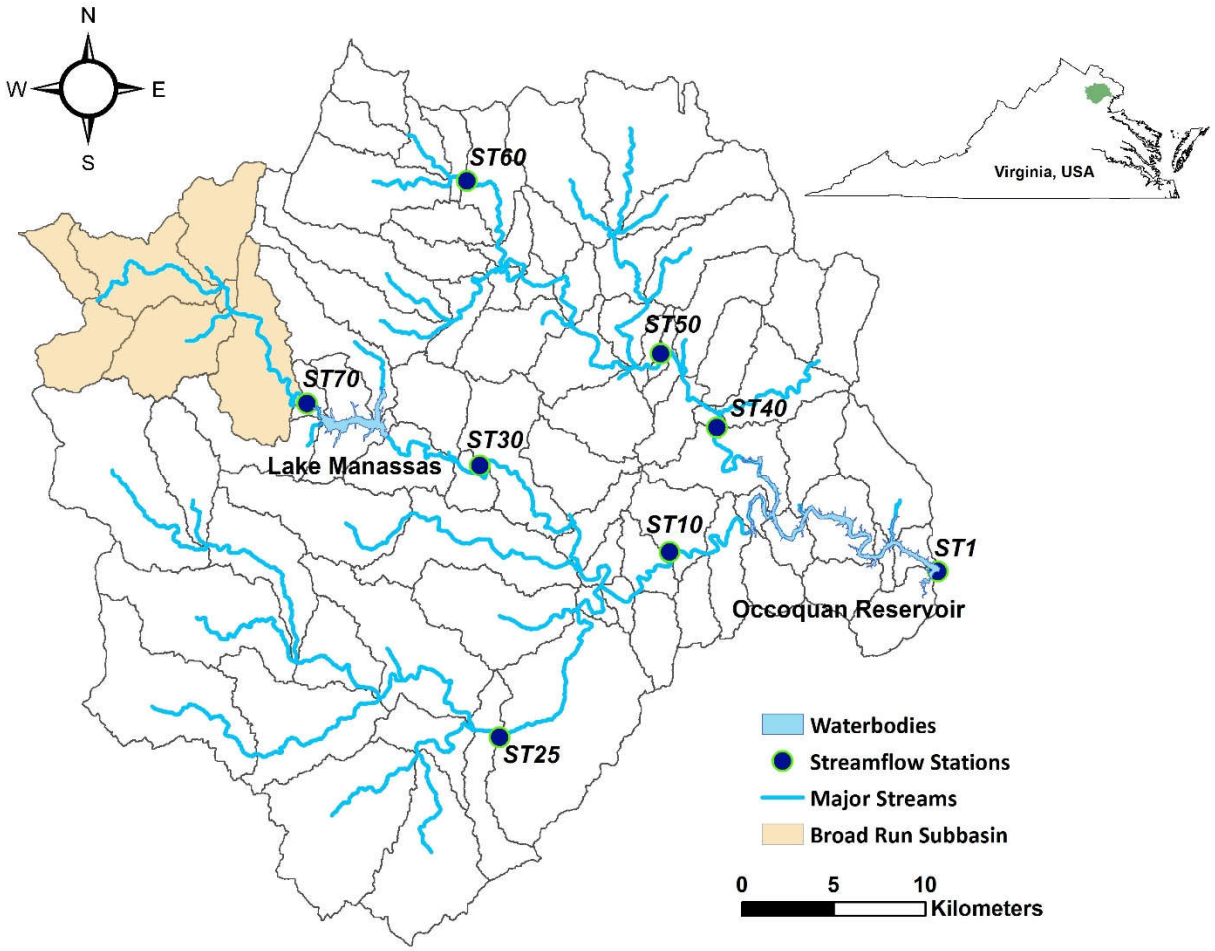

Figure 3-1. Location of the Broad Run watershed within the Occoquan watershed with major streams and streamflow stations.

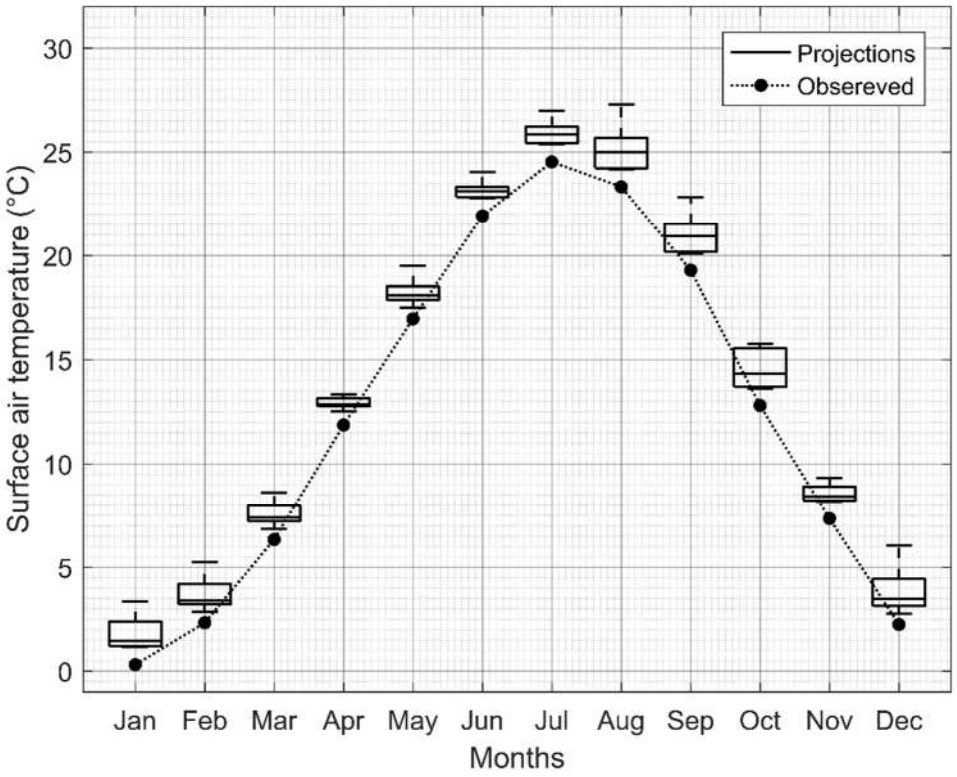

Figure 3-2. Monthly variation of projected surface air temperature for the mid 21st century.

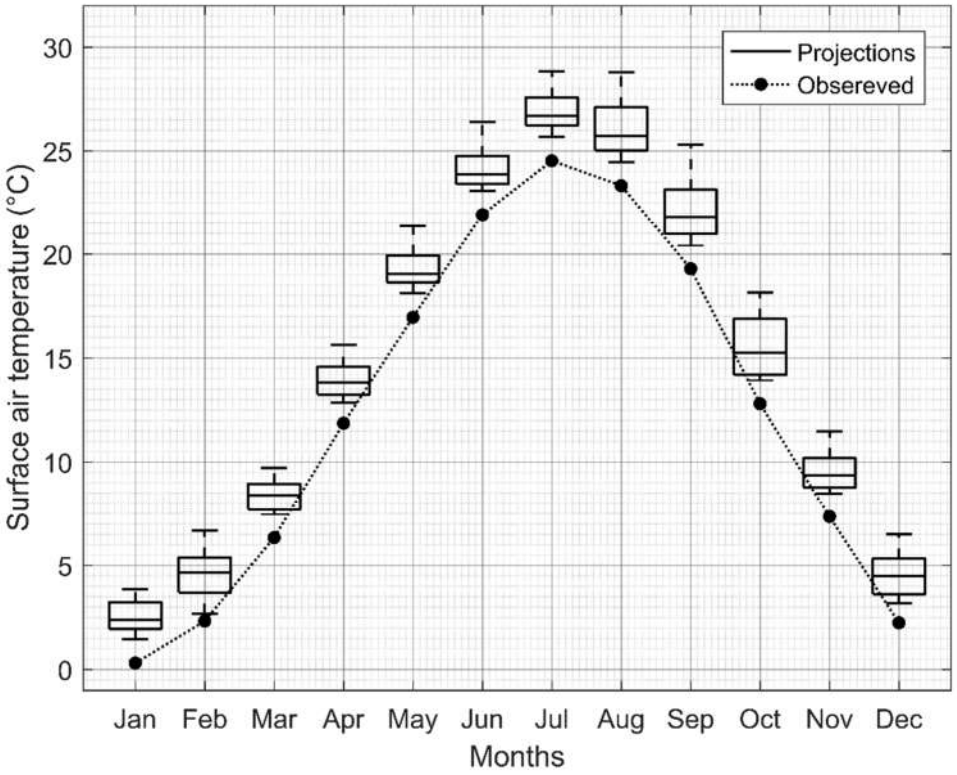

Figure 3-3. Monthly variation of projected surface air temperature for the late 21st century.

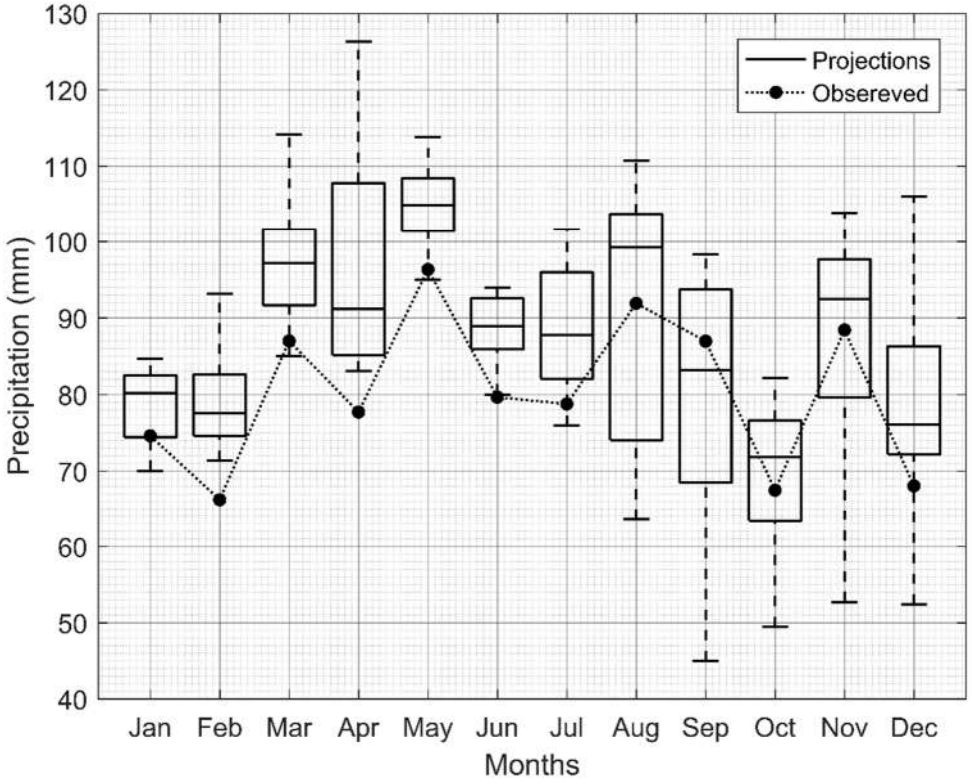

Figure 3-4. Monthly variation of projected precipitation for the mid 21st century.

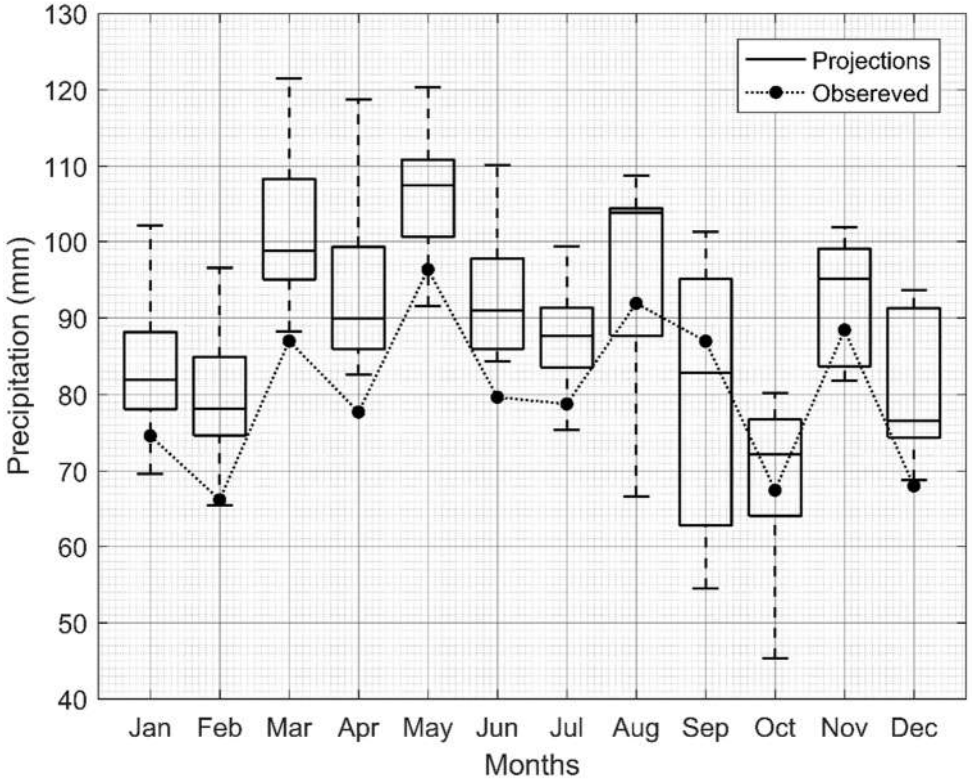

Figure 3-5. Monthly variation of projected precipitation for the late 21st century.

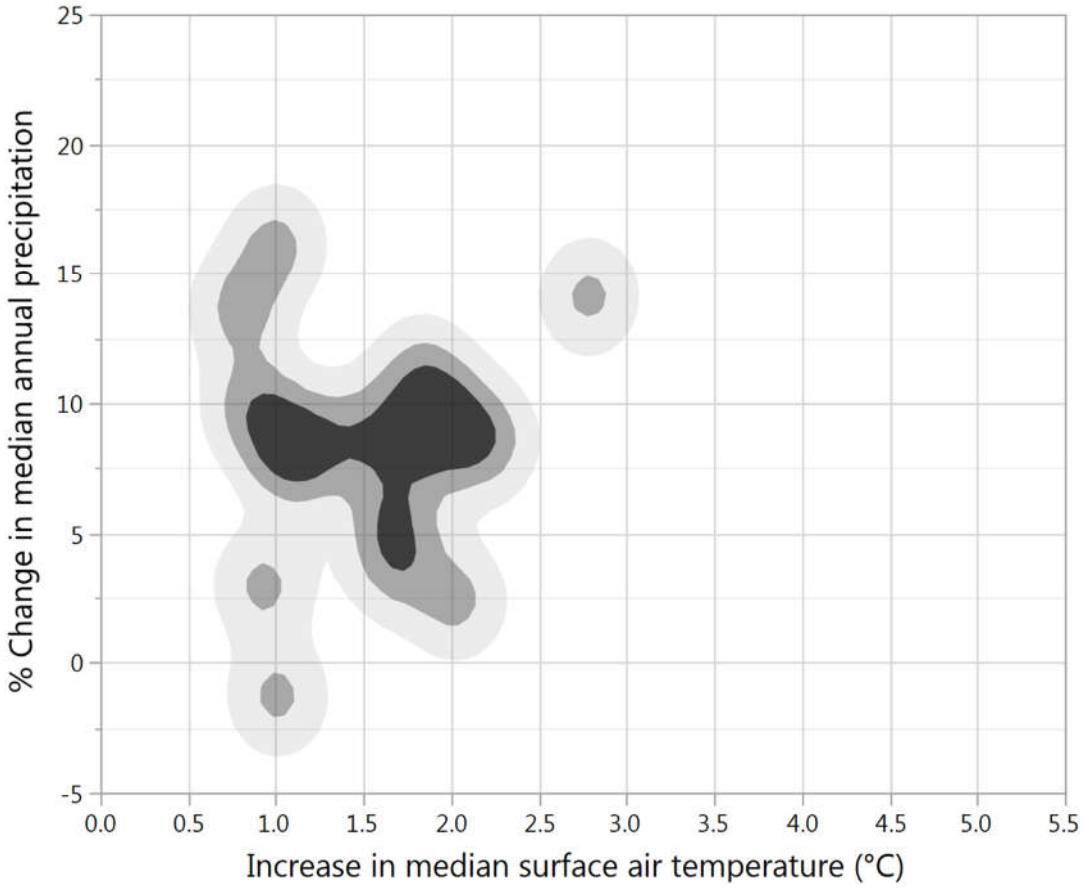

Figure 3-6. Increase in the median of annual surface air temperature against percent change in the median of annual precipitation for mid 21st century.

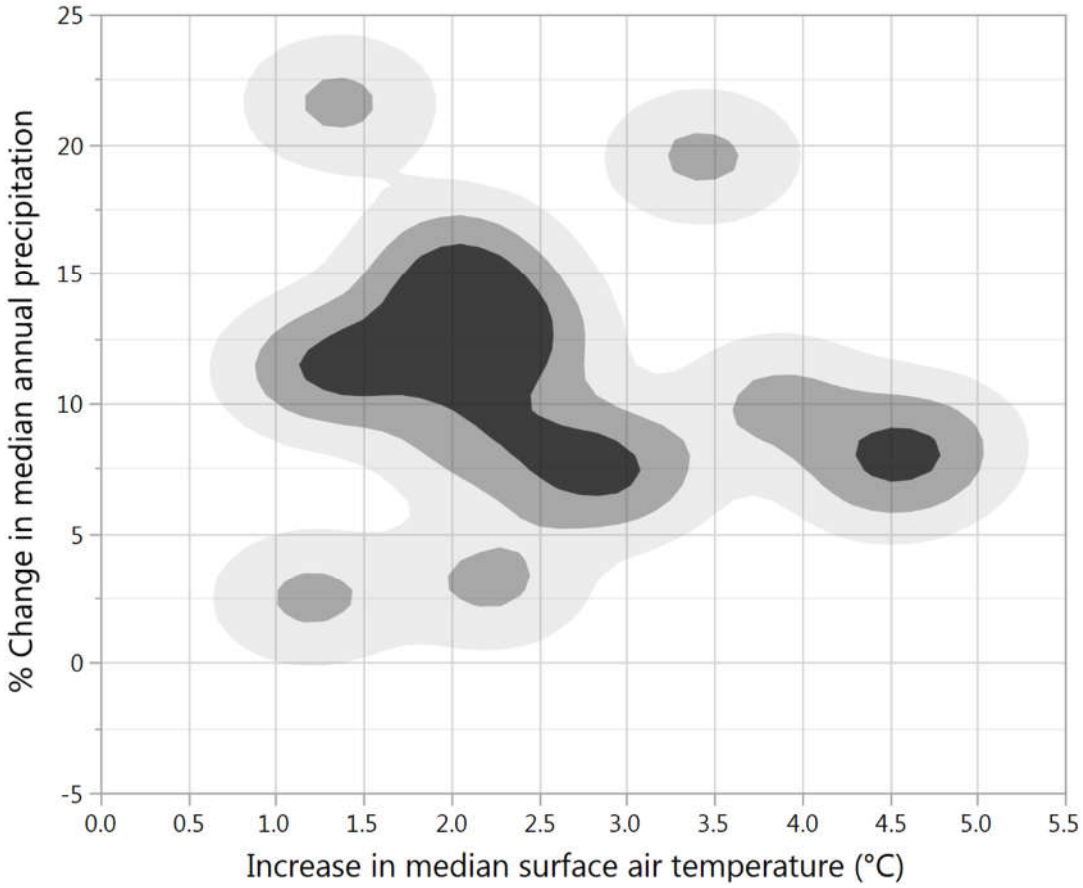

Figure 3-7. Increase in the median of annual surface air temperature against percent change in the median of annual precipitation for late 21st century.

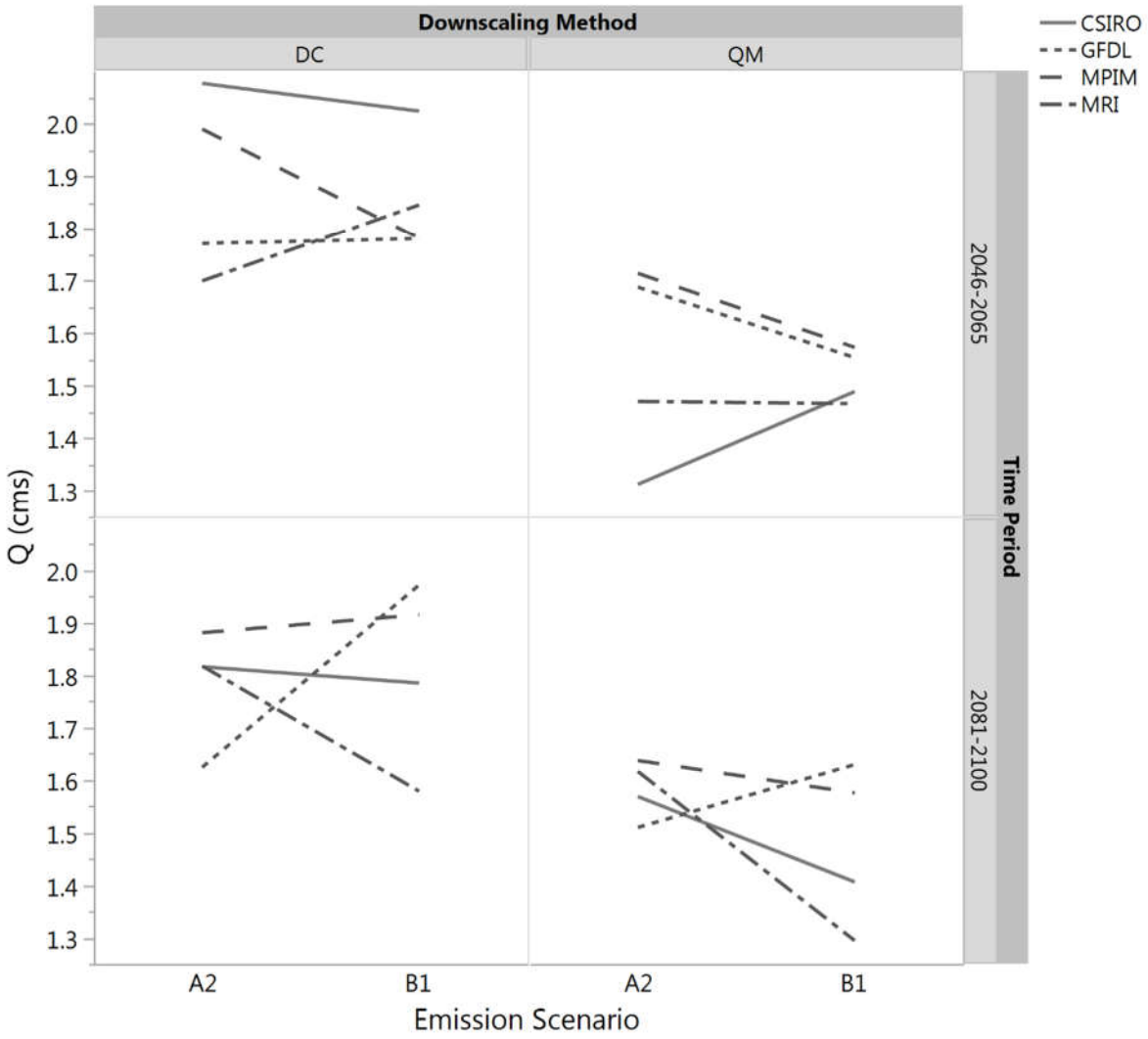

Figure 3-8. Interactions of model groups for four-way ANOVA design with consideration of four different impacting factors (i.e., a choice of emission scenario (two levels), a choice of GCM (four levels), a choice of downscaling method (two levels) and a choice of simulation period (two levels)).

Chapter 4 An Integrated System Modeling for Studying the Individual and Combined Impacts of Climate and Land Use Changes on Occupation Watershed Streamflows in Northern Virginia

Ayden A. Baran[1]; Glenn E. Moglen[2]; Adil N. Godrej[3]
Occoquan Watershed Monitoring Laboratory, 9408 Prince William Street, Manassas, VA 20110, U.S.A.

[1] Ph.D. Candidate, Occoquan Watershed Monitoring Laboratory, Virginia Tech, Manassas, VA, USA, (corresponding author). Email: abaran@vt.edu,

[2] Supervisory Research Hydrologist, USDA-ARS Hydrology and Remote Sensing Laboratory, Beltsville, MD, USA,

[3] Research Associate Professor, Occoquan Watershed Monitoring Laboratory, Virginia Tech, Manassas, VA, USA.

To be submitted to *The Journal of the American Water Resources Association (JAWRA)*

4.1 Abstract

Climate change and land use change are two major driving forces that can alter the streamflow responses to precipitation. In this paper, the singly and jointly impacts of climate change and land use change on the Occoquan watershed located in northern Virginia were studied. The combination of these two driving forces has created four themes, and an integrated complexly-linked watershed-reservoir model was used to run the simulations. The alteration in streamflow responses to the climate change and land use change evaluated at two streams draining to the Occoquan reservoir. The watersheds responsible for these streamflows are Bull Run and Occoquan Creek.

Ensembles of climate change projections were created using two emission scenarios, four GCMs, and two downscaling methods for two periods (i.e., mid and late 21st century). Climate change is projected to increase surface air temperature, precipitation depth, and evapotranspiration in the study area in the future. Moreover, shifts in precipitation patterns are likely to change the hydrological processes in the Occoquan watershed. Specifically, the high flows are projected to increase while the low flows are expected to decrease.

The study area has experienced rapid population growth and urbanization during the last few decades. These increases in population and urbanization are projected to continue and were simulated using two SRES storylines for the mid and late 21st century. The effects of land use

change on streamflow responses are projected to be drastic, specifically in the less urbanized Occoquan Creek.

The combined effects of climate change and land use change are synergistic and amplify the changes in the mean annual flows and high flows. However, climate change tends to dampen the impacts of land use change in the low flows.

The outcome of this study emphasizes the importance of planned urbanization and adequate stormwater infrastructure development facing future modifications in climate and land use. The methodology used in this paper, an integrated modeling system for analyzing the individual and combined impacts of climate change and land use change, can assist regional water resources managers for future planning, integrated adaptation, and mitigation strategies.

Keywords: Climate change; land use change; scenario development; water quantity; water resources management

4.2 Introduction

Among various driving forces affecting a watershed, climate change and land use change are considered as two primary components that can have a long term impact on the hydrological processes of a watershed. In recent years, many studies have addressed the impact of climate change on regional water resources. In this context, the main factors considered in changing the hydrological cycles in local watersheds were surface air temperature and precipitation (Camici et al. 2013; Fiseha et al. 2012; Mohammed et al. 2017). The changes in these factors can cause shifts in the mean, as well as the intensity of the discharges in a river basin (Immerzeel 2008). To project the future climate, many modelers use Global Circulation Models (GCMs). However, there are uncertainties associated with the progression of applying global climate models to a regional watershed level. Kay et al. (2009) categorized the sources of these uncertainties as (1) future greenhouse gas emissions, (2) General Circulation Models (GCMs), (3) downscaling from GCMs, (4) hydrological models, (5) hydrological model parameters, and (6) internal variability of the climate systems. Various approaches have been implemented by researchers to address these uncertainties often by using multiple choices of emission scenarios, GCMs, downscaling methods, and model parameter optimization (Afshar et al. 2017; Dobler et al. 2012; LaFond et al. 2014; Sunyer et al. 2012; Veijalainen et al. 2010; Vetter et al. 2017; Zareian et al. 2017). Consequently, in the development of a climate change impact study, an ensemble of projections

is created. The created ensemble provides upper and lower ends of the possible outcomes. The same method was implemented in this research to create a range of projections for studying the impact of climate change on the Occoquan watershed.

Changes in land use/cover can affect watershed hydrological processes such as interception, evapotranspiration, and infiltration (Niraula et al. 2015; Wang et al. 2014). Urbanization can increase impervious areas and inversely decrease the amount of water infiltration into the soil, resulting in increases of peak flood discharges and total runoff volumes (Beighley and Moglen 2002; Hejazi and Moglen 2008; Wang et al. 2014).

The information provided by the Intergovernmental Panel on Climate Change (IPCC) for future land use change is relatively coarse and only applies to a few sectors (Farjad et al. 2017). These limitations restrict the scale of usefulness of this information for environmental and water resources management (Sleeter et al. 2012). Additionally, this information often requires translation to smaller spatial scales (van Vuuren et al. 2010). Researchers have tried to develop models to create the necessary links between the global and local scale land use projections based on IPCC's Special Report on Emissions Scenarios (SRES). Still, these efforts were local to a city or country or did not produce some of the essential details including housing densities or impervious surfaces (Farjad et al. 2017). In this respect, a tool has been developed by the U.S. EPA as part of the Integrated Climate and Land Use Scenarios (ICLUS) project for the 48 contiguous U.S. states. The constructed scenarios in the ICLUS tool are aligned with the storylines of population growth, greenhouse-gas emissions, and socio-economic changes developed by the IPCC (EPA 2009).

The individual effects of climate change or land use change have been widely addressed in the literature in recent years (Amin et al. 2017; Camici et al. 2013; Reshmidevi et al. 2018; Vetter et al. 2017). However, fewer studies have compared the individual and combined effects of these two driving forces. It is important to note that the direct and indirect influence of the combination of these two components can alter streamflow characteristics in a watershed (Farjad et al. 2017; Gathenya et al. 2011; Maldonado and Moglen 2012; Stagge and Moglen 2017; Zhang et al. 2016). In this context, Hejazi and Moglen (2008) have examined the effect of climate change and land use change on flow duration in the Maryland Piedmont region. They used two GCM models and assumed that future urbanization would add 10% to impervious

lands. Under the joint impact of these two components, they observed reductions in low flows and increases in peak flows. They found that the two driving forces created an amplified effect while climate change alone had a stronger effect on changes in flow duration as Piedmont region was an already urbanized watershed. Maldonado and Moglen (2012) considered the effects of climate change and land use change in investigating the low-flow variations on a reservoir in northern Virginia. Their study revealed that these two components amplified each other's effects and the effects of climate change were much less than land use change. Serpa et al. (2015) investigated the impacts of climate change and land use change on two watersheds in Portugal. Their findings showed decreases in streamflows due to climate change and increases in streamflows because of the land use change. In their research, the two environmental stressors were offsetting each other and climate change was the more dominant factor. Setyorini et al. (2017) assessed the effects of the climate variability and land use/land cover (LULC) change on hydrological processes in the Upper Brantas river basin, Indonesia. They found that these two components dampened each other's effects on streamflows, although the effects of the climate change were overridden. Farjad et al. (2017) used two emission scenarios, two GCM models, one downscaling method, and two periods to predict the effects of the climate change and land use change on hydrological processes in a watershed in southern Alberta, Canada. Their study showed that the impacts of the climate and land use changes are positively correlated in winter and spring while the interactions between these two forces change in other seasons. The influence of land use change was more significant according to their study.

In this research effort, an integrated modeling approach was implemented to form an ensemble of scenarios with an objective to address the following questions: a) How will the streamflow characteristics change if the climate change and land use change are imposed separately or jointly? b) Which of the driving forces has a stronger effect? c) Will these driving forces exacerbate or offset their individual effects on the streamflow characteristics?

4.3 Study Area and Observed Data

The Occoquan watershed is part of the Washington, D.C. metropolitan area (WMA) located in the Mid-Atlantic region of the United States, with four distinctive seasons (

Figure **4-1**). The average elevation of the Watershed is 300 meters with an average slope of 21%. The total drainage area of the Watershed is 1,480 km² (570 mi²) that ends into Occoquan reservoir. The Occoquan reservoir serves as a principal source of potable water for more than 1.7 million residents in northern Virginia.

There are nine primary land use types in the study area with the following coverages, forest (57%), pasture (7%), high tillage cropland (5%), low tillage cropland (5%), townhouse/garden apartment (2%), low density residential (13%), medium density residential (6%), industrial/commercial (4%), and institutional (1%), creating an overall 6% impervious surface areas. Approximately 35% of the soils are categorized as B of NRCS (Natural Resources Conservation Service) hydrological soil group, which features a moderate infiltration rate when thoroughly wetted while the remainder of soil groups are A (10%), C (25%), D (20%) and the rest are water, swamps and alluvial lands (USDA 2017).

Rapid population growth in recent decades has been one of the primary contributors to land use change in northern Virginia. For instance, according to the United States Census Bureau, the population in one of the counties within the Occoquan watershed (Prince William County) has increased by 260% from 1970 to 2010. Urbanization is an ongoing theme in the study area which can greatly influence a watershed's response to precipitation (Leopold, 1968).

Daily meteorological data are collected from 16 weather stations within and nearby the study location. Cloud cover, dew point temperature, solar radiation, and wind speed are obtained from Washington Dulles International Airport (

Figure **4-1**). Observed annual precipitation varies from 730 mm to 1380 mm with an average of 971 mm per year. Observed mean annual surface air temperature is about 12.4 °C with a maximum monthly mean surface air temperature of 30.6 °C in July and a minimum monthly mean surface air temperature of -4.7 °C in January. Table 4-1 presents the observed meteorological data for the study area. Evapotranspiration was simulated using Hamon's potential evapotranspiration formula which relates potential evapotranspiration to maximum possible incoming radiant energy as well as saturation vapor pressure (Lu et al. 2005). Radiant energy is computed by using daylight hours, sunset hour angle, Julian day of the year, and latitude of the study area. The potential moisture-holding capacity of the air was calculated at the prevailing surface air temperature in the study area.

4.4 Models and Methods

Xu et al. (2005) arrayed a general scheme for assessing the effects of climate change on hydrological regimes as (1) employment of GCMs representing future climate scenarios because of increases in greenhouse gases, (2) application of downscaling techniques to downscale GCMs to the compatible scale for hydrological modeling, (3) implementation of hydrological models to simulate the response of hydrological regimes due to climate change. The possible consecutive uncertainties in this framework also can be known as a cascade of uncertainties. It is a general practice to consider a cascade of uncertainties in developing climate models and related scenarios for the climate change impact, adaptation, and mitigation assessment studies (Smithson 2002). The adapted methodology framework for analyzing climate change and land use change impacts on streamflows is represented in Figure 4-2 and described in the following sections.

4.4.1 Watershed Model

For modeling purposes, the Occoquan watershed is delineated into seven smaller subbasin models and two reservoir models, creating a complexly-linked watershed-reservoir hydrology and water quality model known as the Occoquan Model (Figure 4-3). The hydrological processes were simulated with the Hydrological Simulation Program - FORTRAN (HSPF), and the receiving waterbodies were simulated using CE-QUAL-W2.

HSPF is a comprehensive process-based watershed model that has the ability to integrate watershed hydrology and water quality simulations. The extended period structure of HSPF allows users to simulate pervious and impervious land surfaces as well as in-stream hydraulic and sediment-chemical interactions (EPA 2015). HSPF has been widely used as an analytical tool for planning, designing, and operating water resources systems throughout North America and numerous countries around the globe with different climatic regimes (EPA 2015).

CE-QUAL-W2 is a two-dimensional hydrodynamic and water quality model that can provide a detailed description of hydrodynamics and water quality processes in receiving waterbodies, such as rivers, lakes, reservoirs and estuaries (Cole and Wells 2006). In CE-QUAL-W2, waterbodies are defined by a series of control volumes with horizontal layers in the vertical direction of each longitudinal segment (Xu et al. 2007). CE-QUAL-W2 has been applied

extensively to simulate waterbodies worldwide and the example applications can be found in Cole and Wells (2006).

Calibration and validation of the Occoquan Model is an ongoing comprehensive effort which is maintained by the Occoquan Watershed Modeling Laboratory (OWML). The calibration and validation of the Occoquan Model have been carried out using several water quantity and quality parameters including flows, nitrogen, phosphorous, and total suspended solids (TSS). The uncertainties arising from model calibration can also be included in the aforementioned cascade of uncertainty, however, they were not considered in this study. The version of the Occoquan Model that was used in this study was calibrated from 2002 to 2005 and validated from 2006 to 2007. The calibrated process aimed to maximize the coefficient of determination (R^2), Nash-Sutcliffe efficiency (NSE) (Nash and Sutcliffe 1970), and minimize percent bias (PBIAS), and the ratio of the root mean square error to the standard deviation of measured data (RSR) (Moriasi et al. 2007). Table 4-2 displays the model calibration performance for streamflow at the selected stream stations (

Figure **4-1**).

4.4.2 Modeling Climate Change Impact

In creating an ensemble of models to address the uncertainties arising from each source of uncertainty, two emission scenarios, four GCMs, and two downscaling methods have been employed (Table **4-2**Table 4-3).

4.4.3 Emission Scenarios

Green House Gas (GHG) emissions can be seen as a newly added component to the Earth's climate system introduced by humans. Driving forces of GHG emission scenarios are highly dynamic, connecting several components including demographic development, socio-economic progress, agricultural practices, and technological changes (Smithson 2002). IPCC has developed different storylines and scenario families to cover the extensive possible ranges of uncertainties and future changes using available data and existing knowledge of GHG patterns (Bernstein et al. 2008).

To address the uncertainty within GHG emission scenarios, a choice of two extreme sides of the spectrum of the SRES has been considered to create upper and lower limits in future scenarios.

On the upper side of the range, the A2 scenario focuses on regional and economic growth counting for increasing global population, local-oriented economic growth, and fragmented and slower technological advancement. On the lower side of the range, the B1 scenario emphasizes on environmental awareness, the introduction of clean technologies, and global growth attributing on convergent global population after mid 21st century (Bernstein et al. 2008).

4.4.4 GCMs

Each GCM represents the Earth's climate system differently by applying various initial and boundary conditions. To address the uncertainty specifically arising from the GCMs, a group of four GCMs have been considered (Table 4-3).

4.4.5 Statistical Downscaling

Simulated data from GCMs are primarily used to demonstrate the Earth's climate system on a global scale. However, for regional use, these models can be translated to the scale of the watershed being studied. For this reason, the use of an appropriate downscaling method is required. In this study two statistical downscaling methods were applied for producing necessary regional data sets: Delta Change (Anandhi et al. 2011; Arnell 1996; Camici et al. 2013; Wilby et al. 2004) and Quantile Mapping (Bennett et al. 2014; Camici et al. 2013; Maurer and Hidalgo 2008; Piani et al. 2010; Thrasher et al. 2012; Wood et al. 2004).

Delta Change method

The Delta Change (DC) method is one of the simplest forms of downscaling transfer functions or change factor methodologies. In this method, different formulations can be used based on temporal scale and/or mathematical operation (usually additive or multiplicative) (Anandhi et al. 2011). In this study, an additive change factor (Equations 4-1 and 4-2) have been used for downscaling surface air temperatures and multiplicative change factor was applied (Equations 4-3 and 4-4) for downscaling precipitation.

$$\delta_{at} = FC_{at} - HC_{at} \quad (4\text{-}1)$$

$$LF_{at} = LH_{at} + \delta_{at} \quad (4\text{-}2)$$

where FC_{at} is future climate surface air temperature, HC_{at} is historical climate surface air temperature, δ_{at} is change factor for surface air temperatures, LH_{at} is local historical surface air temperatures, and LF_{at} is local future surface air temperature.

$$\delta_{pr} = FC_{pr} \big/ HC_{pr} \tag{4-3}$$

$$LF_{pr} = LH_{pr} \times \delta_{pr} \tag{4-4}$$

where FC_{pr} is future climate precipitation, HC_{pr} is historical climate precipitation, δ_{pr} is change factor for precipitation, LH_{pr} is local historical precipitation, and LF_{pr} is local future precipitation.

Quantile mapping method

In the Quantile Mapping (QM) method, cumulative distribution functions (CDFs) of observed and GCM time series are generated for the variable of interest (e.g., temperature and precipitation), one based on the GCM simulations and one based on the aggregated observations. The mapping procedure is based on a simple nonparametric lookup practice that matches statistical moments of the observed data to the simulated ones. Quantile mapping method can reflect the changes in mean and variance of climate variables matching all statistical moments of GCMs with corresponding observed variables. On the other hand, the delta change method only considers the mean change of the GCM variables. Different variations of quantile mapping methods have been used in previous studies. In this study, bijective (predictors are the same parameters as predictands) and parameter-free (empirical cumulative distribution function) QM has been implemented. Furthermore, an equidistant cumulative distribution function (EDCDF) matching method has been used for downscaling surface air temperatures (Equation 4-5) (Li et al. 2010). EDCDF has limitations for bias correcting precipitation where negative values are not acceptable. Alternatively, an equiratio cumulative distribution function (ERCDF) matching method has been employed for downscaling precipitation data (Equation 4-6) (Wang and Chen 2014).

$$LF_{at} = FC_{at} + \left(LH_{at}^{-1}(FC_{at})\right) - \left(HC_{at}^{-1}(FC_{at})\right) \tag{4-5}$$

$$LF_{pr} = FC_{pr} \times \left(LH_{pr}^{-1}(FC_{pr}) \right) \Big/ \left(HC_{pr}^{-1}(FC_{pr}) \right) \quad (4\text{-}6)$$

Downscaled climate variables

The target application and end-user requirements of climate-scenario models dictate the type of variables to be used in the impact study models. For example, for disaster management, the extremes of temperature, wind, and sea level data might be of more interest. In agricultural applications, precipitation, temperature, solar radiation, and humidity might be more important. General climate variables that have been used in water resources management (water quantity and quality assessments) are precipitation and temperature (Camici et al. 2013; Fiseha et al. 2012). In this study, surface air temperatures (including maximum and minimum), precipitation, and wind were used as the primary predictor variables (Table 4-4).

4.4.6 Modeling Land Use Change Impact

Developed by the U.S. EPA, ICLUS (Integrated Climate and Land-Use Scenarios) was used to simulate the impact of land use change over the watershed. This tool uses the projected population of each county as a major driver of growth. Then the population growth is converted into housing units. In the next step, housing density growth is spatially allocated by population growth rate, neighboring housing density, and transportation infrastructure using Spatially Explicit Regional Growth Model (SERGoM) (Theobald 2005).

The major benefit of using ICLUS for estimating the land use change is the use of mathematical models to produce spatially explicit projections of population and statistical models to render impervious surface areas based on IPCC's SRES storylines (Bierwagen and Morefield 2014). Detail overview of ICLUS modeling process is depicted in Figure 4-4.

4.4.7 Simulation Periods

Impact of future climate change have been analyzed in two periods, in the mid (2046-2065) and late (2081-2100) 21st century. Table 4-5 and Figure 4-5 depict historical and future periods used in this study. The land use changes are simulated every 10 years from 2040 to 2100. The average changes in projected land use in each period was calculated and the center of each period was used to represent the land use changes of that period. To simulate the impact of climate change, the entire 20 years period was used.

4.4.8 Simulation Scenarios

To consider the single and joint impacts of the climate change and land use change, four themes have been developed, as shown in Table 4-6.

Theme 1: Present Climate, Present Land Use

This theme serves as a baseline for which the other simulated themes are compared.

Theme 2: Future Climate, Present Land Use

This theme examines the influence of future climate conditions in the study area. In this theme, a range of future climate projections were explored to forecast the impact of climate change on flow characteristics. Land use condition is set at present levels.

Theme 3: Present Climate, Future Land Use

This theme investigates how continued land use change (i.e., urbanization) affects streamflow in the study area. Climate is set at present conditions.

Theme 4: Future Climate, Future Land Use

This theme considers the combined effects of both climate change and land use change. Comparing the results of this theme against the previous three themes identifies whether the combination of climate change and land used change are amplifying or dampening each other's effects relative to the components acting alone.

Considering these four themes and all of the choices of model set up (two GHG emissions, four GCMs, two downscaling methods, and two periods) resulted in 69 scenarios (68 projection simulations and 1 historical period simulation). For further analyses, the flow regime alterations using these 69 scenarios were studied at two streamflow stations (i.e., ST 10 and ST 40) entering the Occoquan reservoir. The subwatersheds creating these streamflow are Bull Run and Occoquan Creek (

Figure **4-1**).

An in-house software, URUNME, was used to simulate the 69 scenarios (Lodhi et al. 2018). URUNME enables water resources and environmental modelers to link, couple, and run their entire simulation process with various scenarios on one platform. Moreover, URUNME provides

modelers with flexible and interactive visualization and analytical tools to post-process model results.

4.5 Results and Discussion

4.5.1 Climate Change

Surface air temperature

All models predict an increase in annual average surface air temperatures ranging from 0.9 to 4.8 °C. On average, an increase of 11% to 19% for annual surface air temperature is predicted across all models for 2046-2065 and 2081-2100 periods, respectively. Annual maximum surface air temperatures are also projected to increase by 7% and 13% on average for the first and second periods. Annual minimum surface air temperatures are showing 21% and 36% increases for the first and second periods compared to the historical data. Minimum surface air temperatures are rising at slightly higher rates compared to maximum surface air temperatures. This leads to a decrease in an annual average of diurnal temperature range which is the difference between daily maximum and minimum temperatures. This range decreases more in the second period. Rises in temperature sums and minimum temperatures could be one of the factors that can affect future physiological processes of plants' ecosystem and biogeochemical cycling modes in different ways, including phenophase transitions to spring and budburst timing, autumn leaf abscission, and cold hardening (Team 2008). Overall, these increases are more prominent in the late 21st century using A2 scenarios while B1 scenarios in the mid 21st century are showing fewer changes.

Figure 4-6 and Figure 4-7 depict monthly surface air temperature for all the models for both the mid and late 21st century. The highest rises in average monthly surface air temperature occur in summer months (June, July, and August) by 9%, with August having peak monthly average surface air temperatures of 27.3 and 31.6 °C for the mid and late 21st century. Monthly average maximum surface air temperature is estimated to increase more in summer months. However, monthly average minimum surface air temperature is anticipated to have more changes in fall (September, October, and November) with an increase of 1.7 and 2.8 °C for the first and second periods, respectively.

Precipitation

Mean annual precipitation is projected to increase ranging from 2% to 17% with the median of 9% and 11% increases for mid and late 21st century. Overall, models with the emission scenario A2 in the late 21st century display more precipitation than B1 in the mid 21st century. The seasonal increase in median precipitation ranges from 3% in fall to 13% in spring. In the first period, the highest amount of predicted change in monthly precipitation is anticipated in July while the amount of precipitation is expected to decrease in September. In the second period, except for the month of September, the median precipitations are higher with the higher projected precipitations in May and December. Figure 4-8 and Figure 4-9 depict the monthly variation of precipitation for mid and late 21st century.

4.5.2 Land Use Change

Figure 4-10 and Figure 4-11 show an estimated percent of the current impervious surface areas in the Occoquan watershed. The Bull Run is more urbanized with an average impervious surface area of 12%, while the Occoquan Creek is mostly forest, pastures, and low-density residential with an average impervious surface area of 4%. Percent impervious surface areas are projected using SRES's storylines, economic vs. environmental and local vs. global driven developments. These projections can be different based on the initial states of a watershed. These initial states depend on travel time to urban cores and household sizes. The B1 scenario assumes smaller household sizes and denser growth patterns near existing urban cores, whereas the A2 scenario reflects larger household sizes as well as longer travel time to urban centers.

As mentioned earlier, 20-years simulations were used for each period (i.e., 2046-2065 and 2081-2100) while the land use for each of these periods was set at the middle of that period (i.e., 2055 and 2090). B1 scenario projects higher values of impervious land in the Bull Run compared to the A2 scenario until the last decade of the 21st century. In the Occoquan Creek, the A2 scenario always projects higher percentages of impervious lands compared to the B1 scenario. The highest projected percent impervious surface area for the Occoquan Creek is 13% at the end of the 21st century. The rate of change in urbanization in the Occoquan Creek is 1.7 times higher than the Bull Run (Figure 4-11).

Figure 4-12, Figure 4-13, Figure 4-14 and Figure 4-15 show the projected percent impervious surfaces for each of the emission scenarios for the center of each of the simulation periods. The changes are shown in the small subcatchments that are used in the Occoquan Model. These

smaller delineations have been performed based on local geographic characteristics such as topography, land use, and soil properties (Xu et al. 2007).

4.5.3 Streamflow Alterations

The impacts of climate change and land use change have been studied using four flow alteration indicators. These flow alteration indicators quantify the changes in mean annual flows, high flows, low flows, and dispersion of flows using the upper and lower quartiles of the flows. The extreme high and low flows are also evaluated (i.e., Q_1 and Q_{99}). Table 4-7 shows the details of changes in the flow characteristics of each of the Bull Run and Occoquan Creek at their drainage points to the Occoquan reservoir.

Impact of climate change:

In both watersheds, the differences between historical and future projections of mean annual flows fall within the same values of the historical rates for A2 and B1 scenarios in both periods. The interquartile range, which is an indicator of dispersion of the central 50% of data, is increased in both A2 and B1 scenarios in both periods, though these changes are higher in the first period. Generally, the high flows increase and the low flows decrease in all the scenarios, although the changes in low flows in the Occoquan Creek are more profound. As mentioned earlier, the surface air temperature and precipitation depth will increase as a result of climate change in the study area. However, evapotranspiration will become more dominant in future projections, especially in the second period and for the Occoquan Creek. Overall, while the projected mean annual flows seem to vary within the bounds of the historical values, the climate change will impact the high flow, low flows, as well as the dispersion of the flows.

Impact of land use change:

Land use change shows dramatic changes in flow characteristics in both watersheds for all of the scenarios. The alterations in flows are extreme in the Occoquan Creek. These substantial changes indicate that the impact of land use change on less urbanized watersheds will be more drastic. It is worth mentioning that in the historical period, the percent impervious surface areas in the Bull Run is more than twice that of the Occoquan Creek, while the area of the Bull Run is approximately half of that of the Occoquan Creek. Furthermore, historically, the Bull Run generates almost twice the mean annual flow as compared to Occoquan Creek. Alterations in the

mean annual flows, high flows, and low flows are projected to be higher in the late 21st century in both watersheds. In the Bull Run, the B1 scenario shows more significant changes in alteration indices while, in the Occoquan Creek, the A2 scenario predicts more changes in flow alteration indicators.

The directionality of streamflow trends usually tends to follow precipitation trends. However, urbanization can affect the hydrologic response of a watershed and change the orientation of these trends (Beighley and Moglen 2002). These alterations can be significant, as seen in the Occoquan Creek, and imply the fact that the current land use conditions should be considered in future land development.

Combined effects of climate change and land use change:

The combined effects of climate change and land use change amplifies the mean annual flows and high flows. The amplified effects are greater than the of each of the individual driving forces alone. Conversely, in the low flows, climate change tends to dampen the extreme effects of the land use change, and the dampening effects are greater than the direct arithmetic sum of each individual component. Further, there is no significant trend in amplifying or dampening effects in any of the scenarios.

Figure 4-16, Figure 4-17, Figure 4-18 and Figure 4-19 depict the monthly variations of streamflow for both watersheds in two periods using the medians of baseline model, climate change models, land use change models, and the combination of climate change and land use models using A2 and B1 scenarios for two periods for both watersheds. The green bound created by the individual models presents the maximum and minimum possible projections. The envelope is larger in February, March, and April in both watersheds. The deviation from median towards high flows is likely to happen in these months. The envelope gets narrower in July, August, September, and October. Specifically, in Bull Run, the climate change scenarios project lower amounts of low flows. During these months, climate change has dampening effects on the land use change. The land use change scenarios and combined scenarios show higher median flows in all months. The results of A2 and B1 scenarios are comparable in both watersheds for the mid and late 21st century. Figure 4-20 compares the changes in the median of mean annual flows in each watershed. As depicted, the effects of land use change will be dominant in both watersheds for both periods. The effects are more significant for Occoquan Creek.

4.5.4 Flow Duration Curve

Figure 4-21, Figure 4-22, Figure 4-23 and Figure 4-24 show the flow duration curves for each scenario for both subwatersheds. The solid lines show the baseline while the dashed lines are medians for each of the climate change, land use change, and combined climate change and land use change scenarios. The envelopes bound the maximum and minimum possible exceedance probabilities for each watershed. Ultimately, all scenarios show higher levels of peaks for both periods. Higher peaks are distinctive in both Bull Run and Occoquan Creek during both periods. Extreme peaks are distinctive using land use change modification, specifically for the less urbanized Occoquan Creek.

4.6 Summary and Conclusions

The impact of climate change on watersheds' hydrological processes have been a subject of many recent studies. In principle, the effects of climate change are intertwined with other anthropologic driving forces such as land use change. This paper studied the impacts of the indiviual and combined effects of climate change and land use change on the Occoquan watershed. The Occoquan watershed was divided as two subwatersheds, Bull Run and Occoquan Creek. The impacts of climate change and land use change are studied at two streams draining from these two subwatersheds into the Occoquan reservoir. For this purpose, four themes have been defined using the combination of these driving forces. To implement the arising uncertainties in the future projections, two emission scenarios, four GCMs, two downscaling methods and two periods were applied. Collectively 68 projections were simulated and ensembles of these projections were created to analyze the single and joint effects of these driving forces on streamflow characteristics.

Under the climate change scenarios, the Occoquan watershed will likely experience increases in surface air temperatures. These changes are expected to be more prevalent in the late 21st century. The A2 scenario shows higher increases compared to the B1 scenario, with highest changes during the summer months. The maximum and minimum surface air temperatures are also expected to increase. Furthermore, the climate change models projected increases in the total amount of precipitation. The overall rise in the amount of precipitation is higher in the second period and with the A2 scenario. On a seasonal basis, the increase in precipitation is more prominent in the Summer and projected to decrease in the fall. Additionally, as the annual

surface air temperature is projected to increase more in the late 21st century, the amount of evapotranspiration is also likely to be greater.

The impacts of climate change and land use change on streamflow characteristics were evaluated using various alteration indices. In both subwatersheds, projected mean annual flows are expected to fall within the same values of historical rates. However, the high flows are projected to increase and the low flows are projected to decrease. This expansion creates a broader range between the high and low flows.

The changes in flow characteristics considering the future land use change will likely be more drastic as compared to the base scenario in the Occoquan watershed. These changes will be more noticeable in spring. The substantial increases in flows will be more dominant in Occoquan Creek, as the changes due to urbanization will be more pronounced. The outcome of this research shows dramatic alterations of flows caused by urbanization. This emphasizes the necessity to evaluate the state of watersheds for future planning and development with a close consideration of the impact of deforestation and urbanization.

The alteration in flow characteristics will be significant under the joint examination of climate change and land use change. Climate change and land use change have amplifying effects on the mean annual flows and high flows. In contrast, climate change is projected to dampen the extreme increases in the low flows created by the land use change. The projected alterations are synergistic and more than the arithmetic sum of each individual driving forces.

Results show augmented discharges, especially in the high flows under urbanized scenarios. The findings of this study also highlight the importance of the initial state of a watershed in analyzing the impacts of climate change and land use change.

4.7 Acknowledgments

The authors gratefully acknowledge the financial support provided by Australian Water Quality Centre (SA Water) and Occoquan Watershed Monitoring Laboratory (OWML) for this study. The views expressed in the paper are those of the authors and not necessarily of the funding bodies.

4.8 References

Afshar, A. A., Hassanzadeh, Y., Besalatpour, A. A., and Bilondi, M. P. (2017). "Seasonal Changes of Precipitation and Temperature of Mountainous Watersheds in Future Periods with Approach of Fifth Report of Intergovernmental Panel on Climate Change (Case study&58; Kashafrood Watershed Basin)." Majallah-i āb va Khāk, 30(5), 1718-1732.

Amin, M., Shaaban, A., Ercan, A., Ishida, K., Kavvas, M., Chen, Z., and Jang, S. (2017). "Future climate change impact assessment of watershed scale hydrologic processes in Peninsular Malaysia by a regional climate model coupled with a physically-based hydrology model." Science of The Total Environment, 575, 12-22.

Anandhi, A., Frei, A., Pierson, D. C., Schneiderman, E. M., Zion, M. S., Lounsbury, D., and Matonse, A. H. (2011). "Examination of change factor methodologies for climate change impact assessment." Water Resources Research, 47(3).

Arnell, N. W. (1996). Global warming, river flows and water resources, John Wiley & Sons Ltd.

Beighley, R. E., and Moglen, G. E. (2002). "Trend assessment in rainfall-runoff behavior in urbanizing watersheds." Journal of Hydrologic Engineering, 7(1), 27-34.

Bennett, J. C., Grose, M. R., Corney, S. P., White, C. J., Holz, G. K., Katzfey, J. J., Post, D. A., and Bindoff, N. L. (2014). "Performance of an empirical bias-correction of a high-resolution climate dataset." International Journal of Climatology, 34(7), 2189-2204.

Bernstein, L., Bosch, P., Canziani, O., Chen, Z., Christ, R., and Riahi, K. (2008). "IPCC, 2007: climate change 2007: synthesis report." IPCC.

Bierwagen, B., and Morefield, P. (2014). "Integrated Climate and Land Use Scenarios (ICLUS). Web page. Washington, DC: US Environmental Protection Agency (USEPA). Accessed September 25."

Camici, S., Brocca, L., Melone, F., and Moramarco, T. (2013). "Impact of climate change on flood frequency using different climate models and downscaling approaches." Journal of Hydrologic Engineering, 19(8), 04014002.

Cole, T. M., and Wells, S. A. (2006). "CE-QUAL-W2: A two-dimensional, laterally averaged, hydrodynamic and water quality model, version 3.5."

Dobler, C., Hagemann, S., Wilby, R., and Stötter, J. (2012). "Quantifying different sources of uncertainty in hydrological projections in an Alpine watershed." Hydrology and Earth System Sciences, 16(11), 4343-4360.

EPA, U. (2015). "BASINS 4.1 (Better Assessment Science Integrating point & Non-point Sources) Modeling Framework." (02/02/2018).

EPA, U. S. (2009). "Land-Use Scenarios: National-Scale Housing-Density Scenarios Consistent with Climate Change Storylines (Final Report)." EPA/600/R-08/076F.

Farjad, B., Gupta, A., Razavi, S., Faramarzi, M., and Marceau, D. J. (2017). "An Integrated Modelling System to Predict Hydrological Processes under Climate and Land-Use/Cover Change Scenarios." Water, 9(10), 767.

Fiseha, B., Melesse, A., Romano, E., Volpi, E., and Fiori, A. (2012). "Statistical downscaling of precipitation and temperature for the Upper Tiber Basin in Central Italy." International journal of water sciences, 1.

Gathenya, M., Mwangi, H., Coe, R., and Sang, J. (2011). "Climate-and land use-induced risks to watershed services in the Nyando River Basin, Kenya." Experimental Agriculture, 47(2), 339-356.

Hejazi, M. I., and Moglen, G. E. (2008). "The effect of climate and land use change on flow duration in the Maryland Piedmont region." Hydrological Processes, 22(24), 4710-4722.
Immerzeel, W. (2008). "Historical trends and future predictions of climate variability in the Brahmaputra basin." International Journal of Climatology, 28(2), 243-254.
Kay, A., Davies, H., Bell, V., and Jones, R. (2009). "Comparison of uncertainty sources for climate change impacts: flood frequency in England." Climatic Change, 92(1-2), 41-63.
LaFond, K. M., Griffis, V. W., and Spellman, P. "Forcing Hydrologic Models with GCM Output: Bias Correction vs. the" Delta Change" Method." Proc., World Environmental and Water Resources Congress 2014, 2146-2155.
Li, H., Sheffield, J., and Wood, E. F. (2010). "Bias correction of monthly precipitation and temperature fields from Intergovernmental Panel on Climate Change AR4 models using equidistant quantile matching." Journal of Geophysical Research: Atmospheres, 115(D10).
Lodhi, A., Godrej, A. N., Baran, A., and Sen, D. (2018). "URUNME: A Software Platform for Integrated Environmental Modeling to Help 'You Run Models Easily'." Manuscript in preparation.
Lu, J., Sun, G., McNulty, S. G., and Amatya, D. M. (2005). "A comparison of six potential evapotranspiration methods for regional use in the southeastern United States." JAWRA Journal of the American Water Resources Association, 41(3), 621-633.
Maldonado, P. P., and Moglen, G. E. (2012). "Low-flow variations in source water supply for the Occoquan reservoir system based on a 100-year climate forecast." Journal of Hydrologic Engineering, 18(7), 787-796.
Maurer, E. P., and Hidalgo, H. G. (2008). "Utility of daily vs. monthly large-scale climate data: an intercomparison of two statistical downscaling methods."
Mohammed, K., Saiful Islam, A., Tarekul Islam, G., Alfieri, L., Bala, S. K., and Uddin Khan, M. J. (2017). "Impact of High-End Climate Change on Floods and Low Flows of the Brahmaputra River." Journal of Hydrologic Engineering, 22(10), 04017041.
Moriasi, D. N., Arnold, J. G., Van Liew, M. W., Bingner, R. L., Harmel, R. D., and Veith, T. L. (2007). "Model evaluation guidelines for systematic quantification of accuracy in watershed simulations." Transactions of the ASABE, 50(3), 885-900.
Nash, J. E., and Sutcliffe, J. V. (1970). "River flow forecasting through conceptual models part I—A discussion of principles." Journal of hydrology, 10(3), 282-290.
Niraula, R., Meixner, T., and Norman, L. M. (2015). "Determining the importance of model calibration for forecasting absolute/relative changes in streamflow from LULC and climate changes." Journal of Hydrology, 522, 439-451.
Piani, C., Weedon, G., Best, M., Gomes, S., Viterbo, P., Hagemann, S., and Haerter, J. (2010). "Statistical bias correction of global simulated daily precipitation and temperature for the application of hydrological models." Journal of Hydrology, 395(3-4), 199-215.
Reshmidevi, T., Kumar, D. N., Mehrotra, R., and Sharma, A. (2018). "Estimation of the climate change impact on a catchment water balance using an ensemble of GCMs." Journal of Hydrology, 556, 1192-1204.
Serpa, D., Nunes, J., Santos, J., Sampaio, E., Jacinto, R., Veiga, S., Lima, J., Moreira, M., Corte-Real, J., and Keizer, J. (2015). "Impacts of climate and land use changes on the hydrological and erosion processes of two contrasting Mediterranean catchments." Science of the Total Environment, 538, 64-77.

Setyorini, A., Khare, D., and Pingale, S. M. (2017). "Simulating the impact of land use/land cover change and climate variability on watershed hydrology in the Upper Brantas basin, Indonesia." Applied Geomatics, 9(3), 191-204.
Sleeter, B. M., Sohl, T. L., Bouchard, M. A., Reker, R. R., Soulard, C. E., Acevedo, W., Griffith, G. E., Sleeter, R. R., Auch, R. F., and Sayler, K. L. (2012). "Scenarios of land use and land cover change in the conterminous United States: Utilizing the special report on emission scenarios at ecoregional scales." Global Environmental Change, 22(4), 896-914.
Smithson, P. A. (2002). "IPCC, 2001: climate change 2001: the scientific basis. Contribution of Working Group 1 to the Third Assessment Report of the Intergovernmental Panel on Climate Change, edited by JT Houghton, Y. Ding, DJ Griggs, M. Noguer, PJ van der Linden, X. Dai, K. Maskell and CA Johnson (eds). Cambridge University Press, Cambridge, UK, and New York, USA, 2001. No. of pages: 881. Price£ 34.95, US $49.95, ISBN 0-521-01495-6 (paperback).£ 90.00, US $130.00, ISBN 0-521-80767-0 (hardback)." International Journal of Climatology, 22(9), 1144-1144.
Stagge, J. H., and Moglen, G. E. (2017). "Water Resources Adaptation to Climate and Demand Change in the Potomac River." Journal of Hydrologic Engineering, 22(11), 04017050.
Sunyer, M., Madsen, H., and Ang, P. (2012). "A comparison of different regional climate models and statistical downscaling methods for extreme rainfall estimation under climate change." Atmospheric Research, 103, 119-128.
Team, B. A. (2008). Assessment of climate change for the Baltic Sea basin, Springer Science & Business Media.
TERRA, A. (2012). "HSPF Support." (05/05/2017), AQUA TERRA.
Theobald, D. (2005). "Spatially explicit regional growth model (SERGOM) v2 methodology." Report for Trust for Public Lands, Fort Collins, CO.
Thrasher, B., Maurer, E. P., McKellar, C., and Duffy, P. (2012). "Bias correcting climate model simulated daily temperature extremes with quantile mapping." Hydrology and Earth System Sciences, 16(9), 3309.
USDA, N. (2017). "Soil Survey Staff." Natural Resources Conservation Service, United States Department of Agriculture. Web Soil Survey. Available online at http://websoilsurvey.nrcs.usda.gov (accessed December 12, 2017).
van Vuuren, D. P., Smith, S. J., and Riahi, K. (2010). "Downscaling socioeconomic and emissions scenarios for global environmental change research: a review." Wiley Interdisciplinary Reviews: Climate Change, 1(3), 393-404.
Veijalainen, N., Lotsari, E., Alho, P., Vehviläinen, B., and Käyhkö, J. (2010). "National scale assessment of climate change impacts on flooding in Finland." Journal of Hydrology, 391(3-4), 333-350.
Vetter, T., Reinhardt, J., Flörke, M., van Griensven, A., Hattermann, F., Huang, S., Koch, H., Pechlivanidis, I. G., Plötner, S., and Seidou, O. (2017). "Evaluation of sources of uncertainty in projected hydrological changes under climate change in 12 large-scale river basins." Climatic Change, 141(3), 419-433.
Wang, L., and Chen, W. (2014). "Equiratio cumulative distribution function matching as an improvement to the equidistant approach in bias correction of precipitation." Atmospheric Science Letters, 15(1), 1-6.
Wang, R., Kalin, L., Kuang, W., and Tian, H. (2014). "Individual and combined effects of land use/cover and climate change on Wolf Bay watershed streamflow in southern Alabama." Hydrological Processes, 28(22), 5530-5546.

Wilby, R. L., Charles, S., Zorita, E., Timbal, B., Whetton, P., and Mearns, L. (2004). "Guidelines for use of climate scenarios developed from statistical downscaling methods." Supporting material of the Intergovernmental Panel on Climate Change, available from the DDC of IPCC TGCIA, 27, -.

Wood, A. W., Leung, L. R., Sridhar, V., and Lettenmaier, D. (2004). "Hydrologic implications of dynamical and statistical approaches to downscaling climate model outputs." Climatic change, 62(1-3), 189-216.

Xu, C.-y., Widén, E., and Halldin, S. (2005). "Modelling hydrological consequences of climate change—progress and challenges." Advances in Atmospheric Sciences, 22(6), 789-797.

Xu, Z., Godrej, A. N., and Grizzard, T. J. (2007). "The hydrological calibration and validation of a complexly-linked watershed–reservoir model for the Occoquan watershed, Virginia." Journal of Hydrology, 345(3-4), 167-183.

Zareian, M., Eslamian, S., Gohari, A., and Adamowski, J. (2017). "The Effect of Climate Change on Watershed Water Balance." Mathematical Advances Towards Sustainable Environmental Systems, Springer, 215-238.

Zhang, L., Nan, Z., Xu, Y., and Li, S. (2016). "Hydrological impacts of land use change and climate variability in the headwater region of the Heihe River Basin, Northwest China." PloS one, 11(6), e0158394.

Table 4-1. Baseline meteorological data for the study area from 1981 to 2000.

Month	Surface Air Temperature (tas) (°C)	Maximum Surface Air Temperature (tasmax) (°C)	Minimum Surface Air Temperature (tasmin) (°C)	Precipitation (P) (mm)	Evapotranspiration (ET) (mm)
January	0.2	5.2	-4.7	71	32
February	2.3	7.8	-2.9	68	21
March	6.3	12.3	0.5	86	28
April	11.9	18.4	5.4	80	33
May	17.0	23.4	10.6	98	60
June	21.9	28.1	15.9	82	63
July	24.5	30.6	18.7	86	77
August	23.3	29.4	17.5	89	77
September	19.3	25.5	13.4	88	76
October	12.8	19.6	6.3	69	55
November	7.3	13.3	1.6	85	61
December	2.2	7.3	-2.5	69	34
Average ([a]) or Sum ([s])	12.4[a]	18.4[a]	6.7[a]	971[s]	617[s]

Table 4-2. Performance criteria for calibration and validation of the Occoquan Model.

Procedure	Performance Criteria	Streamflow Station				
		ST25	ST30	ST45	ST60	ST70
Calibration	R^2	0.85	0.85	0.90	0.86	0.77
	NSE	0.81	0.85	0.87	0.83	0.75
	PBIAS	10.5	2.7	6.3	6.8	8.0
	RSR	0.44	0.39	0.36	0.41	0.50
Validation	R^2	0.82	0.88	0.84	0.84	0.76
	NSE	0.88	0.84	0.84	0.90	0.86
	PBIAS	-5.3	18.6	6.6	-6.1	4.3
	RSR	0.44	0.46	0.44	0.41	0.50

Table 4-3. GCM used in this study.

Model Name	Agency/Organization	Country
CSIRO MK3	Australia's Commonwealth Scientific and Industrial Research Organization	Australia
GFDL CM2.0	Geophysical Fluid Dynamics Laboratory	USA
MPIM:ECHAM5	Max Planck Institute for Meteorology	Germany
MRI-CGCM2.3.2	Meteorological Research Institute, Japan Meteorological Agency	Japan

Table 4-4. Climate variables used in this study.

Predictor Variables	Precipitation
	Surface Air Temperature
	Maximum Surface Air Temperature
	Minimum Surface Air Temperature
	Wind

Table 4-5. Time horizons for observed and GCM data.

Model set		Period	Abbreviation used in this paper
Observed		1981-2000	Baseline
GCM	Historical	1981-2000	20c3m
	Future	2046-2065	F1
		2081-2100	F2

Table 4-6. Developed themes for assessing the impacts of climate change and land use change.

Theme	Climate	Land Use
1	Present	Present
2	Future	Present
3	Present	Future
4	Future	Future

Table 4-7. Streamflow characteristics caused by climate change and land use change in mid and later 21st century.

Alteration Index	Subwatershed	Scenario											
		F1 (2046-2065)						F2 (2081-2100)					
		CC (A2)	CC (B1)	LUC (A2)	LUC (B1)	CC+LUC (A2)	CC+LUC (B1)	CC (A2)	CC (B1)	LUC (A2)	LUC (B1)	CC+LUC (A2)	CC+LUC (B1)
% Change in median of mean annual flow	Bull Run	1.8	1.7	13	18	16	21	0.47	-0.53	19	23	23	24
	Occoquan Creek	2.1	-0.22	73	72	78	74	-3.7	1.3	76	73	74	77
% Change Q_{IQR}	Bull Run	17	15	13	18	25	28	13	14	18	22	26	32
	Occoquan Creek	15	12	58	56	83	77	14	11	58	58	77	74
% Change Q_1	Bull Run	10	12	9	13	21	27	16	10	14	17	30	30
	Occoquan Creek	5	7	77	76	83	85	11	4	78	77	93	83
% Change Q_5	Bull Run	8	2	10	14	18	17	4	-2	15	18	20	15
	Occoquan Creek	12	-1	73	72	90	71	3	-2	77	73	82	69
% Change Q_{10}	Bull Run	15	9	12	17	27	26	13	13	19	23	34	35
	Occoquan Creek	11	7	73	73	92	83	8	9	74	73	90	89
% Change Q_{90}	Bull Run	-3	-4	17	22	16	21	-8	-3	26	30	20	28
	Occoquan Creek	-30	-26	190	194	139	146	-41	-35	219	193	122	124
% Change Q_{95}	Bull Run	-5	-4	17	23	14	19	-7	-4	24	28	19	27
	Occoquan Creek	-13	-12	268	294	225	223	-20	-14	239	282	209	212
% Change Q_{99}	Bull Run	-16	-7	13	16	-8	5	-16	-12	16	19	-4	2
	Occoquan Creek	-31	-26	238	225	165	183	-39	-28	277	235	137	160

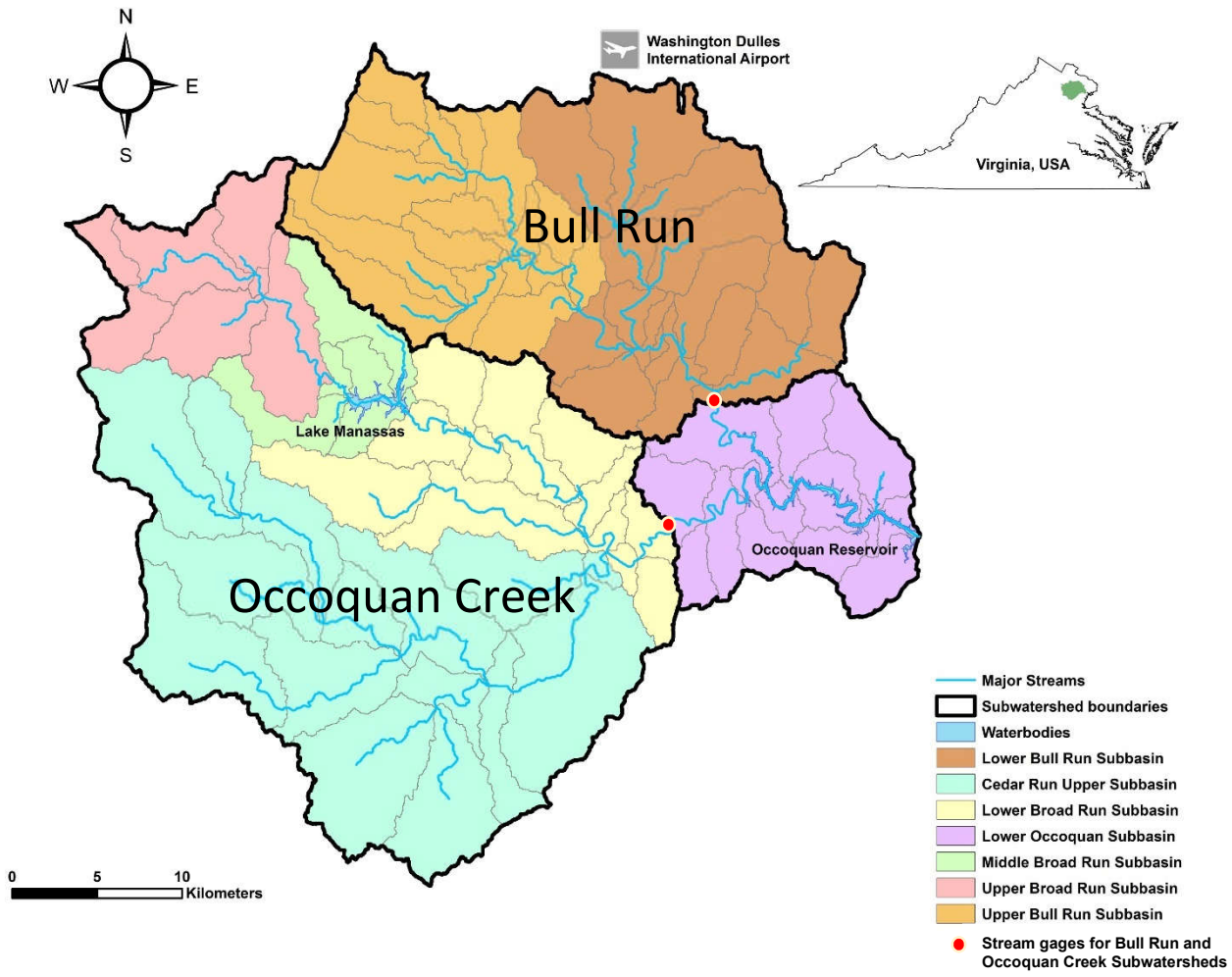

Figure 4-1. Occoquan watershed with major streams and subbasins.

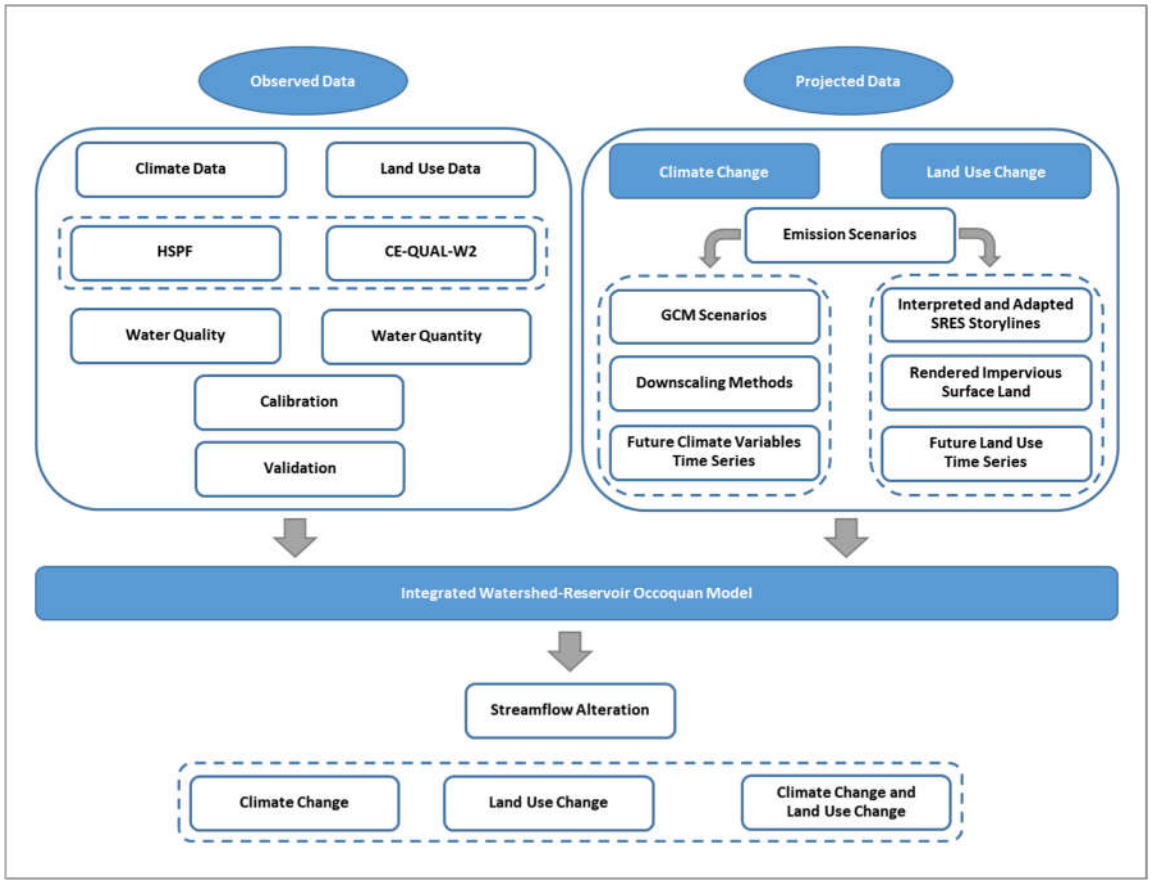

Figure 4-2. Designed study framework for quantifying streamflow alteration due to the climate change and land use change in the study area.

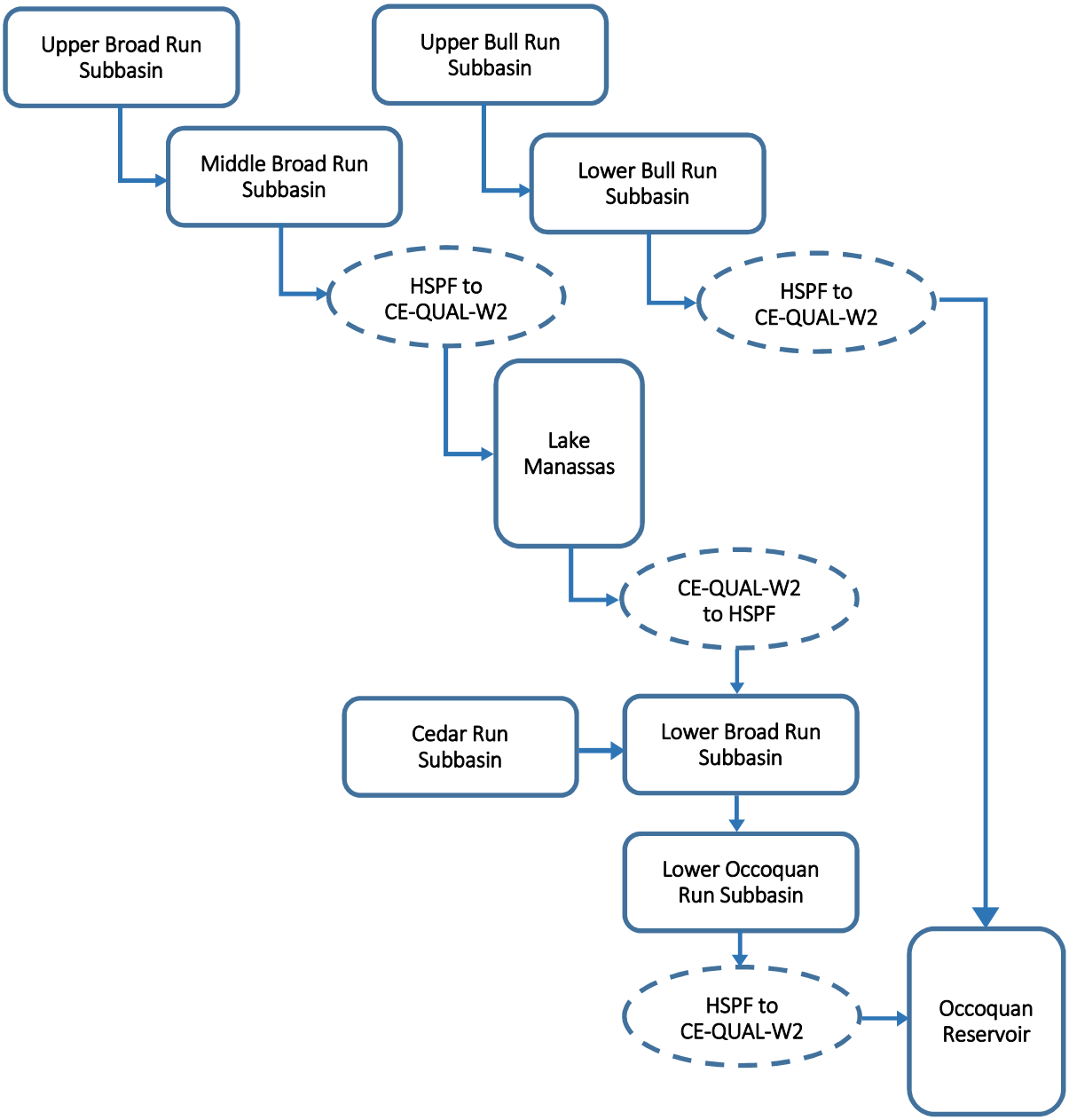

Figure 4-3. Schematic of Occoquan linked watershed-reservoir model.

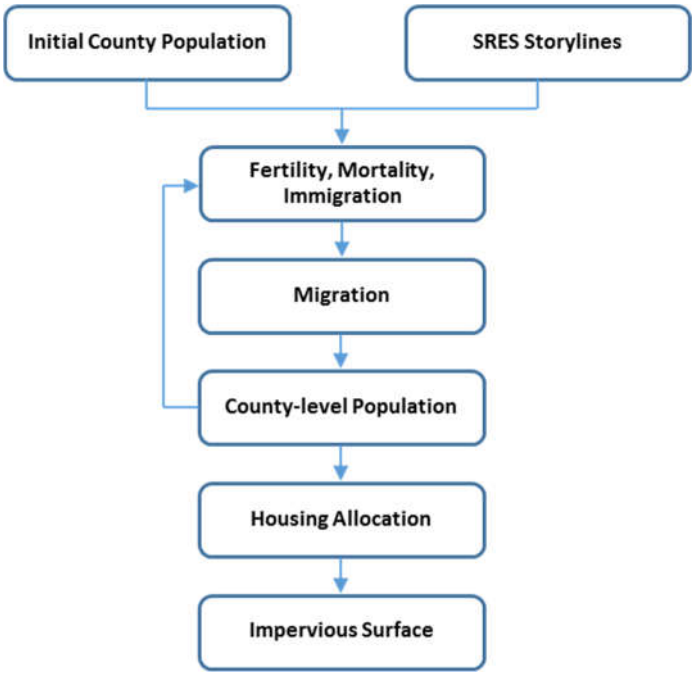

Figure 4-4. Overview of ICLUS modeling process (Bierwagen and Morefield 2014).

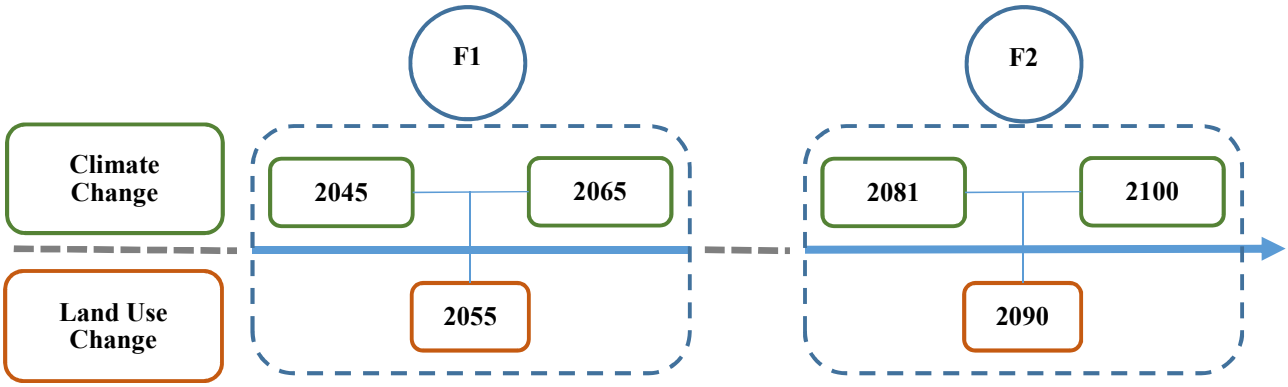

Figure 4-5. Future climate change (green) and land use change (orange) horizons for two future time periods (2046-2065 (F1) and 2081-2100 (F2)).

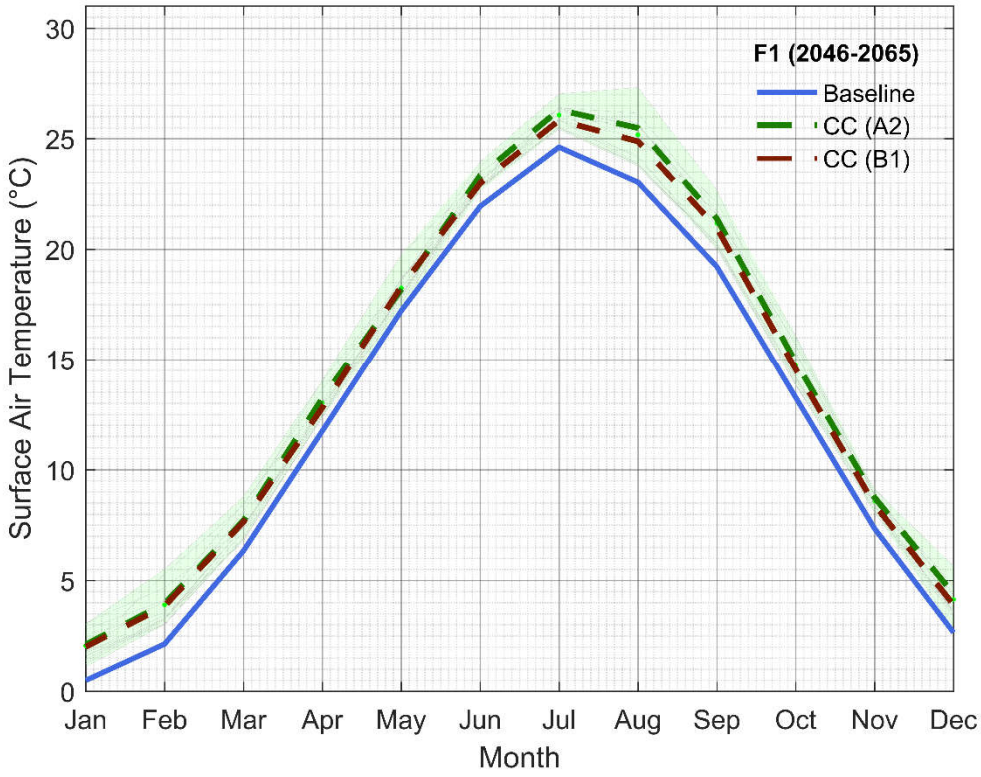

Figure 4-6. Monthly variations of projected Climate Change (CC) surface air temperatures for the mid 21st century (F1). The solid blue line represents the historical values and the light green shaded area envelopes the possible maximums and minimums of the projections while the dashed lines are depicting the medians of climate change projected surface air temperatures categorized based on A2 and B1 emission scenarios.

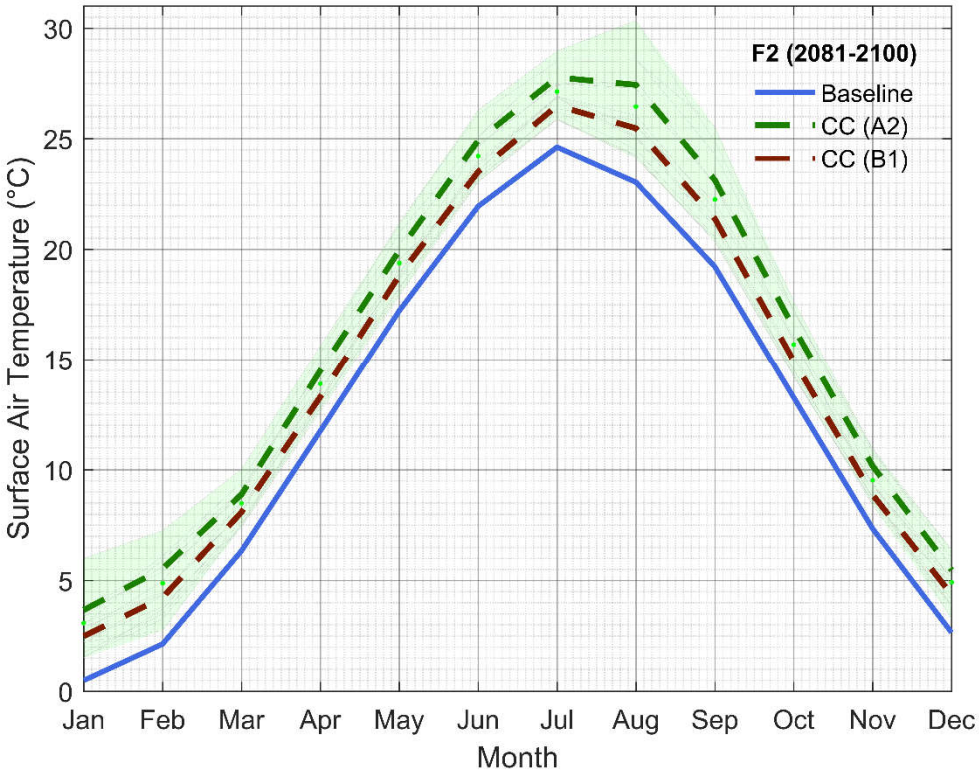

Figure 4-7. Monthly variations of projected Climate Change (CC) surface air temperatures for the late 21st century (F2). The solid blue line represents the historical values and the light green shaded area envelopes the possible maximums and minimums of the projections while the dashed lines are depicting the medians of climate change projected surface air temperatures categorized based on A2 and B1 emission scenarios.

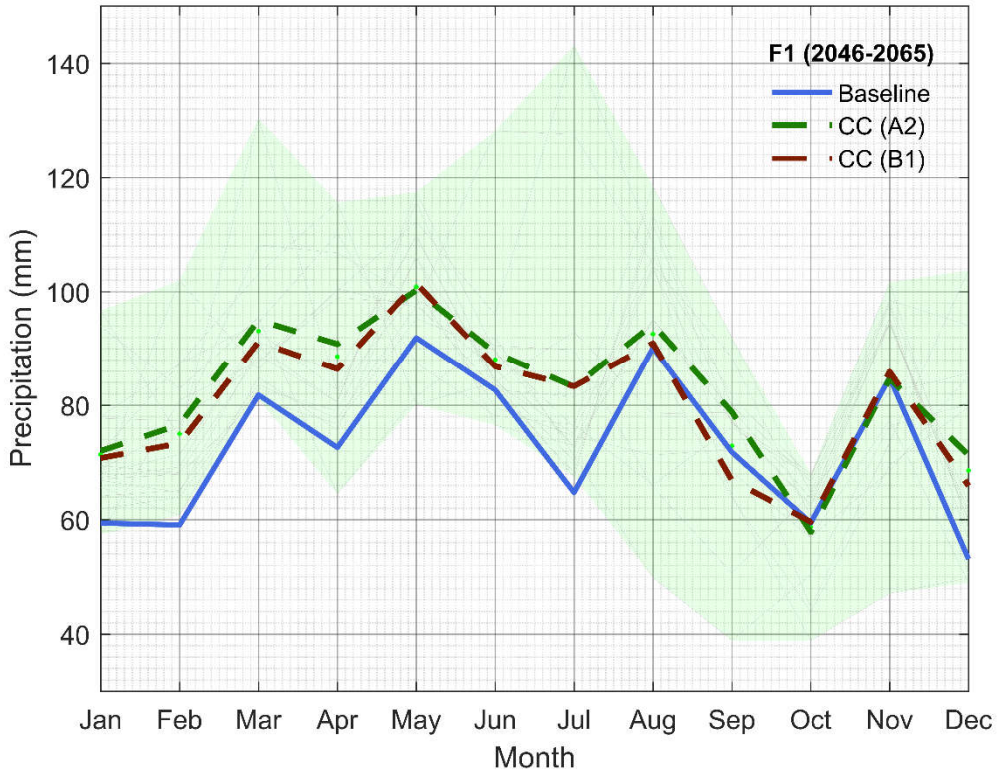

Figure 4-8. Monthly variations of projected Climate Change (CC) precipitations for the mid 21st century (F1). The solid blue line represents the historical values and the light green shaded area envelopes the possible maximums and minimums of the projections while the dashed lines are depicting the medians of climate change projected precipitations categorized based on A2 and B1 emission scenarios.

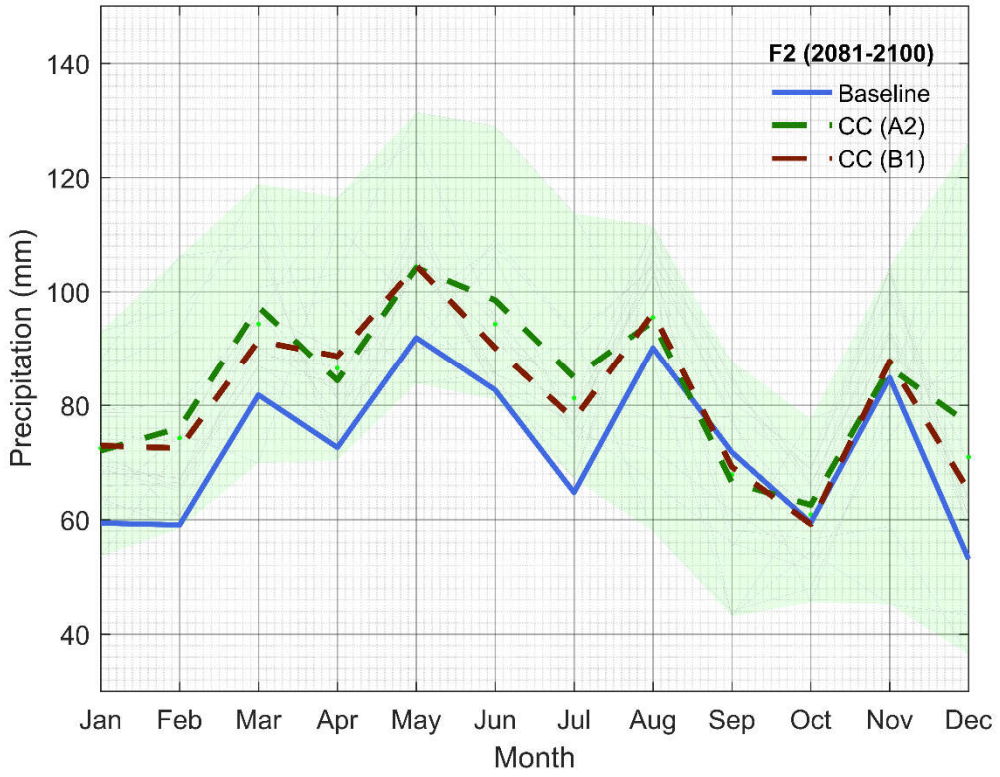

Figure 4-9. Monthly variations of projected Climate Change (CC) precipitations for the late 21st century (F2). The solid blue line represents the historical values and the light green shaded area envelopes the possible maximums and minimums of the projections while the dashed lines are depicting the medians of climate change projected precipitations categorized based on A2 and B1 emission scenarios.

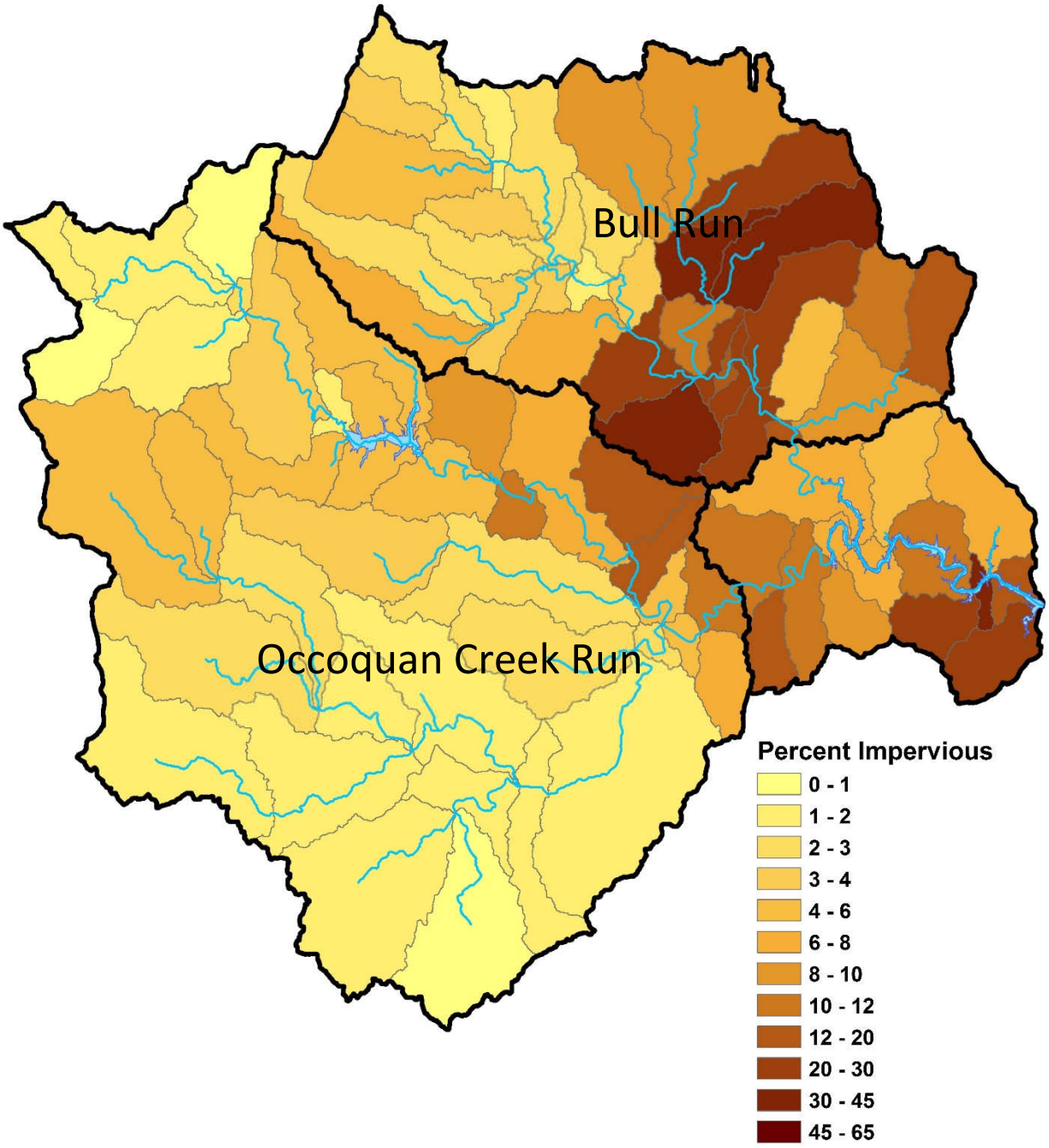

Figure 4-10. Estimate percent impervious surface areas for Occoquan watershed in the historical period. Further delineation (gray lines) was carried out based on 1) rainfall or important meteorological data; 2) soil type; 3) land use conditions; 4) reach characteristics; 5) any other important physical characteristic (infiltration, overland slope, etc.) (Xu et al. 2007).

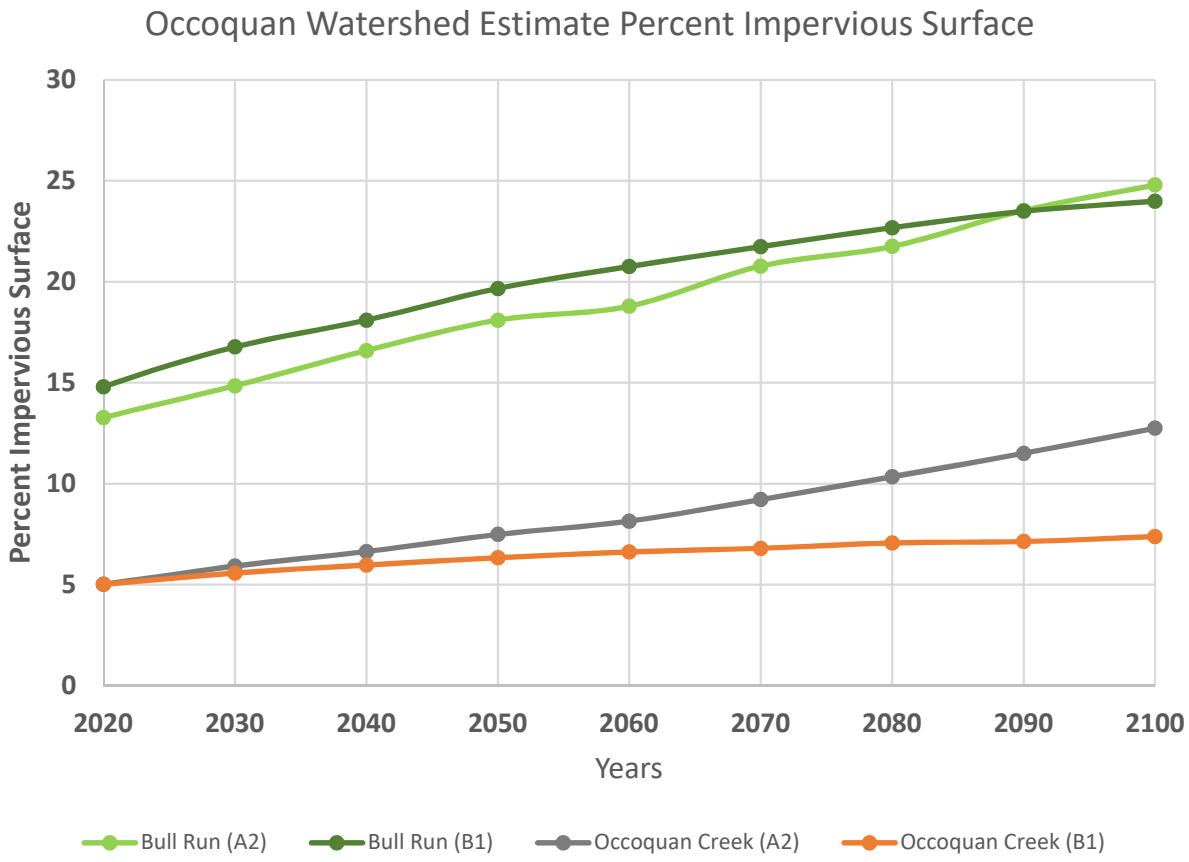

Figure 4-11. Estimate percent impervious surface for Occoquan watershed for future projections in Bull Run and Occoquan Creek using A2 and B1 emission scenarios.

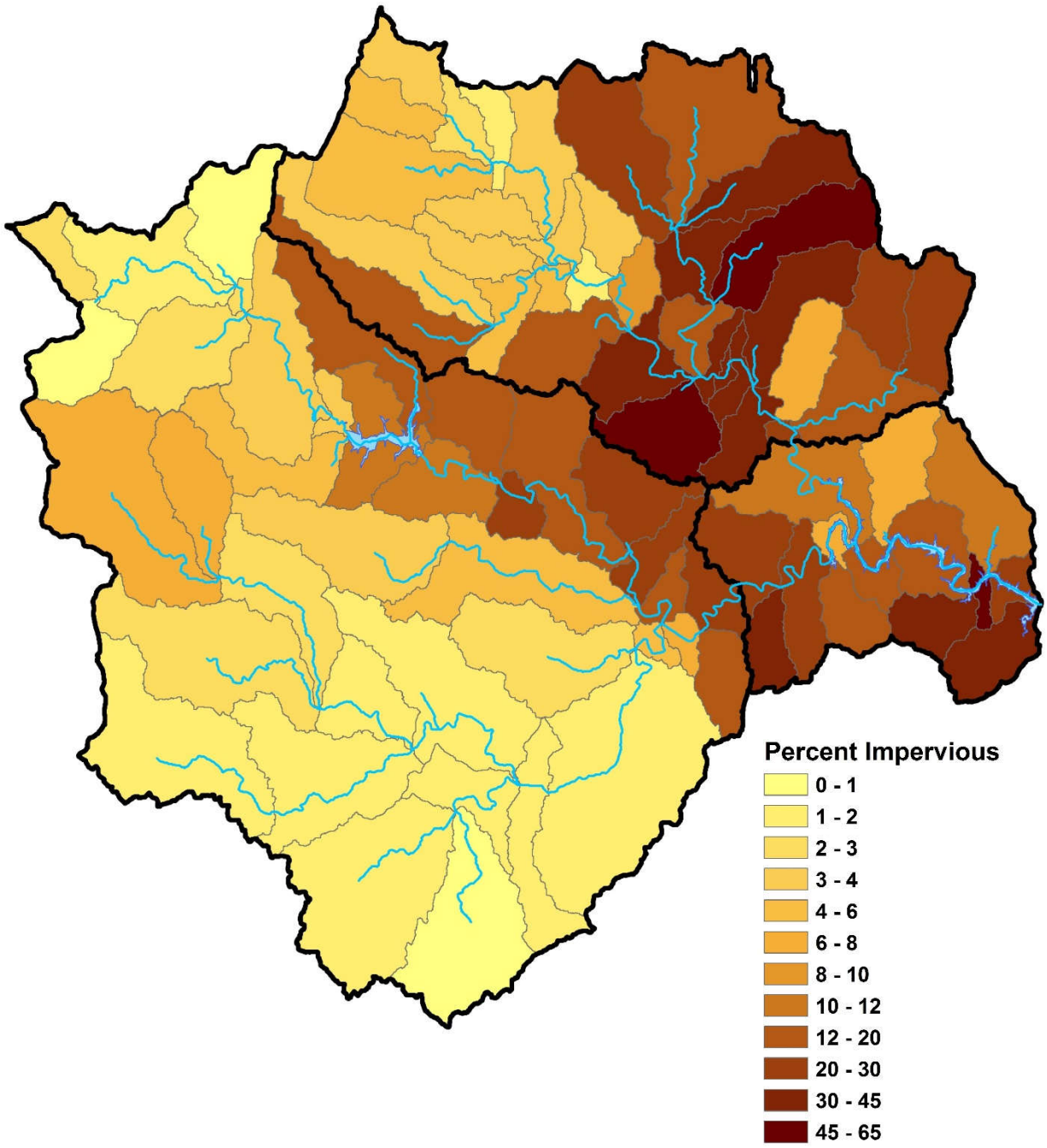

Figure 4-12. Estimate percent impervious surface areas in Occoquan watershed for middle of mid 21st period (2055) using A2 emission scenario.

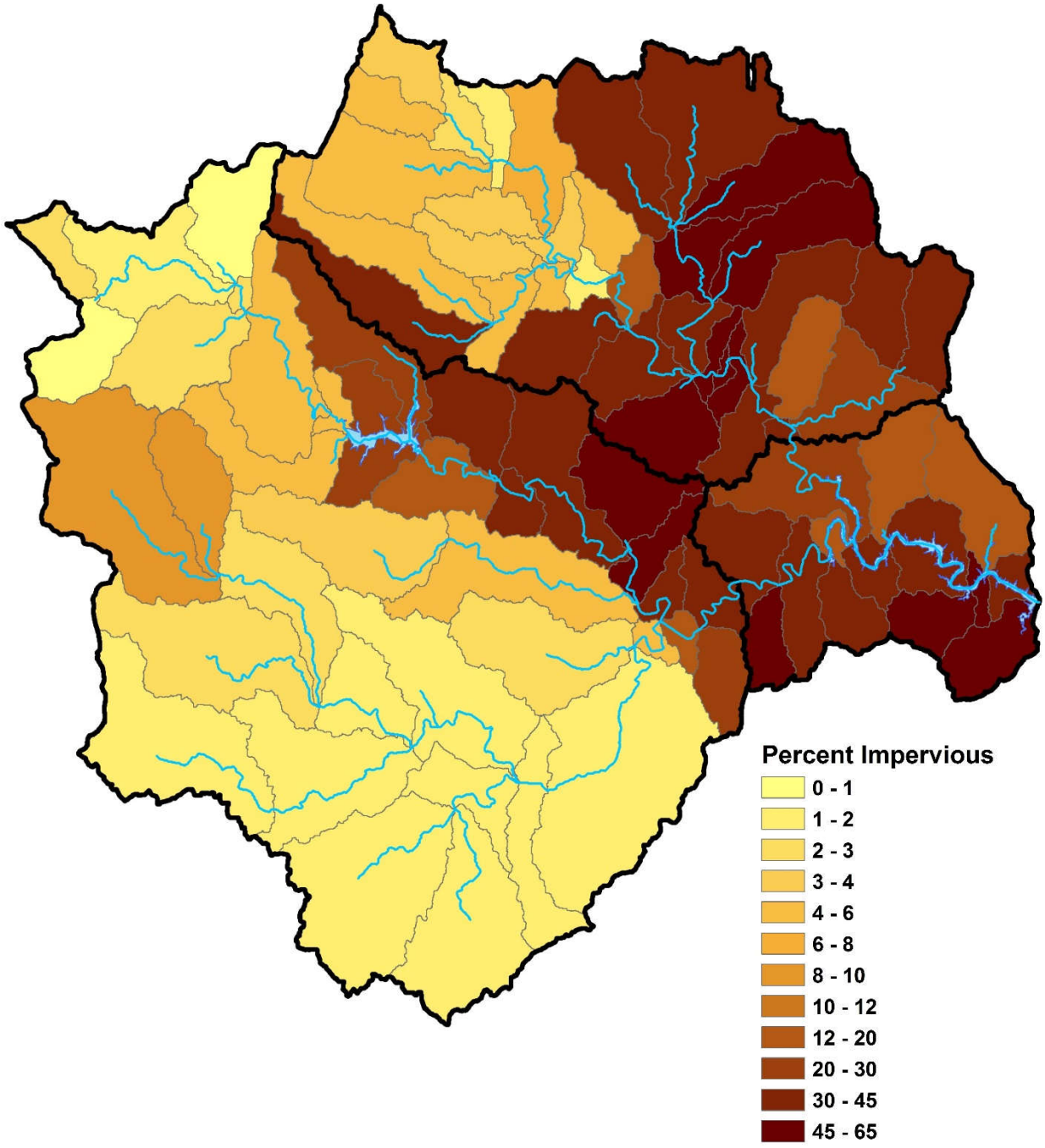

Figure 4-13. Estimate percent impervious surface areas in Occoquan watershed for middle of later 21st period (2090) using A2 emission scenario.

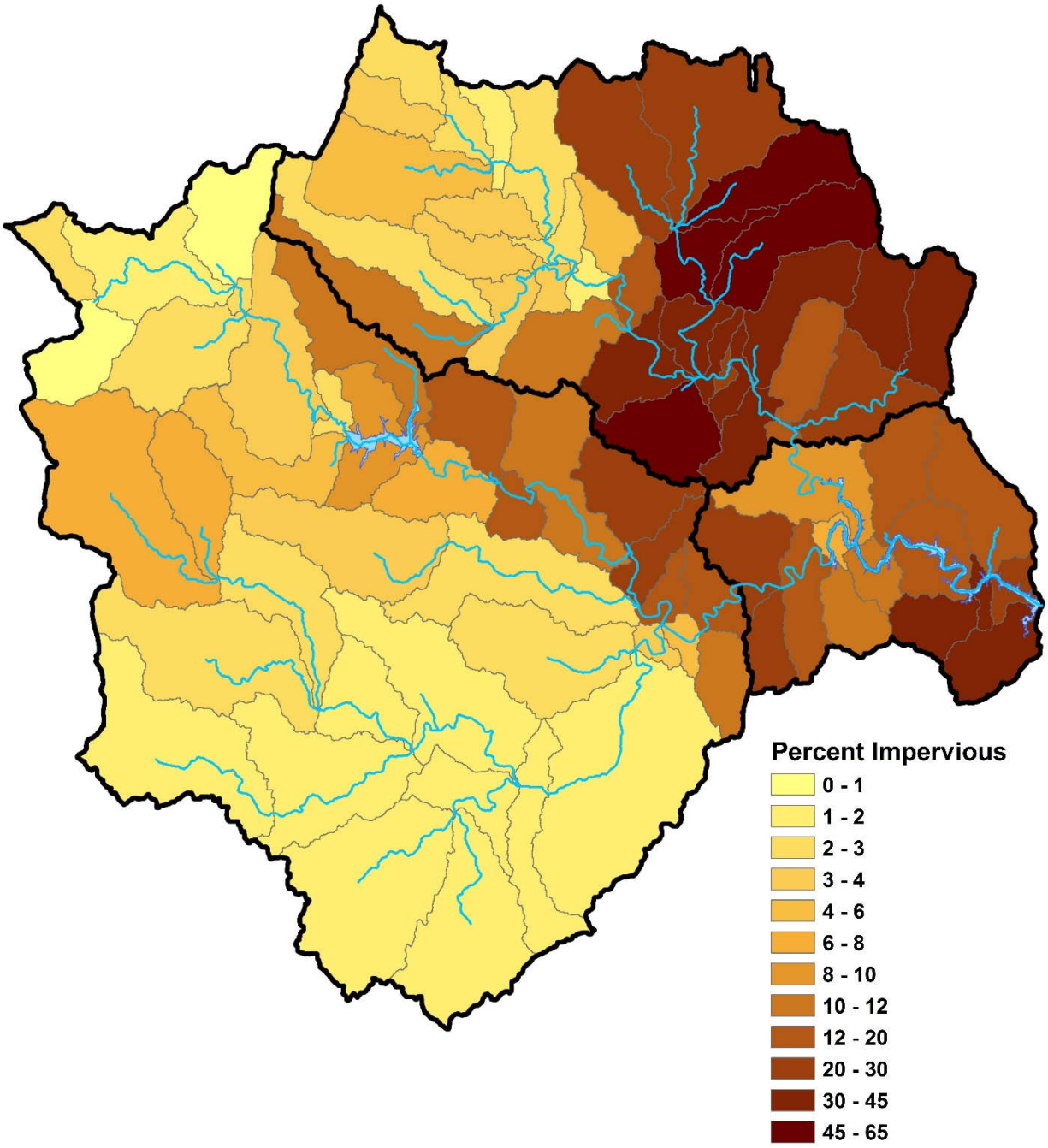

Figure 4-14. Estimate percent impervious surface areas in Occoquan watershed for middle of mid 21st period (2055) using B1 emission scenario.

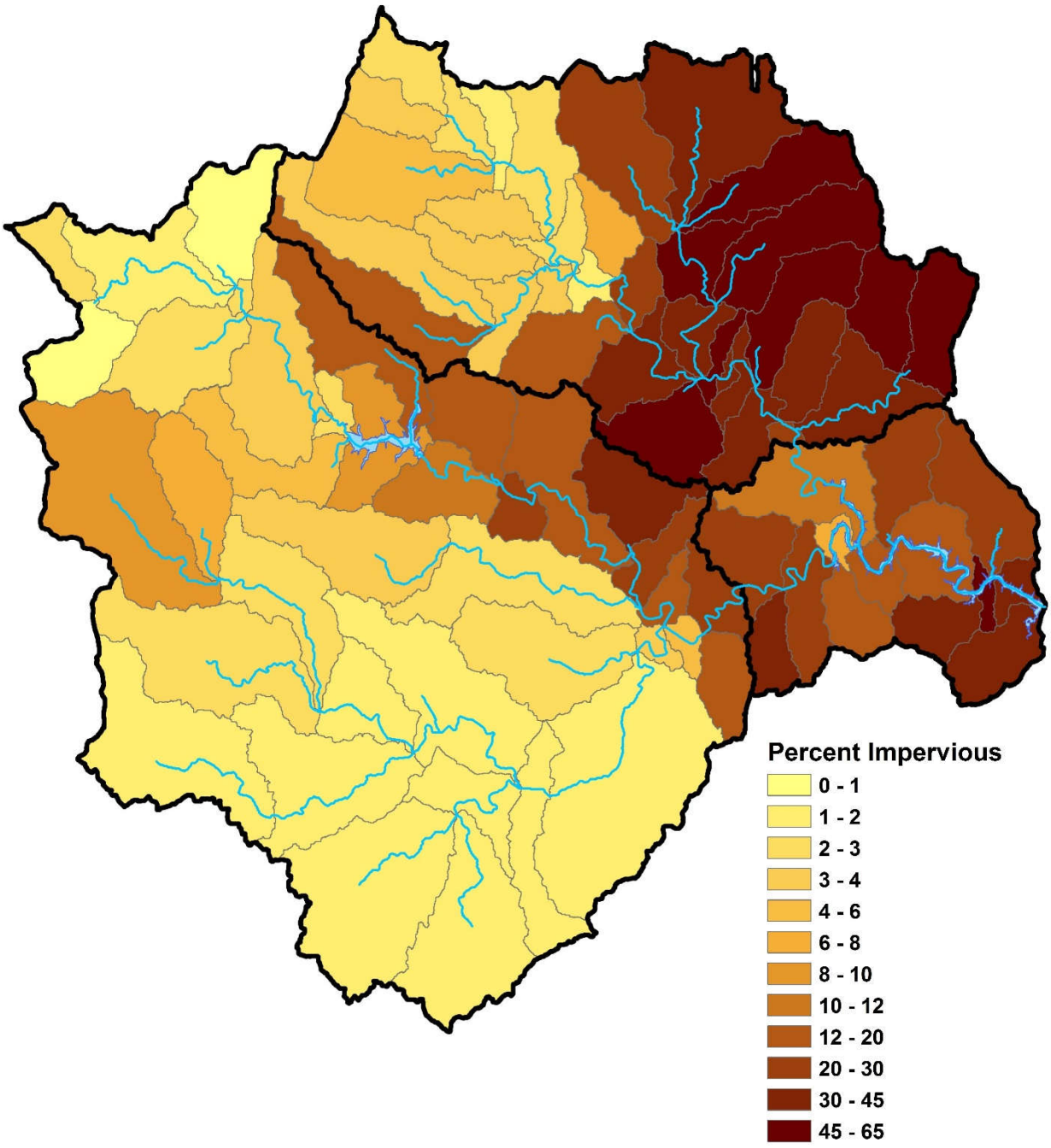

Figure 4-15. Estimate percent impervious surface areas in Occoquan watershed for middle of late 21st period (2090) using B1 emission scenario.

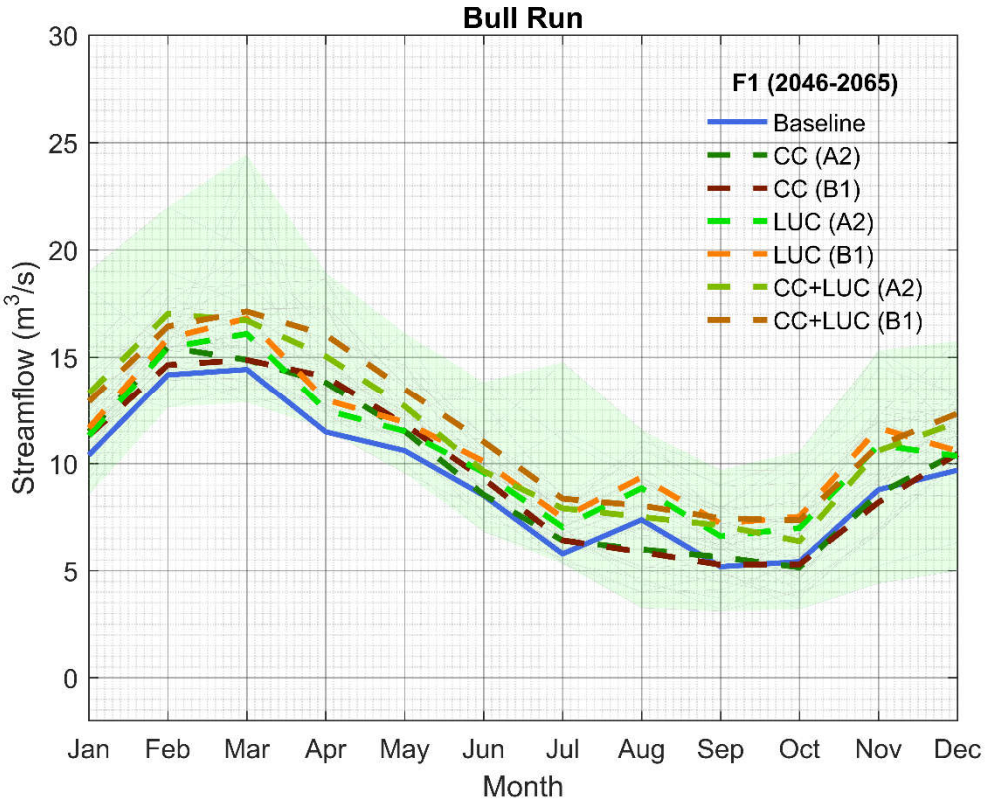

Figure 4-16. Median of monthly variations of flows using Climate Change (CC), Land Use Change (LUC) and combined (CC+LUC) effects for Bull Run in mid 21st century (2046-2065). The solid blue line represents the historical values and the light green shaded area envelopes the possible maximums and minimums of the projections while the dashed lines are depicting the medians of models grouped based on climate change and land use change projections and A2 and B1 emission scenarios.

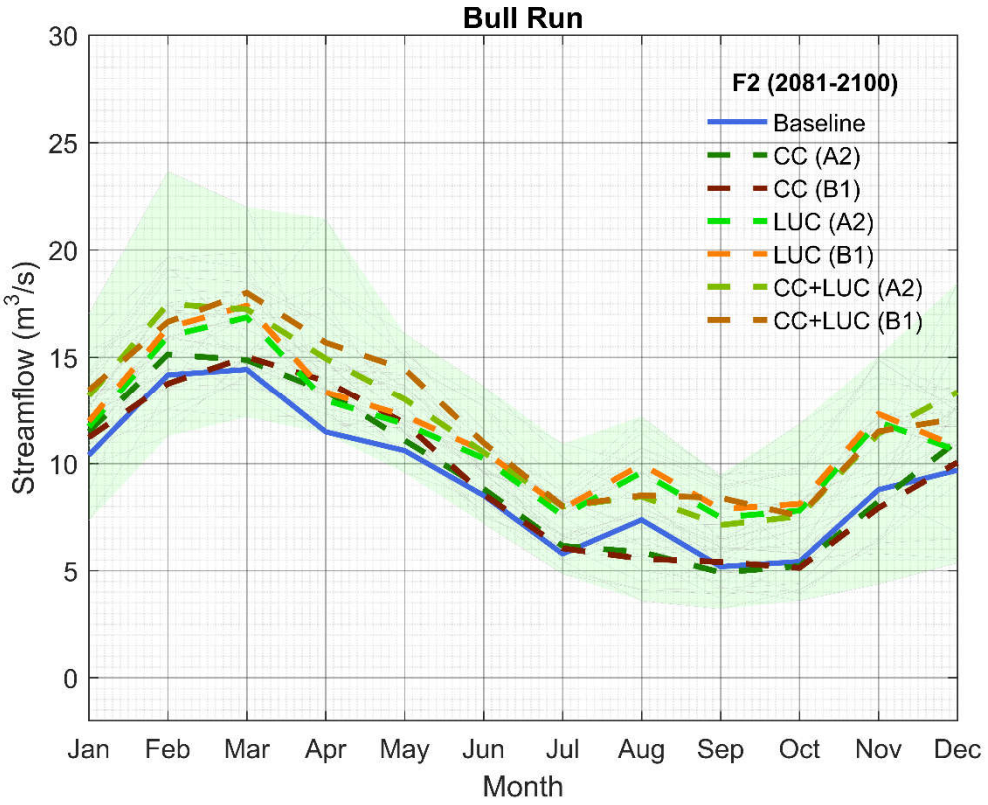

Figure 4-17. Median of monthly variations of flows using Climate Change (CC), Land Use Change (LUC) and combined (CC+LUC) effects for Bull Run in late 21st century (2081-2100). The solid blue line represents the historical values and the light green shaded area envelopes the possible maximums and minimums of the projections while the dashed lines are depicting the medians of models grouped based on climate change and land use change projections and A2 and B1 emission scenarios.

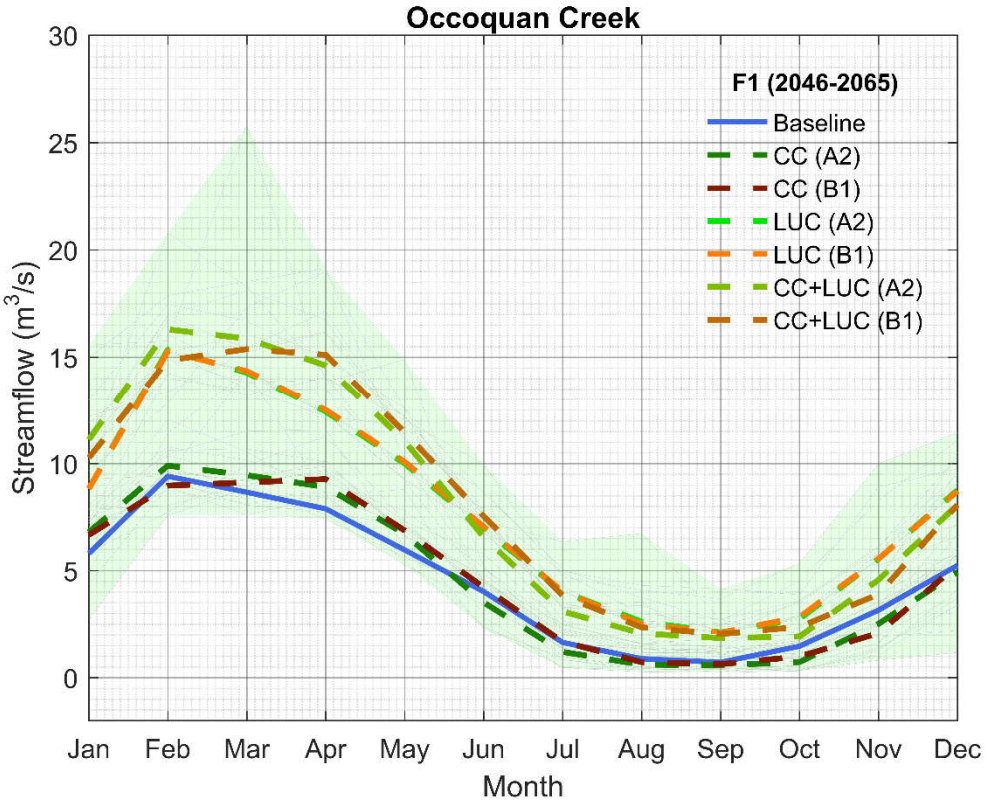

Figure 4-18. Median of monthly variations of flows using Climate Change (CC), Land Use Change (LUC) and combined (CC+LUC) effects for Occoquan Creek in mid 21st century (2046-2065). The solid blue line represents the historical values and the light green shaded area envelopes the possible maximums and minimums of the projections while the dashed lines are depicting the medians of models grouped based on climate change and land use change projections and A2 and B1 emission scenarios.

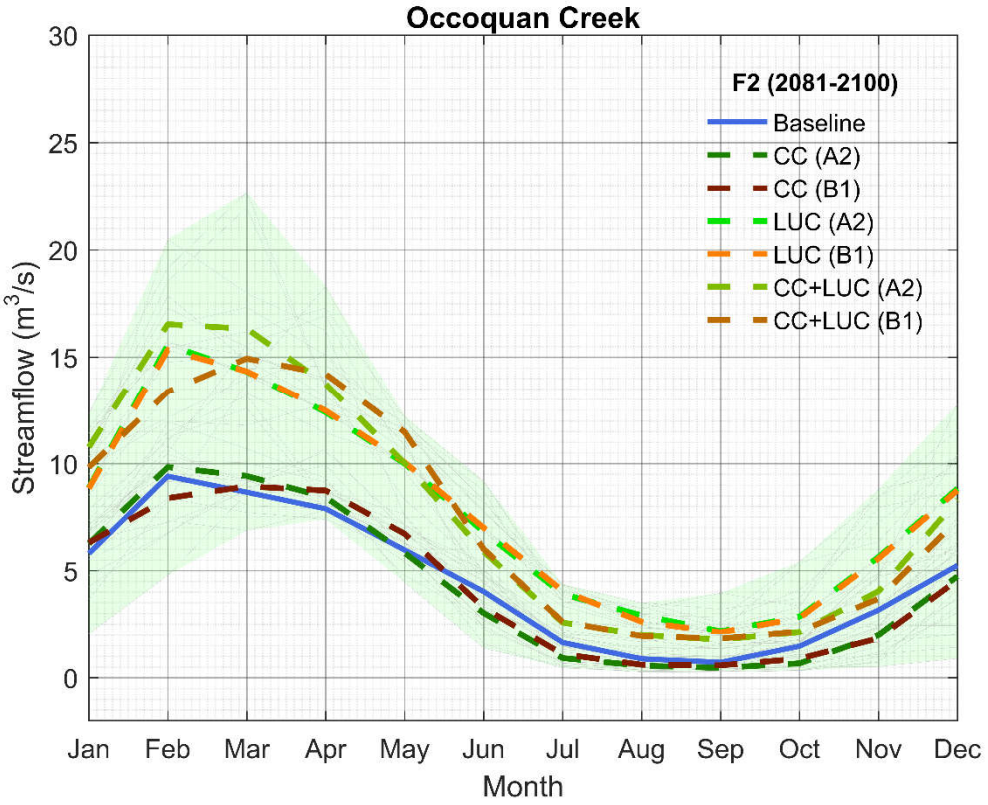

Figure 4-19. Median of monthly variations of flows using Climate Change (CC), Land Use Change (LUC) and combined (CC+LUC) effects for Occoquan Creek in late 21st century (2081-2100). The solid blue line represents the historical values and the light green shaded area envelopes the possible maximums and minimums of the projections while the dashed lines are depicting the medians of models grouped based on climate change and land use change projections and A2 and B1 emission scenarios.

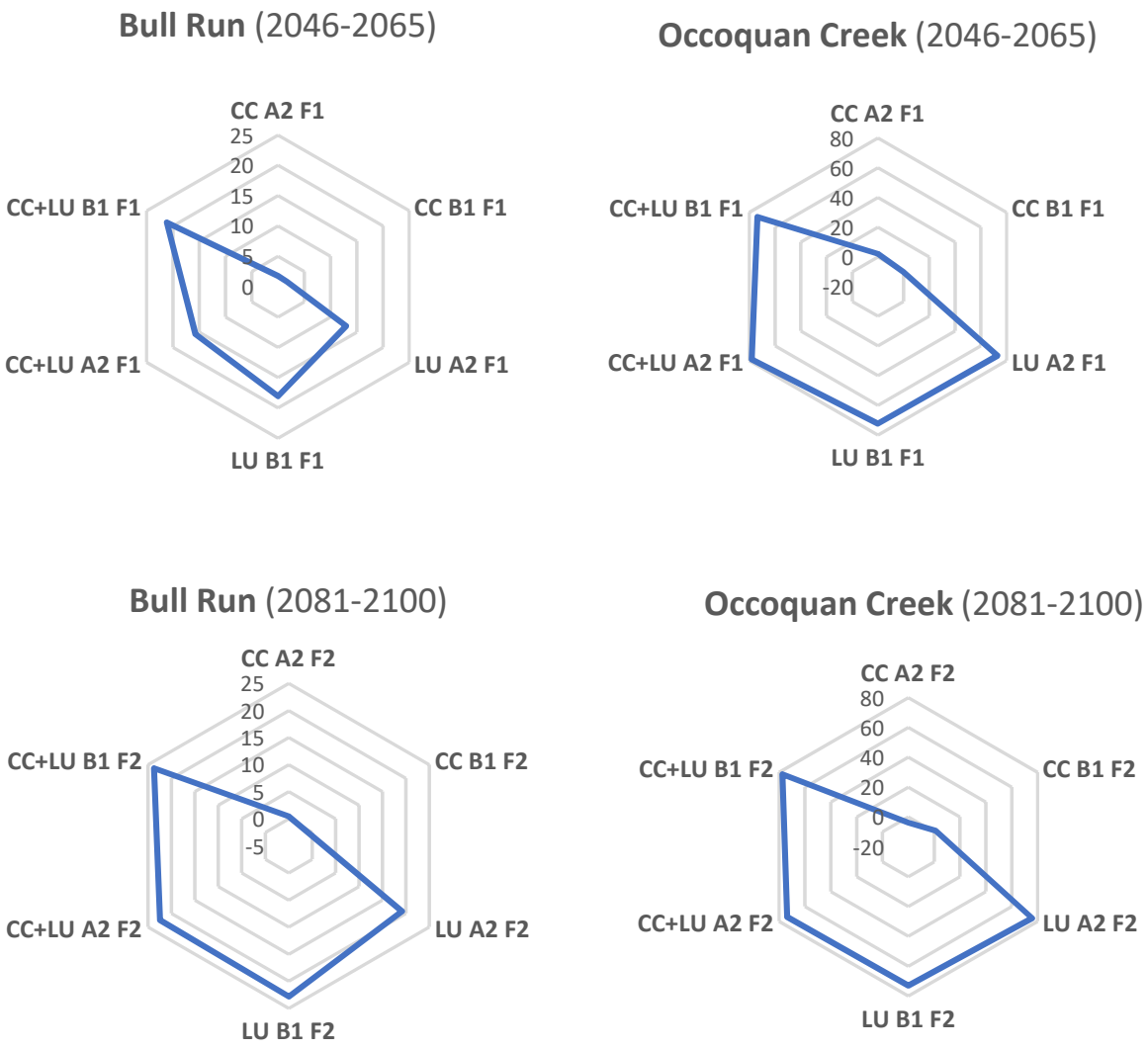

Figure 4-20. Median of monthly variations of flows for Bull Run and Occoquan Creek grouped based on Climate Change (CC), Land Use Change (LUC) and combined effects (CC+LUC) and A2 and B1 emission scenarios in mid and late 21st century (2046-2065 (F1) and 2081-2100 (F2)).

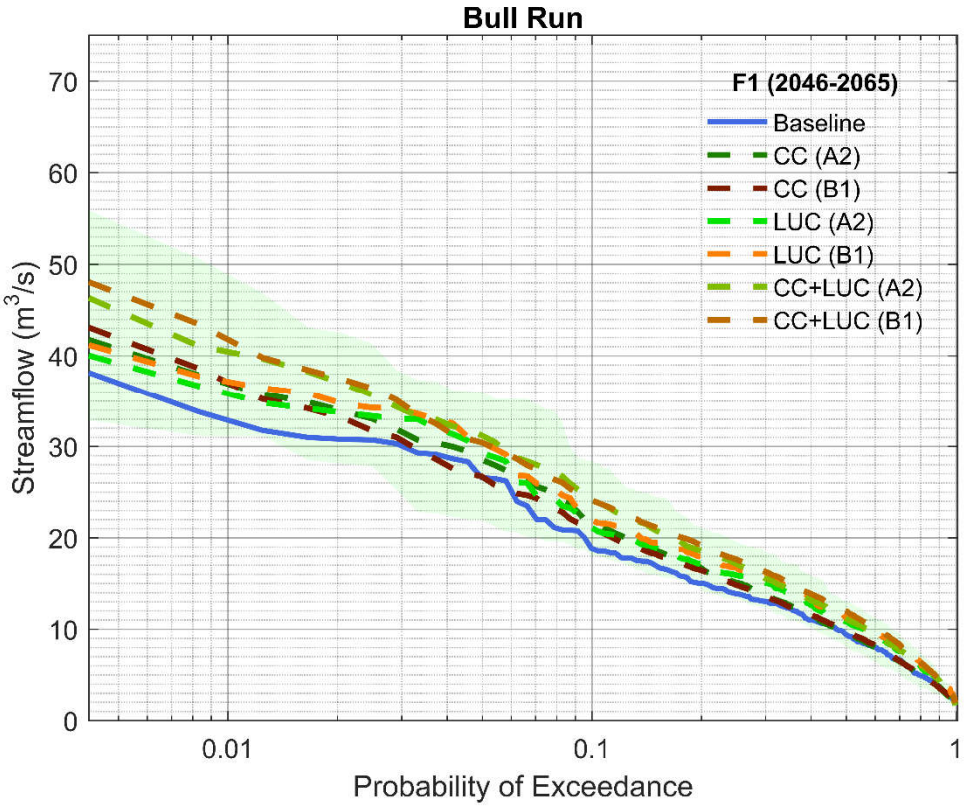

Figure 4-21. Flow duration curves for Bull Run using Climate Change (CC), Land Use Change (LUC) and combined (CC+LUC) effects in mid 21st century (2046-2065). The solid blue line represents the historical values and the light green shaded area envelopes the possible maximums and minimums of the projections while the dashed lines are depicting the medians of models grouped based on climate change and land use change projections and A2 and B1 emission scenarios.

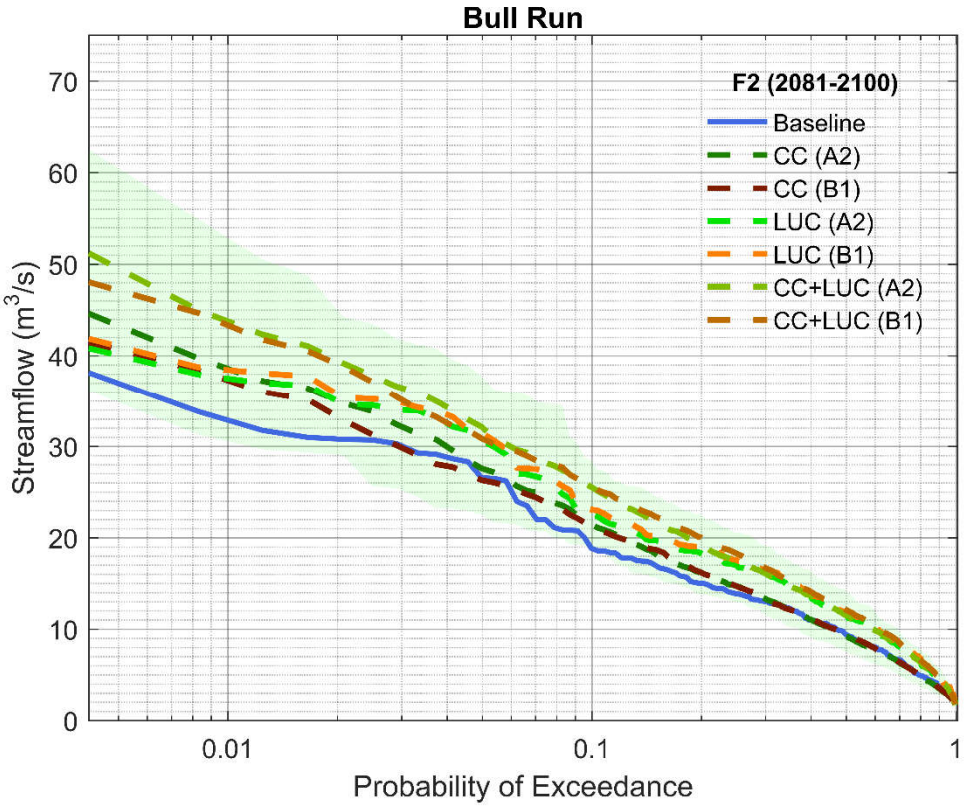

Figure 4-22. Flow duration curves for Bull Run using Climate Change (CC), Land Use Change (LUC) and combined (CC+LUC) effects in mid late century (2081-2100). The solid blue line represents the historical values and the light green shaded area envelopes the possible maximums and minimums of the projections while the dashed lines are depicting the medians of models grouped based on climate change and land use change projections and A2 and B1 emission scenarios.

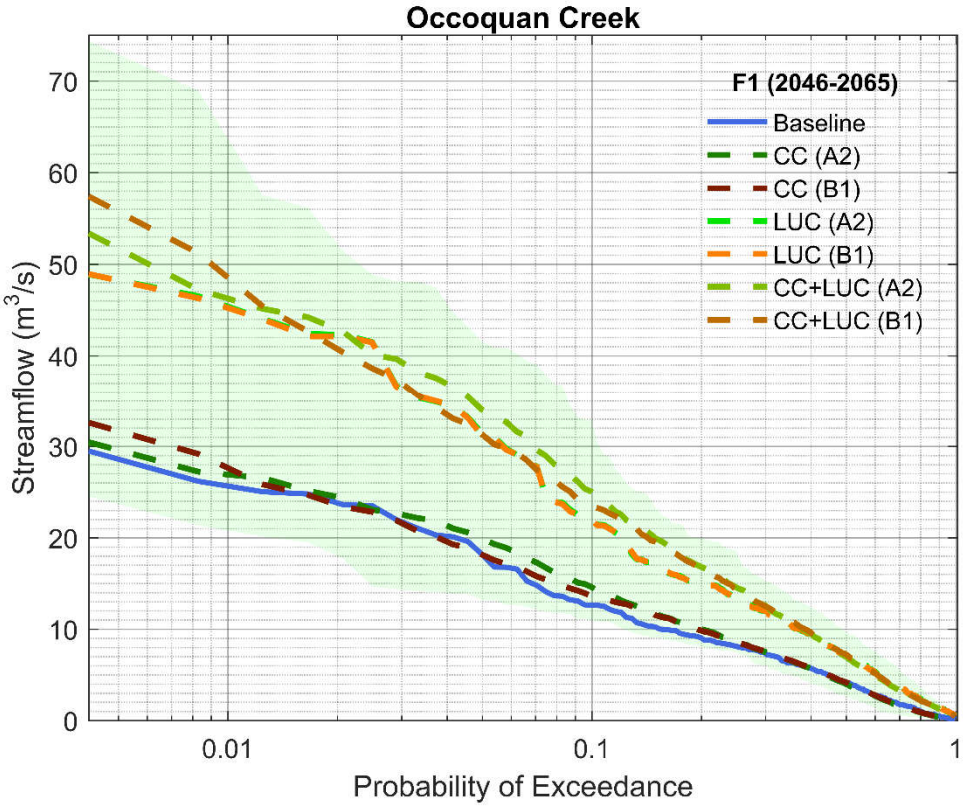

Figure 4-23. Flow duration curves for Occoquan Creek using Climate Change (CC), Land Use Change (LUC) and combined (CC+LUC) effects in mid 21st century (2046-2065). The solid blue line represents the historical values and the light green shaded area envelopes the possible maximums and minimums of the projections while the dashed lines are depicting the medians of models grouped based on climate change and land use change projections and A2 and B1 emission scenarios.

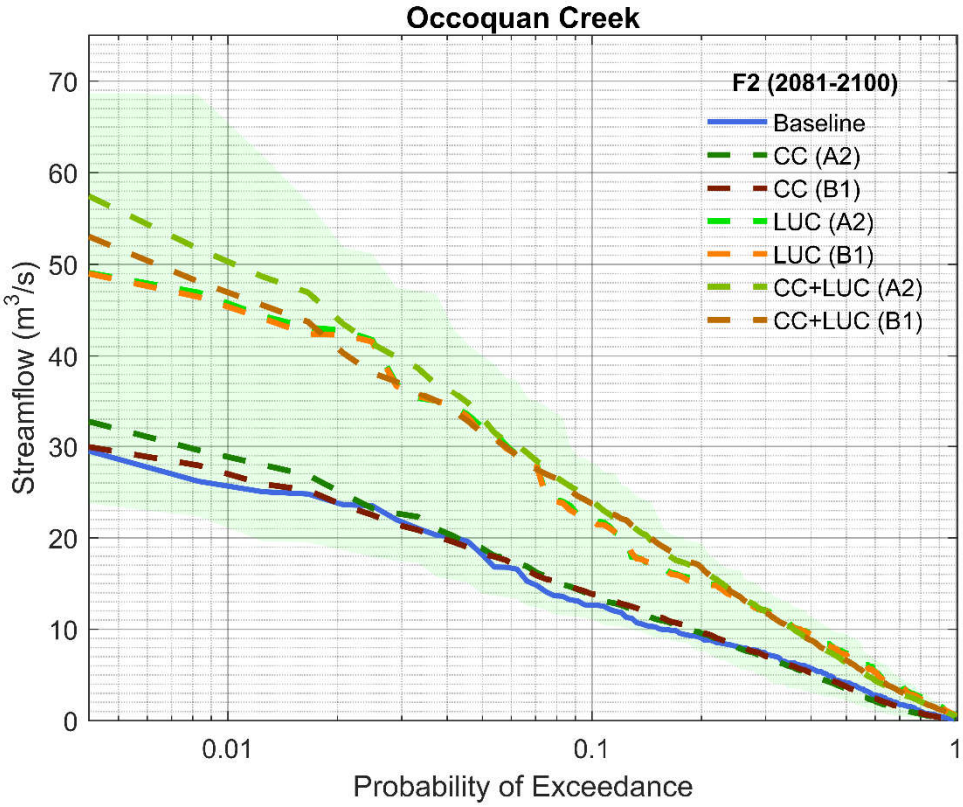

Figure 4-24. Flow duration curves for Occoquan Creek using Climate Change (CC), Land Use Change (LUC) and combined (CC+LUC) effects in late 21st century (2081-2100). The solid blue line represents the historical values and the light green shaded area envelopes the possible maximums and minimums of the projections while the dashed lines are depicting the medians of models grouped based on climate change and land use change projections and A2 and B1 emission scenarios.

Chapter 5 Climate Change and Land Use Change Impacts on Water Quality in the Occoquan Reservoir, Virginia, USA

Ayden A. Baran[1]; Adil N. Godrej[2]; Glenn E. Moglen[3]
Occoquan Watershed Monitoring Laboratory, 9408 Prince William Street, Manassas, VA 20110, U.S.A.

[1]Ph.D. Candidate, Occoquan Watershed Monitoring Laboratory, Virginia Tech, Manassas, VA, USA, (corresponding author). Email: abaran@vt.edu,

[2]Research Associate Professor, Occoquan Watershed Monitoring Laboratory, Virginia Tech, Manassas, VA, USA.

[3] Supervisory Research Hydrologist, USDA-ARS Hydrology and Remote Sensing Laboratory, Beltsville, MD, USA,

To be submitted to the *International Journal on Ecological Modelling and Systems Ecology*

5.1 Abstract

Climate change and land use change are two major driving forces that can change water quality in lakes and reservoirs. This paper studies the singly and jointly impacts of climate change and land use change in the Occoquan reservoir located in northern Virginia. The combination of these two driving forces has created four themes, and an integrated complexly-linked watershed-reservoir model was used to run the simulations.

Ensembles of climate change projections were created using two emission scenarios, four GCMs, and two downscaling methods for two periods (i.e. 2046-2065 and 2081-2100). Climate change is projected to increase surface water temperatures in the study area. Moreover, shifts in precipitation patterns are likely to change the hydrological processes and inflows to the Occoquan reservoir. Specifically, the high flows are projected to increase while the low flows are expected to decrease.

Moreover, the study area has experienced rapid population growth and urbanization during the last few decades. These increases in population and urbanization are projected to continue and were simulated using two SRES storylines for the mid and late 21st century (2046-2065 and 2081-2100). Land use change projections were simulated to account for the anticipated increase of inflows into the Occoquan reservoir.

The combined effects of climate change and land use change synergistically amplify the changes in water quality characteristics. However, climate change tends to dampen the impact of land use change on the surface water dissolved oxygen levels. Results show that land use change tends to have a stronger impact than climate change. Stratification is anticipated to intensify. This increase in metalimnion thickness will be more noticeable in summer months and may result in a stronger hypolimnion and higher stability of thermocline.

The outcome of this study, an integrated modeling system for analyzing the individual and combined impacts of climate change and land use change, emphasizes the importance of planned urbanization and adequate water infrastructure development. The methodology used in this paper can assist regional water resources managers in future planning, integrated adaptation, and mitigation strategies, especially for the protection and preservation of natural water resources and their ecosystems.

Keywords: Climate change; land use change; scenario development; water quality; water resources management

5.2 Introduction

In the global scale, freshwater supplies are experiencing accelerated rates of quantitative and qualitative degradation (Wetzel 1992). In specific, waterbodies are facing human-induced stressors such as growing urbanization, climate change, and a lack of water management policies and institutional framework (Malsy et al. 2017; Syaukat 2012). The growth of population and urbanization not only affects water supply demand patterns and environmental resource utilization but also influences qualitative characteristics of the receiving waterbodies and metabolic responses of aquatic ecosystems (Wetzel 2001). Climate change, as an indirect imposed anthropogenic stressor, can reduce water quality in freshwater resources by modifications in thermal and mixing dynamics caused by alterations in atmospheric patterns. Many researchers have only addressed the individual impacts of climate change or land use change on water quality in receiving waterbodies (Butcher et al. 2015; Calder et al. 1995; Chang et al. 2015; Roberts and Prince 2010; Schwefel et al. 2016; Taner et al. 2011). The combined impacts of climate change and land use change on water quality in lakes and reservoirs have been an interest to researchers as well as water resource managers. However, changes in water quality characteristics and alterations in the response of waterbodies to the physical and

hydroclimatic modulations are not well understood (Butcher et al. 2015). In this context, Records et al. (2014) investigated the effects of climate change and wetland loss on water quality in a river in the western United States. They concluded that the impact of climate change on water quality could be comparable to past conditions. However, the combined effects of climate change and wetland loss can distinctively increase nutrient loads.

Mehdi et al. (2015) used an ensemble of seven climate models with two emission scenarios and three agricultural land use change scenarios to evaluate the effects of climate change and land use change on streamflow water quality in Bavaria, Germany in the mid 21st century. They found that although climate change alone can increase nitrogen loads and decrease phosphorus loads to some degree, the combination of climate change and land use change can significantly increase nitrogen and phosphorous up to 3 and 8 folds, respectively. Bussi et al. (2017) coupled a land use allocation model with a water quality model and imposed future climatic modifications to assess the impact on land use and water quality for the river Thames catchment in the UK in the mid and late 21st century. They found that the average concentration of nitrate is likely to reduce while the average concentration of phosphorous is expected to steadily increase towards the end of the century.

Wang and Kalin (2017) applied four General Circulation Models (GCM), three emission scenarios, and three land use projections to study the combined effects of climate change and land use change on a watershed in southern Alabama, USA. They concluded that climate change and land use change have synergetic effects on water quality. If the effects of these components are in the same direction, they amplify each other, and if their effects are at the opposite direction, they offset each other. They also found that the combined effects have higher impacts than just the linear summation of each component.

Malsy et al. (2017) assessed the effects of climate change and socio-economic development on water quality in Selenga Basin. Selenga Basin is the main inflow contributor to the Lake Baikal. They used three water quality parameters and an integrated water resources model to estimate the loading and concentrations in the 2071-2100 period using three weather types (average, dry, and wet). They concluded that there would be a substantial increase in loading and concentration in the future scenario conditions. Couture et al. (2018) utilized a set of chain models consisting of a global climate model, hydrological model, catchment phosphorus (P) model, lake model, and

Bayesian Network to evaluate the individual effects of climate change and land use change in Lake Vansjø in southern Norway. Their results indicated that, in the future climate, the precipitation and runoff would increase, but these changes will not have a significant effect on the water quality in Lake Vansjø. On the other hand, future management and land-use can positively or negatively affect the lake's ecological status.

Bucak et al. (2018) studied the effects of climate change and land use change on phytoplankton and water quality in Lake Beyşehir, Turkey. They used five GCMs, two greenhouse gas concentration trajectories, and three different land use scenarios. They linked a catchment model to two different lake models to analyze these effects in two periods (2025–2034 and 2055–2064). Their findings revealed differences in the magnitude of lake models' outputs while the direction of changes was similar. Overall, they noticed decreases in inflows and nutrient loads into the lake. Moreover, they found minor changes in chlorophyll-A and an increased abundance of cyanobacteria in future scenarios, which may deteriorate the drinking water potential in Lake Beyşehir.

For the purposes of studying the impacts of climate change and land use change on water quality in the Occoquan reservoir located in the Occoquan watershed, an integrated modeling system approach was implemented to form an ensemble of scenarios with an objective to address the following questions: a) How will the water quality characteristics change if climate change and land use change are imposed separately or jointly? b) Which of these driving forces has a stronger effect? c) Will these driving forces exacerbate or offset their individual effects on the water quality characteristics?

5.3 Study Area and Observed Data

The Occoquan watershed is part of the Washington, DC metropolitan area (WMA) located in the Mid-Atlantic region of the United States, with four distinctive seasons (

Figure **5-1**). The average elevation of the Watershed is 300 meters with the total drainage area of 1,480 km² (570 mi²) that ends into Occoquan reservoir.

There are nine primary land use types in the study area with the following coverages, forest (57%), pasture (7%), high tillage cropland (5%), low tillage cropland (5%), townhouse/garden apartment (2%), low density residential (13%), medium density residential (6%),

industrial/commercial (4%), and institutional (1%), creating an overall 6% impervious surface areas. Approximately 35% of the soils are categorized as B for the SCS (Soil Conservation Society) hydrological soil group, which features a moderate infiltration rate when thoroughly wetted while the remainder of soil groups are A (10%), C (25%), D (20%) and the rest are water, swamps and alluvial lands (USDA 2017).

Rapid population growth in recent decades has been one of the primary contributors to land use change in northern Virginia. For instance, according to the United States Census Bureau, the population in one of the counties within the Occoquan watershed (Prince William County) has increased by 260% from 1970 to 2010. Urbanization is an ongoing theme in the study area which can greatly influence a watershed's response to precipitation (Leopold 1968).

Daily meteorological data are collected from 16 weather stations within and nearby the study location. Cloud cover, dew point temperature, solar radiation, and wind speed are obtained from Washington Dulles International Airport (

Figure **5-1**). Observed annual precipitation varies from 730 mm to 1380 mm with an average of 971 mm per year. Observed mean annual surface air temperature is about 12.4 °C with a maximum monthly mean surface air temperature of 30.6 °C in July and a minimum monthly mean surface air temperature of -4.7 °C in January. Table 5-1 shows the observed meteorological data for the study area. Evapotranspiration was simulated using Hamon's potential evapotranspiration formula which relates potential evapotranspiration to maximum possible incoming radiant energy as well as saturation vapor pressure (Lu et al. 2005). Radiant energy is computed by using daylight hours, sunset hour angle, Julian day of the year, and latitude of the study area. The potential moisture-holding capacity of the air was calculated at the prevailing surface air temperature in the study area.

The Occoquan reservoir serves as a principal source of potable water for more than 1.7 million residents in northern Virginia. The reservoir is a relatively long and narrow constructed impoundment with a full-pool volume of 3.1×107 m^3 and a full-pool area of 616 ha. The Occoquan reservoir's average depth is 5.1 m, and the maximum depth is approximately 19 m at the Occoquan dam (Figure 5-4). The Occoquan reservoir has a relatively high flushing rate, with a mean hydraulic residence time of less than 20 days (Table 5-2) (Xu et al. 2007).

5.4 Models and Methods

Xu et al. (2005) arrayed a general scheme for assessing the effects of climate change on hydrological regimes as (1) employment of GCMs representing future climate scenarios because of increases in greenhouse gases, (2) application of downscaling techniques to downscale GCMs to the compatible scale for hydrological modeling, (3) implementation of hydrological models to simulate the response of hydrological regimes due to climate change. The possible consecutive uncertainties in this framework also can be known as a cascade of uncertainties. It is a general practice to consider a cascade of uncertainties in developing climate models and related scenarios for the climate change impact, adaptation, and mitigation assessment studies (Smithson 2002). The adapted methodology framework for analyzing climate change and land use change impacts on streamflows is represented in Figure 5-2 and described in the following sections.

5.4.1 Occoquan Watershed Model

For modeling purposes, the watershed is delineated into seven smaller subbasin models and two reservoir models creating a complexly-linked watershed-reservoir hydrology and water quality model known as the Occoquan Model (Figure 5-3). The hydrological processes were simulated with Hydrological Simulation Program - FORTRAN (HSPF) and the receiving waterbodies were simulated using CE-QUAL-W2.

HSPF is a comprehensive process-based watershed model that has the ability to integrate watershed hydrology and water quality simulations. The extended period structure of HSPF allows users to simulate pervious and impervious land surfaces as well as in-stream hydraulic and sediment-chemical interactions (EPA 2015). HSPF has been widely used as an analytical tool for planning, designing, and operating water resources systems throughout North America and numerous countries around the globe with different climatic regimes (TERRA 2012).

Watershed models' outputs serve as upstream boundary conditions for the Occoquan reservoir model that simulated using CE-QUAL-W2. CE-QUAL-W2 is a two-dimensional hydrodynamic and water quality model that can provide a detailed description of hydrodynamics and water quality processes in receiving waterbodies, such as rivers, lakes, reservoirs and estuaries (Cole and Wells 2006). CE-QUAL-W2 has been applied extensively to simulate waterbodies worldwide and the example applications can be found in Cole and Wells (2006). In CE-QUAL-

W2, waterbodies are defined by a series of laterally averaged, 2-dimensional systems (Xu et al. 2007).

The Occoquan reservoir consists of two primary tributaries: Bull Run and Occoquan Creek. The Bull Run subbasin is located in the northern portion of the watershed. Occoquan Creek receives flows from the Broad Run and Cedar Run subbasins (

Figure **5-1**). The confluence of the two major tributaries is located approximately 14 km upstream of the Occoquan dam and occurs within the reservoir, such that the upper reaches of the Reservoir are split into two arms: the Bull Run Arm and the Occoquan Creek Arm. Based on a prior delineation of the Reservoir into riverine, transitional, and lacustrine zones (Saji 2008), stations RE02 and RE15 are located in the Reservoir's lacustrine zone, while stations RE30 and RE35 are found in the Reservoir's transitional zone.

For modeling purposes, the Occoquan reservoir model is comprised of 69 longitudinal segments, averaging 0.5 km in length, divided into 4 branches. Branch 1 is the main channel, beginning in the Occoquan Creek Arm of the reservoir and extending downstream to the Occoquan dam. Branch 2 is the Bull Run Arm of the reservoir model, connecting the Lower Bull Run watershed model to the confluence of Bull Run and Occoquan Creek. Branches 3 and 4 are Sandy Run and Hooes Run, respectively, and are lesser tributaries to the reservoir.

Calibration and validation of the Occoquan Model is an ongoing comprehensive effort maintained by Occoquan Watershed Modeling Laboratory (OWML). The calibration and validation of the Occoquan Model have been carried out by using several water quantity and quality parameters including flows, nitrogen, phosphorous and total suspended solids (TSS). The uncertainties arising from model calibration can also be included in the aforementioned cascade of uncertainty, however, they were not considered in this study. The version of the Occoquan Model that was used in this study was calibrated from 2002 to 2005 and validated from 2006 to 2007. The calibrated process aimed to maximize the coefficient of determination (R^2), Nash-Sutcliffe efficiency (NSE) (Nash and Sutcliffe 1970), and minimize percent bias (PBIAS), and the ratio of the root mean square error to the standard deviation of measured data (RSR) (Moriasi et al. 2007). Table 5-3 displays the model calibration performance for streamflow at the selected stream stations (

Figure **5-1**). Table 5-4 shows calibration performance criteria of the selected sampling stations in the Occoquan reservoir.

5.4.2 Modeling Climate Change Impact

In creating an ensemble of models to address the uncertainties arising from each source of uncertainty, two emission scenarios, four GCMs, and two downscaling methods have been employed (Table 5-2).

5.4.3 Emission Scenarios

Green House Gas (GHG) emissions can be seen as a newly added component to the Earth's climate system introduced by humans. Driving forces of GHG emission scenarios are highly dynamic, connecting several components including demographic development, socio-economic progress, agricultural practices, and technological changes (Smithson 2002). IPCC has developed different storylines and scenario families to cover the extensive possible ranges of uncertainties and future changes using available data and existing knowledge of GHG patterns (Bernstein et al. 2008).

To address the uncertainty within GHG emission scenarios, a choice of two extreme sides of the spectrum of the SRES has been considered to create upper and lower limits in future scenarios. On the upper side of the range, the A2 scenario focuses on regional and economic growth counting for increasing global population, local-oriented economic growth, and fragmented and slower technological advancement. On the lower side of the range, the B1 scenario emphasizes on environmental awareness, introduction of clean technologies, and global growth attributing on convergent global population after mid 21st century (Bernstein et al. 2008).

5.4.4 GCMs

Each GCM represents the Earth's climate system differently by applying various initial and boundary conditions. To address the uncertainty specifically arising from the GCMs, a group of four GCMs has been considered (Table 5-5).

5.4.5 Statistical Downscaling

Simulated data from GCMs are primarily used to demonstrate the Earth's climate system on a global scale. However, for regional use, these models can be translated to the scale of the

watershed under study. For this reason, the use of an appropriate and reliable downscaling method is required. In this study two statistical downscaling methods were applied for producing necessary regional data sets: Delta Change (Anandhi et al. 2011; Arnell 1996; Camici et al. 2013; Wilby et al. 2004) and Quantile Mapping (Bennett et al. 2014; Camici et al. 2013; Maurer and Hidalgo 2008; Piani et al. 2010; Thrasher et al. 2012; Wood et al. 2004).

Delta Change method

The Delta Change (DC) method is one of the simplest forms of downscaling transfer functions or change factor methodologies. In this method, different formulations can be used based on a temporal scale and/or mathematical operation (usually additive or multiplicative) (Anandhi et al. 2011). In this study, an additive change factor (Equations 5-1 and 5-2) have been used for downscaling surface air temperatures and multiplicative change factor was applied (Equations 5-3 and 5-4) for downscaling precipitation.

$$\delta_{at} = FC_{at} - HC_{at} \tag{5-1}$$

$$LF_{at} = LH_{at} + \delta_{at} \tag{5-2}$$

where, FC_{at} is future climate surface air temperature, HC_{at} is historical climate surface air temperature, δ_{at} is change factor for surface air temperatures, LH_{at} is local historical surface air temperatures, and LF_{at} is local future surface air temperature.

$$\delta_{pr} = FC_{pr} \big/ HC_{pr} \tag{5-3}$$

$$LF_{pr} = LH_{pr} \times \delta_{pr} \tag{5-4}$$

where, FC_{pr} is future climate precipitation, HC_{pr} is historical climate precipitation, δ_{pr} is change factor for precipitation, LH_{pr} is local historical precipitation, and LF_{pr} is local future precipitation.

Quantile mapping method

In the Quantile Mapping (QM) method, cumulative distribution functions (CDFs) of observed and GCM time series are generated for the variable of interest (e.g., temperature and precipitation), one based on the GCM simulations and one based on the aggregated observations. The mapping procedure is based on a simple nonparametric lookup practice that matches

statistical moments of the observed data to the simulated ones. Quantile mapping method can reflect the changes in mean and variance of climate variables matching all statistical moments of GCMs with corresponding observed variables. On the other hand, the delta change method only considers the mean change of the GCM variables. Different variations of quantile mapping methods have been used in previous studies. In this study bijective (predictors are the same parameters as predictands) and parameter-free (empirical cumulative distribution function), QM has been implemented. Furthermore, an equidistant cumulative distribution function (EDCDF) matching method has been used for downscaling surface air temperatures (Equation 5-5) (Li et al. 2010). EDCDF has limitations for bias correcting precipitation where negative values are not acceptable. Alternatively, an equiratio cumulative distribution function (ERCDF) matching method has been employed for downscaling precipitation data (Equation 5-6) (Wang and Chen 2014).

$$LF_{at} = FC_{at} + \left(LH_{at}^{-1}(FC_{at})\right) - \left(HC_{at}^{-1}(FC_{at})\right) \tag{5-5}$$

$$LF_{pr} = FC_{pr} \times \left(LH_{pr}^{-1}(FC_{pr})\right) \Big/ \left(HC_{pr}^{-1}(FC_{pr})\right) \tag{5-6}$$

Downscaled climate variables

The target application and end-user requirements of climate-scenario models dictate the type of variables to be used in the impact study models. For example, for disaster management, the extremes of temperature, wind, and sea level data might be of more interest. In agricultural applications, precipitation, temperature, solar radiation, and humidity might be more important. General climate variables that have been used in water resources management (water quantity and quality assessments) are precipitation and temperature (Camici et al. 2013; Fiseha et al. 2012). In this study, surface air temperatures (including maximum and minimum), precipitation, and wind were used as the primary predictor variables (Table 5-6).

5.4.6 Modeling Land Use Changes Impact

Developed by the U.S. EPA, ICLUS (Integrated Climate and Land-Use Scenarios) was used to simulate the impact of land use change over the watershed. This tool uses the projected population of each county as a major driver of growth. Then the population growth is converted into housing units. In the next step, housing density growth is spatially allocated by population

growth rate, neighboring housing density, and transportation infrastructure using Spatially Explicit Regional Growth Model (SERGoM) (Theobald 2005).

The major benefit of using ICLUS for estimating the land use change is the use of mathematical models to produce spatially explicit projections of population and statistical models to render impervious surface areas based on IPCC's SRES storylines (Bierwagen and Morefield 2014). Detail overview of ICLUS modeling process is depicted in Figure 5-5.

5.4.7 Simulation Periods

Impact of future climate change have been analyzed in two periods the mid (2046-2065) and late (2081-2100) 21st century. Table 5-7 and Figure 5-6 depict historical and future periods used in this study. The land use changes are simulated every 10 years from 2040 to 2100. The average changes in projected land use in each period were calculated and the middle of each period was used to represent the land use changes of that period. To simulate the impact of climate change, the entire 20 years in each period was used.

5.4.8 Simulated Scenarios

To consider the single and joint impacts of the climate change and land use change, four themes have been developed, as shown in Table 5-8.

Theme 1: Present Climate, Present Land Use

This theme serves as a baseline for which the other simulated themes are compared.

Theme 2: Future Climate, Present Land Use

This theme examines the influence of future climate conditions in the study area. In this theme, a range of future climate projections were explored to forecast the impact of climate change on flow characteristics. Land use conditions are set at present levels.

Theme 3: Present Climate, Future Land Use

This theme investigates how continued land use change (i.e., urbanization) affects streamflows in the study area. Climate is set at present conditions.

Theme 4: Future Climate, Future Land Use

This theme considers the combined effects of both climate change and land use change. Comparing the results of this theme against the previous three themes identifies whether the

combination of climate change and land used change are amplifying or dampening each other's effects relative to the components acting alone.

Considering these four themes and all of the choices of the model set up (two GHG emissions, four GCMs, two downscaling methods, and two periods) resulted in 69 scenarios. For further analyses, the flow regime alterations using these 69 scenarios, were studied at two streamflow stations (i.e., ST 10 and ST 40) entering the Occoquan reservoir. The subwatersheds creating these streamflows are Bull Run and Occoquan Creek (

Figure **5-1**). The projections were compared to historical values at the station near the reservoir dam (RE02).

An in-house software, URUNME, was used to simulate the 69 scenarios (Lodhi et al. 2018). URUNME enables water resources and environmental modelers to link, couple, and run their entire simulation process with various scenarios on one platform. Moreover, URUNME provides modelers with flexible and interactive visualization and analytical tools to post-process model results.

5.5 Results and Discussion

5.5.1 Climate Change

Surface air temperature

All models predict an increase in annual average surface air temperatures ranging from 0.9 to 4.8 °C. On average, an increase of 11% to 19% for annual surface air temperature is predicted across all models for 2046-2065 and 2081-2100 periods, respectively. Annual maximum surface air temperatures are also projected to increase by 7% and 13% on average for the first and second periods. Annual minimum surface air temperatures are showing 21% and 36% increases for the first and second periods compared to the historical data. Minimum surface air temperatures are rising at slightly higher rates compared to maximum surface air temperatures. This leads to a decrease in an annual average of diurnal temperature range which is the difference between daily maximum and minimum temperatures. This range decreases more in the second period. Rises in temperature sums and minimum temperatures could be one of the factors that can affect future physiological processes of plants' ecosystem and biogeochemical cycling modes in different ways, including phenophase transitions to spring and budburst timing, autumn leaf abscission

and cold hardening (Team 2008). Overall, these increases are more prominent in the late 21st century using A2 scenarios while B1 scenarios in mid 21st century are showing fewer changes.

Figure 5-7 and Figure 5-8 depict monthly surface air temperature for all the models for both the mid and late 21st century. The highest rises in average monthly surface air temperature occur in summer months (June, July, and August) by 9%, with August having peak monthly average surface air temperatures of 27.3 and 31.6 °C for the mid and late 21st century. Monthly average maximum surface air temperature is estimated to increase more in summer months. However, monthly average minimum surface air temperature is anticipated to have more changes in fall (September, October, and November) with an increase of 1.7 and 2.8 °C for the first and second periods, respectively.

Precipitation

Mean annual precipitation is projected to increase ranging from 2% to 17% with the median of 9% and 11% increases for mid and late 21st century. Overall, models with the emission scenario A2 in the late 21st century display more precipitation than B1 in the mid 21st century. The seasonal increase in median precipitation ranges from 3% in fall to 13% in spring. In the first period, the highest amount of predicted change in monthly precipitation is anticipated in July while the amount of precipitation is expected to decrease in September. In the second period, except for September, the median precipitations are higher with the higher projected precipitations in May and December. Figure 5-9 and Figure 5-10 depicts the monthly variation of precipitation for mid and late 21st century.

5.5.2 Land Use Change

Figure 5-11 shows an estimated percent of the current impervious surface areas in the Occoquan watershed. The Bull Run is more urbanized with an average impervious surface area of 12%, while the Occoquan Creek is mostly forest, pastures and low-density residential with an average impervious surface area of 4%. Percent impervious surface areas are projected using SRES's storylines, economic vs. environmental and local vs. global driven developments. These projections can be different based on the initial states of a watershed. These initial states depend on travel time to urban cores and household sizes. The B1 scenario assumes smaller household

sizes and denser growth patterns near existing urban cores, whereas the A2 scenario reflects larger household sizes as well as longer travel time to urban centers.

As mentioned earlier, 20 years simulations were used for each period (i.e., F1 and F2) while the land use for each of these periods was set at the middle of that period (i.e., 2055 and 2090). B1 scenario projects higher values in the Bull Run compared to the A2 scenario until the last decade of the 21st century. In the Occoquan Creek, the A2 scenario always projects higher percentages of impervious lands compared to the B1 scenario. The highest projected percent impervious surface area for the Occoquan Creek is 13% at the end of the 21st century. The rate of change in urbanization in the Occoquan Creek is 1.7 times higher than the Bull Run (Figure 5-12). Figure 5-13, Figure 5-14, Figure 5-15 and Figure 5-16 show the projected percent impervious surfaces for each of the emission scenarios for the center of each of the simulation periods. The changes are shown in the small subcatchments that are used in the Occoquan Model. These smaller delineations have been performed based on local geographic characteristics such as topography, land use, and soil properties (Xu et al. 2007).

5.5.3 Impacts of Climate Change and Land Use Change on Occupation Reservoir Water Temperature

Water temperature is one of the most important characteristics of lakes and reservoirs. Nearly all of the physiochemical cycles of waterbodies are regulated by thermal energy content and density stratification (Wetzel 2001). As mentioned earlier, surface air temperature is anticipated to increase in the study area. These changes will be more noticeable in the late 21st century using the A2 emission scenario and will affect water temperature in the Occoquan reservoir both at the surface and at the bottom.

As the surface water temperature increases, thermal resistance to vertical mixing also increases (Butcher et al. 2015). In the mid 21st century, the annual surface water temperature will increase by 6% and 5% for the A2 and B1 emission scenarios. The amount of increase in the late 21st century will be 9% and 6% for the A2 and B1 emission scenarios, respectively. In the mid 21st century land use change effect on thermal conditions of surface water temperature is not noticeable. However, in the second period, land use change will slightly increase the surface water temperature due to higher inputs of warmer streamflows to the reservoir. Annual maximum surface water temperature will increase by 4% and 6% in the mid and late 21st

century. Annual minimum surface water temperature also will increase by 7% and 9% for the first and second periods, respectively. Overall, an increase in water temperatures are projected that will be more pronounced in the summer months (Table 5-9).

At the bottom of the reservoir, water temperature is anticipated to increase by 6% and 5% using A2 and B1 emission scenarios for the mid 21st century and 8% and 6% for the late 21st century, applying the same scenarios. Similar to the surface water temperature, land use change will slightly increase bottom water temperature during the second period. Maximum bottom water temperature is expected to remain at the historical measures while the minimum bottom water temperature is predicted to increase by 7% and 5% in the first and second periods, respectively. The sole effect of land use change on bottom water temperatures are comparable to the historical values. However, bottom water temperatures are slightly higher with the addition of the land use change to the climate change impacts. Figure 5-17 shows the surface and bottom water temperatures in both modeling periods.

Current research suggests that higher water temperatures will promote decreased oxygen solubility and greater heterotrophy. This increase in phytoplankton production will likely lead to more intense and more frequent episodes of hypoxia (Najjar et al. 2010). In the study area, the departure between temperatures in the surface and bottom of the reservoir display higher values in the second part of the 21st century. As the differences between the surface and bottom temperatures increase, intensified stratification is anticipated in this period with an increase of metalimnion thickness.

5.5.4 Dissolved Oxygen

The amount of dissolved oxygen concentration and its distribution through the water column are fundamental in assessing water quality in lakes and reservoirs. In particular, oxygen distribution affects the solubility of many inorganic nutrients. As the water temperature increases, oxygen solubility in water decreases (Wetzel 2001). In the face of future climate change, surface DO concentrations tend to decrease in both the mid and late 21st century. The reduction is more prevalent in the second period with highest decrease in September. However, land use change amplifies the amount of DO in the reservoir due to higher levels of oxygen-rich streamflow flowing to the reservoir. Comparing the combined effects of climate change and land use change, land use change is more dominant in the mid 21st century, meaning that the levels of DO

concentrations at the surface will be higher, but, in the second period, climate change will be overriding the overall effect with the decline of DO levels on the surface of the reservoir (Table 5-10). In contrast, the bottom of the reservoir will experience lower amounts of DO compare to historical records due to climate change. These effects are more noticeable in the second period by about 6% reduction in DO. The effect of land use on DO at the bottom of the lake is not very different from historical data. Considering the combination of both driving forces, climate change is the leading factor in DO reduction at the bottom of the reservoir.

Figure 5-18 depicts that oxygen concentration at the lowest stratum is mainly regulated by biological processes resulting in the complete depletion of stored oxygen in the hypolimnion in summer. This supports a hypolimnion shift from aerobic to anaerobic, with anaerobic conditions persisting during the stratification period.

5.5.5 Nutrients

In freshwater and lakes, ammonia, nitrate, and nitrite are the dominant forms of nitrogen (Wetzel 2001). Among other nutrients in freshwaters, nitrogen is the primary constituent that effects the organisms' productivity although phosphate is generally the limiting nutrient in the Occoquan reservoir.

Ammonia nitrogen (NH_3)

As part of freshwater metabolism, ammonia is produced by biological dissimilation of proteins and other nitrogenous organic compounds. Substantial quantities of ammonia indicate a lack of oxygen in the water column to completely oxidize ammonia into nitrate and nitrite. At the surface of the reservoir, besides some variation in winter months, ammonia nitrogen concentrations are usually very low and close to the trace levels (Figure 5-19).

Nitrate-nitrite nitrogen ($NO_x - N$)

The simulated results indicate a high demand of nitrate-nitrite nitrogen (NO_x-N) close to the sediment layer during summer when the lake is thermally stratified. This results in a decrease in NO_x and complete denitrification throughout the hypolimnion. Figure 5-20 shows the nitrate-nitrite nitrogen levels in surface and bottom of the reservoir in both periods.

Orthophosphate phosphorus (OP)

A prominent form of phosphorus is orthophosphate phosphorus (OP). OP is soluble and readily available (bioavailable) for algae and other aquatic ecosystems. Phosphorus concentrations are often higher nearer to the interstitial water of the sediments mostly due to reduced concentrations of oxygen in the ecological redox sequence. At the sediment-water interface, the exchange equilibria are mostly unidirectional towards the sediments in aerobic settings (Wetzel 2001). However, in anaerobic conditions, exchange of inorganic matter at the sediment-water interface is heavily determined by redox potential and generally directed from the sediment to the water column (Frevert 1979). Considering the impact of climate change and comparison to historical values, the projected models show less dissolved oxygen during the autumn turnover in the hypolimnion. This phenomenon supports the possibility of a greater upward flux of phosphorus back to the water column from the sediments in the autumn turnover (Figure 5-21).

5.6 Summary and Conclusions

The impact of climate change on water quality has been a subject of many recent studies. In principle, the effects of climate change are intertwined with other anthropologic driving forces such as land use change. This paper examined the impacts of the individual and combined effects of climate change and land use change on the Occoquan reservoir's water quality. Four themes have been developed using the combination of these driving forces. To implement the arising uncertainties in the future projections, two emission scenarios, four GCMs, two downscaling methods, and two periods were applied. Collectively, 68 projections were simulated and ensembles of these projections were created to analyze the single and joint effects of these driving forces on streamflow characteristics.

Under the climate change scenarios, the Occoquan reservoir will likely experience increases in surface water temperatures. These changes are expected to be more in the late 21st century. The A2 scenario shows higher increases compared to the B1 scenario, with highest changes in summer months. The maximum and minimum surface water temperatures are also expected to increase. As a result, it is likely that future thermal stratification be intensified due to climate change resulting in a more stable lake with a stronger thermocline and more distinct epilimnion, metalimnion, and hypolimnion layers during the stratification period. It is also expected that the thermal stratification period will expand, which will start in late spring (June instead of July) and end at the beginning of the fall (October instead of September). Lesser amounts of DO

concentrations are projected at the bottom of the reservoir. The period of anaerobic nutrient interaction between the sediment layer and water column may increase due to stronger thermal stratification and the extended anoxic period in the hypolimnion layer. This can promote an upward movement of nutrient fluxes from the reduced environment of the bottom layer to the surface during autumn turnover.

In essense, it is expected that higher water temperatures will promote decreased oxygen solubility and greater heterotrophy. Moreover, longer anoxic conditions are projected at the bottom of the reservoir. It can be seen from the results that higher water temperature will increase the denitrifying capacity of the reservoir, especially during summer months, further reducing the nitrate concentration in the reservoir. However, due to higher projected water temperature and high DO deficiency, the release of ammonia, phosphorus, and other nuisance substances may increase in the future.

5.7 Acknowledgment

The authors gratefully acknowledge the financial support provided by Australian Water Quality Centre (SA Water) and Occoquan Watershed Monitoring Laboratory (OWML) for this study. The views expressed in the paper are those of the authors and not necessarily of the funding bodies.

5.8 References

Anandhi, A., Frei, A., Pierson, D. C., Schneiderman, E. M., Zion, M. S., Lounsbury, D., and Matonse, A. H. (2011). "Examination of change factor methodologies for climate change impact assessment." Water Resources Research, 47(3).

Arnell, N. W. (1996). Global warming, river flows and water resources, John Wiley & Sons Ltd.

Bennett, J. C., Grose, M. R., Corney, S. P., White, C. J., Holz, G. K., Katzfey, J. J., Post, D. A., and Bindoff, N. L. (2014). "Performance of an empirical bias-correction of a high-resolution climate dataset." International Journal of Climatology, 34(7), 2189-2204.

Bernstein, L., Bosch, P., Canziani, O., Chen, Z., Christ, R., and Riahi, K. (2008). "IPCC, 2007: climate change 2007: synthesis report." IPCC.

Bierwagen, B., and Morefield, P. (2014). "Integrated Climate and Land Use Scenarios (ICLUS). Web page. Washington, DC: US Environmental Protection Agency (USEPA). Accessed September 25."

Bucak, T., Trolle, D., Tavşanoğlu, Ü. N., Çakıroğlu, A. İ., Özen, A., Jeppesen, E., and Beklioğlu, M. (2018). "Modeling the effects of climatic and land use changes on phytoplankton and water quality of the largest Turkish freshwater lake: Lake Beyşehir." Science of The Total Environment, 621, 802-816.

Bussi, G., Janes, V., Whitehead, P. G., Dadson, S. J., and Holman, I. P. (2017). "Dynamic response of land use and river nutrient concentration to long-term climatic changes." Science of the Total Environment, 590, 818-831.
Butcher, J. B., Nover, D., Johnson, T. E., and Clark, C. M. (2015). "Sensitivity of lake thermal and mixing dynamics to climate change." Climatic Change, 129(1-2), 295-305.
Calder, I. R., Hall, R. L., Bastable, H. G., Gunston, H. M., Shela, O., Chirwa, A., and Kafundu, R. (1995). "The impact of land use change on water resources in sub-Saharan Africa: a modelling study of Lake Malawi." Journal of Hydrology, 170(1-4), 123-135.
Camici, S., Brocca, L., Melone, F., and Moramarco, T. (2013). "Impact of climate change on flood frequency using different climate models and downscaling approaches." Journal of Hydrologic Engineering, 19(8), 04014002.
Chang, C.-H., Cai, L.-Y., Lin, T.-F., Chung, C.-L., van der Linden, L., and Burch, M. (2015). "Assessment of the impacts of climate change on the water quality of a small deep reservoir in a humid-subtropical climatic region." Water, 7(4), 1687-1711.
Cole, T. M., and Wells, S. A. (2006). "CE-QUAL-W2: A two-dimensional, laterally averaged, hydrodynamic and water quality model, version 3.5."
Couture, R.-M., Moe, S. J., Lin, Y., Kaste, Ø., Haande, S., and Solheim, A. L. (2018). "Simulating water quality and ecological status of Lake Vansjø, Norway, under land-use and climate change by linking process-oriented models with a Bayesian network." Science of the Total Environment, 621, 713-724.
EPA, U. (2015). "BASINS 4.1 (Better Assessment Science Integrating point & Non-point Sources) Modeling Framework." (02/02/2018).
Fiseha, B., Melesse, A., Romano, E., Volpi, E., and Fiori, A. (2012). "Statistical downscaling of precipitation and temperature for the Upper Tiber Basin in Central Italy." International journal of water sciences, 1.
Frevert, T. (1979). "The pe-redox concept in natural sediment-water systems; its role in controlling phosphorus release from lake sediments." Arch. Hydrobiol.[Supp.], 55, 278-297.
Leopold, L. B. (1968). "Hydrology for urban land planning: A guidebook on the hydrologic effects of urban land use."
Li, H., Sheffield, J., and Wood, E. F. (2010). "Bias correction of monthly precipitation and temperature fields from Intergovernmental Panel on Climate Change AR4 models using equidistant quantile matching." Journal of Geophysical Research: Atmospheres, 115(D10).
Lodhi, A., Godrej, A. N., Baran, A., and Sen, D. (2018). "URUNME: A Software Platform for Integrated Environmental Modeling to Help 'You Run Models Easily'." Manuscript in preparation.
Lu, J., Sun, G., McNulty, S. G., and Amatya, D. M. (2005). "A comparison of six potential evapotranspiration methods for regional use in the southeastern United States." JAWRA Journal of the American Water Resources Association, 41(3), 621-633.
Malsy, M., Flörke, M., and Borchardt, D. (2017). "What drives the water quality changes in the Selenga Basin: climate change or socio-economic development?" Regional Environmental Change, 17(7), 1977-1989.
Maurer, E. P., and Hidalgo, H. G. (2008). "Utility of daily vs. monthly large-scale climate data: an intercomparison of two statistical downscaling methods."

Mehdi, B., Ludwig, R., and Lehner, B. (2015). "Evaluating the impacts of climate change and crop land use change on streamflow, nitrates and phosphorus: A modeling study in Bavaria." Journal of Hydrology: Regional Studies, 4, 60-90.
Moriasi, D. N., Arnold, J. G., Van Liew, M. W., Bingner, R. L., Harmel, R. D., and Veith, T. L. (2007). "Model evaluation guidelines for systematic quantification of accuracy in watershed simulations." Transactions of the ASABE, 50(3), 885-900.
Najjar, R. G., Pyke, C. R., Adams, M. B., Breitburg, D., Hershner, C., Kemp, M., Howarth, R., Mulholland, M. R., Paolisso, M., and Secor, D. (2010). "Potential climate-change impacts on the Chesapeake Bay." Estuarine, Coastal and Shelf Science, 86(1), 1-20.
Nash, J. E., and Sutcliffe, J. V. (1970). "River flow forecasting through conceptual models part I—A discussion of principles." Journal of hydrology, 10(3), 282-290.
Piani, C., Weedon, G., Best, M., Gomes, S., Viterbo, P., Hagemann, S., and Haerter, J. (2010). "Statistical bias correction of global simulated daily precipitation and temperature for the application of hydrological models." Journal of Hydrology, 395(3-4), 199-215.
Records, R., Arabi, M., Fassnacht, S., Duffy, W., Ahmadi, M., and Hegewisch, K. (2014). "Climate change and wetland loss impacts on a western river's water quality." Hydrology and Earth System Sciences, 18(11), 4509-4527.
Roberts, A. D., and Prince, S. D. (2010). "Effects of urban and non-urban land cover on nitrogen and phosphorus runoff to Chesapeake Bay." Ecological Indicators, 10(2), 459-474.
Saji, N. (2008). "Development of a Guide to Lake and Reservoir Zone Determination." Virginia Tech.
Schwefel, R., Gaudard, A., Wüest, A., and Bouffard, D. (2016). "Effects of climate change on deepwater oxygen and winter mixing in a deep lake (Lake Geneva): Comparing observational findings and modeling." Water Resources Research, 52(11), 8811-8826.
Smithson, P. A. (2002). "IPCC, 2001: climate change 2001: the scientific basis. Contribution of Working Group 1 to the Third Assessment Report of the Intergovernmental Panel on Climate Change, edited by JT Houghton, Y. Ding, DJ Griggs, M. Noguer, PJ van der Linden, X. Dai, K. Maskell and CA Johnson (eds). Cambridge University Press, Cambridge, UK, and New York, USA, 2001. No. of pages: 881. Price£ 34.95, US $49.95, ISBN 0-521-01495-6 (paperback).£ 90.00, US $130.00, ISBN 0-521-80767-0 (hardback)." International Journal of Climatology, 22(9), 1144-1144.
Syaukat, Y. (2012). Irrigation in Southern and Eastern Asia in figures, FAO the United Nation.
Taner, M. Ü., Carleton, J. N., and Wellman, M. (2011). "Integrated model projections of climate change impacts on a North American lake." Ecological Modelling, 222(18), 3380-3393.
Team, B. A. (2008). Assessment of climate change for the Baltic Sea basin, Springer Science & Business Media.
TERRA, A. (2012). "HSPF Support." (05/05/2017), AQUA TERRA.
Theobald, D. (2005). "Spatially explicit regional growth model (SERGOM) v2 methodology." Report for Trust for Public Lands, Fort Collins, CO.
Thrasher, B., Maurer, E. P., McKellar, C., and Duffy, P. (2012). "Bias correcting climate model simulated daily temperature extremes with quantile mapping." Hydrology and Earth System Sciences, 16(9), 3309.
USDA, N. (2017). "Soil Survey Staff." Natural Resources Conservation Service, United States Department of Agriculture. Web Soil Survey. Available online at http://websoilsurvey.nrcs.usda.gov (accessed December 12, 2017).

Wang, L., and Chen, W. (2014). "Equiratio cumulative distribution function matching as an improvement to the equidistant approach in bias correction of precipitation." Atmospheric Science Letters, 15(1), 1-6.
Wang, R., and Kalin, L. (2017). "Combined and synergistic effects of climate change and urbanization on water quality in the Wolf Bay watershed, southern Alabama." Journal of Environmental Sciences.
Wetzel, R. G. (1992). "Clean water: a fading resource." Hydrobiologia, 243(1), 21-30.
Wetzel, R. G. (2001). Limnology: Lake and River Ecosystems, Academic Press, San Diego.
Wilby, R. L., Charles, S., Zorita, E., Timbal, B., Whetton, P., and Mearns, L. (2004). "Guidelines for use of climate scenarios developed from statistical downscaling methods." Supporting material of the Intergovernmental Panel on Climate Change, available from the DDC of IPCC TGCIA, 27, -.
Wood, A. W., Leung, L. R., Sridhar, V., and Lettenmaier, D. (2004). "Hydrologic implications of dynamical and statistical approaches to downscaling climate model outputs." Climatic change, 62(1-3), 189-216.
Xu, C.-y., Widén, E., and Halldin, S. (2005). "Modelling hydrological consequences of climate change—progress and challenges." Advances in Atmospheric Sciences, 22(6), 789-797.
Xu, Z., Godrej, A. N., and Grizzard, T. J. (2007). "The hydrological calibration and validation of a complexly-linked watershed–reservoir model for the Occoquan watershed, Virginia." Journal of Hydrology, 345(3-4), 167-183.

Table 5-1. Baseline meteorological data for the study area from 1981 to 2000.

Month	Surface Air Temperature (tas) (°C)	Maximum Surface Air Temperature (tasmax) (°C)	Minimum Surface Air Temperature (tasmin) (°C)	Precipitation (P) (mm)	Evapotranspiration (ET) (mm)
January	0.2	5.2	-4.7	71	32
February	2.3	7.8	-2.9	68	21
March	6.3	12.3	0.5	86	28
April	11.9	18.4	5.4	80	33
May	17.0	23.4	10.6	98	60
June	21.9	28.1	15.9	82	63
July	24.5	30.6	18.7	86	77
August	23.3	29.4	17.5	89	77
September	19.3	25.5	13.4	88	76
October	12.8	19.6	6.3	69	55
November	7.3	13.3	1.6	85	61
December	2.2	7.3	-2.5	69	34
Average([a]) or Sum([s])	12.4[a]	18.4[a]	6.7[a]	971[s]	617[s]

Table 5-2. Summary of Occoquan reservoir physical characteristics (Xu et al. 2007).

Occoquan reservoir physical characteristics	
Watershed drainage area (km^2)	1480
Volume (m^3)	31.4×10^6
Surface Area (ha)	616
Length (m)	2.25×10^4
Mean Depth (m)	5.1
Maximum Depth (m)	19
Mean Width (m)	150
Maximum Width (m)	275
Safe Yield (m^3/day)	2.5×10^5
Average Inflow (m^3/day)	1.6×10^6
Dam Crest Height above Mean Sea Level (m)	37.2
Hydraulic Residence Time (day)	19.6

Table 5-3. Performance criteria for calibration and validation.

Procedure	Performance Criteria	Streamflow Station				
		ST25	ST30	ST45	ST60	ST70
Calibration	R^2	0.85	0.85	0.90	0.86	0.77
	NSE	0.81	0.85	0.87	0.83	0.75
	PBIAS	10.5	2.7	6.3	6.8	8.0
	RSR	0.44	0.39	0.36	0.41	0.50
Validation	R^2	0.82	0.88	0.84	0.84	0.76
	NSE	0.88	0.84	0.84	0.90	0.86
	PBIAS	-5.3	18.6	6.6	-6.1	4.3
	RSR	0.44	0.46	0.44	0.41	0.50

Table 5-4. Calibration performance criteria for calibration of the Occoquan reservoir.

Reservoir Sampling Station	Constituent	Location	NSE	PBIAS
RE02	DO	Surface	0.40	-0.01
		Bottom	0.86	-0.03
	Temperature	Surface	0.95	0.03
		Bottom	0.93	-0.03
	NO_3	Surface	0.50	-0.05
		Bottom	0.40	-0.28
	OP	Surface	-0.34	0.18
		Bottom	0.02	-0.27
	NH_4	Surface	-0.37	0.02
		Bottom	0.45	-0.07
RE15	DO	Surface	-0.28	-0.10
		Bottom	0.83	0.02
	Temperature	Surface	0.96	0.01
		Bottom	0.86	-0.05
	NO_3	Surface	0.61	0.02
		Bottom	0.37	-0.46
	OP	Surface	-0.48	0.10
		Bottom	-5.28	2.15
	NH_4	Surface	-0.46	-0.06
		Bottom	0.62	-0.20

Table 5-5. GCM used in this study.

Model Name	Agency/Organization	Country
CSIRO MK3	Australia's Commonwealth Scientific and Industrial Research Organization	Australia
GFDL CM2.0	Geophysical Fluid Dynamics Laboratory	USA
MPIM:ECHAM5	Max Planck Institute for Meteorology	Germany
MRI-CGCM2.3.2	Meteorological Research Institute, Japan Meteorological Agency	Japan

Table 5-6. Climate variables used in this study.

Predictor Variables	Precipitation
	Surface Air Temperature
	Maximum Surface Air Temperature
	Minimum Surface Air Temperature
	Wind

Table 5-7. Time horizons for observed and GCM data.

Model set		Period	Abbreviation used in this paper
Observed		1981-2000	Baseline
GCM	Historical	1981-2000	20c3m
	Future	2046-2065	F1
		2081-2100	F2

Table 5-8. Developed themes for assessing the impacts of climate change and land use change.

Theme	Climate	Land Use
1	Present	Present
2	Future	Present
3	Present	Future
4	Future	Future

Table 5-9. Projected monthly differences between surface and bottom (surface-bottom) layers for water temperature.

Month	Scenario												
	Historical	F1 (2046-2065)						F2 (2081-2100)					
	Base	CC (A2)	CC (B1)	LUC (A2)	LUC (B1)	CC+LUC (A2)	CC+LUC (B1)	CC (A2)	CC (B1)	LUC (A2)	LUC (B1)	CC+LUC (A2)	CC+LUC (B1)
Jan	-0.75	-0.43	-0.61	-0.81	-0.76	-0.38	-0.60	-0.28	-0.44	-0.78	-0.77	-0.12	-0.41
Feb	-0.27	0.19	0.18	-0.32	-0.29	0.19	0.19	0.18	0.10	-0.28	-0.28	0.42	0.23
Mar	1.71	2.08	2.00	1.68	1.69	2.07	2.20	2.03	2.20	1.72	1.72	2.33	2.33
Apr	5.99	6.46	6.31	6.19	6.14	6.51	6.41	6.81	6.44	6.22	6.18	7.17	6.54
May	12.29	12.84	12.94	12.33	12.12	12.64	12.75	13.41	12.86	12.26	12.05	13.57	12.57
Jun	16.98	17.30	17.07	16.71	16.61	17.03	16.88	17.85	17.22	16.62	16.58	17.98	16.94
Jul	19.03	19.52	19.20	18.67	18.65	19.14	19.04	20.08	19.58	18.61	18.62	20.06	19.27
Aug	17.17	18.25	18.03	16.71	16.63	17.96	17.73	18.81	18.12	16.67	16.63	18.80	17.92
Sep	13.09	14.11	13.86	12.74	12.69	13.83	13.59	14.66	14.00	12.72	12.70	14.77	13.81
Oct	5.97	6.81	6.82	5.46	5.44	6.61	6.64	7.47	6.68	5.43	5.48	7.51	6.53
Nov	0.90	0.90	0.77	0.77	0.79	0.88	0.81	1.21	0.99	0.80	0.78	1.24	0.92
Dec	0.04	0.34	0.17	-0.01	0.04	0.39	0.27	0.42	0.26	0.00	0.05	0.47	0.29

Table 5-10. Projected monthly differences between surface and bottom (surface-bottom) layers for DO concentrations.

Month	Scenario												
	Historical	F1 (2046-2065)						F2 (2081-2100)					
	Base	CC (A2)	CC (B1)	LUC (A2)	LUC (B1)	CC+LUC (A2)	CC+LUC (B1)	CC (A2)	CC (B1)	LUC (A2)	LUC (B1)	CC+LUC (A2)	CC+LUC (B1)
Jan	0.73	0.54	0.50	0.58	0.54	0.49	0.58	0.46	0.54	0.51	0.54	0.45	0.55
Feb	0.48	0.33	0.34	0.58	0.55	0.33	0.39	0.29	0.34	0.57	0.55	0.41	0.39
Mar	0.53	0.99	0.96	0.61	0.61	1.04	1.05	1.11	0.93	0.60	0.60	1.22	1.06
Apr	3.99	5.06	4.80	4.45	4.33	5.40	5.27	5.07	4.79	4.41	4.34	5.81	5.32
May	8.40	8.58	8.59	8.99	8.96	9.18	9.12	8.55	8.56	9.11	9.06	9.21	9.24
Jun	7.86	7.78	7.81	8.17	8.15	8.10	8.16	7.72	7.80	8.23	8.21	8.14	8.16
Jul	7.17	7.12	7.23	7.36	7.42	7.37	7.48	7.08	7.11	7.51	7.49	7.42	7.43
Aug	6.63	6.70	6.73	6.82	6.82	6.93	6.96	6.74	6.66	6.85	6.84	7.03	6.97
Sep	6.14	6.25	6.32	6.34	6.39	6.42	6.54	6.24	6.26	6.41	6.42	6.41	6.54
Oct	7.23	6.87	6.96	7.41	7.43	7.10	7.18	6.82	6.93	7.49	7.47	6.96	7.15
Nov	1.75	2.14	2.14	1.42	1.49	1.97	1.92	2.82	2.23	1.38	1.41	2.84	2.09
Dec	0.27	0.21	0.21	0.25	0.29	0.21	0.26	0.19	0.21	0.22	0.25	0.24	0.20

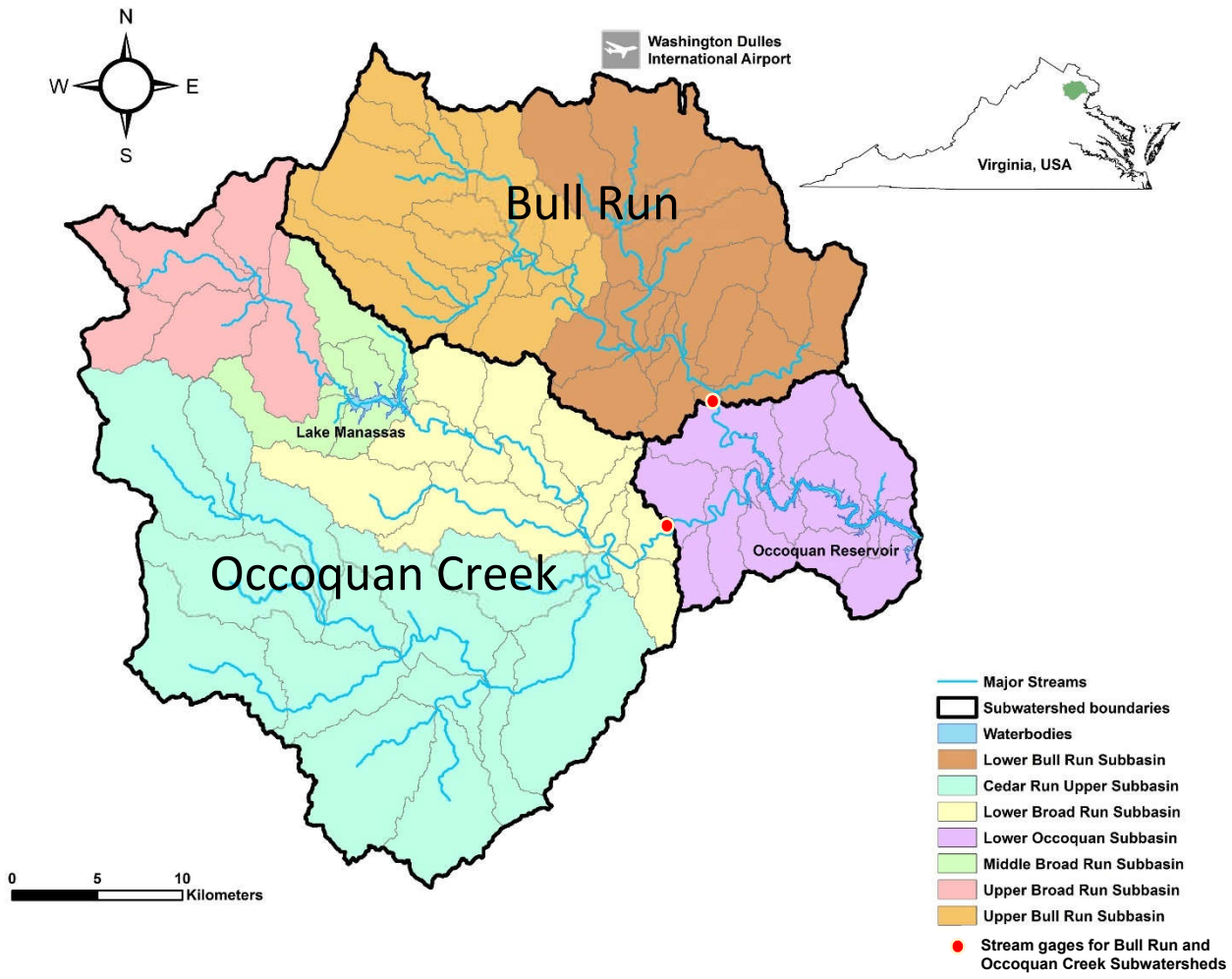

Figure 5-1. Occoquan reservoir within the Occoquan watershed with major streams and subbasins.

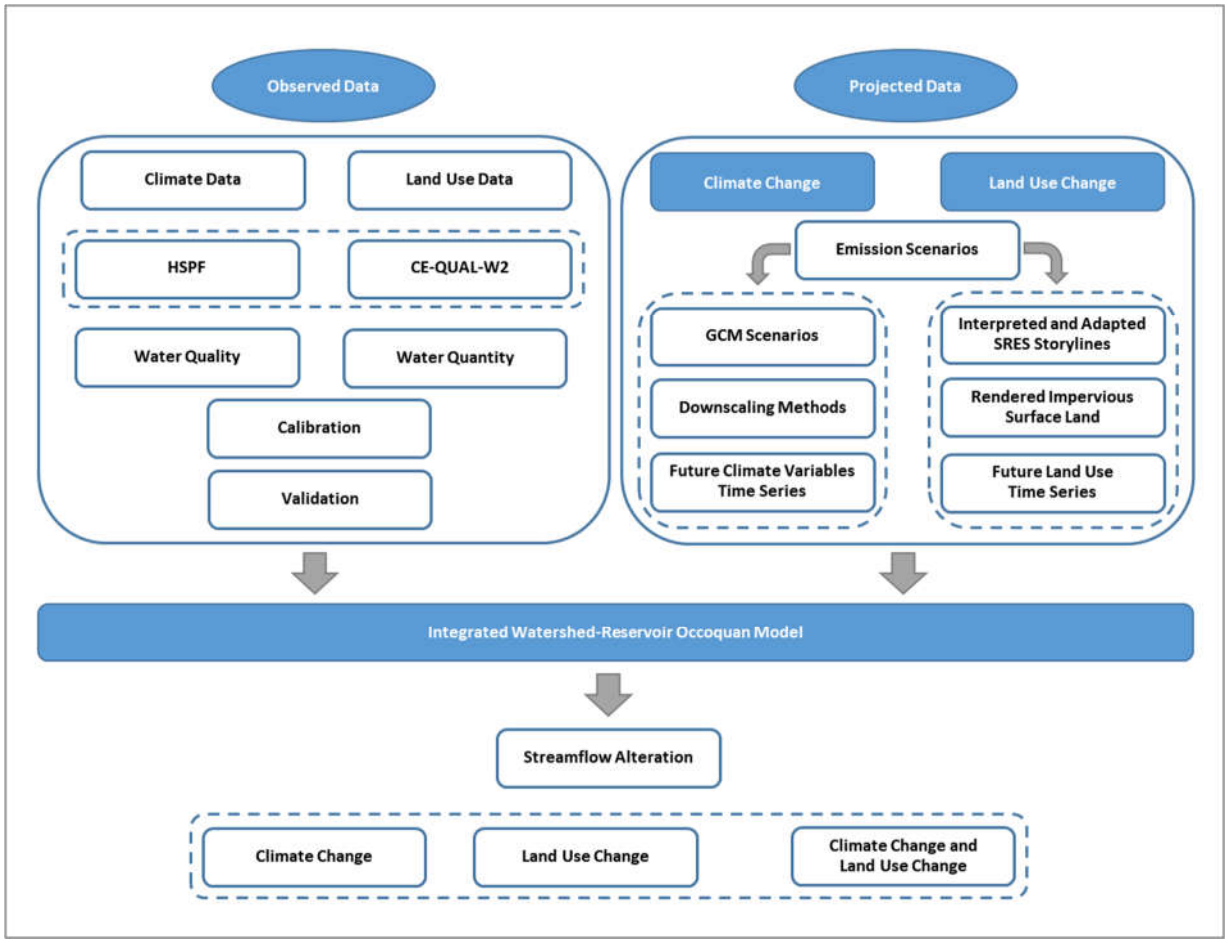

Figure 5-2. Designed study framework for quantifying water quality alteration due to the climate change and land use change in the study area.

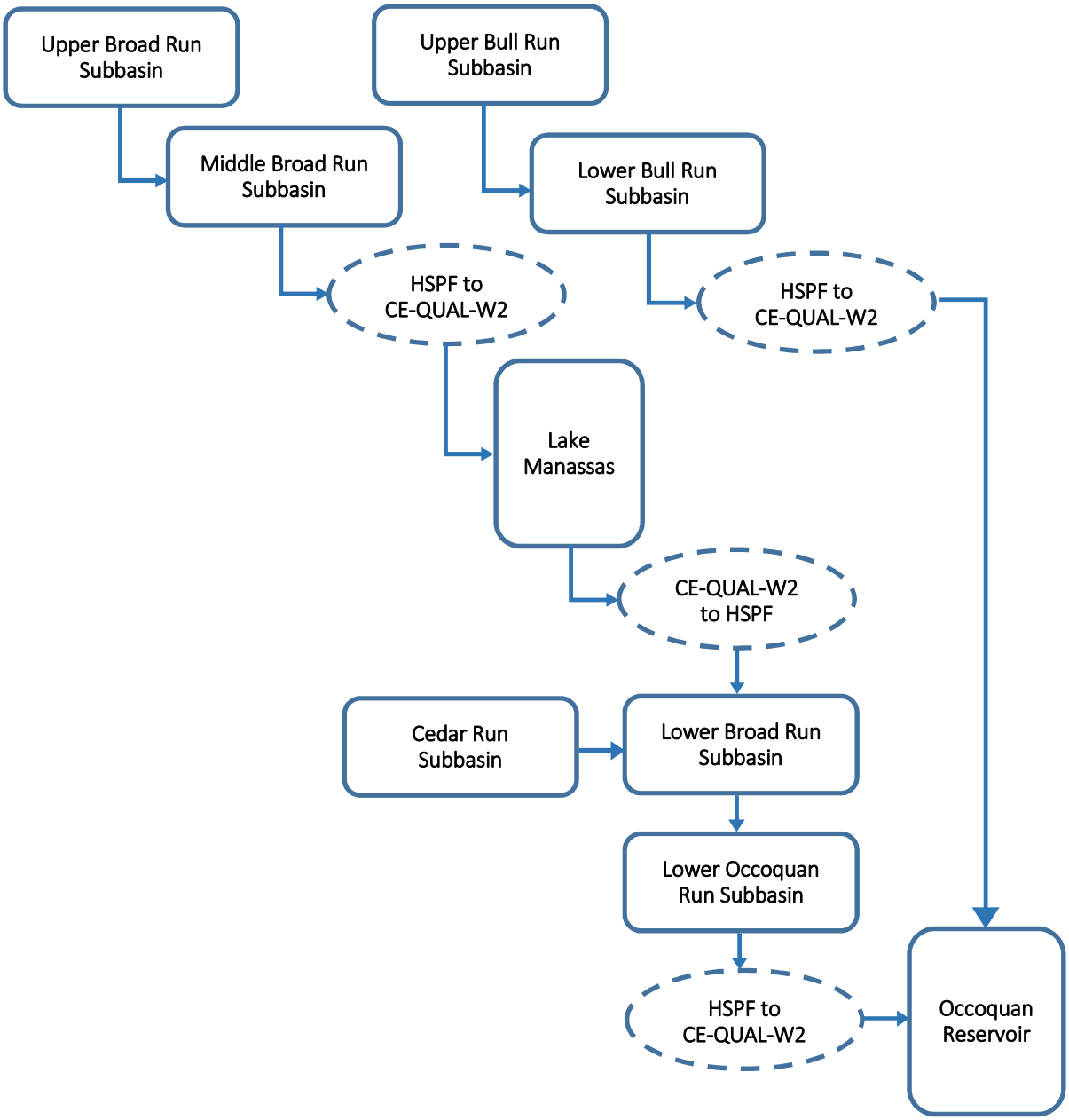

Figure 5-3. Schematic of Occoquan linked watershed-reservoir model.

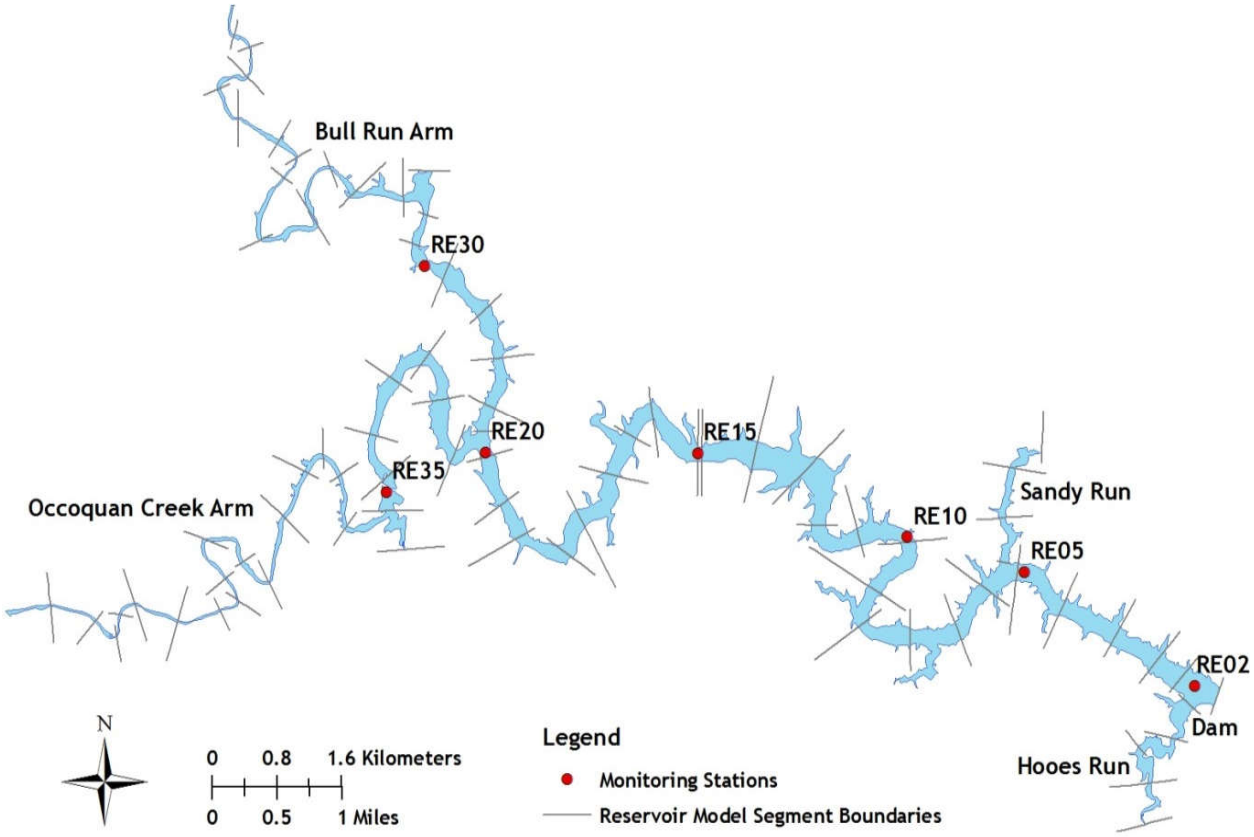

Figure 5-4. Occoquan reservoir segmentations and monitoring station locations.

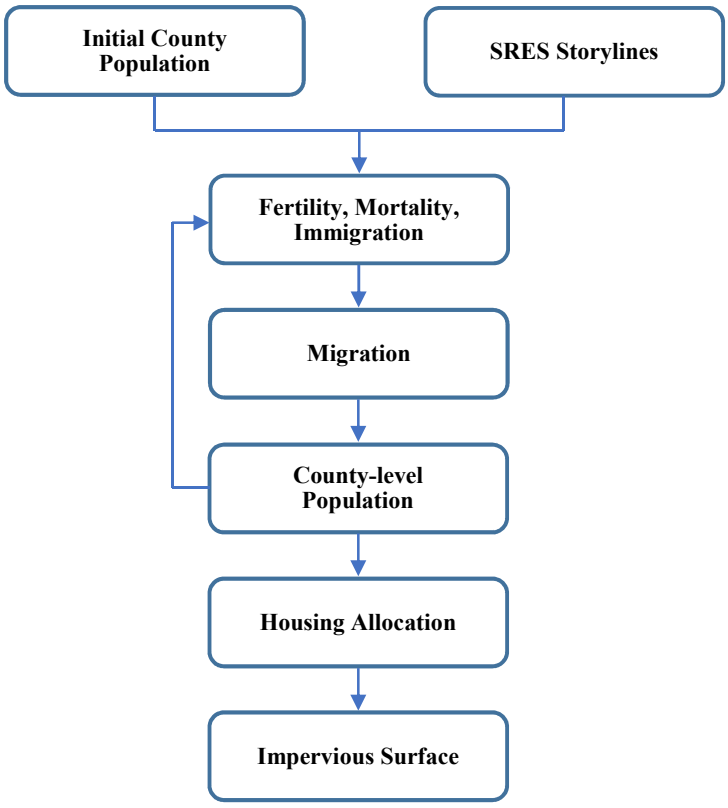

Figure 5-5. Overview of ICLUS modeling process (Bierwagen and Morefield 2014).

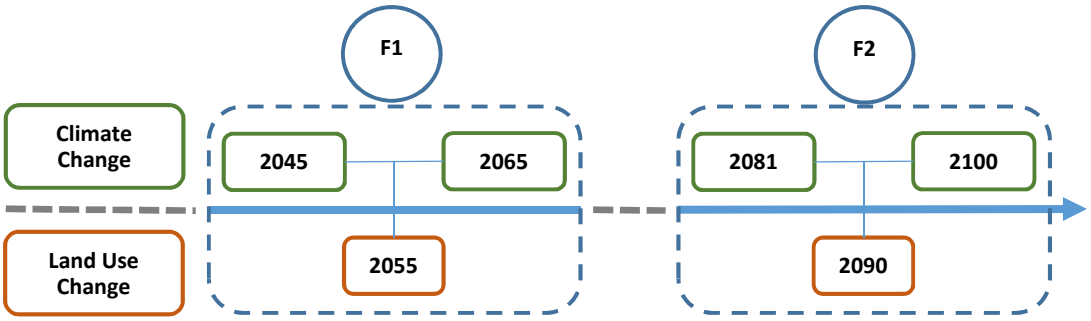

Figure 5-6. Future climate change (green) and land use change (orange) horizons for two future time periods (2046-2065 (F1) and 2081-2100 (F2)).

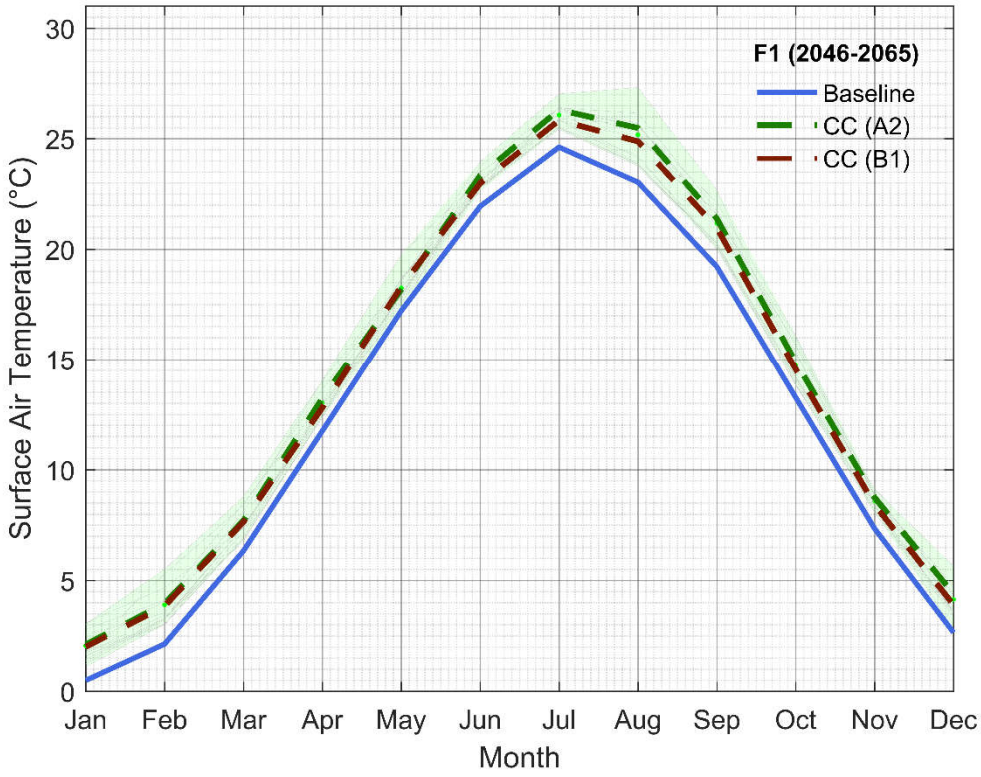

Figure 5-7. Monthly variations of projected Climate Change (CC) surface air temperatures for the mid 21st century (F1). The solid blue line represents the historical values and the light green shaded area envelopes the possible maximums and minimums of the projections while the dashed lines are depicting the medians of climate change projected surface air temperatures categorized based on A2 and B1 emission scenarios.

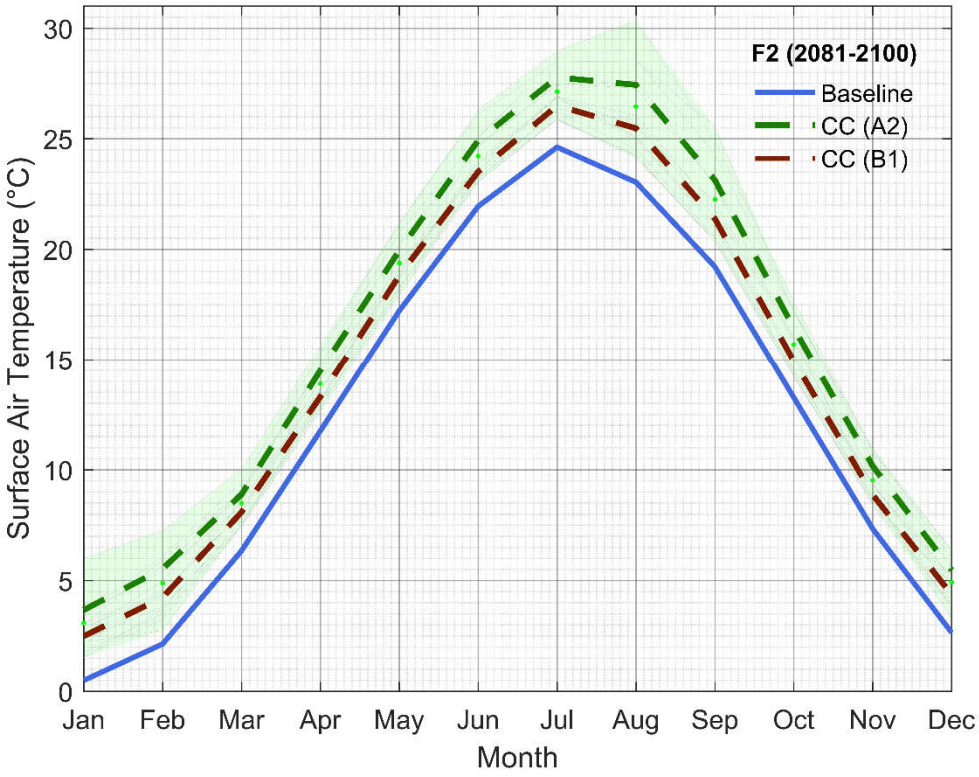

Figure 5-8. Monthly variations of projected Climate Change (CC) surface air temperatures for the late 21st century (F2). The solid blue line represents the historical values and the light green shaded area envelopes the possible maximums and minimums of the projections while the dashed lines are depicting the medians of climate change projected surface air temperatures categorized based on A2 and B1 emission scenarios.

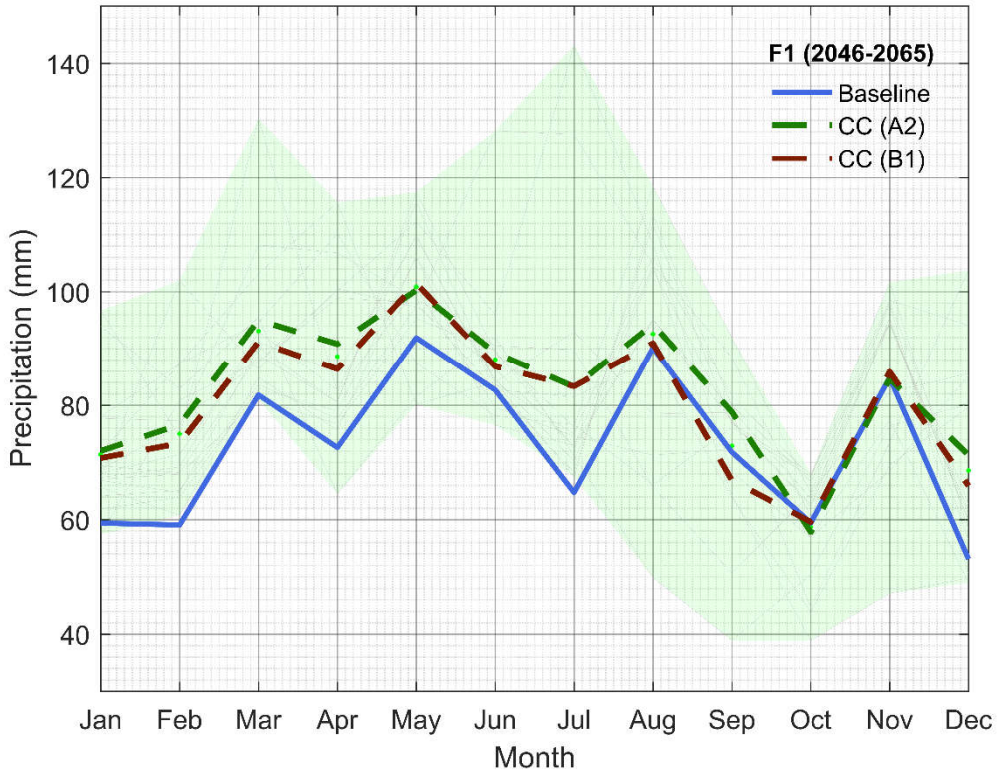

Figure 5-9. Monthly variations of projected Climate Change (CC) precipitations for the mid 21st century (F1). The solid blue line represents the historical values and the light green shaded area envelopes the possible maximums and minimums of the projections while the dashed lines are depicting the medians of climate change projected precipitations categorized based on A2 and B1 emission scenarios.

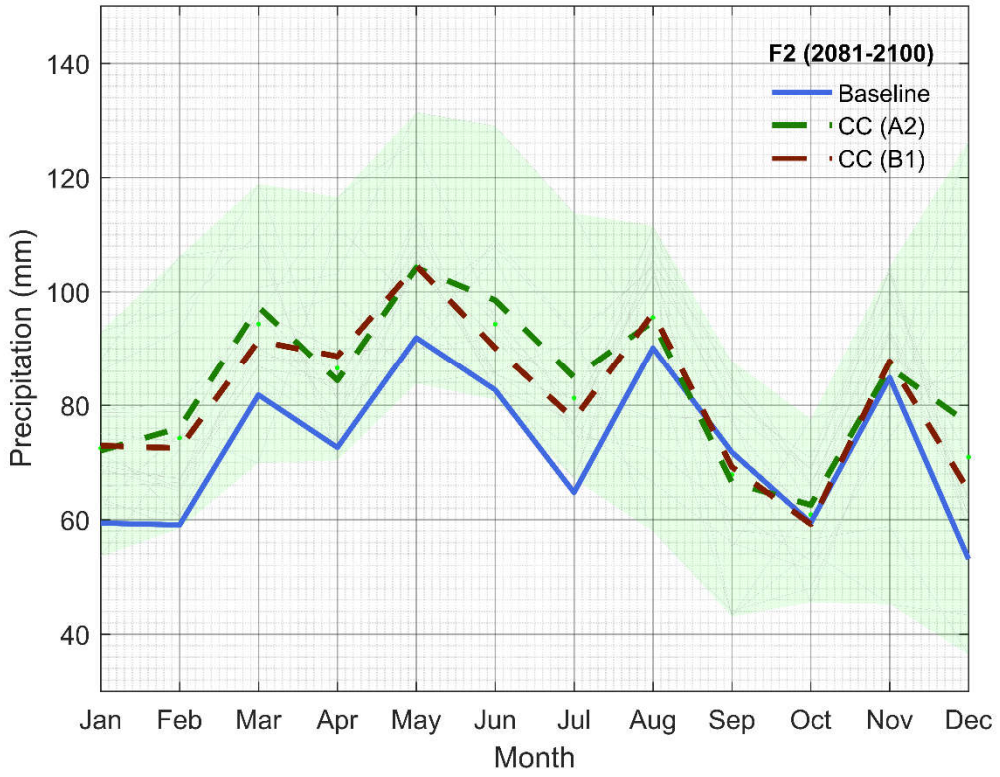

Figure 5-10. Monthly variations of projected Climate Change (CC) precipitations for the late 21st century (F2). The blue solid line represents the historical values and the light green shaded area envelopes the possible maximums and minimums of the projections while the dashed lines are depicting the medians of climate change projected precipitations categorized based on A2 and B1 emission scenarios.

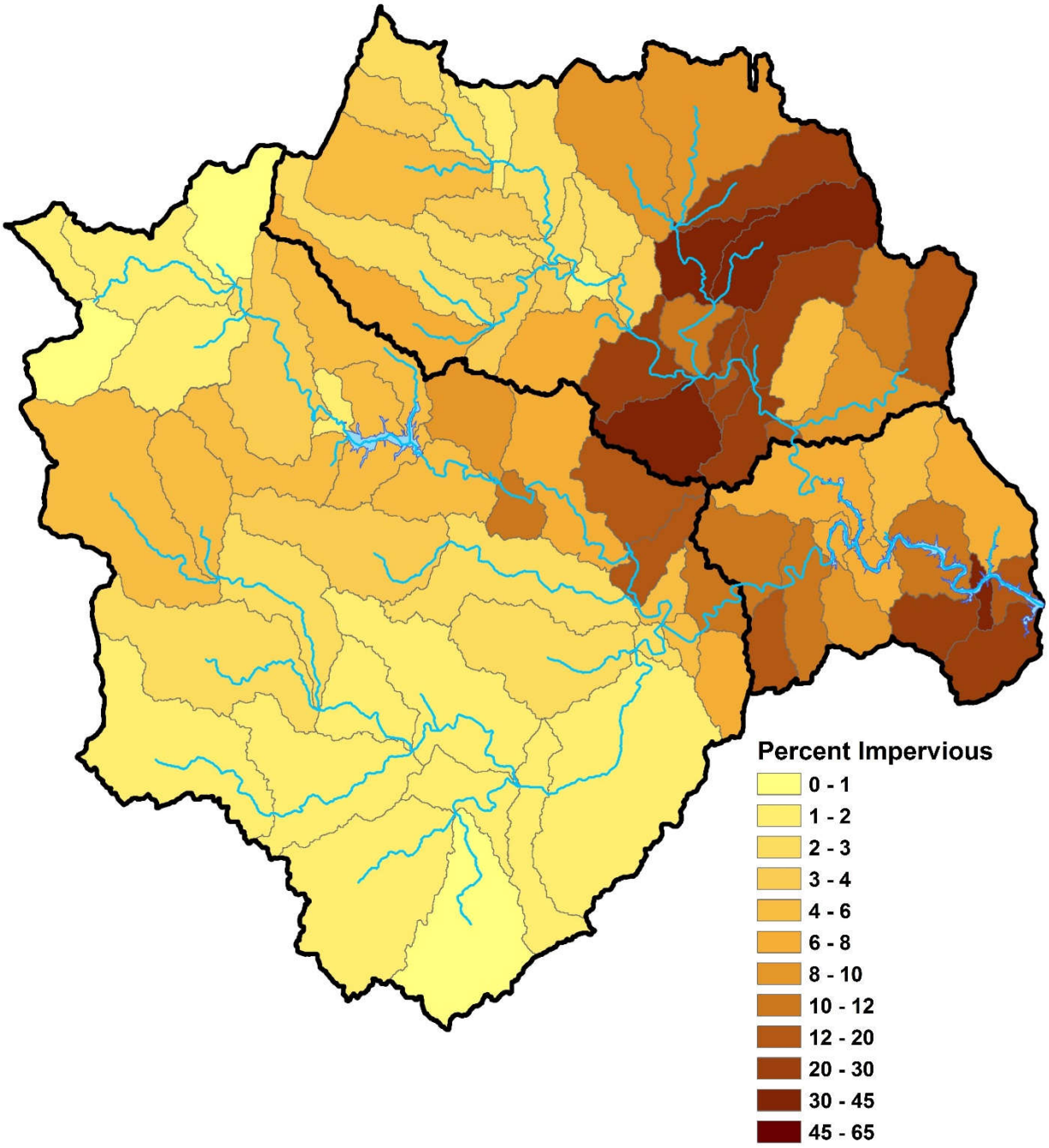

Figure 5-11. Estimate percent impervious surface areas for Occoquan watershed in the historical period. Further delineation (gray lines) was carried out based on 1) rainfall or important meteorological data; 2) soil type; 3) land use conditions; 4) reach characteristics; 5) any other important physical characteristic (infiltration, overland slope, etc.) (Xu et al. 2007).

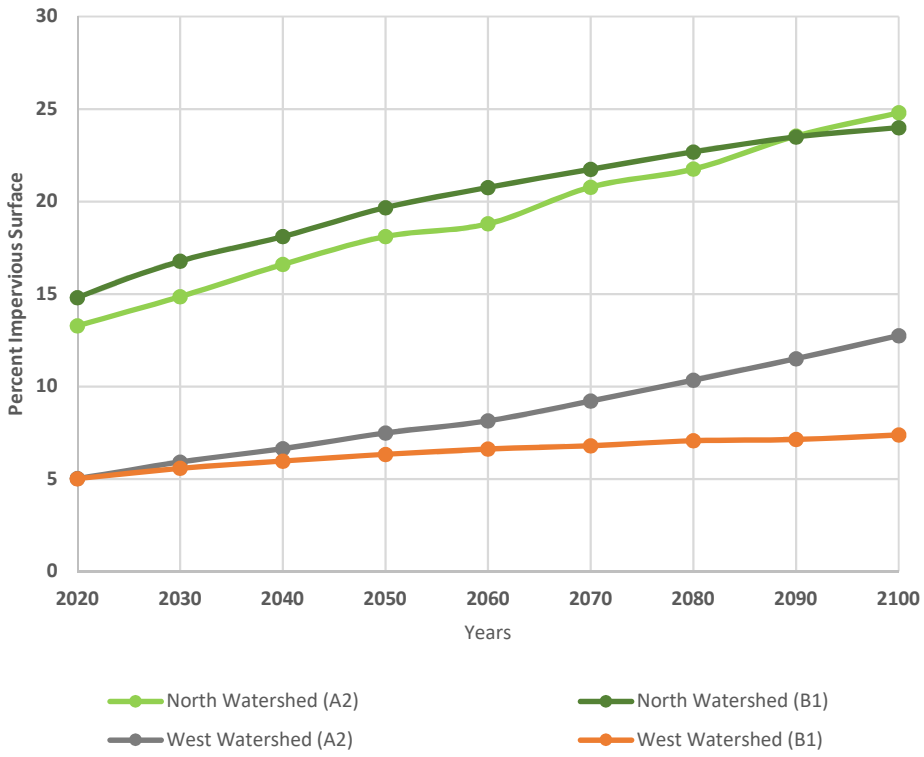

Figure 5-12. Estimate percent impervious surface for Occoquan watershed for future projections in Bull Run and Occoquan Creek using A2 and B1 emission scenarios.

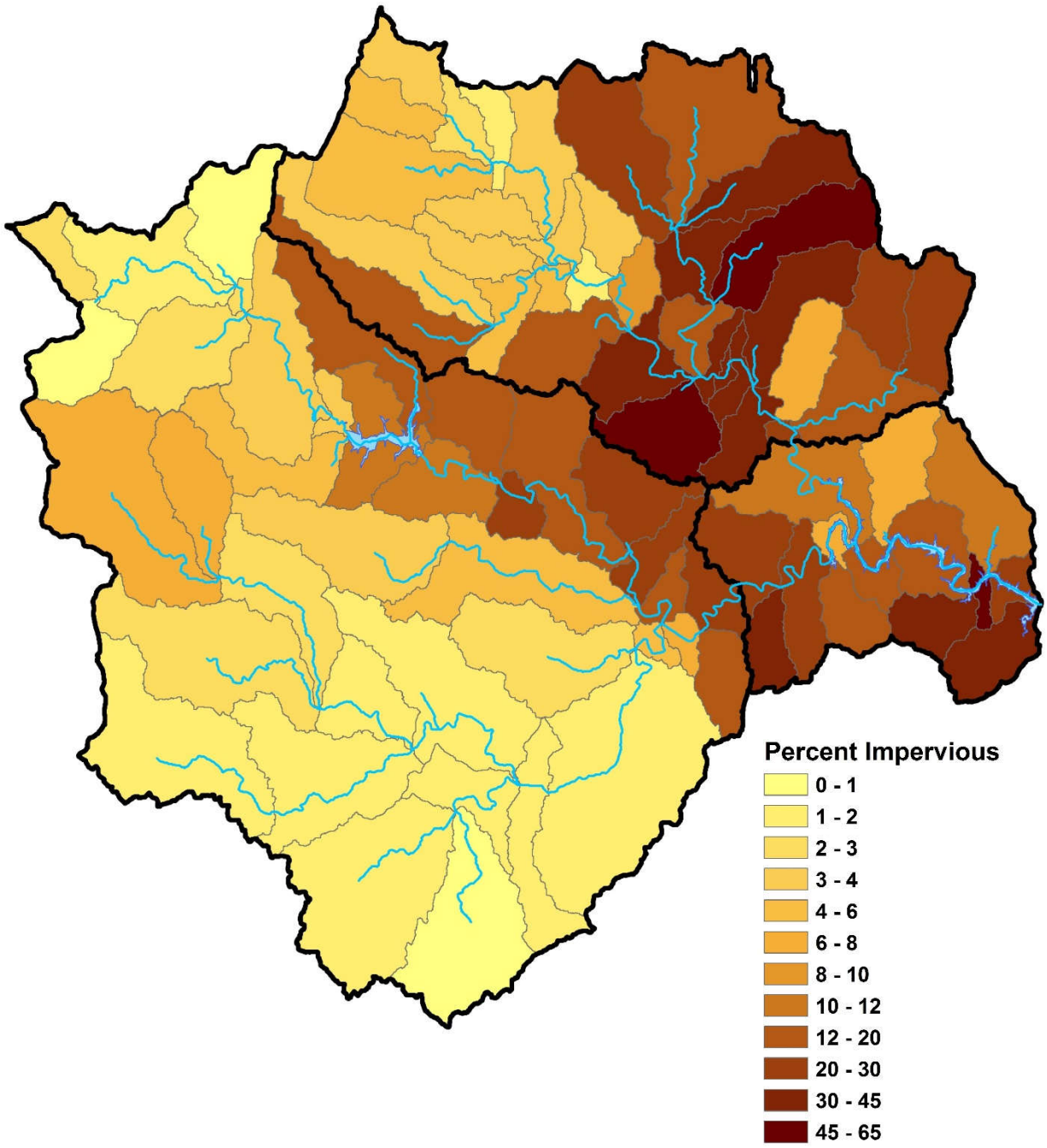

Figure 5-13. Estimate percent impervious surface areas in Occoquan watershed for middle of mid 21st period (2055) using A2 emission scenario.

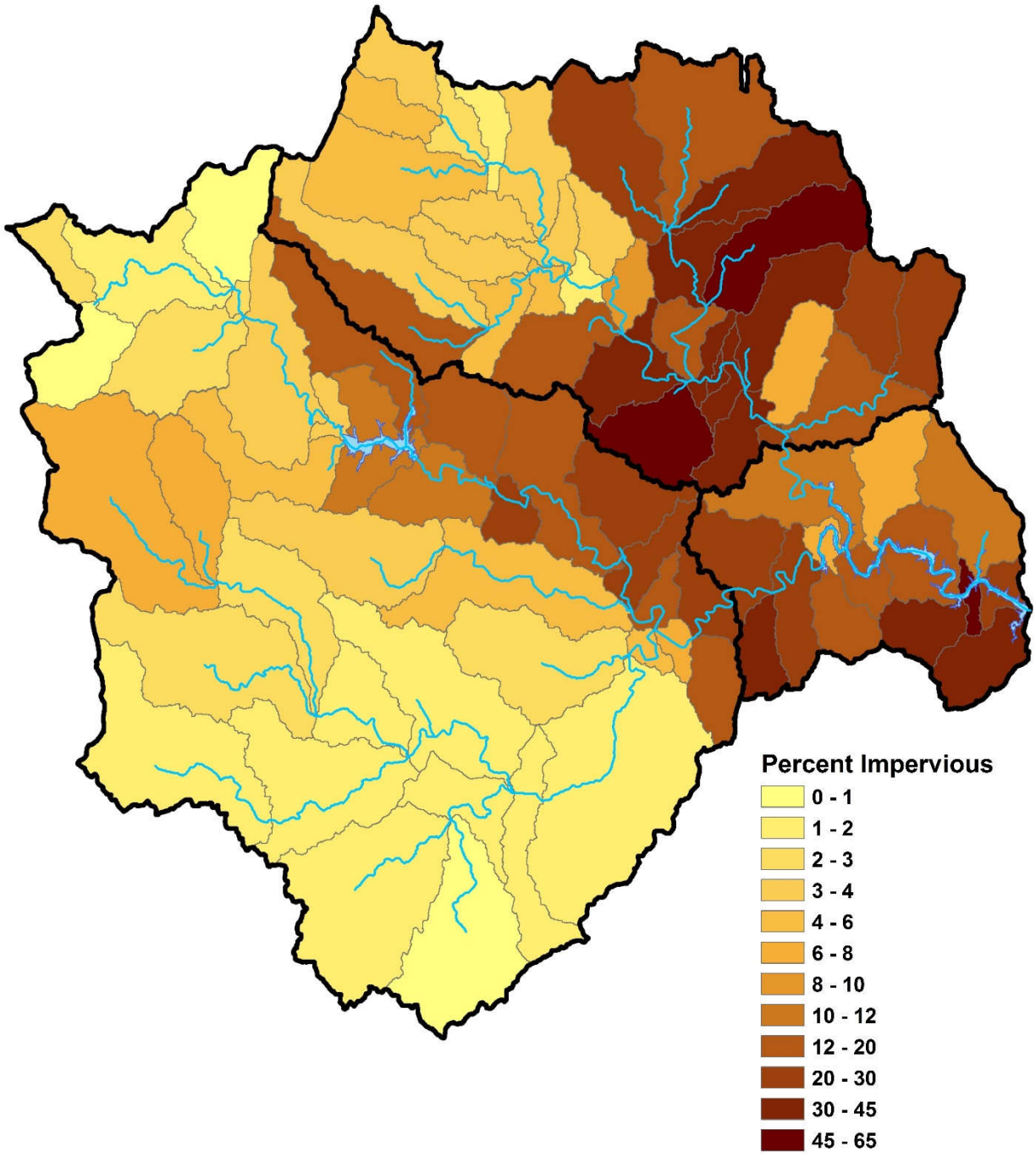

Figure 5-14. Estimate percent impervious surface areas in Occoquan watershed for middle of later 21st period (2090) using A2 emission scenario.

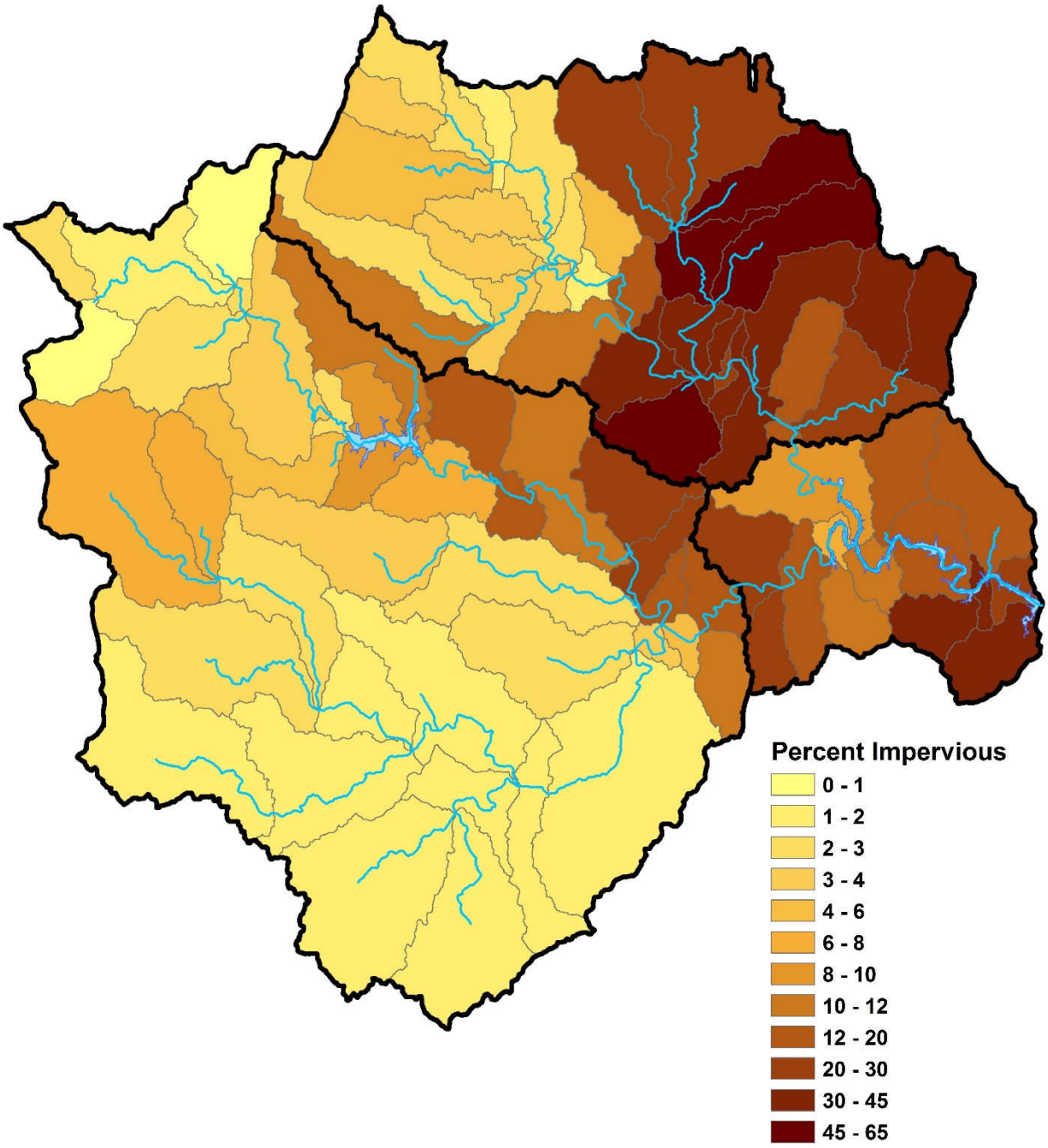

Figure 5-15. Estimate percent impervious surface areas in Occoquan watershed for middle of mid 21st period (2055) using B1 emission scenario.

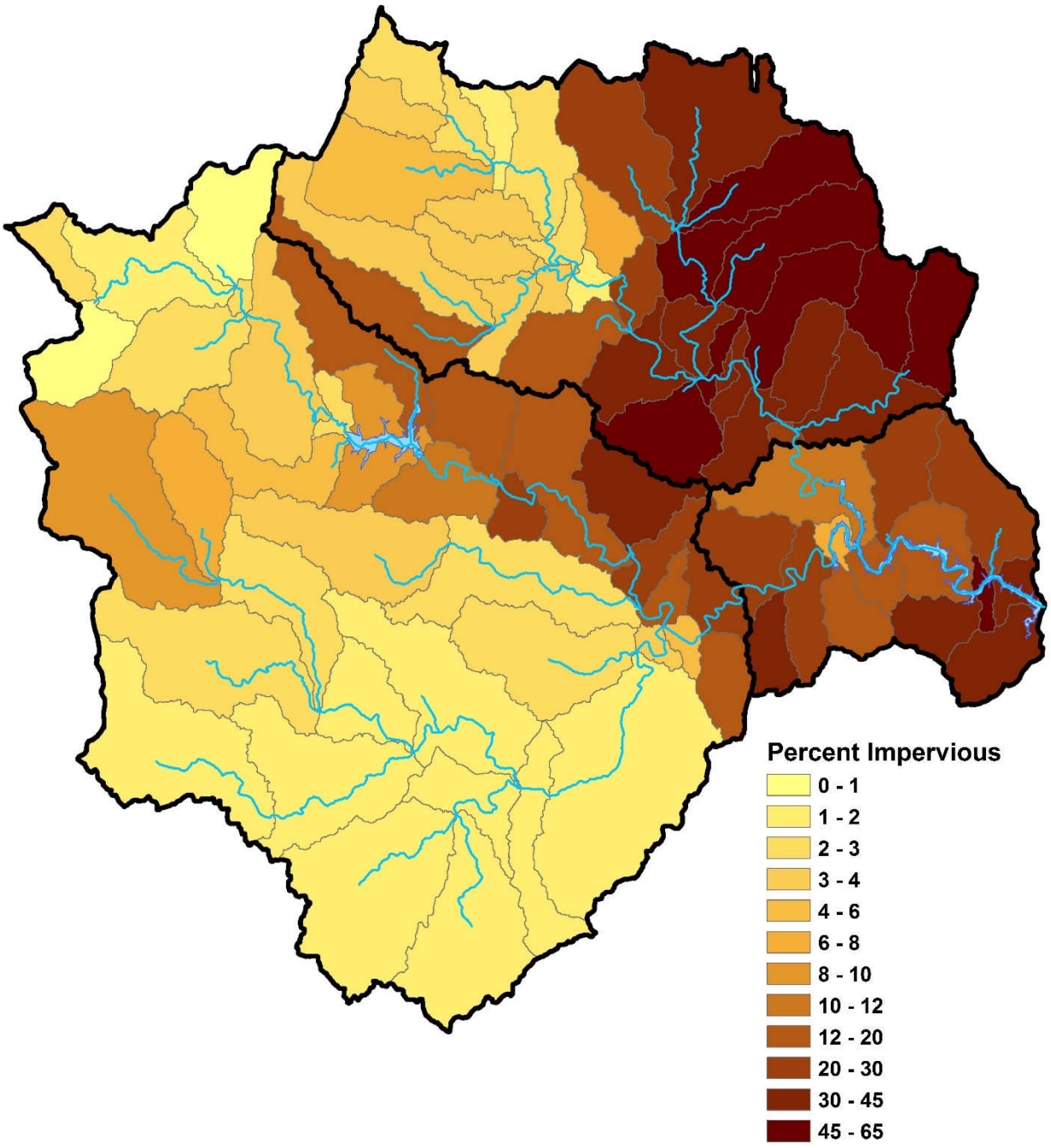

Figure 5-16. Estimate percent impervious surface areas in Occoquan watershed for middle of late 21st period (2090) using B1 emission scenario.

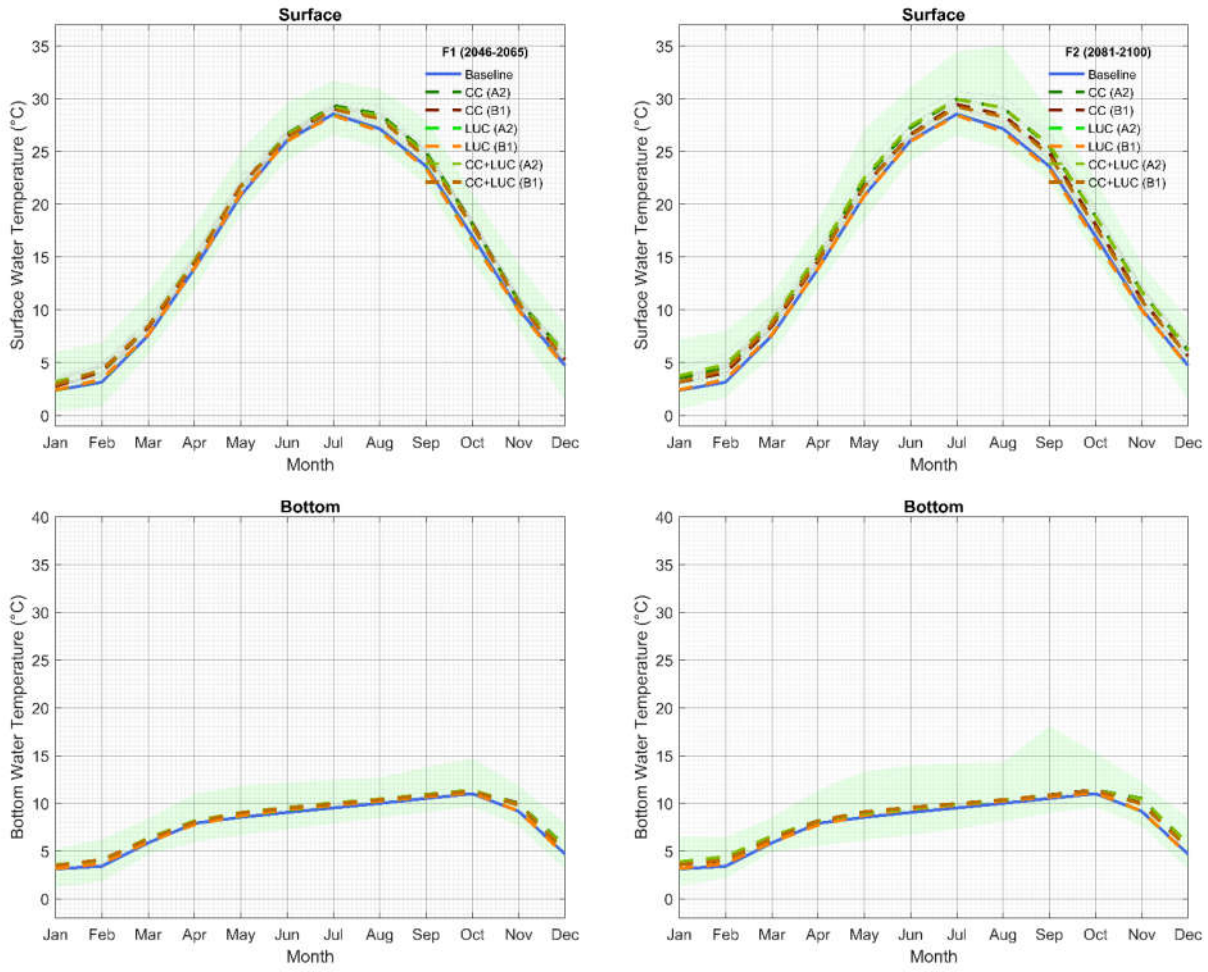

Figure 5-17. Projected monthly variations of surface and bottom water temperatures for the Occoquan reservoir at RE02 using Climate Change (CC), Land Use Change (LUC) and combined (CC+LUC) effects in mid and late 21st century (F1 and F2). The solid blue line represents the historical values and the light green shaded area envelopes the possible maximums and minimums of the projections while the dashed lines are depicting the medians of models grouped based on climate change and land use change projections and A2 and B1 emission scenarios.

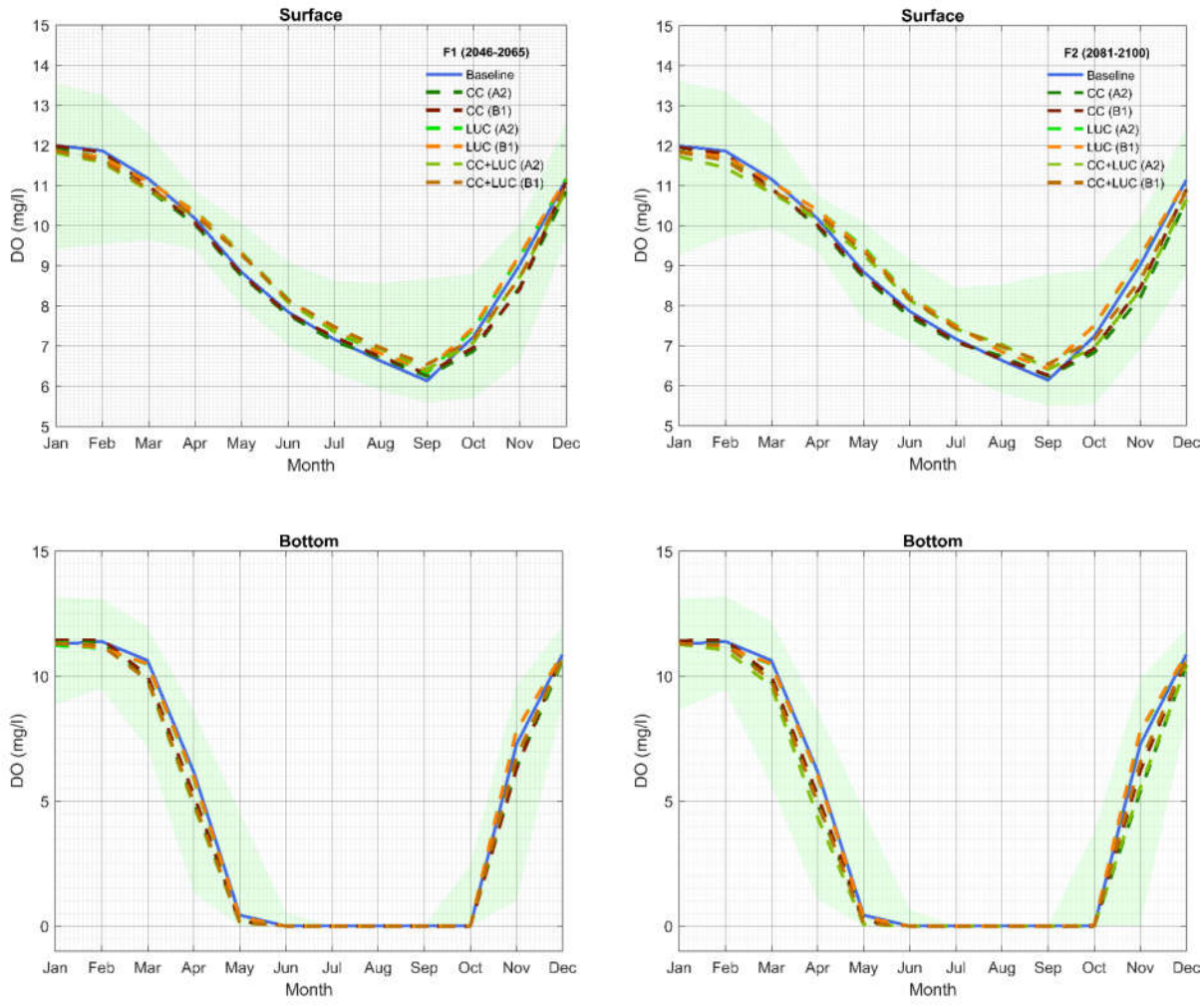

Figure 5-18. Projected monthly variations of surface and bottom dissolved oxygen concentration levels for the Occoquan reservoir at RE02 using Climate Change (CC), Land Use Change (LUC) and combined (CC+LUC) effects in mid and late 21st century (F1 and F2). The solid blue line represents the historical values and the light green shaded area envelopes the possible maximums and minimums of the projections while the dashed lines are depicting the medians of models grouped based on climate change and land use change projections and A2 and B1 emission scenarios.

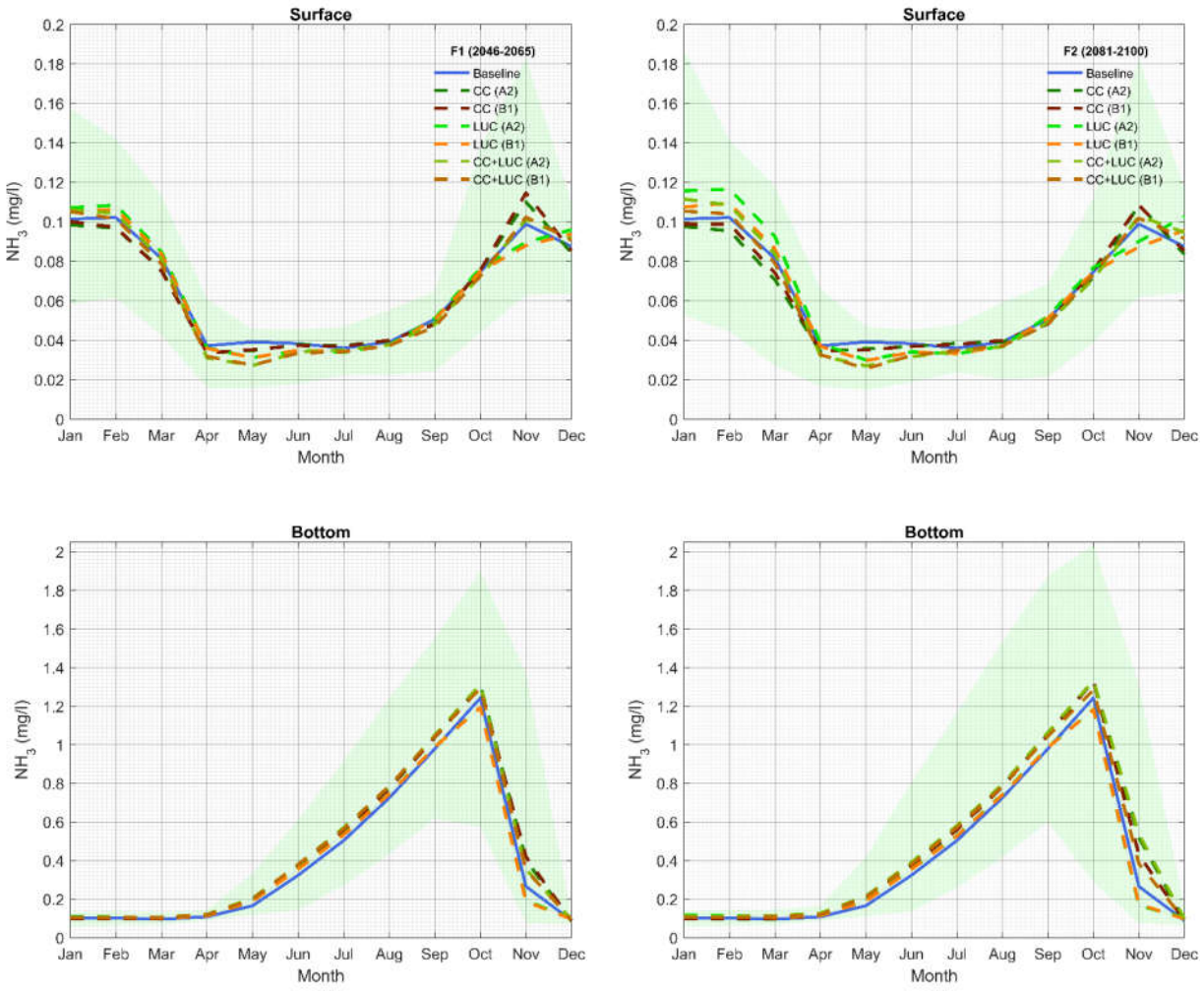

Figure 5-19. Projected monthly variations of surface and bottom ammonia concentration levels for the Occoquan reservoir at RE02 using Climate Change (CC), Land Use Change (LUC) and combined (CC+LUC) effects in mid and late 21st century (F1 and F2). The solid blue line represents the historical values and the light green shaded area envelopes the possible maximums and minimums of the projections while the dashed lines are depicting the medians of models grouped based on climate change and land use change projections and A2 and B1 emission scenarios.

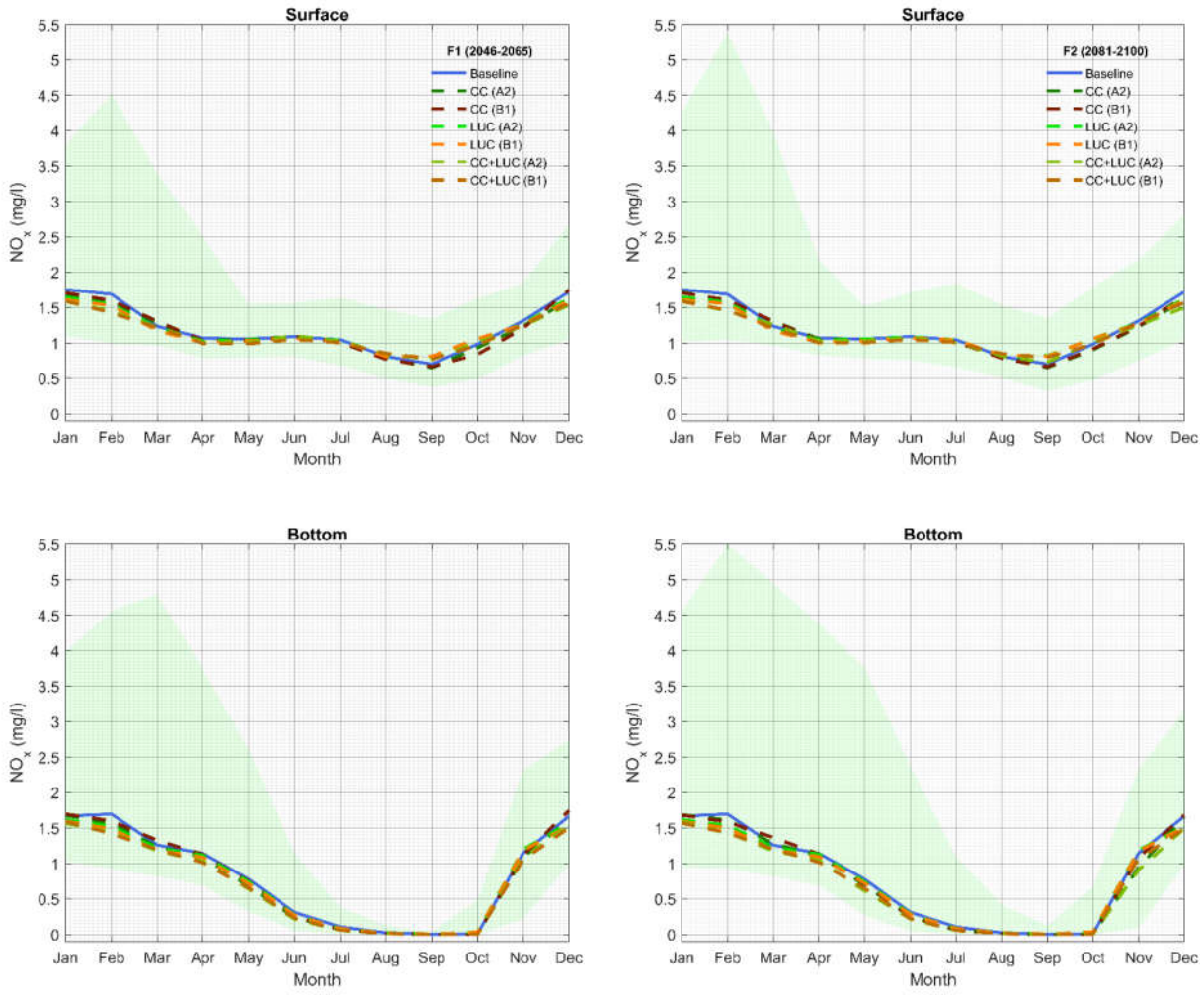

Figure 5-20. Projected monthly variations of surface and bottom nitrate-nitrite nitrogen concentration levels for the Occoquan reservoir at RE02 using Climate Change (CC), Land Use Change (LUC) and combined (CC+LUC) effects in mid and late 21st century (F1 and F2). The solid blue line represents the historical values and the light green shaded area envelopes the possible maximums and minimums of the projections while the dashed lines are depicting the medians of models grouped based on climate change and land use change projections and A2 and B1 emission scenarios.

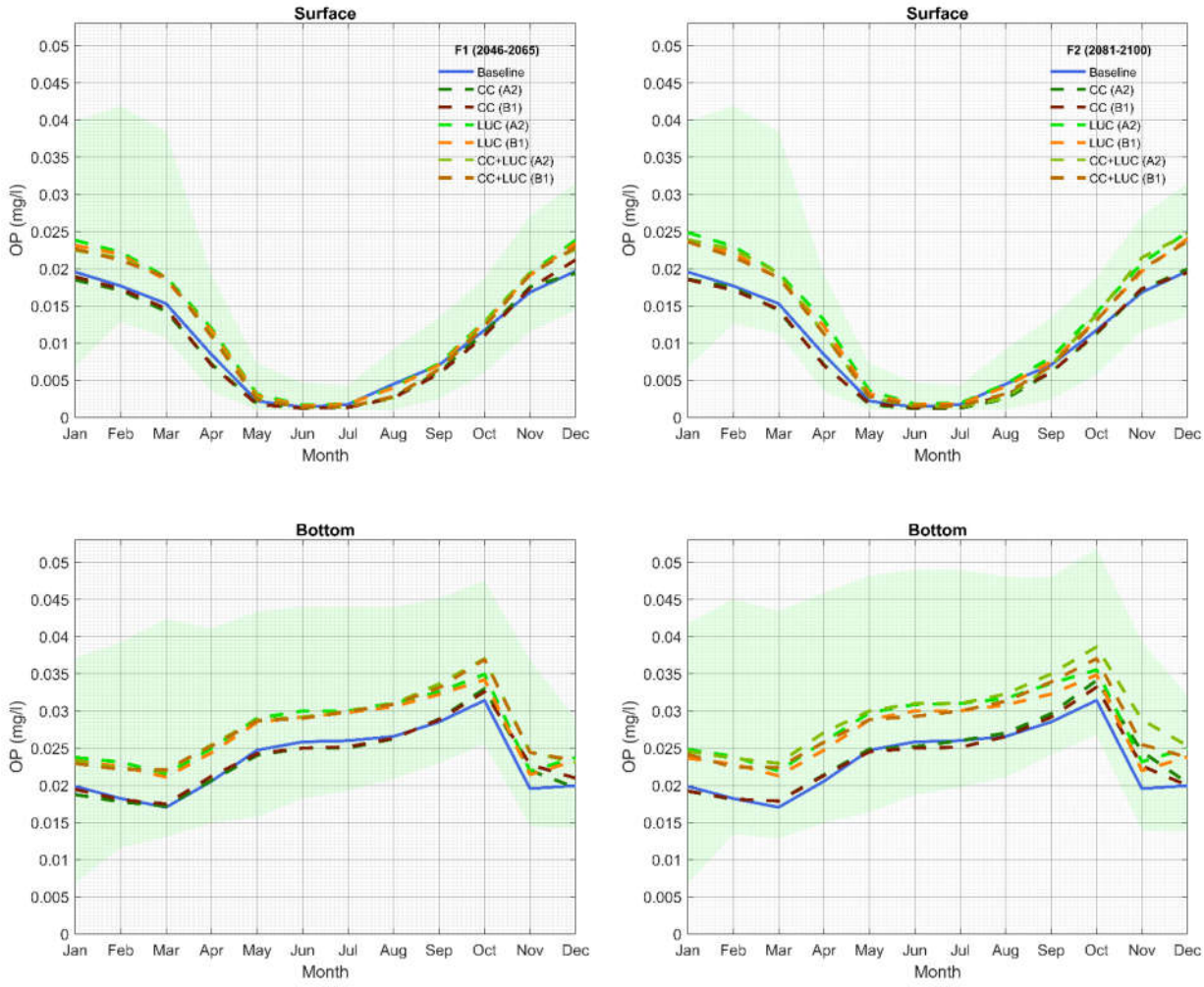

Figure 5-21. Projected monthly variations of surface and bottom orthophosphate phosphorus concentration levels for the Occoquan reservoir at RE02 using Climate Change (CC), Land Use Change (LUC) and combined (CC+LUC) effects in mid and late 21st century (F1 and F2). The solid blue line represents the historical values and the light green shaded area envelopes the possible maximums and minimums of the projections while the dashed lines are depicting the medians of models grouped based on climate change and land use change projections and A2 and B1 emission scenarios.

Chapter 6 Summary, Conclusions, and Recommendations for Further Study

6.1 Summary

This research has presented climate change and land use change impact assessment conducted using the Occoquan Model, a complexly-linked network of seven watershed models and two reservoir models. Water quantity and quality were analyzed using four different themes (1. present climate, present land use; 2. future climate, present land use; 3. present climate, future land use; 4. future climate, future land use) using two future time periods (2046-2065 and 2081-2100).

The first study included a hydrological impact assessment of climate change on Broad Run watershed with the focus on identifying the main factors affecting the climate change projection models. A total of 32 model projections were developed using two emission scenarios, four GCMs, two downscaling methods, and two time periods. The results have shown that some of these model projections estimated up to a 30% increase in the median of mean annual flows. On average, an 8% increase in the median of mean annual flows was projected for both the mid and late 21st century. These changes were more prominent using the Quantile Mapping (QM) downscaling method compared to Delta Change (DC) method. An ANOVA test was used to identify which factors are affecting climate change projection models the most (two emission scenarios, four GCMs, and two downscaling methods and two periods in the mid and late 21st century). Results indicated that only the downscaling method had a statistically significant effect on the mean response, whereas the other factors did not.

In the second study, the impact of individual and combined effects of climate change and land use change on the Occoquan watershed was studied. Streamflow characteristics were analyzed separately as Bull Run and Occoquan Creek subbasins. The Bull Run is more urbanized with an average impervious surface area of 12%, while the Occoquan Creek is mostly forest, pastures, and low-density residential with an average impervious surface area of 4%. The results indicated that the entire watershed would experience increases in annual average surface air temperatures under the climate change scenarios ranging from 11% to 19%. These changes are expected to be more prevalent in the late 21st century. The maximum and minimum surface air temperatures are also expected to increase. Overall, increases in surface air temperatures are more prominent in the late 21st century using A2 scenarios while B1 scenarios in mid 21st century are showing least

amounts of increases. Furthermore, the climate change models have projected an increase in the total amount of precipitation. The seasonal increase in median precipitation ranges from 3% in fall to 13% in spring.

Under the climate change projections alone, it is expected that high flows (Q_{10}) will increase in both the mid and late 21st century ranging from 9% to 13%, while low flows (Q_{90}) are projected to decrease ranging from 6% to 38% with greater shifts in the late 21st century compared to the mid century. Moreover, the Q_{IQR}, is projected to increase in both time horizons. On the other hand, changes in flow characteristics are more pronounced when only future land use changes are considered. The flow increase is more noticeable in spring and in the Occoquan Creek which projected to experience a rapid urbanization. Both high flows (Q_{10}) and low flows (Q_{90}) are projected to increase ranging from 15% to 75% and 20% to 206%, respectively. Additionally, the Q_{IQR} is projected to increase ranging from 16% to 58%. Finally, under the joint examination of both future climate and land use change, an amplifying effect on the mean annual flows and high flows is observed. In contrast, climate change is projected to dampen the extreme increases in the low flows created by the land use change. The projected alterations are synergistic and more than the arithmetic sum of each individual driving forces.

The third research study examined the impact of the individual and combined effects of climate change and land use change on the Occoquan reservoir's water quality. Under the climate change projections alone, the Occoquan reservoir will experience increases in surface water temperatures (annual average, maximum and minimum). These increases are expected to be more in the late 21st century. The A2 scenario shows higher increases compared to the B1 scenario, with the highest changes in summer months. On the other hand, the effect of only land use change on the surface water temperature is not very noticeable. It is expected that higher water temperatures will promote decreased oxygen solubility and greater heterotrophy. Moreover, longer anoxic conditions are projected at the bottom of the reservoir. It can be seen from the results that higher water temperature will increase the denitrifying capacity of the reservoir, especially during summer months, further reducing the nitrate concentration in the reservoir. However, due to higher projected water temperature and high DO deficiency, the release of ammonia, phosphorus, and other nuisance substances may increase in the future.

This research has demonstrated the importance of comprehensive regional climate change and land use change impact studies. It also confirms the concerns regarding the inadequacy of current stormwater infrastructure which may not be unable to meet the future requirements imposed by climate change and land use change in the study area (Beighley and Moglen 2002; Hejazi and Moglen 2008; Moglen and Rios Vidal 2014; Stagge and Moglen 2017). This study has also shed some light of the possible adverse effect of projected climate and land use change on the water quality of the Occoquan reservoir due to higher water temperatures and consequently extended anoxic condition during the summer.

6.2 Conclusions

The key findings of this research were as follows:

- All projection models showed increases in mean annual surface air temperatures. The A2 scenario showed higher increases compared to the B1 scenario, with highest changes during the summer months.
- The shift in location and dispersal in mean annual surface air temperatures were higher in the late 21st century than the mid 21st century (2081-2100 compared to 2046-2065).
- Both the maximum and minimum surface air temperatures were projected to increase in both future time periods.
- Annual maximum surface air temperatures are projected to increase by 7% and 13% on average for the two future time periods (2046-2065 and 2081-2100), respectively.
- Annual minimum surface air temperatures are projected to increase by 21% and 36% for the first and second periods, respectively. Minimum surface air temperatures are expected to rise at slightly higher rates compared to maximum surface air temperatures. This leads to a decrease in an annual average of the diurnal temperature range, which is the difference between daily maximum and minimum temperatures.
- The highest rises in average monthly surface air temperature occur in summer months (June, July, and August) by 9%, with August having peak monthly average surface air temperatures of 27.3 and 31.6 °C for the 2046-2065 and 2081-2100 periods.
- Increases in surface air temperatures are more prominent in the late 21st century using A2 scenarios while B1 scenarios in mid 21st century are showing least amounts of increases.

- The higher amounts of precipitation are projected in the study area in both future periods. Mean annual precipitation is projected to increase ranging from 2% to 17% with the median of 9% and 11% increases for mid and late 21st century. Projection models with the emission scenario A2 in the late 21st century display more precipitation than B1 in the mid 21st century.
- In the first period (2046-2065), the highest amount of predicted monthly precipitation increase is projected in July while the amount of precipitation is expected to decrease in September. In the second period, the median of projected precipitations are higher for all of the months except for September.
- On a seasonal basis, the increase in precipitation is more prominent in the summer and projected to decrease in the fall.
- Considering two emission scenarios, four GCMs, two downscaling methods and two periods in the mid and late 21st century. The choice of the downscaling method had a statistically significant effect on the mean runoff response, whereas the other factors did not.
- Under the climate change scenarios for both Bull Run and Occoquan Creek, for both future time periods, the median of mean annual flows are close to the historical values.
- In the Bull Run, under the climate change scenarios, the high flows (Q_{10}) are projected to increase by 12% and 13% and the low flows (Q_{90}) are projected to decrease by 4% and 6% for mid and late 21st century. Furthermore, the Q_{IQR} is projected to increase by 16% and 14% for the 2046-2065 and 2081-2100 periods.
- Similarly, using climate change scenarios, in the Occoquan Creek, the high flows (Q_{10}) are projected to increase by 9% for both future time periods while the low flows (Q_{90}) are projected to decrease by 28% and 38% for mid and late 21st century. Additionally, the Q_{IQR} is projected to increase by 14% and 13% for mid and late 21st century.
- Land use change shows dramatic changes in flow characteristics in both watersheds for all of the scenarios.
- By applying the land use change in the Bull Run, the median of mean annual flows are projected to increase by 16% and 21% for mid and late 21st century. The high flows (Q_{10}) are projected to increase by 15% and 21% and the low flows (Q_{90}) are projected to increase by 20% and 28% for mid and late 21st century, respectively. The Q_{IQR} is projected to increase by 16% and 20% for mid and late 21st century.

- Land use change will have more drastic effects on flow characteristics in the Occoquan Creek. The median of mean annual flows are projected to increase by 73% and 75% for mid and late 21st century. The high flows (Q_{10}) are projected to increase by 73% and 74%, while the low flows (Q_{90}) are projected to increase by 192% and 206% for the 2046-2065 and 2081-2100 periods, respectively. The Q_{IQR} is projected to increase by 57% and 58% for mid and late 21st century.
- Using the climate change scenarios, the Occoquan reservoir will likely experience increases in water temperatures both at the surface and at the bottom. In the mid 21st century, the annual surface water temperature will increase by 6% and 5% for the A2 and B1 emission scenarios. The amount of increase in the late 21st century will be 9% and 6% for the A2 and B1 emission scenarios, respectively.
- Climate change is projected to increase annual maximum surface water temperature by 4% and 6% in the mid and late 21st century. Annual minimum surface water temperature also projected to increase by 7% and 9% for the first and second periods, respectively. Overall, an increase in water temperatures are projected be more pronounced in the summer months.
- Land use change effect on thermal conditions of surface water temperature will not be noticeable.
- By applying the climate change scenarios, at the bottom of the reservoir, water temperature is anticipated to increase by 6% and 5% using A2 and B1 emission scenarios for the mid 21st century and 8% and 6% for the late 21st century. Maximum bottom water temperature is expected to remain at the historical measures while minimum bottom water temperature is predicted to increase by 7% and 5% in the first and second periods, respectively.
- The sole effect of land use change on bottom water temperatures are comparable to the historical values.
- Increases in water temperatures are expected to be more prevalent in the late 21st century.
- Using climate change scenarios, reduced DO concentrations are projected both at the surface and bottom of the Occoquan reservoir.
- Using both driving forces, more extended anoxic conditions are projected at the bottom of the reservoir.

- It is projected that the thermal stratification period is likely to expand, which will start in late spring (June instead of July) and end at the beginning of the fall (October instead of September).
- Lower DO concentrations are projected in the bottom of the Occoquan reservoir applying both driving forces. These decreases are more distinct using climate change scenarios.
- Increased period of anoxic nutrient interaction between the sediment layer and water column may increase due to stronger thermal stratification. This may promote an upward movement of nutrient fluxes from the reduced environment of the bottom layer to the surface.
- Under land use change, higher amounts of distributed and stream inflows are projected to flow into the Occoquan reservoir.
- Higher water temperatures are projected to increase the denitrifying capacity of the reservoir, especially during summer months, further reducing the nitrate concentration in the reservoir.
- Warmer water temperature induced by climate change may increase higher OP concentration due to the anoxic environment during summer months.

6.3 Recommended Future Research

While these studies all yielded valuable insight regarding the possible impacts of climate change and land use change on the Occoquan watershed, they also revealed avenues for further research.

- Using the Regional Climate Model (RCM) instead of GCM can improve the accuracy of the climatic projections. An RCM is a three-dimensional mathematical model with a higher resolution than GCM. While the RCM domain is typically nested within the grid used by a GCM, its application is more computationally intensive. As such, a good computing infrastructure can significantly increase the outcome of climate change impact studies.
- The choice of the downscaling method in this study emerged as the main source of uncertainty. Application of other downscaling methods can shed light on the suitability of those methods for such studies.
- While land use change based on IPCC's fifth Assessment Report (AR5) has not been yet developed for the United States, availability of such information can lead the use of Representative Concentration Pathway (RCP) trajectories innated of SRES.
- While these studies affirmed the importance of comprehensive integrated scenario-based climate change and land use impact studies, the additional research recommended in this

chapter would improve the predictive capabilities of such research in the Occoquan watershed in future.

6.4 References

Beighley, R. E., and Moglen, G. E. (2002). "Trend assessment in rainfall-runoff behavior in urbanizing watersheds." Journal of Hydrologic Engineering, 7(1), 27-34.

Hejazi, M. I., and Moglen, G. E. (2008). "The effect of climate and land use change on flow duration in the Maryland Piedmont region." Hydrological Processes: An International Journal, 22(24), 4710-4722.

Moglen, G. E., and Rios Vidal, G. E. (2014). "Climate change and storm water infrastructure in the mid-Atlantic region: Design mismatch coming?" Journal of Hydrologic Engineering, 19(11), 04014026.

Stagge, J. H., and Moglen, G. E. (2017). "Water Resources Adaptation to Climate and Demand Change in the Potomac River." Journal of Hydrologic Engineering, 22(11), 04017050.

Appendix

A.1 Model Implementation

This research has presented climate change and land use change impact assessment conducted using the Occoquan Model, a complexly-linked network of seven watershed models and two reservoir models. The hydrological processes were simulated with the Hydrological Simulation Program - FORTRAN (HSPF) (EPA 2015), and the receiving waterbodies were simulated using CE-QUAL-W2 (Cole and Wells 2006). The 2002-2007 version of Occoquan Model was used in this study. Implementation of the models and input/output procedure have been heavily discussed by Xu et al. (2007).

A.2 Data Management Plan

A.2.1 Global Circulation Models Data

The initial step to downscale GCM data to the region of study area is to download these data from the IPCC website. Hence, IPCC Fourth Assessment Report (AR4) data for each of the climate variables were downloaded and organized based on alphabetical order. These data are free to access and can be downloaded through IPCC's website (www.ipcc-data.org). The historical period in this study was from 1981 to 2000 and labeled as 20c3m in the dataset. The two future periods were from 2046 to 2065 and 2081 to 2100 and labeled as F1 and F2, respectively.

As explained in previous chapters, two downscaling methods (i.e. Delta Change and Quantile Mapping) have been implemented to downscale the climate variables. The downloaded data were in NetCDF (Network Common Data Form) format. NetCDF is a file format that supports storage of multidimensional scientific data (variables). In this format, each variable has three dimensions. For example, for a specific region, surface air temperature has three dimensions, two of these dimensions are showing the spatial resolution (latitude, longitude) and the third dimension is the temporal resolution (time). Figure A - 1 shows the basic structure of a NetCDF file.

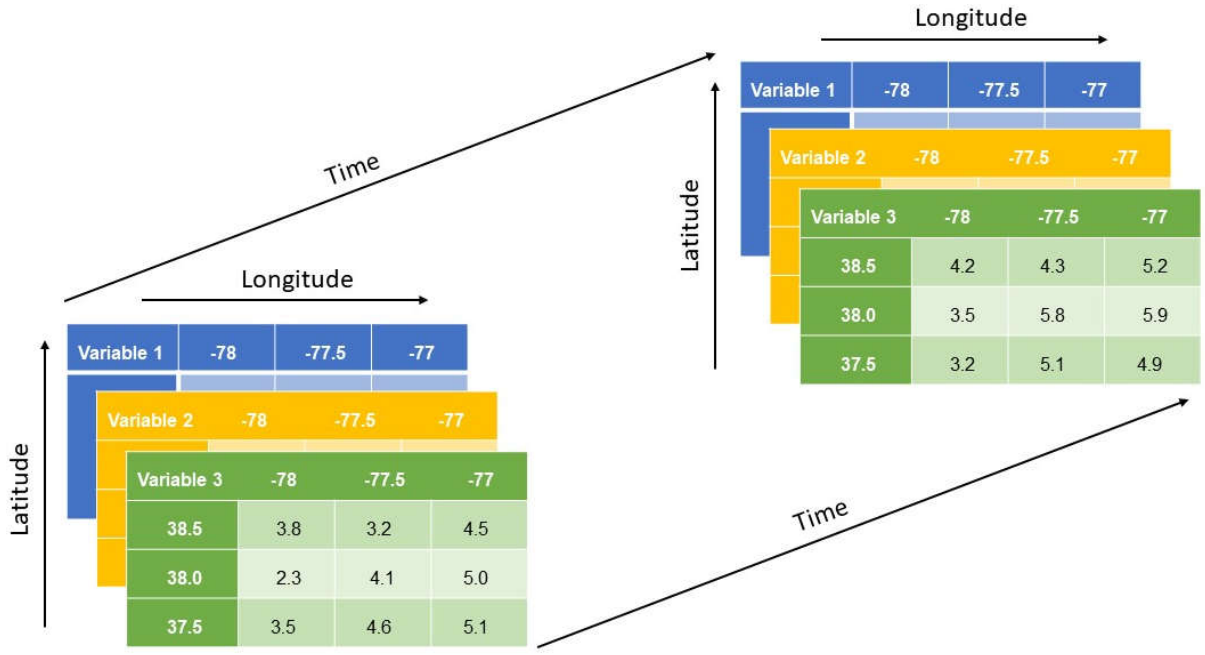

Figure A - 1. The basic structure of NetCDF file.

The NetCDF data are array-oriented and Matlab scripts have been developed to read these data, extract the necessary information and save them in a .mat format for further analysis. After downscaling the data, the downscaled timeseries were stored in relational database system using SQLite software (please refer to section A.2.5).

A.2.2 Land Use Data

All of the historical and projected land use data were set up in accordance with Occoquan watershed segmentations as well as land use types based on pervious and impervious lands. An example of land use data for Low Broad Run subbasin in mid 21st century using A2 emission scenario is shown in Table A - 1. It is worth mentioning that ratios of land development types were kept constant based on the county and city codes. For example, the ratio of impervious land of townhouses to the total occupied land needs to be maximum 35%.

Table A - 1. Land use data for Low Broad Run subbasin using A2 emission scenario for mid 21st century.

#	Segment	Pasture	Forest	Low Density Res.	Low Till. Corps	High Till. Corps	Industrial	Institutional	Medium Density Res.	Townhouse/garden apt.	Sum
		Land Use (Acre)									
		1	2	3	4	5	6	7	8	9	
Pervious Land											
1	50	0.0	23.0	5.5	0.0	0.0	423.9	208.1	1975.0	101.8	**2737.3**
2	51	0.2	43.0	8.8	4.8	1.6	550.7	56.6	3965.4	241.2	**4872.3**
3	64	631.7	3809.6	982.5	1623.5	775.1	30.0	4.1	403.5	2.0	**8262.0**
4	65	0.0	413.7	220.6	0.0	198.4	43.9	24.4	908.7	96.6	**1906.3**
5	66	44.6	501.1	379.2	0.0	0.0	2.4	2.0	230.1	0.0	**1159.4**
6	68	0.0	700.4	92.6	0.0	0.0	1.3	0.0	35.9	0.0	**830.1**
7	69	0.0	1266.5	747.4	0.0	0.0	11.3	29.7	409.0	0.0	**2463.9**
8	75	0.0	23.8	1.8	0.0	0.0	398.8	13.5	2090.8	55.8	**2584.5**
9	76	228.6	809.5	505.4	452.2	207.8	15.0	6.2	1246.5	47.9	**3519.2**
10	82	43.5	13.8	125.4	40.3	0.0	15.4	41.3	966.4	73.9	**1320.1**
11	83	8.6	419.0	923.6	28.6	0.0	7.6	22.7	505.7	0.0	**1915.8**
12	84	580.7	4879.5	1275.9	242.9	341.1	35.6	24.9	309.5	0.0	**7690.0**
Sub-Total		**1537.9**	**12902.9**	**5268.7**	**2392.3**	**1524.0**	**1535.9**	**433.5**	**13046.5**	**619.2**	**39260.9**
Impervious Land											
1	50	0.0	23.0	5.5	0.0	0.0	423.9	112.0	919.4	54.8	**1538.6**
2	51	0.2	43.0	8.8	4.8	1.6	550.7	30.5	1170.5	129.9	**1940.0**
3	64	12.9	43.3	51.7	50.2	24.0	30.0	2.2	100.9	1.1	**316.3**
4	65	0.0	10.8	11.6	0.0	6.1	43.9	13.2	227.2	52.0	**364.8**
5	66	0.9	7.5	20.0	0.0	0.0	2.4	1.1	57.5	0.0	**89.4**
6	68	0.0	7.5	4.9	0.0	0.0	1.3	0.0	9.0	0.0	**22.7**
7	69	0.0	18.0	39.3	0.0	0.0	11.3	16.0	102.2	0.0	**186.8**
8	75	0.0	23.8	1.8	0.0	0.0	398.8	7.3	954.6	30.1	**1416.4**
9	76	4.7	20.3	26.6	14.0	6.4	15.0	3.3	311.6	25.8	**427.7**
10	82	0.9	8.4	6.6	1.2	0.0	15.4	22.3	241.6	39.8	**336.2**
11	83	0.2	10.4	48.6	0.9	0.0	7.6	12.2	126.4	0.0	**206.3**
12	84	11.9	50.8	67.2	7.5	10.5	35.6	13.4	77.4	0.0	**274.3**
Sub-Total		**31.7**	**266.8**	**292.6**	**78.6**	**48.6**	**1535.9**	**233.5**	**4298.3**	**333.5**	**7119.5**
Total		**1569.6**	**13169.7**	**5561.3**	**2470.9**	**1572.6**	**3071.8**	**667.0**	**17344.8**	**952.7**	**46380.4**

A.2.3 Local Data and Data Infilling

OWML operates a system of automated stream and rainfall stations which allows capturing the spatial coverage of Occoquan watershed along with the Occoquan reservoir. These data are managed in an internal database by OWML and FoxPro software was used to retrieve the

necessary data. FoxPro has been abandoned by its developers and after retrieving the necessary data, they were stored in relational database using SQLite software. Data recorded over time by monitoring stations shown in Table A - 2 and Table A - 3 were used to build and calibrate the Occoquan Model.

Table A - 2. Occoquan watershed flow monitoring stations.

Station	STORET NO.	Distance Above Dam		Drainage Area		Date Active
		km	mi	km^2	mi^2	
Occoquan Reservoir Outlet	ST01	0	0	1484	573	01/01/1982
Occoquan River near Manassas	ST10	25.8	16	888	343	NA
Cedar Run near Aden	ST25	46.1	28.8	401	155	10/01/1972
Broad Run near Bristow	ST30	46.6	29.1	232.1	89.6	10/01/1974
Bull Run at 28 near Yorkshire	ST45	29.9	18.6	385.9	149	11/16/1984
Cub Run near Bull Run	ST50	34.9	21.8	129.2	49.9	10/01/1972
Bull Run near Catharpin	ST60	49.9	31.2	66.8	25.8	05/01/1969
Broad Run near Buckland	ST70	59.7	37.3	130.8	50.5	10/01/1950

Table A - 3. Occoquan reservoir monitoring stations.

Station	STORET No.	Distance Above Dam	
		km	mi
Occoquan Reservoir at Occoquan Dam	RE01	0	0
Occoquan Reservoir at 2nd power line	RE02	0.5	0.3
Occoquan Reservoir below Sandy Run	RE05	2.9	1.8
Occoquan Reservoir at Jacob's Rock	RE10	6.4	4.0
Occoquan Reservoir at Ryan's Dam	RE15	9.8	6.1
Occoquan Reservoir below confluence	RE20	12.6	7.9
Occoquan Creek above con. Bull Run	RE25	15.8	9.9
Occoquan Reservoir (Bull Run)	RE30	16.8	10.5
Occoquan Creek at Ravenwood Bridge	RE35	18.0	11.2

For the purpose of this study, an additional set of data was required from other meteorological stations in the vicinity of the watershed area. Altogether these observed historical data were used in developing the climate change models. The three long-established meteorological stations in this region are Washington Dulles International Airport, Reagan National Airport, and the Plains. Table A - 4 shows the weather stations within and in the vicinity of the Occoquan watershed.

Table A - 4. Weather stations within and nearby Occoquan watershed.

No.	Weather Station	Latitude	Longitude	Abbreviation
1	Lorton Water Treatment Plant	38.7012	-77.2073	LRTN
2	Occoquan Watershed Monitoring Laboratory	38.7488	-77.4806	OWML
3	Lake Manassas Water Treatment Plant	38.7623	-77.6222	LMAN
4	Prince William County Regional Landfill	38.6374	-77.4281	LNDF
5	Balls Ford Rd. Yard Waste Facility	38.7880	-77.5642	BLFD

6	Lake Jackson Dam	38.7050	-77.4480	LKJK
7	Airlie	38.7796	-77.8020	AIRL
8	Fair Oaks Police Department	38.8719	-77.3701	FOAK
9	C. Hunter Ritchie Elem. School	38.7606	-77.6956	RITC
10	Cedar Run Wetlands	38.6213	-77.5558	CEDA
11	Clifton Elementary School	38.7840	-77.3887	CLIF
12	Camp Snyder Wetlands	38.8288	-77.6659	CSNY
13	Crockett Park	38.6208	-77.7227	CROK
14	Evergreen Fire Department	38.8805	-77.6341	EVGR
15	Dulles International Airport	38.9401	-77.4632	DULL
16	Reagan Washington National Airport	38.8482	-77.0338	REAG
17	The Plains 2 NNE	38.8939	-77.7541	PLAI
18	Warrenton 3 SE	38.6811	-77.7672	WARN

Historical data availability has always been a challenge for modeling purposes. Often the data in the local stations do not go back far enough or have sections with missing data. Filling the missing data has been a big question for many researchers, hydrologists and water resources engineers. Over time and based on the purpose and practical aspects of filling the missing data, this issue has been addressed differently.

In many studies, for filling the missing hydrological data, the predictive models were developed based on the data in surrogate locations that collected the basic hydrological data including precipitation along with other similar data. These data usually were used to compare and understand how the climate conditions compare across the study area and the sites near the target station with missing data.

In general, the data infilling strategies are classified into three major categories. The first category is using statistical relationships between the target station with missing data and nearby stations with a full set of data. This starts from a simple regression to more advanced methods including autoregressive models to different variations of artificial neural networks models. The second category uses spatial interpolation alike kriging, Thiessen polygons interpolation, Voronoi tessellation, etc. for filling the missing data. The last category uses mathematical formulas to generate time series based on the specified limits, distributions, and criteria defined by the user. These parameters can be set up based on observed values. The simulator uses these constraints and random numbers to generate a new time series as an imitation of the data in the missing period. An example of this category is the Soil and Water Assessment Tool (SWAT)'s Weather Generator (WG) which requires the user to input the probability of a wet day. Then, by using a first-order Markov chain, SWAT generates a random number to appropriate wet day's

probability. Next, the amount of precipitation is calculated using two different distributions, namely the skewed distribution and exponential distribution.

It is also important to note that strategies to fill in data sets could be different compared to filling in the other type of hydrological data sets (e.g. precipitation compared to temperature). In the case of precipitation, mostly due to the spatial nature of rainfall, particularly if the rainfall events are more convective rather than stratiform, On the other hand, for example, Hubbard (1994) found that one station every 60 km in a relatively simple terrain was adequate to capture 90% of the spatial variability in daily temperature. However, for the same site, the network resolution for capturing daily precipitation variability was about an order of magnitude higher (5 km).

In the following section, demonstrations the methodology to quantify a model that can satisfactorily fill the missing data. Table A - 5 lists the required set of hydrological inputs for the Occoquan Model.

Table A - 5. List of required inputs for the Occoquan model

No.	Constituent	Abbreviation	Unit
1	Precipitation	PREC	Inches (in)
2	Air Temperature	ATEM	Fahrenheit (°F)
3	Dew Point	DEWP	Fahrenheit (°F)
4	Wind Speed	WIND	Mile per Hour (mph)
5	Cloud Cover	CLOUD	Decimus
6	Solar Radiation	SOLR	Langley (Ly)
7	Pan Evaporation	EVAP	Inches (in)
8	Potential Evapotranspiration	PEVT	Inches (in)

A.2.4 An example of model selection procedure for infilling the historical precipitation data. A case study: Upper Broad Run subbasin

Summary

For downscaling the climate data to local stations, there is a need for local historical hydrological data. Many of these local stations do not have historical data. The goal of this section is to explore the use to a model for constructing historical precipitation time series. For this reason, different variations of three methods have been compared for filling the missing data. 19 models were made and various performance metrics have been used to measure the performance of each model. Finally, Closet Station Method (CSM) method was selected based on its performance ratings. As an example, this method has been used to create historical precipitation data for the

local stations in Upper Broad subbasin. The comparison between constructed and recorded data showed that the method could effectively build the missing historical data.

Introduction

In part of downscaling the climate data, Local Historical (LH) information is needed for several stations across the watershed. Often the data in the local stations do not go back far enough for the downscaling purposes. These local stations are usually missing some hydrological data including precipitation and temperature. Filling the missing data has been a big question for many researchers, hydrologists and water resources engineers. Over time and based on the purpose and practical aspects of filling the missing data this question has been addressed differently.

In many studies, for filling the missing hydrological data, the predictive models were developed based on the data in surrogate locations that collected the basic hydrological data including precipitation along with other similar data. These data usually were used to compare and understand how the climate conditions compare across the study area and the sites near the target station with missing data.

In the case of precipitation, mostly due to the spatial nature of rainfall, particularly if the rainfall events are more convective rather than stratiform, strategies to fill in data sets could be different oppose to filling in the other type of hydrological data sets (e.g. temperature). For example, Hubbard (1994) found that one station every 60 km in a relatively simple terrain was adequate to capture 90% of the spatial variability in daily temperature. However, for the same site, the network resolution for capturing daily precipitation variability was about an order of magnitude higher (5 km).

Materials and methods

In general, the filling strategies are classified into three major categories. The first category is using statistical relationships between the target station with missing data and nearby stations with a full set of data. This starts from a simple regression to more advanced methods including autoregressive models to different variations of artificial neural networks models. The second category uses spatial interpolation alike kriging, Thiessen polygons interpolation, Voronoi tessellation, etc. for filling the missing data. The last category uses mathematical formulas to

generate time series based on the specified limits, distributions, and criteria defined by the user. These parameters can be set up based on observed values. The simulator uses these constraints and random numbers to generate a new time series as an imitation of the data in the missing period. An example of this category is the Soil and Water Assessment Tool (SWAT)'s Weather Generator (WG) which requires the user to input the probability of a wet day. Then, by using a first-order Markov chain, generates a random number to appropriate wet day's probability. Next, the amount of precipitation is calculated using two different distributions, namely the skewed distribution and exponential distribution.

The goal of this section is to quantify a model that can satisfactorily fill the missing data. The three stations that have been investigated here are located in the Upper Broad subbasin (Figure A - 2). These three stations do not have historical hydrological data. Six years of observed data (2002-2007), four nearby stations and three different methods have been investigated to fill the missing historical precipitation data (1970-2001). The list of weather stations has been shown in Table A - 6. The methods that have been used to model the missing data are shown in Table A - 7.

Table A - 6. Stations used in this study

Name of the weather station	Abbreviation	Latitude	Longitude	Elevation (m)
Dulles International Airport	DULL	38.940	-77.463	88.4
Reagan Washington National Airport	REAG	38.848	-77.034	3.00
The Plains 2 NNE	PLAI	38.894	-77.754	161.5
Warrenton 3 SE	WARN	38.681	-77.767	152.4
Airlie	AIRL	38.780	-77.802	N/A
Camp Snyder Wetlands	CSNY	38.829	-77.666	N/A
C. Hunter Ritchie Elementary School	RITC	38.761	-77.696	N/A

Table A - 7. Methods that have been used for creating models for filling the historical precipitation data

No.	Method name	Abbreviation
1	Closest Station Method	CSM
2	Inverse Distance Weighting Interpolation	IDW
3	Normal Ratio Method	NRM

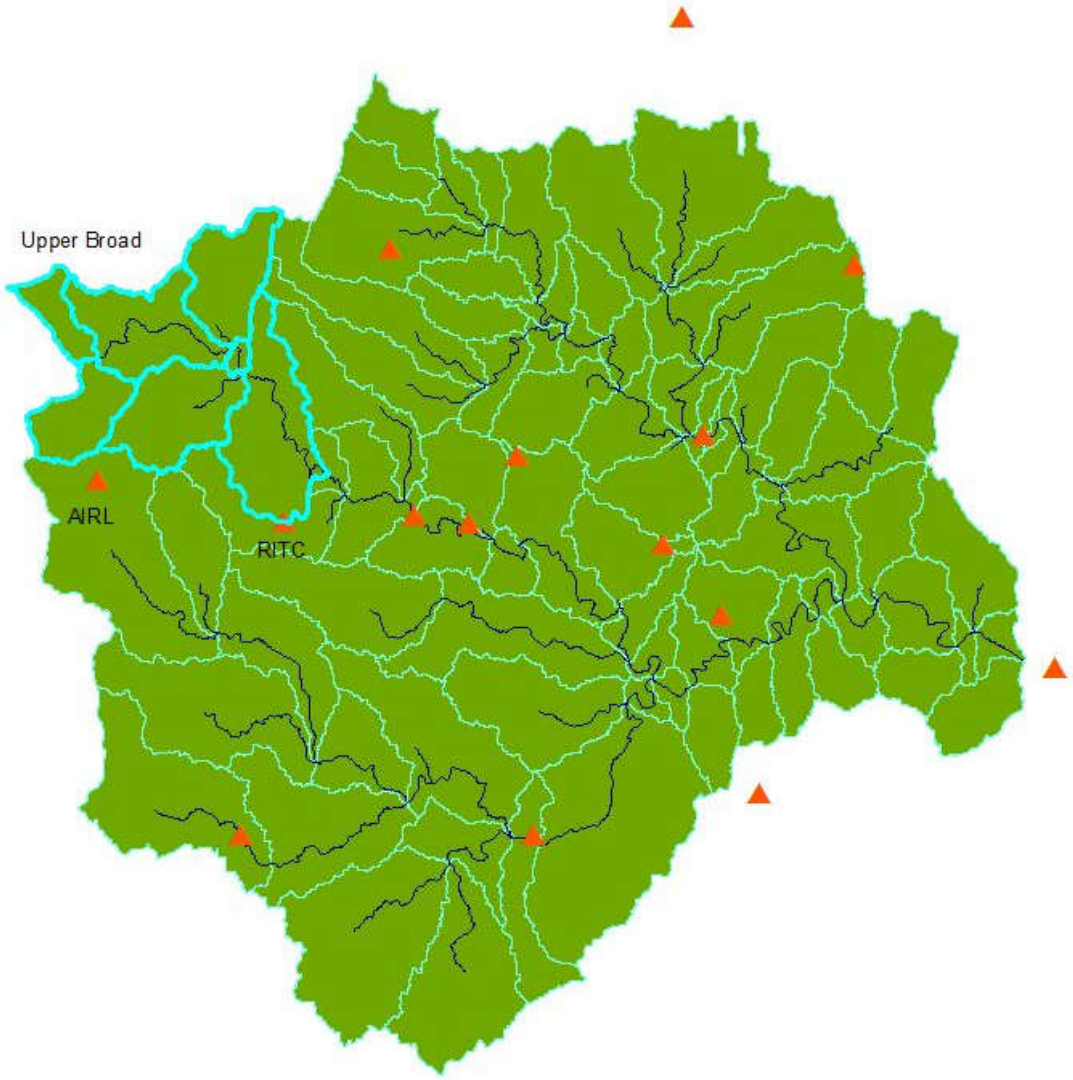

Figure A - 2. Location of Upper Broad subbasin in the Occoquan Watershed

Closest station method (CSM)

This method uses the first and second moments of available data between target station and the station with a full set of data for filling the missing data. In the first step, the first and the second moment of available data in the both target and neighbor station are calculated. In the second step, the first and the second moment of historical data in the neighbor station are calculated and scaled using the mean and the standard deviation of the first step. Then using Equation A - 1 the amount of precipitation is calculated for the target station. This method assumes that the dry/wet days in the target station were same as the neighboring station.

$$\frac{x_i - \mu_x}{\sigma_x} = \frac{y_i - \mu_y}{\sigma_y}$$ Equation A - 1

where

x_i: precipitation in the target station

y_i: precipitation in the nearby station

μ_x: mean of precipitation of the target station

μ_y: mean of precipitation of the nearby station

σ_x: standard deviation of the target station

σ_y: standard deviation of the nearby station

The match paired dry/wet days of the observed data (2002-2007) are shown in Table A - 8. This method was used with the four neighboring weather stations that had the full set of data. The statistics and the performance of each model using this method is shown in Table A - 12.

Table A - 8. Matching dry/wet days observed data (2002-2007) in target stations with neighboring stations

Station name		DULL		REAG		PLAI		WARN	
		Dry	Wet	Dry	Wet	Dry	Wet	Dry	Wet
AIRL	Dry	0.56	0.08	0.58	0.07	0.56	0.09	0.57	0.08
	Wet	0.11	0.25	0.10	0.25	0.12	0.23	0.12	0.23
Matched days		%81		%83		%79		%80	
CSNY	Dry	0.58	0.07	0.60	0.06	0.57	0.08	0.58	0.08
	Wet	0.09	0.25	0.08	0.26	0.10	0.24	0.12	0.23
Matched days		%84		%86		%81		%81	
RITC	Dry	0.59	0.09	0.61	0.07	0.58	0.10	0.59	0.09
	Wet	0.08	0.24	0.08	0.25	0.10	0.23	0.10	0.22
Matched days		%83		%86		%81		%81	

Inverse Distance Weighting interpolation method (IDW)

This method is based on the Tobler's first law of geography: Everything is related to everything else, but near things are more related than distant things (Tobler, 1970). This deterministic method has different variations. The basic or Shepard method has been used in this study.

$$z_p = \frac{\sum_{i=1}^{n} \frac{z_i}{d_{ip}^a}}{\sum_{i=1}^{n} \frac{1}{d_{ip}^a}}$$ Equation A - 2

where

z_p: unknown precipitation in the target station

z_i: precipitation in the nearby stations

i: number of nearby stations

n: number of known points (stations)

d: distances between target station and nearby stations

a: positive real number, called the power parameter

The two factors for using this method are a number of used known points (stations with a full set of data) (n) and the power parameter (a) (Table A - 9). Here, three different combinations of n and four different power parameters (2, 3, 5 and 10) have been explored. The power parameter has a control effect in this formula meaning that by having lower power parameter the nearby stations will be incorporated more uniformly. This will result in smoother estimated values. However, higher power parameters will employ the stations that are closer to the target station. This will accentuate the estimated values by the values of the nearest neighbors. The distance between the target stations and nearby stations with full set of data are shown in Table A - 10. These distances were calculated using Haversine formula (Equation A - 3)

$$d = 2r\arcsin\left(\sqrt{\sin^2\left(\frac{\varphi_2-\varphi_1}{2}\right)+\cos(\varphi_1)\cos(\varphi_2)\sin^2\left(\frac{\lambda_2-\lambda_1}{2}\right)}\right) \qquad \text{Equation A - 3}$$

where

d: distance between the two points

r: radius of the sphere (the Earth)

ϕ_1 and ϕ_2: latitudes of point 1 and point 2

λ_1 and λ_2: longitudes of point 1 and point 2

In this formula, the mean radius of the Earth has been considered (6371.0 km) which is the authalic radius extracted from the surface area (Lide, 2000). Latitude and longitude of each weather station have been shown in Table A - 6.

Table A - 9. Stations used in IDW method.

Number of neighbor stations	Name of the stations
$n = 4$	DULL, REAG, PLAI, WARN
$n = 3$	DULL, PLAI, WARN
$n = 2$	PLAI, WARN

Results of different variations of IDW methods have been shown in Table A - 12.

Table A - 10. Distances between target stations and neighbor stations.

Name of the station	Distance (mi)			
	DULL	REAG	PLAI	WARN
AIRL	21.34	41.62	8.32	7.07
CSNY	13.35	34.03	6.54	11.57
RITC	17.62	36.13	9.74	6.71

Normal Ratio Method (NRM)

NRM first proposed by Paulhus and Kohler (1954) and later modified by Young (1992) (0Equation A - 4). This method considers a weigh for nearby stations base on the correlation coefficient between the target station and the station with full set of data.

$$z_p = \frac{\sum_{i=1}^{n} w_i z_i}{\sum_{i=1}^{n} w_i} \qquad \text{0Equation A - 4}$$

where

z_p: precipitation in the target station

z_i: precipitation in the nearby stations

i: number of nearby stations

n: number of known points (stations)

w_i: weight of ith surrounding stations which can be calculated by 0Equation A - 5

$$w_i = r_i^2 \left(\frac{n_i - 2}{1 - r_i^2}\right) \qquad \textbf{0}\text{Equation A - 5}$$

where

r_i: correlation coefficient between the target station and the ith nearby stations

n_i: number of data points used to derive the correlation coefficient.

Results employing this method using different stations have been shown in Table A - 12.

Performance criteria

There are two general categories for evaluating the model performance consisting of statistical and graphical methods. The qualitative statistical methods, themselves, have been categorized to three major groups: standard regression, dimensionless, and error index. Standard regression statistics determine the strength of the linear relationship between simulated and measured data. Dimensionless techniques provide a relative model evaluation assessment, and error indices quantify the deviation in the units of the data of interest (Legates and McCabe, 1999).

Besides graphical evaluation, in this report, six indexes have been used to measure how the simulated and observed data fit together (Table A - 11).

Table A - 11. Qualitative performance metrics.

No.	Name of the metric	Abbreviation	Type	Optimal value
1	Nash-Sutcliffe efficiency	NSE	dimensionless	1
2	Percent bias	PBIAS	error index	0
3	Root mean square error	RMSE	error index	0
4	RMSE-observations standard deviation ratio	RSR	error index	0
5	Coefficient of determination	R^2	standard regression	1
6	Correlation coefficient	PCC	standard regression	1

Nash-Sutcliffe efficiency (NSE): NSE is a normalized statistic that determines the relative magnitude of the residual variance (noise) compared to the measured data variance (information) (Nash and Sutcliffe, 1970).

Percent bias (PBIAS): PBIAS measures the average tendency of the simulated data to be larger or smaller than their observed counterparts (Gupta et al., 1999).

Root mean square error (RMSE): RMSE represents the sample standard deviation of the differences between predicted values and observed values (Wikipedia).
RMSE-observations standard deviation ratio (RSR): standardizes RMSE using the observations standard deviation, and it combines both an error index and the additional information recommended by Legates and McCabe (1999).

Coefficient of determination (R^2): R^2 describe the degree of collinearity between simulated and measured data (Moriasi et al. 2007).

Correlation coefficient (Pearson product-moment correlation coefficient) (PCC): PCC is a measure of the linear correlation (dependence) between two variables with the maximum and

minimum of +1 and -1 inclusive, where 1 is total positive correlation, 0 is no correlation, and -1 is total negative correlation.

Results and discussions

In many cases, researcher use observed series of data which are considered theoretically related to the missing set of data to fill the missing data by estimation or interpolation. As mentioned earlier there are several methods for filling the missing data. Most of the methods investigate the correlation of the nearby weather stations and develop a correlation equation. Then use the weather station(s) with the best performance metric to fill the data gaps.

In this study, for filling the missing precipitation data, 19 different models have been developed using three methods (Table A - 7). General statistics of each 19 models for the three target stations are shown in Table A - 12.

Table A - 12. Statistics of observed and simulated precipitations.

No.	Method	Max	Min	μ	σ	Med	CV	Skewness	Ave. annual precipitation	% error (Mean of Observed and Simulated)	% error (SD of Observed and Simulated)
1	DULL-Obs	6.69	0.00	0.12	0.35	0.00	2.98	6.49	43.34		
2	REAG-Obs	5.19	0.00	0.11	0.35	0.00	3.05	5.80	41.75		
3	PLAI-Obs	5.48	0.00	0.13	0.37	0.00	2.85	5.63	46.85		
4	WARN-Obs	3.76	0.00	0.12	0.33	0.00	2.79	4.64	42.61		
5	AIRL-Obs	3.53	0.00	0.11	0.33	0.00	2.93	5.00	40.78		
6	CSNY-Obs	3.86	0.00	0.11	0.33	0.00	3.00	5.28	40.76		
7	RITC-Obs	3.66	0.00	0.10	0.31	0.00	3.08	5.46	37.21		
8	AIRL-CSM-DULL	6.19	0.00	0.11	0.33	0.00	2.97	6.47	40.32	1.16	0.15
9	AIRL-CSM-REAG	4.88	0.00	0.11	0.33	0.00	3.02	5.77	39.71	2.69	0.31
10	AIRL-CSM-PLAI	4.91	0.00	0.11	0.33	0.00	2.87	5.65	41.61	2.06	0.24
11	AIRL-CSM-WARN	3.78	0.00	0.12	0.33	0.00	2.82	4.67	42.24	3.58	0.43
12	AIRL-IDW-4P-a-2	3.80	0.00	0.12	0.29	0.00	2.41	4.39	44.29	8.59	10.68
13	AIRL-IDW-4P-a-3	3.81	0.00	0.12	0.29	0.00	2.43	4.39	44.20	8.33	10.20
14	AIRL-IDW-4P-a-5	3.67	0.00	0.12	0.30	0.00	2.47	4.38	43.91	7.61	9.46
15	AIRL-IDW-4P-a-10	3.33	0.00	0.12	0.31	0.00	2.58	4.47	43.31	6.18	6.68
16	AIRL-IDW-3P-a-2	3.82	0.00	0.12	0.29	0.00	2.42	4.39	44.33	8.68	10.50
17	AIRL-IDW-3P-a-3	3.81	0.00	0.12	0.29	0.00	2.43	4.39	44.20	8.42	10.16
18	AIRL-IDW-3P-a-5	3.67	0.00	0.12	0.30	0.00	2.47	4.38	43.91	7.61	9.46
19	AIRL-IDW-3P-a-10	3.33	0.00	0.12	0.31	0.00	2.58	4.47	43.31	6.18	6.68
20	AIRL-IDW-2P-a-2	3.96	0.00	0.12	0.30	0.00	2.43	4.43	44.39	8.86	9.77
21	AIRL-IDW-2P-a-3	3.86	0.00	0.12	0.30	0.00	2.44	4.40	44.22	8.42	9.83
22	AIRL-IDW-2P-a-5	3.67	0.00	0.12	0.30	0.00	2.47	4.39	43.91	7.70	9.40
23	AIRL-IDW-2P-a-10	3.33	0.00	0.12	0.31	0.00	2.58	4.47	43.31	6.18	6.68

24	AIRL-NRM-4P	2.61	0.00	0.07	0.20	0.00	2.66	5.08	26.85	34.20	40.38
25	AIRL-NRM-3P	2.07	0.00	0.06	0.16	0.00	2.74	5.26	21.87	46.37	49.91
26	AIRL-NRM-2P	1.77	0.00	0.04	0.12	0.00	2.85	5.63	15.10	62.94	64.04
27	CSNY-CSM-DULL	6.32	0.00	0.11	0.33	0.00	2.99	6.49	40.87	0.27	0.03
28	CSNY -CSM-REAG	4.98	0.00	0.11	0.33	0.00	3.04	5.78	40.25	1.25	0.15
29	CSNY -CSM-PLAI	5.01	0.00	0.12	0.33	0.00	2.88	5.66	42.19	3.49	0.42
30	CSNY -CSM-WARN	3.85	0.00	0.12	0.33	0.00	2.83	4.68	42.85	5.11	0.60
31	CSNY-IDW-4P-a-2	4.30	0.00	0.12	0.32	0.00	2.54	4.94	45.36	11.29	5.59
32	CSNY-IDW-4P-a-3	4.75	0.00	0.13	0.33	0.00	2.63	5.22	45.92	12.72	0.96
33	CSNY-IDW-4P-a-5	5.24	0.00	0.13	0.35	0.00	2.77	5.51	46.53	14.16	5.38
34	CSNY-IDW-4P-a-10	5.47	0.00	0.13	0.36	0.00	2.84	5.62	46.83	14.96	9.06
35	CSNY -IDW-3P-a-2	4.34	0.00	0.12	0.32	0.00	2.55	4.97	45.44	11.47	5.11
36	CSNY -IDW-3P-a-3	4.76	0.00	0.13	0.33	0.00	2.64	5.23	45.94	12.72	0.81
37	CSNY -IDW-3P-a-5	5.24	0.00	0.13	0.35	0.00	2.77	5.51	46.54	14.16	5.38
38	CSNY-IDW-3P-a-10	5.47	0.00	0.13	0.36	0.00	2.84	5.62	46.83	14.96	9.06
39	CSNY -IDW-2P-a-2	4.85	0.00	0.13	0.32	0.00	2.57	5.16	45.82	12.46	3.50
40	CSNY -IDW-2P-a-3	5.08	0.00	0.13	0.34	0.00	2.66	5.36	46.20	13.35	0.66
41	CSNY -IDW-2P-a-5	5.34	0.00	0.13	0.35	0.00	2.78	5.55	46.62	14.43	6.01
42	CSNY-IDW-2P-a-10	5.47	0.00	0.13	0.36	0.00	2.84	5.62	46.84	14.96	9.06
43	CSNY-NRM-4P	3.02	0.00	0.08	0.22	0.00	2.67	5.14	30.19	25.90	34.06
44	CSNY -NRM-3P	2.50	0.00	0.07	0.19	0.00	2.75	5.30	25.13	38.35	43.48
45	CSNY -NRM-2P	2.03	0.00	0.05	0.14	0.00	2.85	5.63	17.37	57.35	59.48
46	RITC-CSM-DULL	5.92	0.00	0.10	0.31	0.00	3.01	6.51	37.99	2.06	0.22
47	RITC-CSM-REAG	4.66	0.00	0.10	0.31	0.00	3.06	5.80	37.43	0.59	0.06
48	RITC-CSM-PLAI	4.69	0.00	0.11	0.31	0.00	2.90	5.68	39.24	5.50	0.64
49	RITC-CSM-WARN	3.61	0.00	0.11	0.31	0.00	2.85	4.69	39.88	7.16	0.83
50	RITC-IDW-4P-a-2	3.50	0.00	0.12	0.29	0.00	2.42	4.32	43.87	17.86	7.21
51	RITC-IDW-4P-a-3	3.43	0.00	0.12	0.30	0.00	2.48	4.37	43.63	17.27	5.48
52	RITC-IDW-4P-a-5	3.41	0.00	0.12	0.31	0.00	2.60	4.50	43.18	16.00	1.85
53	RITC-IDW-4P-a-10	3.70	0.00	0.12	0.32	0.00	2.75	4.62	42.71	14.82	2.71
54	RITC-IDW-3P-a-2	3.52	0.00	0.12	0.29	0.00	2.43	4.32	43.92	18.06	6.98
55	RITC-IDW-3P-a-3	3.44	0.00	0.12	0.30	0.00	2.48	4.37	43.64	17.27	5.42
56	RITC-IDW-3P-a-5	3.41	0.00	0.12	0.31	0.00	2.60	4.50	43.18	16.00	1.85
57	RITC-IDW-3P-a-10	3.70	0.00	0.12	0.32	0.00	2.75	4.62	42.71	14.82	2.71
58	RITC-IDW-2P-a-2	3.71	0.00	0.12	0.30	0.00	2.46	4.39	43.98	18.16	5.52
59	RITC-IDW-2P-a-3	3.51	0.00	0.12	0.30	0.00	2.51	4.41	43.66	17.27	4.46
60	RITC-IDW-2P-a-5	3.41	0.00	0.12	0.31	0.00	2.61	4.50	43.18	16.00	1.59
61	RITC-IDW-2P-a-10	3.70	0.00	0.12	0.32	0.00	2.75	4.62	42.71	14.82	2.71
62	RITC-NRM-4P	3.00	0.00	0.08	0.22	0.00	2.67	5.16	29.82	19.82	30.39
63	RITC-NRM-3P	2.45	0.00	0.07	0.18	0.00	2.75	5.31	24.44	34.35	41.36
64	RITC-NRM-2P	1.94	0.00	0.04	0.13	0.00	2.85	5.63	16.55	55.54	58.83

Table A - 13 shows the suggested general performance ratings for the selected performance metrics on a monthly time step (Moriasi, 2007).

Table A - 13. General performance ratings for the selected performance metrics on a monthly time step.

Performance rating	Performance metric		
	NSE	PBIAS (%)	RSR
Very good	$0.75 < NSE \leq 1.00$	$PBIAS < \pm 10$	$0.00 \leq RSR \leq 0.50$
Good	$0.65 < NSE \leq 0.75$	$\pm 10 \leq PBIAS < \pm 15$	$0.50 < RSR \leq 0.60$
Satisfactory	$0.50 < NSE \leq 0.65$	$\pm 15 \leq PBIAS < \pm 25$	$0.60 < RSR \leq 0.70$
Unsatisfactory	$NSE \leq 0.50$	$PBIAS \geq \pm 25$	$RSR > 0.70$

As part of demonstrating the selected model, several performance metrics have been examined to quantify the confidence associated with the selected models for each target station (Table A - 14). The CSM models developed using The Plains and Dulles International Airport weather stations are showing satisfactory results using the performance metrics, namely model 'AIRL-CSM-PLAI' for AIRL, model 'CSNY-CSM-PLAI' for CSNY and model 'RITC-CSM-DULL' for RITC. Meaning that these models have the highest NSE, lowest PBIAS, and lowest RSR among other peer models. Monthly performance criteria for different models are shown in Table A - 15.

Table A - 14. Comparing the performance ratings of the selected final models.

Model names	Target stations	Used stations	Method	Performance metrics and ratings		
				NSE	PBIAS (%)	RSR
AIRL_CSM_PLAI	AIRL	PLAI	CMS	0.82	-2.06	0.42
				Very good	Very good	Very good
CSNY_CSM_PLAI	AIRL	PLAI	CMS	0.63	-3.44	0.60
				Satisfactory	Very good	Good
RITC_CSM_DULL	RITC	DULL	CMS	0.73	-2.20	0.51
				Good	Very good	Good

Table A - 15. Monthly performance criteria for different models.

Method	NSE	PBIAS (%)	RSME	RSR	R^2	PCC
AIRL-CSM-DULL	0.60	1.12	1.26	0.63	0.65	0.84
AIRL-CSM-REAG	0.38	2.86	1.56	0.78	0.51	0.75
AIRL-CSM-PLAI	0.82	-2.06	0.84	0.42	0.85	0.85
AIRL-CSM-WARN	0.73	-3.48	1.03	0.52	0.75	0.78
AIRL-IDW-4P-a-2	0.80	-8.51	0.88	0.44	0.84	0.84
AIRL-IDW-4P-a-3	0.80	-8.29	0.89	0.44	0.84	0.83
AIRL-IDW-4P-a-5	0.79	-7.68	0.90	0.45	0.83	0.82
AIRL-IDW-4P-a-10	0.77	-6.20	0.95	0.47	0.80	0.81
AIRL-IDW-3P-a-2	0.80	-8.66	0.88	0.44	0.84	0.84
AIRL-IDW-3P-a-3	0.80	-8.30	0.89	0.44	0.84	0.83
AIRL-IDW-3P-a-5	0.79	-7.69	0.90	0.45	0.83	0.83
AIRL-IDW-3P-a-10	0.77	-6.20	0.95	0.47	0.80	0.81
AIRL-IDW-2P-a-2	0.80	-8.84	0.89	0.44	0.84	0.83
AIRL-IDW-2P-a-3	0.80	-8.43	0.89	0.44	0.84	0.83
AIRL-IDW-2P-a-5	0.79	-7.68	0.90	0.45	0.83	0.82
AIRL-IDW-2P-a-10	0.77	-6.20	0.95	0.47	0.80	0.81
AIRL-NRM-4P	0.35	34.21	1.61	0.80	0.73	0.84
AIRL-NRM-3P	0.05	46.57	1.94	0.97	0.80	0.87
AIRL-NRM-2P	-0.59	62.98	2.51	1.25	0.85	0.85

CSNY-CSM-DULL	0.56	-0.43	1.26	0.66	0.65	0.73
CSNY -CSM-REAG	0.37	1.25	1.52	0.79	0.53	0.63
CSNY -CSM-PLAI	0.63	-3.44	1.16	0.60	0.72	0.74
CSNY -CSM-WARN	0.60	-4.94	1.21	0.63	0.66	0.69
CSNY-IDW-4P-a-2	0.62	-11.28	1.17	0.61	0.75	0.75
CSNY-IDW-4P-a-3	0.58	-12.64	1.23	0.64	0.74	0.75
CSNY-IDW-4P-a-5	0.52	-14.12	1.32	0.69	0.73	0.74
CSNY-IDW-4P-a-10	0.49	-14.95	1.37	0.71	0.72	0.74
CSNY -IDW-3P-a-2	0.62	-11.48	1.18	0.61	0.75	0.75
CSNY -IDW-3P-a-3	0.58	-12.70	1.24	0.64	0.74	0.75
CSNY -IDW-3P-a-5	0.52	-14.12	1.32	0.69	0.73	0.74
CSNY-IDW-3P-a-10	0.49	-14.95	1.37	0.71	0.72	0.74
CSNY -IDW-2P-a-2	0.59	-12.45	1.23	0.64	0.74	0.74
CSNY -IDW-2P-a-3	0.55	-13.41	1.28	0.66	0.73	0.74
CSNY -IDW-2P-a-5	0.51	-14.45	1.34	0.69	0.72	0.74
CSNY-IDW-2P-a-10	0.49	-14.94	1.37	0.71	0.72	0.74
CSNY-NRM-4P	0.47	26.02	1.39	0.72	0.69	0.71
CSNY-NRM-3P	0.22	38.41	1.68	0.88	0.73	0.76
CSNY-NRM-2P	-0.47	57.51	2.32	1.21	0.72	0.74
RITC-CSM-DULL	0.73	-2.20	0.95	0.51	0.77	0.85
RITC-CSM-REAG	0.47	-0.76	1.33	0.72	0.59	0.75
RITC-CSM-PLAI	0.71	-5.47	0.98	0.53	0.77	0.84
RITC-CSM-WARN	0.66	-7.38	1.07	0.58	0.71	0.72
RITC-IDW-4P-a-2	0.65	-17.94	1.08	0.59	0.79	0.80
RITC-IDW-4P-a-3	0.64	-17.13	1.10	0.59	0.78	0.79
RITC-IDW-4P-a-5	0.62	-15.97	1.12	0.61	0.75	0.76
RITC-IDW-4P-a-10	0.60	-14.77	1.15	0.62	0.72	0.73
RITC-IDW-3P-a-2	0.65	-18.03	1.08	0.59	0.79	0.80
RITC-IDW-3P-a-3	0.64	-17.22	1.10	0.60	0.77	0.79
RITC-IDW-3P-a-5	0.62	-15.99	1.12	0.61	0.75	0.76
RITC-IDW-3P-a-10	0.60	-14.77	1.15	0.62	0.72	0.73
RITC-IDW-2P-a-2	0.62	-18.17	1.12	0.61	0.78	0.79
RITC-IDW-2P-a-3	0.63	-17.29	1.12	0.61	0.76	0.77
RITC-IDW-2P-a-5	0.62	-16.07	1.13	0.61	0.75	0.75
RITC-IDW-2P-a-10	0.60	-14.77	1.15	0.62	0.72	0.73
RITC-NRM-4P	0.65	19.94	1.09	0.59	0.77	0.84
RITC-NRM-3P	0.43	34.42	1.39	0.75	0.83	0.87
RITC-NRM-2P	-0.29	55.62	2.08	1.13	0.78	0.84

After using these models for filling the historical data, the constructed precipitation data were analyzed using the performance metrics for the same period that observed data were available (i.e. 2002 to 2007). The results of these comparisons are shown in Table A - 16.

Table A - 16. Comparing the performance ratings of constructed models with observed records (2002-2007).

Model names	Performance metrics and ratings		
	NSE	PBIAS (%)	RSR
AIRL_CSM_PLAI	0.82	-2.10	0.42
	Very good	Very good	Very good
CSNY_CSM_PLAI	0.63	-3.64	0.60
	Satisfactory	Very good	Good
RITC_CSM_DULL	0.73	-2.14	0.51
	Good	Very good	Good

Conclusion

This section demonstrated an example of data infilling procedure for one of the methodological variables (i.e. precipitation). As precipitation can be quite variable on a short distance, different performance metrics have been examined to find the most suitable nearby weather station for filling the missing precipitation time series. The models using CSM method developed based on the Dulles International Airport and the Plains weather station outperforms the other models. These models were used to populate the missing historical data in the Upper Broad subbasin weather stations. The constructed time series were investigated for their performance. The results showed that the method could successfully construct missing precipitation data. The same methodology was used to construct and infill the missing data for the needed weather stations for this study.

A.2.5 Data Management System

After creating the timeseries for each of the climate and land use variables, all of the timeseries were saved in a database. A relational database management system, namely SQLite software was used to store and retrieve the necessary data on demand. SQLite is a free software and one can query relational data using a query system quickly and efficiently. The following shows an example of querying meteorological variables of Upper Broad Run subbasin for mid 21st century:

```
SELECT F1, LKJK, ATEM, DEWP, WIND, PHI, CLOU
FROM UBRS
WHERE F1 < date('EndDate')
```

where

F1: mid 21st century

UBRS: Upper Broad Run Subbasin

and

LKJK, ATEM, DEWP, WIND, PHI, CLOU: precipitation, surface air temperature, dew point, wind velocity, wind direction and cloud cover data from Lake Jackson Dam weather station, respectively.

Subsequently, this database served as the basis for input and output data of Occoquan Model.

A.3 References

Cole, T. M., and Wells, S. A. (2006). "CE-QUAL-W2: A two-dimensional, laterally averaged, hydrodynamic and water quality model, version 3.5."

Donigian, AS. Jr. (2000) HSPF training workshop handbook and CD. Lecture #19: calibration and verification issues. U.S. Environmental Protection Agency Headquarters, Washington Information Center, 10−14 January, 2000. Prepared for U.S. Environmental Protection Agency, Office of Water, Office of Science and Technology, Washington, DC.

EPA, U. (2015). "BASINS 4.1 (Better Assessment Science Integrating point & Non-point Sources) Modeling Framework." (02/02/2018).

Gupta, H. V., Sorooshian, S. and Yapo, P. O. (1999). Status of automatic calibration for hydrologic models: Comparison with multilevel expert calibration. J. Hydrologic Eng. 4(2): 135-143.

Hubbard, K. G. (1994). Spatial variability of daily weather variables in the high plains of the USA. Agric. For. Meteor., 68, 29-41.

Kashani, M. H. and Dinpashoh, Y. (2012). Evaluation of efficiency of different estimation methods for missing climatological data. Stochastic Environmental Research and Risk Assessment. 01/2011; 26(1). DOI:10.1007/s00477-011-0536-y

Legates, D. R., and McCabe, G. J. (1999). Evaluating the use of 'goodness-of-fit' measures in hydrologic and hydroclimatic model validation. Water Resources Res. 35(1): 233-241.

Lide D. R. (2000). Handbook of Chemistry and Physics (81st edition). CRC. ISBN 0-8493-0481-4.
Nash, J. E. and Sutcliffe, J. V. (1970). River flow forecasting through conceptual models part I - A discussion of principles, Journal of Hydrology, 10 (3), 282–290.
Moriasi, D. N., Arnold, J. G., Van Liew, M. W., Bingner,R. L., Harmel, R. D. and Veith, T. L. (2007). Model evaluation guidelines for systematic quantification of accuracy in watershed simulations, Transactions of the ASABE, 50 (3), 885–900.
Paulhus, J. L. and Kohler, M. A. (1952). Interpolation of missing precipitaion records. Mon. Wea. Rev., 109, 2040-2045.
Shepard, D. (1968). A two-dimensional interpolation function for irregularly-spaced data. Proceedings of the 1968 ACM National Conference. pp. 517–524. doi:10.1145/800186.810616.
Tobler, W. (1970). A computer movie simulating urban growth in the Detroit region. Economic Geography, 46(2): 234-240.
Young, K. C. (1992). A three-way model for interpolating for monthly precipitation values. Monthly Weather Review, vol.120, no.11, pp. 2561–2569, 1992.
Xu, Z., Godrej, A. N., and Grizzard, T. J. (2007). "The hydrological calibration and validation of a complexly-linked watershed–reservoir model for the Occoquan watershed, Virginia." Journal of Hydrology, 345(3-4), 167-183.